Proceedings of the Third National Meeting on

MICROWAVES IN THE ENGINEERING AND IN THE APPLIED SCIENCE

MISA 2006

Proceedings of the Third National Meeting on

MICROWAVES IN THE ENGINEERING AND IN THE APPLIED SCIENCE

MISA 2006

Edited by Eugenio Caponetti

Cover Figure: Radiation from a shaped double reflector system to a cylindrical penetrable target.

With permission of E. Di Giampaolo, F. Bardati and P. Tognolatti

ENEA

Ente per le Nuove tecnologie,
l'Energia e l'Ambiente

Proceedings of the Third National Meeting on

MICROWAVES IN THE ENGINEERING AND IN THE APPLIED SCIENCE

MISA 2006

EDITED BY EUGENIO CAPONETTI

PREFACE

The Third National Meeting on "Microonde nell'Ingegneria e nelle Scienze Applicate – MISA 2006" was held at "Splendid Hotel La Torre" in Palermo (Mondello), Sicily, from May 24 to May 26, 2006. About 50 scientists attended this Meeting to discuss basic and applied research to the physical and chemical processes under microwave irradiation.

In the last three decades, the electromagnetic energy revealed to be a powerful tool for the homogeneous heating of materials and aroused the interest of researcher in various fields of applied research and of industries. The high energetic efficiency and the short treatment time for processes under ultrasonic and microwave irradiation guarantee low energetic consumption, the reduction of pollutants and an improved quality of materials. The Italian Group of "Microonde Applicate ai Materiali ed ai Processi" (GIMAMP), was constituted in the 2001 as Italian branch of AMPERE "Association for Microwave Power in Europe for Research and Education". Several researchers, involved in the applicability of microwaves in the industry as well as in the basic research, joined this group. GIMAMP proposes various activities devoted to the developing of the technology of dielectric heating for safe applications, a First National Meeting held in Cetara (SA) in 2002, followed by a Second one in Ancona in 2004.

The main purpose of the Third National Meeting was to improve the basic understanding on the applicability of the microwave technology to the environment and to the chemical syntheses under extreme conditions, including ultrasounds irradiation. The multidisciplinary approach encompassed related work in the areas of organic as well as inorganic chemistry, and in technological applications. Approximately 30 contributes were presented orally, including two invited talks.

Many people have contributed to the success of this Meeting. First of all, we would like to acknowledge the advice and support of the Advisory Board and of the Organizing Committee. Thanks are due to Dott. E. Di Giampaolo, F. Bardati and P. Tognolatti for kindly providing us the figure reported in the cover.

It would be our great pleasure if the proceeding of MISA 2006, refereed by the Advisory Board, could be helpful for future developments in this field.

November 2006   *Eugenio Caponetti*

                                                         Chairman of the Organizing
                                                         Committee of MISA 2006

Microonde nell'Ingegneria e nelle Scienze Applicate – MISA 2006

The Third National Meeting on "Microonde nell'Ingegneria e nelle Scienze Applicate – MISA 2006" was organized by the Italian Group of "Microonde Applicate ai Materiali ed ai Processi" (GIMAMP). It was supported by: SCI - Società Chimica Italiana - Divisione di Chimica dell'Ambiente e dei Beni Culturali, AMPERE - Association for Microwave Power in Europe for Research and Education, AIMAT - Associazione Italiana di Ingegneria dei Materiali, GRICU - Gruppo Ricercatori di Ingegneria Chimica dell'Università and INCA - Consorzio Interuniversitario Nazionale "La Chimica per l'Ambiente" and Istituto Regionale della Vite e del Vino.

Advisory Board

Domenico Acierno, *Università degli Studi di Napoli "Federico II"*
Alberto Bargagna, *Università degli Studi di Genova*
Eugenio Caponetti, *Università degli Studi di Palermo*
Attilio Citterio, *Politecnico di Milano*
Anna Corradi, *Università degli Studi di Modena e Reggio Emilia*
Giuseppe Conciauro, *Università degli Studi di Pavia*

Giancarlo Cravotto, *Università degli Studi di Torino*
Roberto De Leo, *Università degli Studi di Ancona*
Luca Guasina, *R&D Barilla*
Carlo Mazzocchia, *Politecnico di Milano*
Mauro Panunzio, *ISOF-CNR Bologna*
Gian Carlo Pellacani, *Università degli Studi di Modena e Reggio Emilia*
Innocenzo M. Pinto, *Università degli Studi del Sannio*

Organizing Committee

Eugenio Caponetti, *Università degli Studi di Palermo*
Delia Chillura Martino, *Università degli Studi di Palermo*
Cristina Leonelli, *Università degli Studi di Modena e Reggio Emilia*

Franco Moglie, *Università Politecnica delle Marche*
Serena Riela, *Università degli Studi di Palermo*
Maria Luisa Saladino, *Università degli Studi di Palermo*

INTRODUCTION

Microwave is a term loosely applied to those radio frequency wavelengths which are sufficiently short to exhibit some of the properties of light. Commonly used for frequencies from about 300 MHz to 30 GHz, i.e. a type of electromagnetic radiation with wavelengths between those of infrared radiation and radio waves capable of heating dielectric materials.

Microwave power irradiation of dielectrics is nowadays well recognized and extensively used as an exceptionally efficient and versatile heating technique. Besides this, it revealed since the early 1980s an unexpected, and still far from being elucidated, capacity of causing reaction and yield enhancements (and even reaction pathway modifications) in a great variety of chemical processes, such as polymerization, organic synthesis, ceramics processing, and plasma chemistry.

In addition an area of equal importance is represented by new studies in microwave antennas, wave propagation simulation and microwave integrated circuits as well as microwave characterization/measurements of materials.

Nevertheless a multidisciplinary approach is strongly required for applicator design and development as well as the evaluation of all the environmental aspect of this technology which can really be quoted as benign energy technology. All these aspects has been presented in the four section of the book with the competence of yearly experience colleagues either from the academy as well as from the industrial world make it a milestone for the state of the art in microwave technology in Italy.

November 2006   *Cristina Leonelli*

                                                            Secretary GIMAMP
                                                            Member of the Board of
                                                            Directors of AMPERE

CONTENTS

Section 4. Modeling and applicator design

THE CONTRIBUTION OF MICROWAVES TO THE ENVIRONMENTAL PROTECTION

L. Campanella, M. Pintore

Dipartimento di Chimica – Università degli Studi "La Sapienza"

P.le A. Moro 5, Roma

Introduction

The action of microwaves on a system can be interpreted as a combination of a thermal and a not thermal contribution. In the conceipt of the kinetic advantages, bound to the latter contribution the polarity increase due to a great interaction among all its components following the transition from the fundamental state to the excited one because of the incident radiation, the influence on the Arrhenius's constant, therefore on the activation energy and the higher heating efficiency must be considered.

Interaction with biological systems

The most common knowledge of the microwaves was overall bound till few years ago to their antimicrobial and antialgal activity; for instance they exerted a detoxifying action to free some foods from aflatoxins G1 and B1.

Today the knowledges are more extended: so the microwaves exert an enzymatic inhibition on different protein such as invertase, myrosinase, interferon ruled enzymes, amylase, ATPase, polyphenoloxidase, dehydrogenase, catalase and consequently they can influence the process bound to the brownish of the foods and related to the soil fertility. Beyond the enzymatic activity they are able to inhibit also the enzymatic kinetics depending on water activity; they allow too a rapid stabilisation of the tissues used for analytical aims, furtherly they affect the release of drugs and chemical substances in specific zones of the body and favour the production of radicals without lowering the superoxidismutase activity; they behave as larvicides, affect the antibiotic activity and act as stabilizers of soils (for instance in the transport from the sampling site to the laboratory).

Among the noxious effects of the microwaves we have to remember that they affect the stability of aminoacids, expecially of alanine, lysine, tirosine, arginine, methionine, and they have mutagenic activity, sensitized by thyroid hormons.

Table I - Respirometric ihibition of yeast cells following their exposure to microwaves

TIME (MIN)	% RESPIROMETRIC INHIBITION
0	0
1	0
2	4
5	8
8	12
10	19
12	20
15	13
18	25
20	28

Applications: advantages and dangers

Today the uses of the microwaves are multiple: they are used to sterilize, even if they can produce losses of proteins and vitamins, up to the full destruction within times of about 3 hrs. As an example, in table 2 the effect of the microwaves on beta-carotene through a test performed by monitoring the toxicity of its transformations with the passage of time is shown; the increase of toxicity corresponds to a decrease of the beta-carotene concentration.

The microwaves find also application in medical fields as hyperthermy, neurology, internal medicine, hematology, endocrinology and the defrozing of intravenous infusions, even if it cannot be forgotten that microwaves produce radicals, very noxious species for human organisms, so that the therapeutical use of microwaves should be coupled to a radical scavenging treatment

Table II - Effect of microwaves on beta-carotene

EXPOSURE TIME (MIN)	TOXICITY DEGREE (ARBITRARY UNITS)
10	0
20	1
20	2
40	4
50	8
60	10
90	12

.
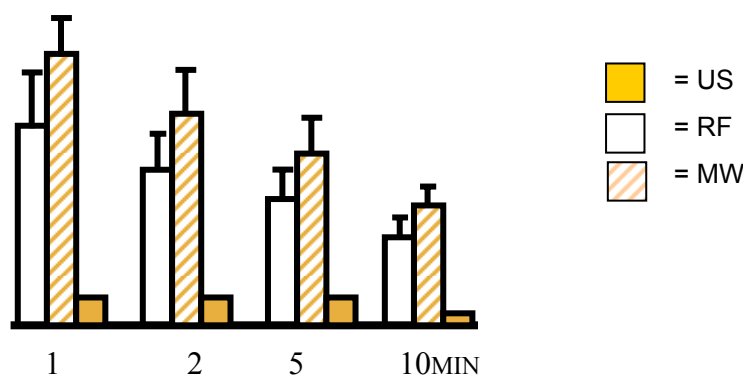
Figure 1 - Comparison of the production rate of radicals by microwaves, radiofrequency and ultrasounds

Table III - Comparison of SOD inhibition due to MW and RF

Power (Watt)	t = 1 min		t = 5min	
	RF	MW	RF	MW
90	10	12	28	35
180	12	15	32	38
360	20	35	45	86

In Figure 1 the production along the time of radicals on exposure of a physiological solution to microwaves, radiofrequency and ultrasounds is shown: it can be observed that the radical concentration increases with the time for all the three considered sources and that microwaves are those ones able to produce the highest radicalic concentration.

The production of radicals from MW, RF, can be also shown by the inhibition by them produced of oxygenasic activity of human kidney toward benzene and of superoxidis-mutasic activity. In this case it can be observed too as the difference between the two energies increases with their power and with the exposure time at 360 w and t = 5 min the contribution of microwaves (MW) to the enzymatic inhibition is about two times that one of radiofrequency (RF) (table III).

The use of microwaves in the chemical processes is has the great advantage of decreasing the reaction times expecially for some synthesis and to save meaning amounts of energy.

The adoption of microwaves in place of heating traditional techniques can be of interest for chemical analysis relatively to the mineralisation step for any kind of matrix expecially foods, biological samples, soils and plants ensuring in any case a gain in terms of needed time and energy: this saving is due to the fact that heating by microwaves is volumetric, so allowing also the conservation of fibrous components. Really in the case of the traditional heating energy is transferred to the matter by convection, conduction and irradiation of the heat from the irradiating surface toward inside the matter to be heated. On using microwaves rather than heat electromagnetic energy is transferred.

Differently the energy associated to microwaves is transferred directly to matter by molecular interactions with electromagnetic field: thence a direct heating characterised by higher selectivity, homogenety and possibility to operate in situ differently from traditional heating follow.

Analytical and environmental applications

The most common applications in the analytical chemical field needing heat sources in the research and in the quality control are

- acid digestion preliminarly to AAS, ICP, or other methods;
- extraction by organic solvents for chromatographic analysis;
- humidity and fats determination, expecially in foods;
- determination of ashes;
- organic and inorganic synthesis;
- hydrolysis of proteins and peptides for the analysis of the formed aminoacids;
- dissolution of polymers ion in order to determine their molecular weight;
- acid digestion of polymeric components for the determination of the fibrous contents
- fixation of biological samples for their microscopy analysis;
- digestion to determine COD

The use of microwaves can find applications in process of environmental interest such as the removal of NO_x and SO_2. Really the removal of NO_x occurring by direct way is based one the adsorption of these gases on carbon filters and following heating by microwaves: so molecular nitrogen and carbon dioxide are evolved into the atmosphere, while carbon is recycled. The removal of SO_2 occurring: by indirect way consists in a reductium of this compound by carbon, in an acid washing able to produce volatile sulphydryl compounds, in a following evaporation of these compounds supported by microwaves and finally in an alkaline washing.

The microwaves also exert a sensitizing activity to the electroanalytical methods.

For instance the determination of the heavy metals in environmental matrixes can be performed by electrochemical way. As an example Figure 2 shows the cathodic branch of eight different cyclic voltammograms representing the hehaviour of solutions containing cadmium. The measurements were performed with glassy carbon as working electrode by 5 scans between –0.2 and –0.8 V, a satured calomel electrode and counter reference electrode in presence and in absence of microwaves.

I = 0, 14, 18, 22, 26, 30, 34, 34, 38 µA.
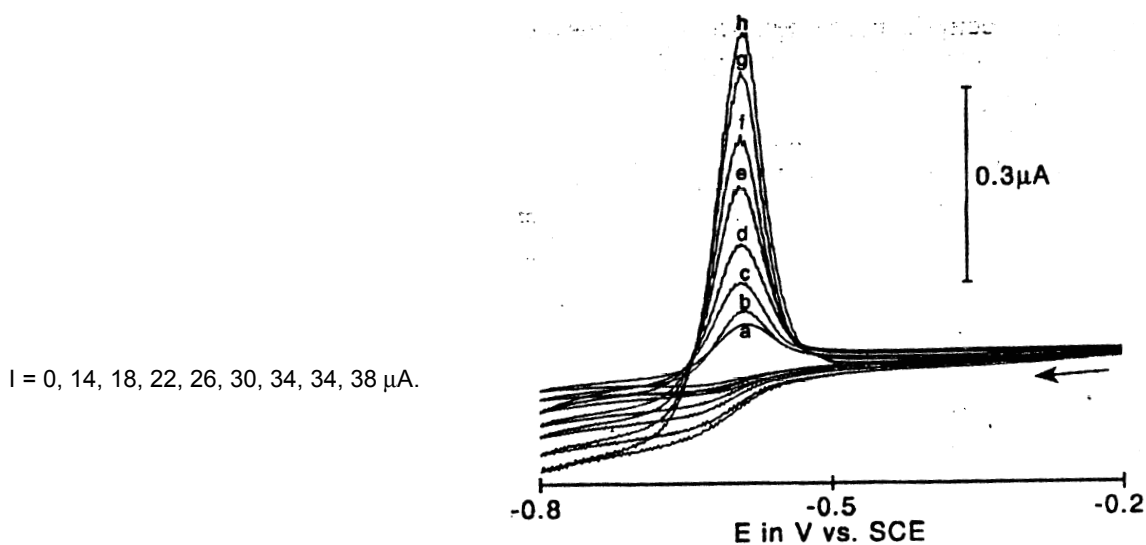
Figure 2 - Cathodic branches of eight different cyclic voltammograms of Cd solutions under different microwave irradiation intensity

Management of wastes and photodegradations

The management of toxic wastes from hospitals occurs by a disposing process foreseeing further treatments due to their possible dangerous activity:

- under vacuum;
- pulsed ozone;
- water vapour;
- microwaves.

Starting from the classification of pollutants based on their dangerous properties (table IV) and considering that their degradability depends on the structure (table V), recent studies have evidenced phenomena for which the use of microwaves coupled to UV irradiation is able to catalyse many kinds of degradative reactions, i.c. it happens that the contribution of microwaves can result into better efficiency if combined with UV light (photodegradation).

During these transformations energy is supplied to the matter (generally organic matter) that suffers degradation, eventually down to mineralisation with production of CO_2, H_2O, mineral acids. Semiconductor oxides, among which TiO2 is the most efficient, activated by UV radiation of optimized wavelength, catalyse the process. Depending on the nature of the semiconductor the activation of the full process can occur by direct and undirect way, in the latter one by carrier substances.

In the photocatalytic cell an acidification occurs due to the produced CO_2, so that from compound containing N, S, Cl atoms the corresponding oxides, acids and anhydrides are formed.

Through rH_2 red-ox potential is related to pH: so due to the occurred pH variation also red-ox potential changes with the following varying red-ox reactions.

17

Table IV - Classification of pollutants basing on their dangerous activity (Increasing from I to III)

Group	Definition	Pollutants
I	Easily degraded and abated, even for their toxicity pollutants	pH, T, colour, odour, coarse solids, sedimented and suspended solids, BOD, COD, sulphides, sulphites, sulphates, chloudes, fluorides, NH_3, fats animal and vegeral oils
II	Toxic Pollutants not possibly accumulated in the aquifer ecosystems	Aluminium, barium, boron, chromium III, iron, manganese, nichel, copper, tin, zinc, cyanide, chlorine, phosphates, mineral oils, aldheydes, organic solvents, surfactories
III	Highly toxic pollutants accumulated in the aquifer ecosystems	Arsenic, cadmium, chromium VI, mercury, lead, selenium, phenols, pesticides

Table V - Degradability of some organic compounds basing on their structure

Kind of compounds	High degradability	Low degradability
Hydrocarbons	Superior alkanes (~12) paraffins, BAH_S	Inferior alkanes, high molecular weight alkanes PAH_s
Substituents in the aromatic ring	-OH -COOH $-NH_2$ $-OCH_3$	-F -Cl $-NO_2$ $-SO_3H$
Aliphatic chlorides	-Cl beyond six carbon atoms from the terminal one	-Cl less than six carbon atoms from the terminal one

According to Lewis's theory acids and bases are characterised by their respective property to behave as acceptor or donor of electrons so basing on the theory even a complexation reaction can be considered as an acid/base one: for instance the complexation reactions in soil between humic acid (donors) and metals (acceptors) can be considered an acid/base reaction and as such influenced by MW able to produce radicals from H^+ and OH^- of water and so to determine pH variation on photodegradation.

The promotion and the efficiency of the photodegradative process depend on O_2 concentration in the solution and on its oxidant activity that is function of pH, on its turn depending on the amount of produced CO_2:

$$O_2 \quad + \quad 4H^+ \quad + \quad 4e^- \quad \longrightarrow \quad 2H_2O$$

MW are able to enhance the photodegradative eventually hardly proceeding reactions.

To lower the pollution level of superficial waters several techniques were applied in the past, to which recently some other ones were codevelopped, in order to increase the efficiency of the removal of pollutants from aquifer systems.

Particularly AOP_s (advanced oxidative processes) resulted to be advantageous in comparison with other chemical and physical methods for different reasons:

- they are able to bring to the full mineralisation of the pollutant
- they are characterised by high capacity even in presence of recalcitrant compounds
- they are simple and easy to be handled
- they are substantially cheap.

AOP_s can be classified into homogeneous and heterogeneous phase ones.

Among the former ones Fenton and UV/H_2O_2 treatments fall. UV/H_2O_2 treatment is not well efficient due to the fact that it is unable to degrade photostable compounds: it can be assisted by soluble Fe (II) salts added to an acid (pH < 3) solution of H_2O_2, but as negative point residual ferrous ions are produced and must be disposed.

On the contrary heterogeneous catalysis is more efficient and offers the advantage of recovering the solid catalyst.

The whole process of heterogeneous photocatalysis can be articled into five steps:

- transfer of the reagent into the fluid phase on the catalyst's surface;
- adsorption of the reagent on the catalyst;
- reaction in the adsorbed phase between catalyst and reagent;
- desorption of the reaction product (or products);
- removal of these products from the catalyst's surface.

On irradiating semiconductor catalyst with an UV light of opportune wavelength the promotion of one or more electrons from the valence to the conductivity band occurs. On depending on the nature of the semiconductor the ideal wavelength must be chosen as it has to correspond as more exactly as possible to the energy gap to be gained by the electrons to be promoted.

Table VI - Energy gaps between valance and conductivity band and corresponding optimal λ for some common semiconductor catalysts

COMPOUND	ENERGY GAP (EV)	Λ (NM)	COMPOUND	ENERGY GAP (EV)	Λ (NM)
ZRO2	5.0	248	CDS	2.4	516
TA2O5	4.0	310	A-FE2O3	2.34	530
SNO2	3.5	354	ZNTE	2.3	539
KTAO3	3.5	354	PBFE12O19	2.3	539
SRTIO3	3.4	365	GAP	2.3	539
NBO5	3.4	365	CDFE2O4	2.3	539
ZNO	3.35	370	CDO	2.2	563
BATIO3	3.3	376	HG2NB2O7	1.8	689
TIO2	3.0-3.3	376-413	HG2TA2O7	1.8	689
SIO	3.0	376	CUO	1.7	729
V2O5	2.8	443	PBO2	1.7	729
BI2O3	2.8	443	CDTE	1.4	885
FETI3	2.8	443	GAAS	1.4	885
PBO	2.76	449	INP	1.3	954
WO3	2.7	459	SI	1.1	1127

Simultaneously to the promotion of the electrons from valence to conductivity band electron holes are produced (h^+) in the valence, behaving as positive charge. The electron/hole couples interact with the adsorbed species on the catalyst's surface according to the corresponding red-ox potential values; the electrons can reduce the oxidising species such as oxygen adsorbed on catalyst (i.e. TiO_2) and at the same time the holes can oxidise the reducing species such as water (Figure 3).

The full result is the production of hydrogen and expecially of hydroxyde and superoxide radicals able to oxidase the compounds to be photodegraded adsorbed on the catalyst. What does it occurs to these processes when microwave irradiation occurs? As said the interaction of microwaves with the materials results in a peculiar and rapid heating due to the tendence to polarization and rotation of the molecular dipoles under microwaves in order to be oriented in this field. The resistance to rotation expecially in the case of large molecular size is the reason of the energy dissipation as heat. It is clear from these concepts that the main property responsable for the interaction of a compound with microwaves is the polarizability of its molecular dipoles. So all the compounds containing such dipoles, even of least energy, are sensitive to microwaves, as all the polar dielectrics, the semiconductors, the magnetic and ferromagentic materials.
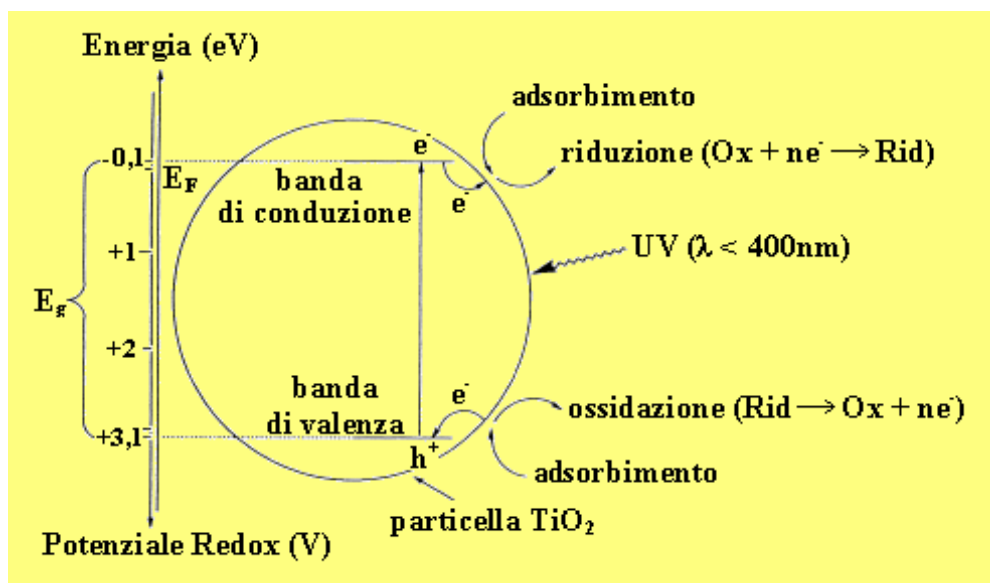
Figure 3 - Scheme of the processes occurring on the catalyst's surface
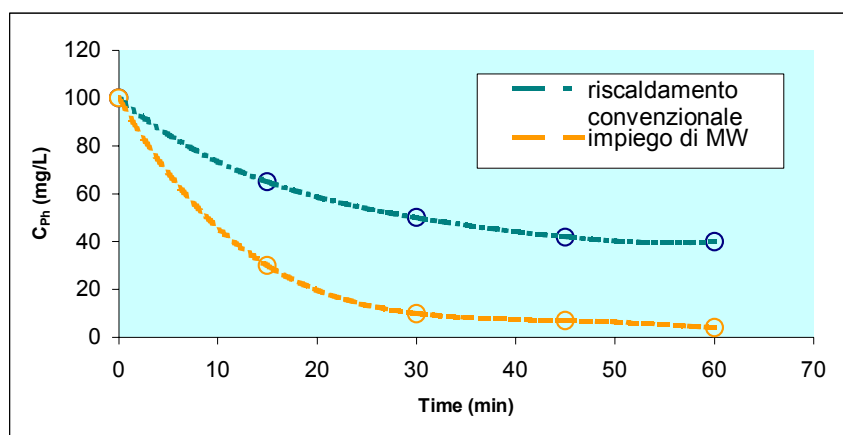
Figure 4 - Effect of microwaves on the degradation of phenol

The heating degree depends on the molecular structure: so in the case of little size molecules no deforming effects are observed coupled to heating, but for larger molecules a structural tension and a following decrease of stabilization occur. This is the case of, for instance, pharmaceutical principles containing polar groups such as - COOH, - OH, - $NHSO_2$. Some examples can help the reader's comprehension Phenol from petrolchemical and coal treatment plants is toxic compound with a limit concentration to protect human health less than 50 ppb. Its toxicity is such that the ingestion of 1 g brings to certain death due to the damages suffered by the nervous central system. Furtherly phenol is responsible for the formation of chlorophenols in water added with chlorine to guarantee its solubrity. Luckily phenol is easily degraded as its COD value is 2.4 mg O_2/mg.

In Figure 4 the behaviour to degradation of phenol in presence and in absence of microwaves is represented.

The treatment of toxic wastes by microwaves assisted degradations is applied to remediation of soil polluted by hydrocarbons, expecially benzene and toluene (for which mineralisation is requested, as the only partial degradation products are often more toxic than the original ones), but also phenanthrene, pentachlorophenol, dioxin and anthraquinone. In order to avoid such dangerous intermediate degradation compounds it is opportune to add carbon to soils, expecially in the case of clayey (more than sandy) soils.

In table VII we report the comparison of the dissolved organic carbon value (DOC) and of the optical absorption at 254 nm of an aqueous solution of humic acids respectively treated for 30 and 60 with UV, MW and UV + MW compared with those ones of an untreated one. From table VII it clearly appears that the treatment with MW brings to a more complete degradation than with only UV; but it is the combination of the two to give the best results.

Table VII - Comparison of DOC values and of optical absorption values at 254 nm of an aqueous solution of humic acid untreated or treated for 30 and 60 min with UV, MW and UV+MW

	AFTER 30 MIN		AFTER 60 MIN	
	DOC (PPM OF C)	UV$_{254}$ (ABS. NORM)	DOC (PPM OF C)	UV$_{254}$ (ABS. NORM)
WITHOUT TREATMENTS	45	1.00	45	1.00
ONLY UV	37	0.90	24	0.41
ONLY MW	43	0.95	34	0.72
ARRANGED MW - UV	28	0.78	11	0.18
DEGRADATION OF HUMIC ACIDS IN AQUEOUS SOLUTION (UV AND MW)				
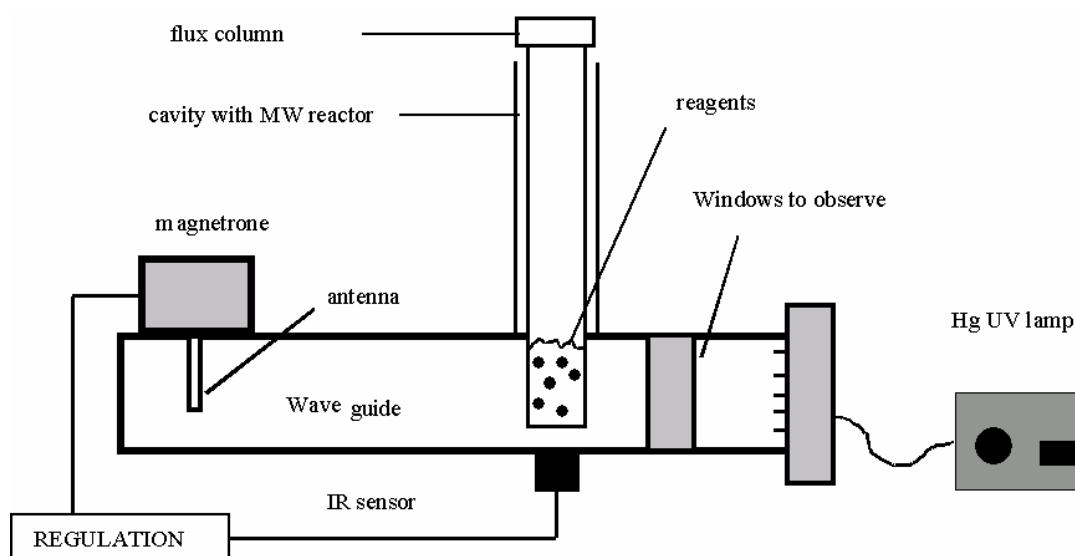
Figure 5 - Scheme of the system for degradation performed by MW assisted UV photodegradation

Our contribution MW + UV: applications to removal of disposed pharmaceuticals

In our lab a research was performed to investigate about the effect of MW assistance heterogeneous photocatalytic degradation of some recalcitrant pollutants.

A great part of the work consisted in the design of an experimental system, as simple and as cheap as possible able to combine the action of ultraviolet rays with that one of microwaves in a way as well integrated as possible. Fundamentally the instrument is formed by two cells, connected each other by tubular ways, on each one of which an opportune wavelength radiation hits; one of the two cells is inserted in a microwave mineralizer. A peristaltic pump allows the solution filling the circuit to pass from one cell to the other. The light sources we used were a germicide lamp characterised by an emission maximum at 254 nm and an over voltaged halogenic dichraic lamps able to simulate the whole solar spectrum. In Figure 7 the photos of the two lamps and the relative emission spectra are presented.
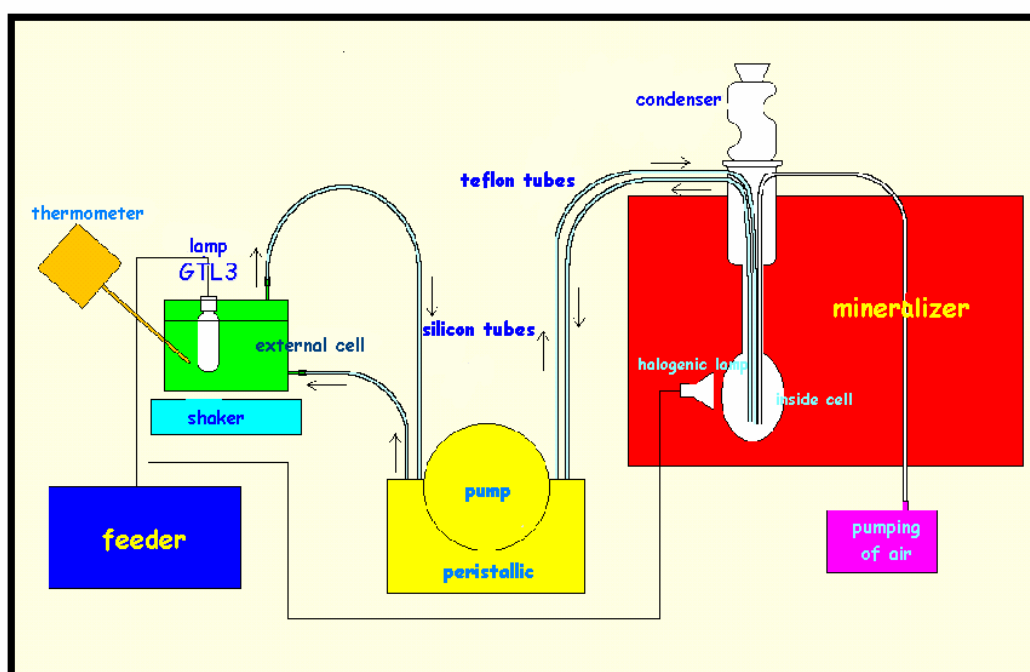
Figure 6 - Scheme of our experimental degrading and cleaning system
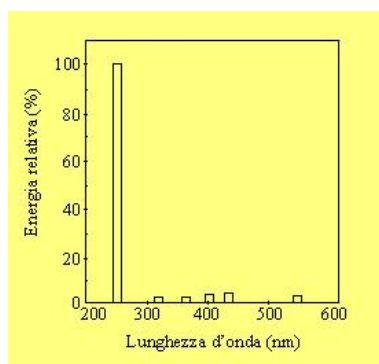
Figure 7a - Germicide lamp GTL3 (3W) and its emission spectrum
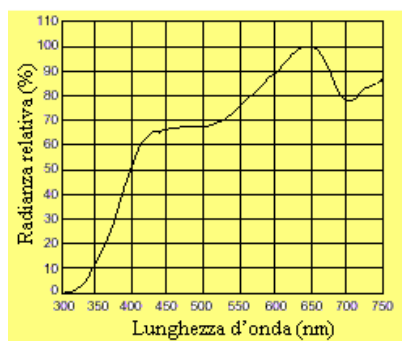
Figure 7b - Halogenic dichroic lamp MR11 (20 W) and its emission spectrum

**Table VIII - Results of photocatalysis performed on the same solution
with various lamps**

LAMP	A_{MAX} INITIAL	A_{MAX} AFTER 1 H OF PHOTOCATALYSIS	A_{MAX} AFTER 4 H OF PHOTOCATALYSIS	% EFFICIENCY AFTER 1 H	% EFFICIENCY AFTER 4 H
FLUORIMPORT JC- TYPE, G4	0.884	0.861	0.821	2.6	7.1
OSRAM WFL	0.866	0.841	0.784	2.9	9.5
GTL$_3$	0.900	0.854	0.773	5.1	14.1
DICROICA MR$_{11}$	0.881	0.821	0.726	6.8	17.6

In order to evaluate the influence of the semiconductor catalyst two different kinds of TiO$_2$ were tested respectively furnished by Aldrich and Degussa, also performing an electronic microscope scan (SEM photos in Figure 8).

While in the first case (Figure 8A) a structure characterised by particles all of almost the same size, is present in the second one the dimension of the particles ranged within a large interval from 60 to 170 nm.

The optimal condition found to get the best efficiency of photodegradation were applied to the degradation of a new class of pollutants, the pharmaceutical principles. Unfortunately this class, practically absent in the past in the environmental matrices, now meaningly contributes to pollution due to the exceptionally high increase rate of the use – we must better speak about abuse – of these substances. For this increase:

CAS N° 13463-67-7
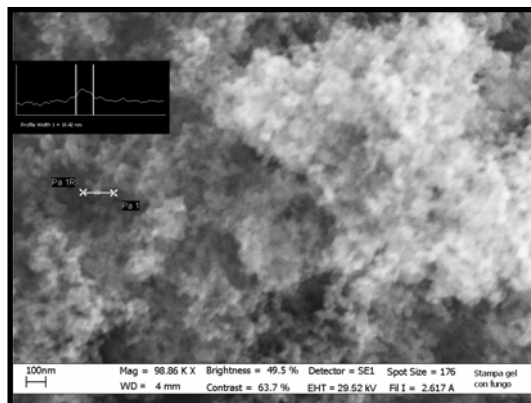
Figure 8a - TiO$_2$ Degussa P25 AG Mean particle diameter 20 nm specific area 50 m^2/g

CAS N° 1317-70-0
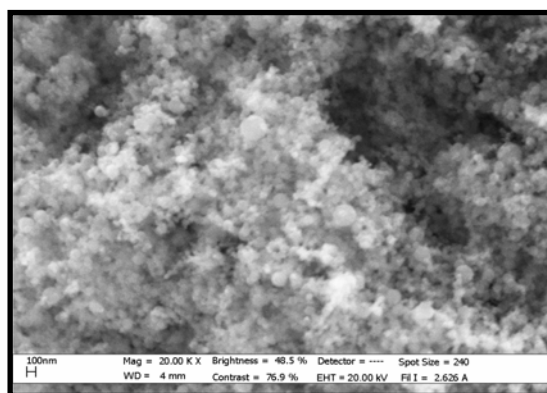
Figure 8b - TiO$_2$ Aldrich Mean particle diameter 100 nm specific area 6 m^2/g

- the increase of the mean human lifetime to which an increasing request of drugs is corresponding
- the progress of the pharmaceutical research able to produce drug always more addressed to the different pathologies
- unproper disposal of extincted drugs
- excretion of active principles
- the increase request for wellfare and well conditions so that drugs are not only assumed in presence of a pathology
- the increase of pathologies and diseases related to the life style and habits of western countries (pollution, stress, bad alimentary education can bring to pathological states unknown few years ago
- the abuse of drugs not for only therapeutical reasons due to the tendency to buy more pakages of needed drugs (resulting in a following problem of desposal) than necessary, the increasing rate of market occupied by selfprescriptions, easy to be obtained, the claims continuously more present in the media and journals suggesting specific drugs for some coummon pathologies such as allergy, colds, local infections expecially of oral cavity

are accounted.

The increase of the pharmacological therapy is one of the main reason accounted for the water pollution.

The traditional plants of treatment of waters are not always able to remove and degrade all the polluting compounds present in water due to the high recalcitrancy of some of them. To the aim of recover this negative situation EU has managed different research projects aiming at the full degradation of the compounds not removed in the water treatment plants. On 27th june 2003 in Göteborg (Sweden) three projects were launched devoted to the monitoring and removal of drugs from surface water and from potable water (ERAMVIS, REMPHARMAWATER, POSEIDON) in order to lower the environmental impact of the above denounced abuses.

The described photocatalytic degradation was performed on six of the pharmaceutical principles reported in table IX. Their choice was suggested by the statistical data of EU about the most consumed drugs (excluding antibiotics), by their high persistence in the environment and by their relatively high concentrations observed in surface waters, expecially in Europe.

In table X the increase of the photodegradation efficiency due to the additive action of MW to the systems is shown.

In table XI the maximum rate values of photodegradation in presence of the microwaves are reported.

Table IX - Pharmaceutical principles tested in photodegradation experiments

CLOFIBRIC ACID

ANTILIPIDEMICO (NOT IN COMMERCE)

2- (4-CLOROFENOSSI) -2 - METIL- PROPANOICO ACID
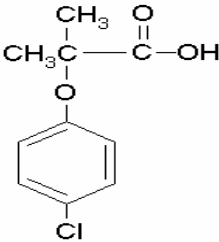
CARBAMAZEPINE

ANTIEPILEPTIC (TEGRETOL) 5H-DIBENZ [B, F] AZEPINA-5-CARBOSSIAMMIDE; 5-CARBAMOIL-5H-DIBENZ [B, F] AZEPINA
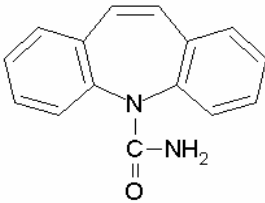
DICLOFENAC

ANTIINFLAMMATORY

(DEALGIC,   DICLOFAN,   FORGENAC,   NOVAPIRINA,
VOLTAREN)

(2- [(2,6-DICLOROFENIL) THEY LOVE] BENZENACETICO
ACID) KNOWS THEM SODICO
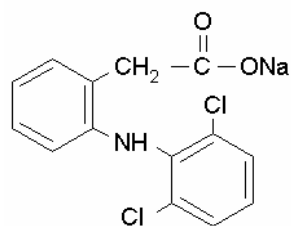
OFLOXACINE

ANTIBACTERIAL (EXOCIN, OFLOCIN)

(±) 9-FLUORINE (4-METIL-1-PIPERAZINIL) - 7-BONE-7H-
PIRIDOL [1,2,3-DE] - CARBOSSILICO 1,4-BENZOSSAZINA-
6-ACID
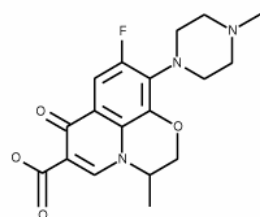
PROPRANOLOL

B-BLOCKER; ANTIHYPERTENSIVE (INDERAL, EUPROVASIN)

1- [(1-METILETIL) LOVES] - 3- (1-NAFTALENILOSSI) - 2-
PROPANOLO
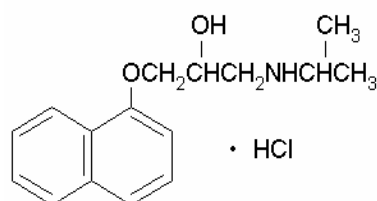
SULPHAMETOXAZOL

ANTIMICROBICO (BACTRIM, EUSAPRIM, GEYMONAT)

N1- (5-METIL-3-ISOSSAZOLIL) SOLFANILAMIDE
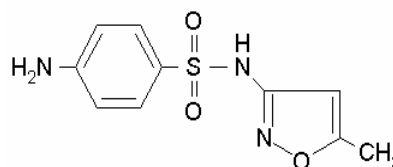
**Table X - % increase of the photodegradation degree following the addition of MW
in the degrading system**

PHARMACEUTICAL PRINCIPLE	% INCREASE OF THE PHOTODEGRADATIVE EFFICIENCY DUE TO ASSISTANCE OF MICROWAVE
CARBAMAZEPINE	196.3
CLOFIBRIC ACID	36.5
SULFAMETOXAZOLE	18.8
OFLOXACINE	11.8
DICLOFENAC	8.1
PROPANOLOL	10.2

Table XI - Highest photodegradation efficiency values obtained by combining UV and MW actions

PRINCIPLE	MAXIMUM VALUES OF PHOTODEGRADATION DEGREE
METHYLTESTOSTERONE	70 ± 5
TOLMETIN	48 ± 3
BACAMPICILLINE	88 ± 5
SULFAMETOXAZOLE	68 ± 3
CLOFIBRIC ACID	85 ± 5
DICLOFENAC SODIUM SALT	72 ± 4
OFLOXACINE	95 ± 5
CARBAMAZEPINE	70 ± 5
PROPANOLOL	75 ± 3

Also the surfactants are dangerous pollutants due to the excess amounts of soaps dispersed into the environment resulting in the entrophication process. The surface tension due to the degradation increases with the passage of the time of exposure to the photodegrading irradiation so representing a marker index of the proceeding photocatalytic degradation.

An example, in Figure 9 the curves representing the variations of the surface tension during the heterogeneous photodegradation of a surfactant assisted or not by MW and the corresponding production of CO_2 are reported; the very good agreement deserves to be pointed out.
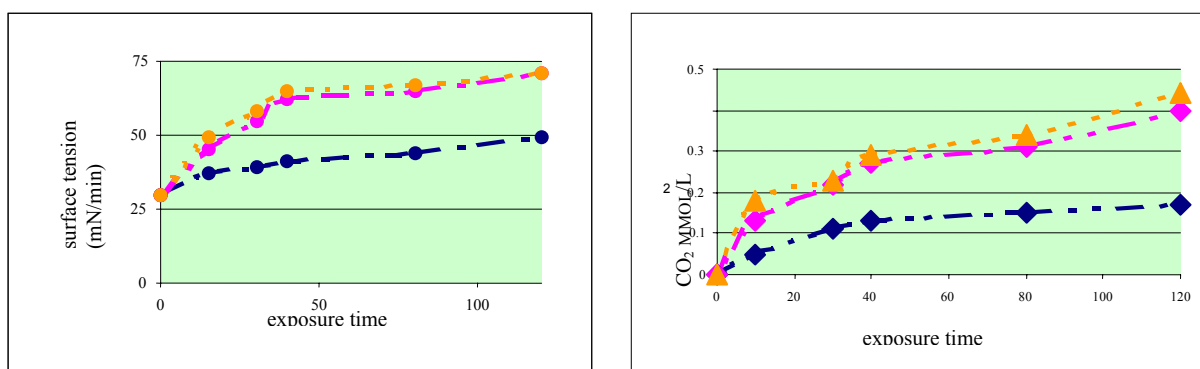
Figure 9 - Curves relative to the variation along the time of the surface tension and CO_2 production on the heterogeneous photocatalytic degradation of a surfactant

In the further developments of this research we modified the catalyst on memebranising TiO_2 in PVC support and adding a conducting polymer (polyaniline) to the membrane according to the composition thickness area. In table 13 we show % photodegradation degree of s pesticide (paraoxon) in solution a photodegraded according three different processes.

Table XII - Composition of the assembled mixed catalyst

POLYANILINE% (W/W)	TiO2 % (W/W)	PVC % (W/W)	SURFACE AREA (CM^2)	THICKNESS (μM)
11.0	18	71	9.8	100

Table XIII - % of photodegradation degree of a paraoxon solution photodegraded by three different ways

TIME (MIN)	% PHOTODEGRADATION		
	(a)	(b)	(c)
10	46	56	34
20	77	85	47
30	78	89	50
40	80	90	56

a = UV+MW +TiO$_2$, b = UV+ MW + mixed Catalyst , c = UV + mixed Catalyst.

From the results reported in table XIII it can be concluded that the use of the catalyst added with the conducting polymers allows getting a higher efficiency of the photo-degradation by combined catalysis UV + MW.

A further improvement of the efficiency was obtained with a pretreatment of the sample in an ultrasound bath in order to remove the present impurities and to obtain an homogenisation of the solution to be degraded which can favour the contact between the catalyst's surface and the target molecule.

MICROWAVES AND POWER ULTRASOUND: A NEW SYNERGY IN GREEN ORGANIC SYNTHESIS

Giancarlo Cravotto

Dipartimento di Scienza e Tecnologia del Farmaco,

Università di Torino - Via P. Giuria 9, 10125 Torino, Italy

giancarlo.cravotto@unito.it

Abstract

Although the vast majority of organic chemists still cling to conductive heating as a means to promote reactions, major advances have recently been made in this connection. Both microwave (MW) and power ultrasound (US) are being increasingly exploited in organic synthesis, and their combined use is one of the most promising innovations. In our work we focus on the advantages arising from the use of MW and US (alone or combined), often in association with unconventional reaction media such as room-temperature ionic liquids (RTILs) or water. The synergies arising from these combinations will certainly go a long way to meet the increasing demand for environmentally benign chemical methods.

1.   Introduction

In the snag-ridden approach to the goal of a sustainable economy, the ''greening'' of chemical processes has become a major issue for academia and industry. US and MW have recently come to play an irreplaceable role in the development of environment-friendly chemical processes. A long way from pioneering approaches, when domestic MW ovens and US cleaning baths were poorly standardized tools, these techniques now have their place in reproducible, high-yield synthetic protocols. In the last few years the systematic use of MW [1] and US [2] has determined an epoch-making change in organic synthesis, as these techniques can dramatically speed up most synthetic reactions and activate poorly reactive substrates. Moreover, MW- and US-promoted reactions can be successfully carried out in aqueous media or RTIL; this approach has revealed a host of interesting synergic effects and resulted in marked gains from the standpoint of green chemistry.

Sonochemical effects are mainly due to acoustic cavitation or *cold boiling*, i.e. to the formation, growth and implosive collapse of gaseous bubbles generated by acoustic waves [2]. Their implosion results in the formation of so-called *hot spots*, sub-microscopic domains of extremely high energy that present a unique environment to chemical reactions [2]. The interaction of acoustic waves with a chemical system does not merely achieve an improved stirring or surface cleaning, as it involves complex physico-chemical phenomena which are currently a matter of advancing research.

As is well known, the thermal effect exerted by MW irradiation on the reaction mixture is due to an oscillating orientation change of molecular dipoles under the alternating electromagnetic field; more specific effects have been accounted for by the *hot spots* theory [1].

In fact even if bulk heating is prevented by strict thermostatic control, reactions are nevertheless accelerated, especially when polar mechanisms are involved, with development of charges and late transition states.

Finding alternative reaction media to replace volatile, flammable and often toxic solvents commonly used in organic syntheses is an important goal towards the development of green chemistry [3]. From both the environmental and the economic point of view it is highly desirable to resort to aqueous media [4] or room-temperature ionic liquids (RTILs) [5]. Although it is well known that the hydrophobic effect may accelerates several reactions [6], water has been avoided as a medium for organic reactions because it dissolved reactants very poorly, or it was incompatible with certain intermediates, or ensuing hydrolysis competed excessively with the desired reaction. Most of these limitations have now been circumvented by working under high-intensity US [7]. RTILs combine to a remarkable extent the properties of molecular solvents and those of molten salts. Being non-flammable and having barely measurable vapour pressures, they can be efficiently recycled and may provide the answer to the problems caused by volatile organic compounds (VOCs). Their high solvent power towards non polar as well as polar compounds confers on them versatility as reaction media that traditional molecular solvents could never approach [8].

MW and US also can induce reactions that would otherwise prove very laborious, enhance heterogeneous catalysis and even bring out unusual chemoselectivities, thus opening up new synthetic pathways. They can be applied in a straightforward manner to some, but certainly not all, reactions; indeed, painstaking preliminaries are often required to identify optimal conditions (Table 1) that often turn out to be quite different from the traditional ones. Recent publications report a variety of straightforward synthetic laboratory-scale procedures, carried out in parallel under MW and US [9-11]; much work is under way for their scale-up, not an easy task by any means [12-14].

Table 1 - US *vs* MW: compared uses and effects

	US	MW
Use of metals	Favorite domain	Limited use
Reaction media	Aqueous and organic solvents	MW-absorbing solvents Solvent-free
Reaction times	From minutes to hours	Very short: often a few minutes
Activation	By cavitation	Thermal effects Specific (non-thermal)
Scaling-up	Relatively easy	Possible with specific set up for each applications
Chemical effects	Acceleration Selectivity changes	Large accelerations Selectivity changes

Recent work showed that combined MW and US irradiation significantly enhanced rates and improved yields of several organic reactions such as the hydrazinolysis of esters [15], the synthesis of ethers (Williamson) [16], the Mannich [17] and the Suzuki-Miyaura reactions [18].

2.   New advances and perspectives

Our main research line, concerning synthetic applications of US and MW (alone or combined), ranges from basic investigations to the development of new reactor prototypes and new synthetic procedures. Because of technical hurdles, combined US/MW irradiation has not been systematically investigated for synthetic purposes as yet, which is reflected in the scarcity of published reports. Simultaneous US/MW irradiation was first described by *Chemat* and co-workers [19], who used a low-viscosity apolar liquid (decaline) to convey US to the outer space of a double-jacketed pyrex vessel placed in a MW oven, the reacting mixture being contained in inner space. Beside describing some synthetic applications, these authors could successfully digest at atmospheric pressure solid and liquid samples for chemical analysis and called their method ''US-assisted MW digestion''[20].

To increase the efficiency of combined US/MW irradiation we developed two different systems:

A) This employs two reaction compartments (one for each kind of irradiation) joined by short lengths of tubing to allow circulation of the reacting liquid mixture between them (Figure 1 and 2).

Figure 1 - Flow US/MW reactor (first prototype for sequential irradiation)

Figure 2 - Professional Flow US/MW reactor

B) Simultaneous irradiation with both energy sources is carried out in a single reaction cell placed inside a MW oven where the horn (made of quartz or pyrex) is directly inserted. Figure 3 and 4 illustrate the devices currently employed in our laboratory with a domestic or a professional multimode MW oven.

Figure 3 - Reactor featuring simultaneous US/MW irradiation (fused-quartz horn)

Figure 4 - Combined US/MW (pyrex horn) with cooled reaction vessel

To begin with the scaling up we developed a 5-liter flow reactor (Figure 5) that sequentially irradiates a circulating reaction mixture with two US generators working at 20 and 300 kHz, while MW irradiation takes place in a modified domestic oven.

1 – Tank
2 – Centrifugal Pump
3 – Recirculation for Mixing
4 – Cooling Coil
5 – Regulation of Inlet to US Cell
6 – US Reaction Cell
7/8 – 300 kHz / 20 KHz Probes
9 – Peristaltic Pump
10/11 – MW Oven / Reaction Coil
12 – Refrigeration Oil from Coaxial Hose
13 – Cooling Oil
14/15 – Valves that regulate the flow of cooling oil
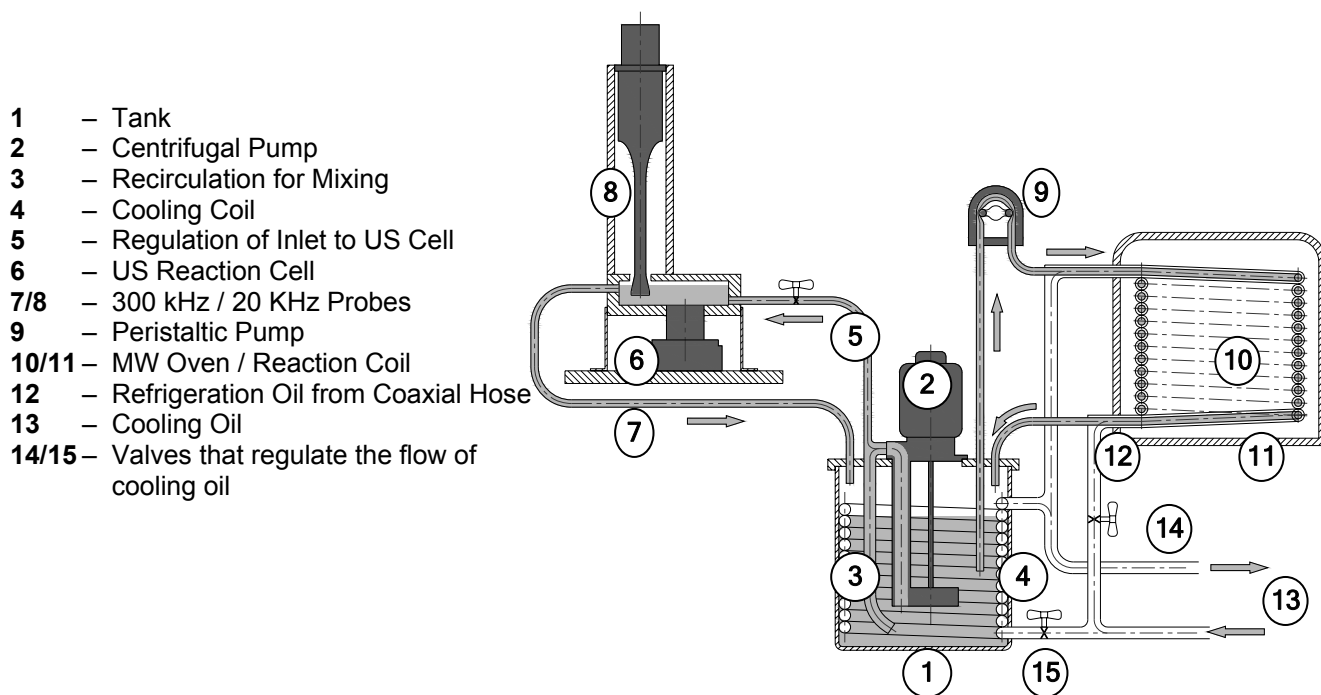
Figure 5 - Pilot Flow Reactor

With the following system, featuring a movable US transducer, we were able to compare combined US/MW irradiation carried out sequentially (*relay race mode)* with that carried out simultaneously (*tandem mode*). The system consists of:

- a 20 kHz US transducer (pyrex horn) that can be used either inside or outside the MW oven

- a Milestone MicroSYNTH MW oven (max power 1000 W)

- a peristaltic pump that circulates the reaction mixture

- two heat exchangers

- an optical fiber thermometer inside the MW reaction cell

- a standard thermometer or thermocouple outside the oven.

Samples can be easily taken during a run from the external tubing without opening the oven. Keeping MW and US power constant, the temperature can be controlled by regulating the flow rate of the reaction mixture or that of the cooling media (water or refrigerated silicon oil).

**Figure 6 - Double set up US/MW reactor: 1) Sequential Flow System or
2) Simultaneous US/MW irradiation**

3. Our recent applications

The synthesis of RTILs was efficiently promoted under US [21] and/or MW [22] irradiation (Figure 7). The two successive synthetic steps were carried out under US/MW simultaneous irradiation, both in sequence or even one-pot. Work is in progress in our laboratory to improve yields and purity of the products. MW- and US-promoted reactions have been successfully carried out in RTILs, revealing a host of interesting synergic effects and resulting in marked advantages from the standpoint of green chemistry.
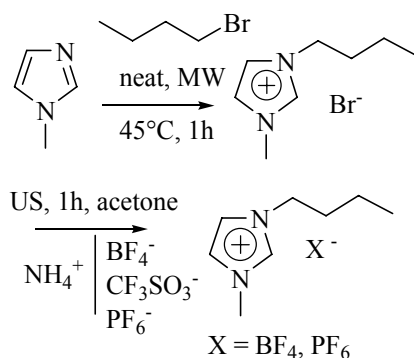
Figure 7 - Non-conventional synthesis of RTILs

We observed additive or synergic effects on several reactions that involve metal catalysts (most in heterogeneous phase) like the Suzuki homo- and cross-coupling [18], Heck and Sonogashira reactions. We disclose an efficient synthetic procedure for the chemoselective reduction of nitroarenes to azo and azoxy compounds using US and MW, alone or combined. The simultaneous irradiation promotes the reaction and increases the yield [23].

In conclusion the MW/US association has been successfully introduced in organic synthesis, although technical hurdles are still hampering a widespread use.

Acknowledgments

References

[1]   A. Loupy, Microwaves in Organic Synthesis, Wiley-VCH, 2002.

[2]   G. Cravotto, P. Cintas, *Chem. Soc. Rev.* **2006**, *35*, 117.

[3]   (a) M. Poliakoff, J. M. Fitzpatrick, T. R. Farren, P. T. Anastas, *Science* **2002**, 297, 807;

       (b) J. M. De Simone, Science, **2002**, 297, 799.

[4]   S. Ribe, P. Wipf, *Chem Comm.* **2001**, 10, 940.

[5]   J.M. Lévêque, G. Cravotto *Chimia* **2006**, *60*(6), 313.

[6]   (a) R. Breslow, D. Rideout, *J. Am. Chem. Soc.***1980**, *102*, 7816. (b) S. Salmar,

       G. Cravotto, A. Tuulmets, H. Hagu, *J. Phys. Chem., B.* **2006**, *110* (11), 5817.

[7]   G. Cravotto, G.M. Nano, G. Palmisano, S. Tagliapietra, A. Penoni, *Eur. J. Org. Chem.* **2003**, *22*, 4438.

[8]   P. Wasserscheid, T. Welton, "Ionic liquids in synthesis", Wiley-VCH, Weinheim, **2002**.

[9]   G. Cravotto, L. Boffa, M. Turello, M. Parenti, A. Barge, *Steroids* **2005**, *70*, 77.

[10]   W. Bonrath, *Ultrason. Sonochem.* **2004**, *11*, 1.

[11]   V. Roy, L. Colombeau, R. Zerrouki, P. Krausz, *Carbohydr. Res.* **2004**, *339*, 1829.

[12]   Nuchter M., Ondruschka B., Bonrath W., Gum A. *Green Chem.* **2004**, *6,* 128.

[13]   Wolkenberg SE, Shipe WD, Lindsley CW, Guare JP, Pawluczyk JM, *Curr. Opin. Drug Disc. & Devel.* **2005**, *8*, 701.

[14] T.J. Mason, D. Peters, 'Practical Sonochemistry. Power Ultrasound: Uses and Applications', Ellis Horwood, Chichester, **2002**.

[15]   Y. Peng, G. Song, *Green Chem.,* **2001**, *3*, 302.

[16]   Y. Peng, G. Song, *Green Chem.*, **2002**, *4*, 349.

[17]   Y. Peng, R. Dou, G. Song, J. Jiang, *Synlett*, **2005**, 2245.

[18]   G. Cravotto, M. Beggiato, G. Palmisano, J.M. Lévêque, W. Bonrath, *Tetrahedron Lett.* **2005**, *46*, 2267.

[19]   (a) F. Chemat, M. Poux, J. L. Di Martino, J. Berlan, *J. Microw. Power Electrom. En.* **1996**, *31*, 19. (b) F. Chemat, M. Poux and S. A. Galema, *J. Chem. Soc., Perkin Trans. 2*, **1997**, 2371.

[20]   S. Chemat, A. Lagha, H. A. Amar and F. Chemat, *Ultrason. Sonochem.*, **2004**, *11*, 5.

[21]   J.M. Lévêque, S. Desset, J. Suptil, C. Fachinger, W. Bonrath, G. Cravotto, *Ultrason. Sonochem*. **2006**, 13, 189.

[22] G. Vo Thanh, B. Pegot, A. Loupy, *Eur. J. Org. Chem.*, **2004**, 1112.

[23] G. Cravotto, L. Boffa, M. Bia, W. Bonrath, M. Curini, *Synlett* **2006***, 20, in press.*

SOLVENT-FREE MICROWAVE EXTRACTION OF ESSENTIAL OIL FROM *SALVIA SOMALENSIS* VATKE

R. Gambaro[1], C. Villa[1], A. Bisio[2], E. Mariani[1], R. Raggio[1]

[1]Dipartimento di Scienze Farmaceutiche,

Viale Benedetto XV, 3 - 16132 Genova

[2]Dipartimento di Chimica e Tecnologie Farmaceutiche ed Alimentari

Via Brigata Salerno -16147 Genova

e.mariani@unige.it

Abstract

Solvent-free microwave extraction (SFME) is a combination of microwave heating and dry-distillation performed without adding any solvent or water. It is mainly used to study fresh plants for recovering volatile chemicals. In this work SFME was used to extract essential oil from an aromatic plant, *Salvia somalensis* Vatke. The solvent-free methodology was compared with conventional techniques, hydro-distillation (HD) and steam distillation (SD) and the best results have been obtained with SFME in terms of speed, efficiency and greenness.

1.   Introduction

The increasing interest for natural products, especially of botanical origin, induces to study new, fast, economic and eco-friendly methodologies to extract actives from plants. In this context, microwave technology may be an alternative energetic source of great interest in green procedures. Since 1970, microwaves have been applied to the analytical sample preparation, especially for a rapid digestion of environmental, toxicological, food and petrochemical samples. More recently the use of microwave technology in the analytical field has promoted the development of several fast and efficient methods to enhance the solvent extraction of organic compounds from geological, botanical, biological matrices and cosmetic products. In this context dielectric heating can be used to heat the solvents with high dielectric loss coefficients, that are in contact with the solid matrices (MAE - Microwave Assisted Extraction) or to heat a suspension of conducting particle in a non-conducting medium (MAP - Microwave Assisted Process).

In recent years a new green microwave extraction method without adding any solvent or water has been developed, Solvent-free Microwave Extraction (SFME). This methodology is an original combination of microwave heating and dry-distillation, performed at atmospheric pressure that provided a new idea in the extraction of essential oil from fresh plant materials [1-3].

Essential oils are a complex mixture of volatile substances, perishable and sensitive to heat, naturally synthesized from plants. The classical extraction methods such as steam distillation (SD) and hydro-distillation (HD) can cause the loss of the most volatile chemicals and the hydrolytic and thermal degradation of some compounds.

In this context SFME can be considered an interesting extraction method: under microwave irradiation the heating of *in situ* water within the botanical material distends the cells causing the rupture of the glands; the essential oil is released and evaporated by plant water and its isolation is performed in a single step. In this study SFME was applied to recover essential oil from *Salvia somalensis* Vatke[4].

To investigate the potential of the solvent-free method, SFME was compared with conventional techniques, hydro-distillation and steam distillation in terms of yields, extraction times, energy and solvent consumption.

By GC-MS a qualitative analysis of the essential oils, extracted by SFME and HD methods, was carried out and the results compared.

2. Experimental

2.1. Plant material

Salvia somalensis Vatke was purchased in spring 2006 from the CeRSAA- Camera di Commercio Industria Artigianato e Agricoltura di Savona collection, Savona, Italy (Figure 1). The specie has been identified by Dr. Gemma Bramley and a voucher speciem is deposited in Kew Herbarium (K).

2.2. SFME Apparatus and procedure

The solvent-free extraction was performed using a monomode microwave reactor (CEM Discover®) equipped with a cooling system using compressed air, thus enabling higher levels of irradiation over the time course of the extraction maintaining a low temperature. This procedure is particularly interesting to recover volatile chemicals and to avoid deterioration of the vegetable matrices. The microwave apparatus provides power emission from 1 to 300 Watts that allows controlling the process temperature. Temperature is monitored by IR detection. Sample vessel is equipped with a Clevenger modified apparatus that permits essential oil bedding over the plant water and the feed back of water excess in the vessel to prevent premature drying out of the irradiated biological material [5] (Figure 2a-b).

The fresh botanical parts (15 g), placed in the microwave reactor without any solvent or water, were irradiated for 15 minutes at 200 Watt, using the cooling system to keep the temperature under 100 °C. The essential oil collected was directly analyzed by GC-MS.
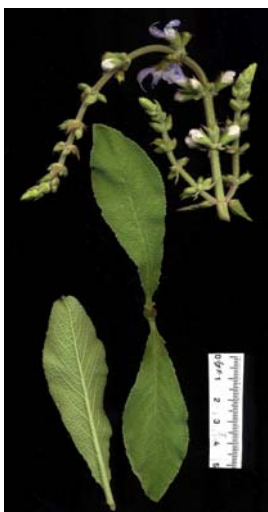
Figure 1 - *Salvia somalensis* Vatke
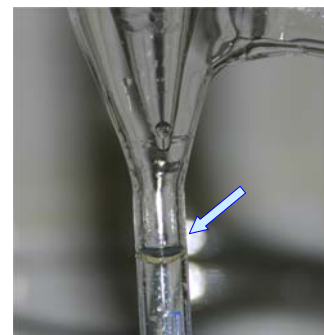
a   b

Figure 2 - (a) Microwave reactor coupled with Clevenger apparatus; (b) Essential oil stratification in Clevenger apparatus

2.3. HD apparatus and procedure

Fifteen grams of fresh plant material were submitted to hydro-distillation with the Clevenger-type apparatus according to the European Pharmacopoeia and extracted with 250 ml of water for 60 minutes (until no more essential oil was obtained). The essential oil collected was directly analyzed by GC-MS.

2.4. SD apparatus and procedure

Fifteen grams of fresh plant material were submitted to steam distillation for 90 minutes. The essential oil was obtained by extracting the condensed water (500 ml) with diethyl ether, the solvent was evaporated under reduced pressure.

2.5. Gas chromatography-mass spectrometry identification

The essential oils were analyzed by gas chromatography coupled to mass spectrometry (Hewlett Packard HPHP6890-5973) using a HP5 95-methyl-5-phenylpolysyloxane capillary column at the following conditions: carrier gas He, constant flux 1ml/min; split 25:1; injection temperature 250 °C; temperature progress: 50 °C for 5 min to 220 °C, 5 °C min; detector MSD. Mode: scan mass 50-500 amu.

3. Results and discussion

Figures 3-6 report the comparisons of the results obtained by SFME, HD and SD in terms of yields, extraction times, energy and solvent consumption. The data show that the most efficient method is SFME: yields are clearly higher (1.21 against 0.58 and 0.28 for HD and SD respectively - Figure 3) within shorter extraction time (15 min against 60 and 90 min - Figure 4) with a consequent neat reduction of energy consumption (Figure 5). Moreover, Clevenger apparatus allows eliminating solvents to collect the essential oil and, in the case of microwave activation no water was added to the extraction process (Figure 6).

The GC-MS qualitative analysis of the essential oils, extracted by SFME and HD methods, showed that the composition of the essential oils obtained with the two extraction methods were much the same. No significant differences were identified, but in the HD extraction some oxygenated compounds such as caryophyllene oxide and limonene oxide were found. These compounds, not present in the SFME essential oil, can be considered as artifacts caused by long extraction time (HD/SFME: 60/15 min) and large amount of water (Figure 7 a-b).
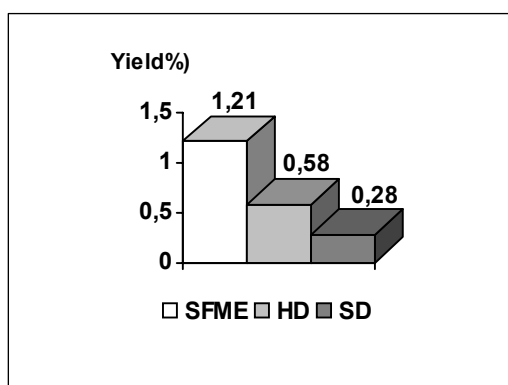
Figure 3 - Yields obtained by SFME, HD and SD
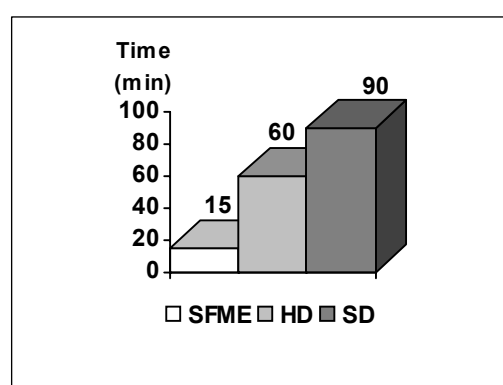
Figure 4 - Extraction time for SFME, HD and SD
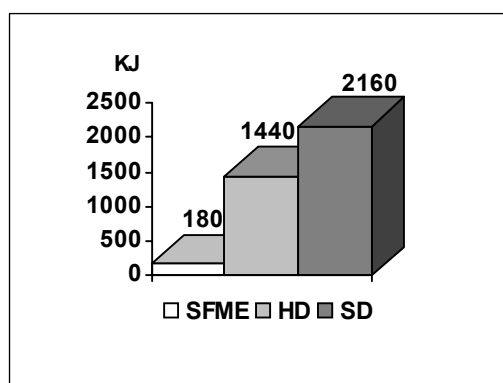
Figure 5 - Energy consumption in SFME, HD and SD used in SFME, HD and SD
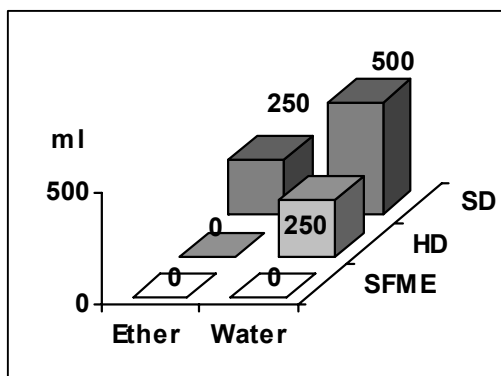
Figure 6 - Amount of solvent and water
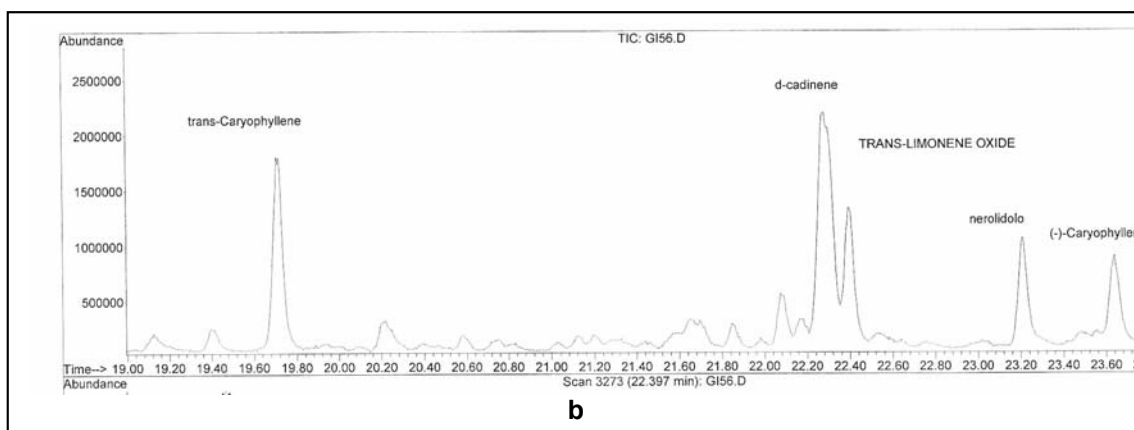
Figure 7 - GC-MS analysis of the essential oils from *Salvia somalensis* Vatke: comparison of the chromatographic detail (a - Essential oil by SFME; b - Essential oil by HD) related to the presence of oxygenated compounds

4. Conclusion

SFME can be considered a green technology, which offers important advantages over classical methods: shorter extraction times, substantial energy and solvent saving, higher yields and easier work-up.

5. References

[1] M.E. Lucchesi, F. Chemat, J. Smadia, Flavour and Frag. J., 19 **(**2004), 134-138,.

[2] M.E. Lucchesi, F. Chemat, J. Smadia, J. Chromogr., 2 (2004), 323-327.

[3] N. Asfaw, P. Licence, A.A. Novitskii, M. Poliakoff,. Green Chem. 7 (2005), 352-356.

[4] F. Chialva, F. Monguzzi, P. Manitto, J. Essent. Oil Res., 4 (1992), 447-455.

[5] F. Chemat, J. Smadja, M. Lucchesi, Eur. Pat 1439218 (2004).

Section 2. Chemical synthesis

INFLUENCE OF MICROWAVES ON THE PREPARATION OF ORGANOCLAYS

S. Baldassari[a], S. Komarneni[b], E. Mariani[a], C. Villa[a]

[a]Di.Sci.Far., Università degli Studi di Genova,

Viale Benedetto XV, 316132 Genova - Italy

[b]Materials Research Institute, The Pennsylvania State University,

University Park, PA 16802 - USA.

e.mariani@unige.it

I.   Abstract

Microwave activation under hydrothermal conditions (M-H) has been used for the preparation of organoclays, materials widely applied as rheological additives. Microwave (MW) irradiation has several advantages over conventional procedures, such as rapid heating and enhanced reaction rates. The combination of microwaves with mild reaction conditions (hydrothermal processing) represents an interesting eco-friendly choice in the context of Green Chemistry.

In this study, the microwave technology was applied to the preparation of organophilic clays by treating synthetic fluorophlogopite-type micas with different quaternary ammonium salts. The full conversion of the clays into their corresponding organophilic derivatives was easily achieved, as shown by the X-Ray Diffraction (XRD) patterns. In most cases microwave irradiation resulted to be superior to conventional heating, yielding a complete intercalation in shorter reaction times.

II.   Introduction

Organoclays are hybrids derived from an ion exchange of the inorganic cations located in the interlayers of clays with long-chained quaternary ammonium salts under hydrothermal conditions [1]. The exchange makes the clay hydrophobic and enables it to swell in non-aqueous media. Organophilic clays are therefore applied as rheological additives in paints, inks, adhesives and cosmetics; moreover, they are used for the preparation of nanocomposites and may be exploited to absorb organic pollutants in soil remediation programs [2-3]. Organoclays are generally prepared from natural smectites; our research has instead focused on the preparation of organophilic derivatives of several synthetic, swelling-type sodium fluorophlogopite micas [4]. Organophilic derivatives of synthetic clays might prove to be more performing technological materials, having reproducible chemical composition and pureness, and featuring specific properties.

In this study an innovative, fast and efficient microwave-assisted hydrothermal procedure was developed to perform the intercalation of the clays. Microwave-activated reactions have acknowledged advantages over conventional procedures, such as rapid heating, enhanced reaction rates by one to two orders of magnitude, formation of novel phases [5-6]. MW irradiation may be successfully associated to the hydrothermal processing of materials, and this methodology, for its fast kinetics and low environmental impact, may be considered a valuable alternative for sustainable chemistry.

We aimed at investigating the influence of microwaves on the intercalation process, thus all syntheses were also performed under conventional hydrothermal (C-H) conditions for comparison.

III.   Discussion

The micas used in this research had been prepared using either kaolinite or silicic acid and aluminum trichloride as aluminosilicate sources and MgO in a solid-state process [7, 8] and were characterized by different layer charges (expressed by their Cation Exchange Capacity, CEC): Na-0.5-micas (CEC 64meq/100g of dry clay, chemical composition $Na_{0.5}Si_{7.5}Al_{0.5}Mg_6O_{20}F_4$), Na-1-micas (CEC 127 meq/100 g, chemical composition $NaSi_7AlMg_6O_{20}F_4$), Na-1.5-micas (CEC 188 meq/100 g, chemical composition $Na_{1.5}Si_{6.5}Al_{1.5}Mg_6O_{20}F_4$) and Na-2-micas (CEC 246 meq/100 g, chemical composition $Na_2Si_6Al_2Mg_6O_{20}F_4$). All the clays used, except the Na-2-mica, were treated with different quaternary ammonium salts to evaluate any difference in intercalation kinetics of organics with different molecular weight: the salts used were decyltrimethylammonium (C10), dodecyltrimethylammonium (C12), tetradecyltrimethylammonium (C14), hexadecyltrimethylammonium (C16), octadecyltrimethylammonium (C18) and didecyldimethylammonium (*Bis*-C10) chloride. The high-charged Na-2-mica, whose intercalation is more difficult due to its high CEC, was treated only with the octadecyltrimethylammonium cation.

The reaction conditions are reported in Table I. For the reactions performed under microwave irradiation, a multimode microwave system (MARS5) made by CEM Corporation was used. The system operates at a frequency of 2.45 GHz as in the case of a domestic microwave oven.

The maximum operating power used was 300 W, modulated from 0% to 100% during the reaction. The temperature, power level and irradiation time can be programmed and the pressure and temperature were continuously monitored during the treatment. Under microwaves, the reaction temperature was reached after a 1-minute irradiation.

As for conventional heating, the reactions performed at 60 °C were carried out in an electric oven and the solutions of the ammonium salt were preheated for 15 minutes before adding the clay. As for processes conducted at 100 °C, the reactions were performed in Teflon-lined Parr bombs and no preheating was carried out.

At the end of all reactions, the clays were centrifuged, washed with deionized water (20 mL) and ethanol 190% proof (15 mL) and finally dried in an electric oven at 60 °C for at least 16 h. All samples were analysed by X-Ray Diffraction.

Table I - Reaction conditions for the preparation of organophilic clays

Mica	Amount of ammonium salt (% CEC)	Concentration of ammonium salt (mM)	Time (min)		Temp. (°C)
Na-0.5-mica	300	0.01	30	M-H	60
			30 + 15	C-H	
Na-1-mica	300	0.02	30	M-H	60
			30 + 15	C-H	
Na-1.5-mica	100	0.01	30	M-H	60
			30 + 15	C-H	
Na-2-mica	1000	0.12	120	M-H	100
			120	C-H	
			240	C-H	
			360	C-H	

It resulted that with the low-charged Na-0.5-mica, Na-1-mica and Na-1.5-mica microwave activation usually yielded a complete ion exchange in 30 minutes at 60 °C, while conventional heating in most cases led to a partial intercalation under the same reaction conditions (Table II).

In Figures 1-3 the XRD spectra of several organophilic derivatives of low-charged micas are shown as examples. The *d*-spacings 12.3-12.4 Å correspond to the (001) reflection of the original clays. The replacement of the inorganic cations by quaternary ammonium cations results in an increase of the basal spacing dependent on the arrangement adopted by the cations in the interlayers: 13-14 Å for lateral monolayer, 17-18Å for lateral bilayer, 23-25 Å for pseudotrilayer, 28-31 Å for paraffin-type monolayer [9, 10]. The co-existence of areas showing different molecular arrangement was found in all samples, but MW-irradiated samples mainly featured a higher packing density compared to the corresponding conventionally-heated hybrids.

Table II - Results of the intercalation processes

Mica	IV ammonium cation	Intercalation M-H	Intercalation C-H
Na-0.5-mica	C10	Complete	Complete
	C12	Complete	Complete
	C14	Almost complete	Partial
	C16	Almost complete	Partial
	C18	Complete	Partial
	Bis – C10	Complete	Partial
Na-1-mica	C10	Complete	Partial
	C12	Partial	Partial
	C14	Complete	Complete
	C16	Complete	Partial
	C18	Complete	Partial
	Bis – C10	Complete	Partial
Na-1.5-mica	C10	Partial	Partial
	C12	Complete	Partial
	C14	Complete	Partial
	C16	Complete	Complete
	C18	Complete	Complete
	Bis – C10	Complete	Complete
Na-2-mica	C18-120min	Almost complete	Partial
	C18-240min	-	Partial
	C18-360min	-	Trace of original clay
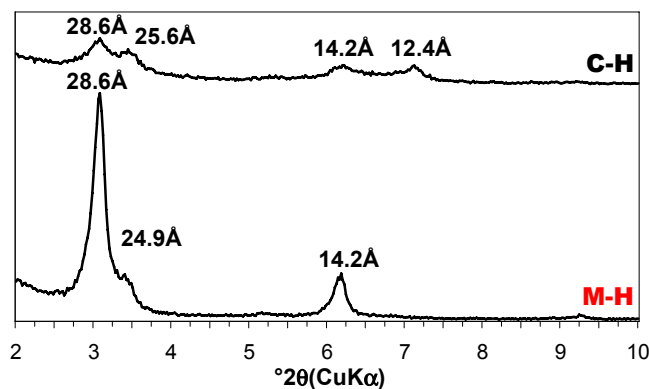
Figure 1 - Powder XRD patterns of the octadecyltrimethylammonium derivative of Na-0.5-mica
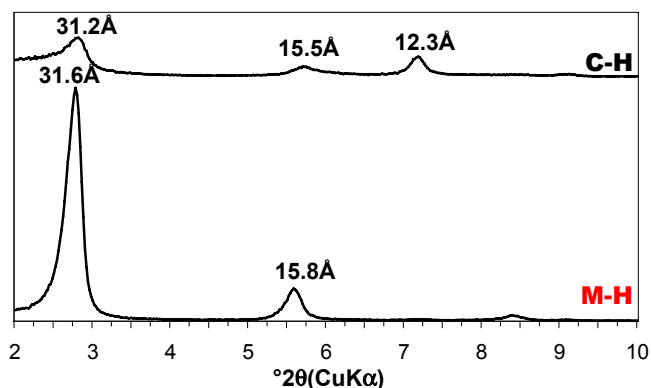
Figure 2 - Powder XRD patterns of the didecyldimethylammonium derivative of Na-1-mica
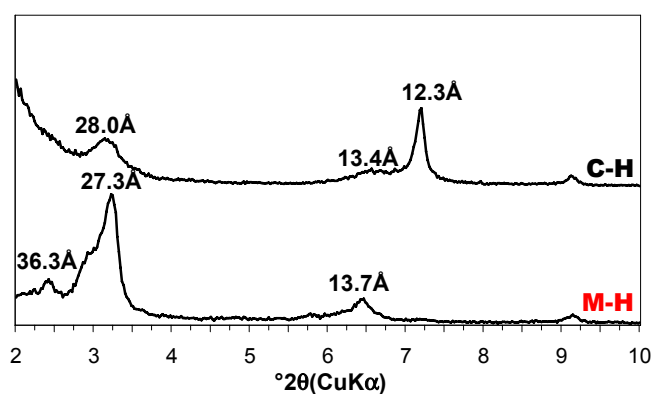
Figure 3 - Powder XRD patterns of the dodecyltrimethylammonium derivative of Na-1.5-mica

In the case of the high-charged Na-2-mica, an almost complete substitution of the inorganic cations in the interlayers was achieved after a 2-hour irradiation at 100 °C. The XRD pattern shows an intense peak corresponding to a *d*-spacing of 29.5Å, proof of paraffin-type monolayer. After 2-hours' conventional heating, the inorganic cations were only partially replaced by the quaternary ammonium cations arranged in lateral monolayer. An almost complete conversion, with a trace of the original clay, was only achieved conventionally heating the mixture for 6 hours.

In Figure 4 the XRD patterns of the octadecyltrimethylammonium derivative of the Na-2-mica are shown.
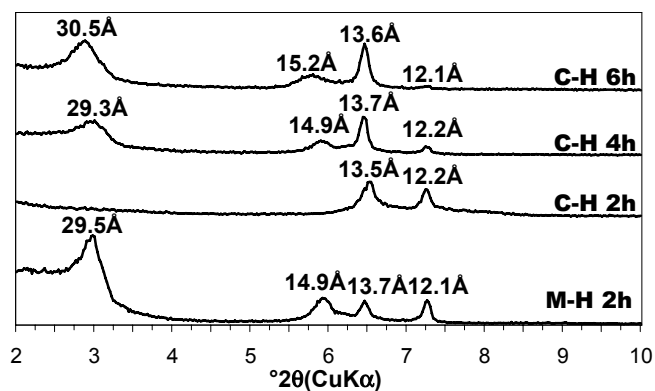
Figure 4 - Powder XRD patterns of the octadecyltrimethylammonium derivative of Na-2-mica (the *d*-spacings 12.1-12.2Å correspond to the (001) reflection of the original clay)

IV.   Conclusion

The preparation of organophilic clays can be successfully performed through a microwave-assisted hydrothermal process. In most cases MW heating has proved to be more efficient than conventional heating, yielding a higher extent of intercalation. Microwaves resulted particularly superior in the treatment of high-charged clays, with significant energy and timesavings.

References

[1] H. Favre, G. Lagaly, Clay Miner. 26 (1991), 19-32.

[2] M.T. Clarke, Rheological additives, in: D. Laba (Ed.), Rheological Properties of Cosmetics and Toiletries. M. Dekker Inc., New York, NY, USA (1993), 55-152.

[3] M.J. Carrizosa, P.J. Rice, W.C. Koskinen, I. Carrizosa, M. Hermosin, Clays Clay Miner. 52 (2004), 341-349.

[4] T. Kodama, T. Higuchi, T. Shimizu, K. Shimizu, S. Komarneni, W. Hoffbauer, H. Schneider, J. Mater. Chem. 11 (2001), 2072-2077.

[5] S. Komarneni, Ionics 21 (1995), 95-98.

[6] S. Komarneni, R. Roy, Q.H. Li, Mater. Res. Bull. 27 (1992), 1393-1405.

[7] M. Park, D.H. Lee, C.L. Choi, S.S. Kim, K.S. Kim, J. Choi, Chem. Mater. 14 (2002), 2582-2589.

[8] S. Komarneni, R. Ravella and M. Park, J. Mat. Chem. 15 (2005), 4241-4245.

[9] Z. Kłapyta, A. Gaweł, T. Fujita, N. Iyi, Clay Miner. 38 (2003), 151-160.

[10] Y. Xi, Z. Ding, H. He, R.L. Frost, J. Colloid Interface Sci. 277 (2004), 116-120.

MICROWAVE ASSISTED ORGANIC SYNTHESIS (MAOS): EASY AND FAST SYNTHESIS OF BIOLOGICALLY ACTIVE COMPOUNDS

Mauro Panunzio*[a], Elisa Bandini,[b] Antonio D'Aurizio [b] and Giorgio Martelli [b]

a: ISOF-CNR, Dipartimento di Chimica "G. Ciamician"

University of Bologna, Via Selmi 2, 40126 Bologna, Italy

b: ISOF-CNR, Area della Ricerca di Bologna, Via Gobetti 101, 40121 Bologna Italy

mauro.panunzio@unibo.it

1.   Introduction

Microwave Chemistry is becoming increasingly popular in synthetic organic chemistry. [1] The research literature, on this field, has literally grown exponentially from the first report on the Microwave Assisted Organic Synthesis (MAOS) in the mid 1980's. Nowadays the problem with MAOS is not what to do with this appealing technique, since it is extending itself to an incredible number of applications in synthetic organic chemistry, but how and why it is so effective, at least on lab-scale. Debates still continue about precisely why microwaves display so high efficiency in many reactions. A few comments are needed in this context: Whereas it may be considered already acquired the very efficiency of MAOS in the building-up small libraries of pharma-ceutically interesting compounds in really very short time, compared with the classical convective heating, the problem of the scaling-up to Kg-lab or, better, to industrial scale, is far away, in our opinion, to be solved. From a practical point of view, this is considered, unfortunately, beside the point. As a simple statement too many papers appear in the literature reporting new applications of MAOS but very few of them take into account the comparison of MAOS with classical technique, few of them the amount of energy involved and less than few deal with scale-up problems. The fact is that microwave heating can do a number of things which conventional heating cannot and it is very convenient to avoid any explanation on these aspects in order to produce and publish as many papers as possible.

Microwave heating is *direct* - energy absorbed by the sample without heating, by external source, the sample vessel. Direct heating also means that it is a highly controllable form of heating. This makes microwave heating *highly efficient*, and in many cases, this efficiency *will over-ride the fact that microwave energy is relatively expensive* compared with convective heating. This is a crucial point that in many papers is forgotten or, in very wrong and un-ethical cases, presented in a form that MAOS is defined a very convenient friendly environmental technique. Too many times MAOS, with particular emphasis to the MAOS associate with solid support technique is presented as a tool to perform green chemistry: this statement is very far away from the true if one look at the cost of the solid supports, at the ponderal ratio with the reagents (1 to 10 at least!!!) and at the need to use, in any case, organic solvents to homogenously distribute the reactants on the support and to remove the obtained products from the solid supports.

The sentence *"Solvent free organic reactions assisted by Microwave to achieve green chemistry"* reported in the titles of many scientific papers is very far away from the true: no mention is dedicated to the environmental cost to produce the solid support and to the high consuming energy the Microwave generator (Magnetron) requires!

2.   Microwaves speed synthesis reactions

Nevertheless in the last few years the use of microwave technology, as a heating source, has become widespread in lab-scale synthesis, both in the academic and in the industry fields. The major part of chemical compounds is obtained *via* reactions that involve the heating of the reaction mixture. The reason of this great interest can be found in the efficiency of the heating process, because it's heating directly the core of the reaction. As a consequence rate enhancement and higher product yield and purity have been observed. From this point of view MAOS technique have, *rightly*, matched the need of pharmaceutical industries: production in very short time of a large amount of samples to undergo to the biological tests, no mention to the future development, which will be performed by classical technologies.

3.   Comparison between conventional and microwave heating

These points together with higher yield and purity of the products are the reason of the popularity of microwave technology. Microwaves technology impact on removing significant bottlenecks and delays from the discover process: it allows chemists to focus on what is most important - the development of new compounds and/or establishing good experimental parameters for improving/generating known and unknown products. Because the speed and the efficiency microwave-enhanced chemistry has become a cutting-edge technology across the pharmaceutical, biotech, polymers, plastics, fine and agrochemical industries. At the beginning domestic microwaves were employed: unfortunately they present several limitations like lack of safety, no control of critical parameter as temperature and pressure, no possibility of fine power regulations. Many results, so far reported, are useless because the lack of reproducibility of the experiments described. Today, fortunately, there are Microwave ovens available in the market dedicated to research in general and to run MAOS in particular. The use of such instruments allows working safely under well-defined and monitored conditions of temperature and pressure as well as knowledge of the output power during the run. In this way the experiment is completely reproducible every time thanks also to the homogeneity of the field in the microwave oven. Two kinds of microwave instruments are nowadays available: monomode or multimode microwave systems. Both the systems have the characteristics mentioned above, but the main differences rely on the number of reactions that can be run simultaneously and the volume of reactants that can be used. Monomode system allows performing reaction between 0.2ml and 20ml total volume, at 200 °C and 20 bar for one reaction at time. In the multimode system instead it's possible to work from 2ml up to litres, at 250 °C and 50bar with the possibility to scale-up reactions from small to large volume without any further optimization of the reaction conditions. The main difference is in the amount of power, usually adjusted automatically by the instrument. In this way the chemists can focus on what is most important: the development of new compounds.

Furthermore, thanks to the homogeneity of the microwave field in the cavity, the multimode system can work with one vessel at time up to several vessels simultaneously, with the possibility to perform the '*real*' parallel synthesis saving a lot of time. In literature thousands of examples are reported regarding the synthesis of compounds or libraries of compounds using a multimode cavity. The next three sections report the results obtained in our laboratory using MAOS technique.

4.   Synthesis of 3-thiophenyl- and 3-thiobenzyl-β-lactams by maos. Comparison between dielectric heathing and convective heathing

The synthetic approaches to 2-azetidinones are almost countless, but the Staudinger approach from ketenes and imines remains the most useful despite its venerable age. [2] An application of this strategy to the synthesis of 3-phenylsulfanyl- and 3-benzylsulfanyl- azetidinones, making use of MAOS technique is reported. [3] In detail, the synthesis involves the preparation of an azadiene, [4] from a *N*-trimethylsilylimine [5] and the corresponding phenylsulfanyl- or benzylsulfanyl-ketene, formed *in situ* from the corresponding phenylsulfanyl- or benzylsulfanyl-acetyl chloride and triethylamine (Scheme 1).

Scheme 1: Sinthesis of β-lactams by MAOS
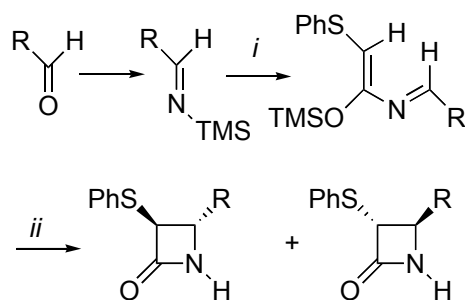
Ring closure to the expected azetidinone was performed by Microwave Assisted Organic Synthesis. Comparison of the same reaction performed by refluxing overnight in dry toluene is reported as well (Table 1).

The configuration of the azadiene has been assigned by Noe experiments and that of the azetidinones obtained on the basis of coupling constant between the C_3H and C_4H (usually between 0-3Hz for *trans* derivatives and 3-7Hz for the *cis* ones). By this protocol a diastereomeric mixture of *N*H-β-lactams has been obtained after usual work-up and silica gel flash chromatography in yields and diastereomeric ratios varying from the substituents of the azadiene. The yields of azetidinones are based on the starting aldehydes (Scheme 1) and are calculated on the pure isolated compounds. Table 1 warrants some comments: although the yields are not high, they have not been optimized and should be considered satisfactory since it must be taken into account that reactions are performed in a one pot, three-step fashion (preparation of the imine, reaction with acyl chloride and ring closure to the β-lactam ring).

Table 1 . *NH*- 3-thiophenyl-β-lactams A and B

R	Solvent	Products	DH-Time 20 → 110 Yields(%)	A/B	CH-Time 350 → 800 Yields(%)	A/B
(PhS/TMSO imine, OTIPS methyl)	Cl-benxene	A / B (OTIPS methyl β-lactams)	50	50/50		
	Toluene		---	---	50	65/35
	neat		18	50/50	Traces	
(PhS/TMSO imine, OTIPS isopropyl)	Cl-benxene	A / B (OTIPS isopropyl β-lactams)	50	84/16		
	Xilene		75	72/28	35	57/43
	Toluene					
(PhS/TMSO imine, OTIPS Ph)	Cl-benxene	A / B (OTIPS Ph β-lactams)	52	50/50		
	Toluene				44	55/45
(PhS/TMSO imine, C6H4–NO2)	Toluene	(PhS β-lactam, C6H4–NO2)	15(*)	Trans	14(*)	Trans
(PhS/TMSO imine, C6H4–OMe)	Cl-benzene	(PhS β-lactam, C6H4–OMe)	20	Trans		
	Toluene				15	Trans
(PhS/TMSO imine, thiophene)	Cl-benzene	(PhS β-lactam, thiophene)	30	Trans		
	neat		25	Trans		
	Toluene				25	Trans
(PhS/TMSO imine, alkyne–Ph)	Cl-benzene	(PhS β-lactam, alkyne–Ph)	30	Trans		
	Toluene			Trans	25	Trans
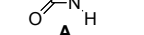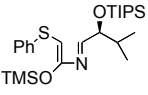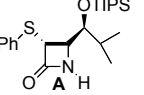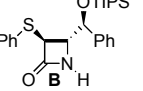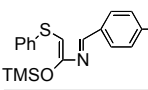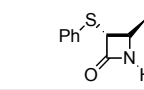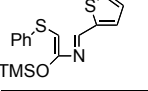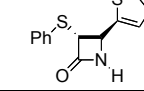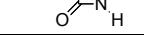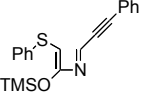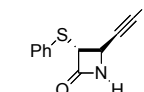
DH: Dielectric Heating; CH: Conventional Heating

The data reported show that the [2+2] cyclization, in term of simple diastereoselectivity, is highly stereo-controlled since only *trans* azetidinones, characterized by coupling constants C_3H–C_4H of 2.0–2.5 Hz at ^{1}H NMR spectra, are obtained. Unfortunately no significant facial-diastereoselectivity is present in all the experiments performed and under the experimental conditions used except for the example of entry 5, Table 1.

The ring closure described using classical heating has been performed using MAOS methodology. Comparison between the data arising from dielectric heating and convective heating shows that the only valuable difference between the two methodologies resides on the shorter reaction time thus certifying that, at least for this example, no further differences, in yield as well as in diastereoselectivity, take place. Of course the MAOS shows itself more convenient if one looks at the possibility to prepare in very short time a small library of β-lactams. The slight increasing in yield confers an extra advantage to the MAOS technology.

The compounds prepared may be used for the synthesis of non-classical β-lactams (*e.g.* see Scheme 2) and of some derivatives known to be used as enzyme inhibitors (*vide infra*).

Scheme 2: Synthesis of non-Classical Thio–β-Lactams
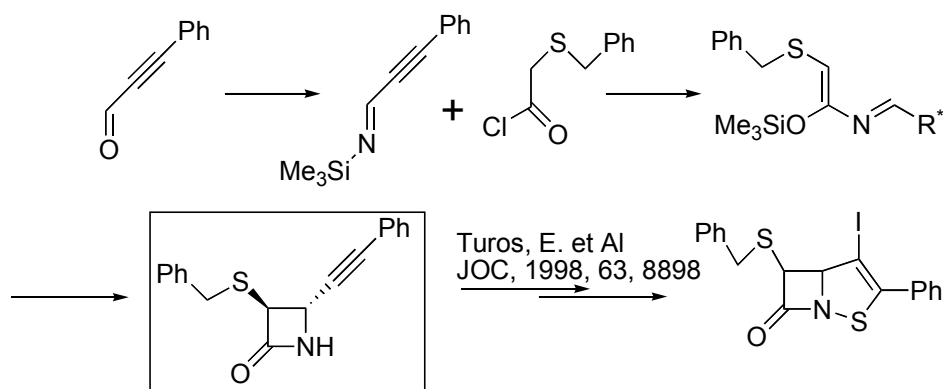
5 Synthesis of (R)- and (S)-Fluoxetines (Prozac®) via MAOS-HDA reaction

Hetero Diels-Alder (HDA) cycloaddition is a versatile strategy for the synthesis of natural compounds containing six-membered heterocyclic rings.[6] Moreover this strategy has found important applications through the elaboration of the cyclic adducts, thus obtained, to acyclic compounds with a well-defined stereo- and regio-control of the present functionalities. Reported herein is the application of hetero Diels-Alder methodology to the synthesis of open-chain compounds containing the 1,3-hydroxy-amino moiety, which is present in a large class of pharmaceutically important compounds as Duloxetine (Cymbalta®) and Fluoxetine (Prozac®). [7] Prozac has been chosen as a target compound being potent and highly selective inhibitor of neutral serotonin-reuptake and among the most important drugs for the treatment of psychiatric disorders and metabolic problems. Last but not least, their market is very interesting from an industrial point of view. As a matter of fact the establishing of new synthetic protocols, which allow the building-up of small libraries, with an easily obtainable different substitution pattern on the scaffold, is of primary importance for researchers involved in the preparation and the study of this class of compounds. MAOS technique has been shown very appealing in our research group in this context. In fact, in continuation of our studies on the use of hetero Diels-Alder strategy in the synthesis of heterocyclic compounds with different substitution pattern and their use for the preparation of acyclic derivatives we have developed the synthesis and the use of the 5-phenylthio-perhydrooxazin-4-ones, valuable intermediates in the preparation of racemic and optically active 1,3- aminoalcohols.

5.1 Synthesis of 5-Thiophenyl-1,3- Oxazinan-4-Ones, intermediates for the preparation of Prozac®

5-Phenyl-thio-1,3-oxazinan-4-ones have been obtained from the easily available 1,3-azadienes, prepared from silylimines and ketenes, and using aldehydes as dienophiles. The starting azadiene has been already used in a previous study for the preparation of a β-lactam ring by a 4p-conrotatory electrocyclization (*See above*).

Scheme 3: Preparation of Fluoxetine by MAOS
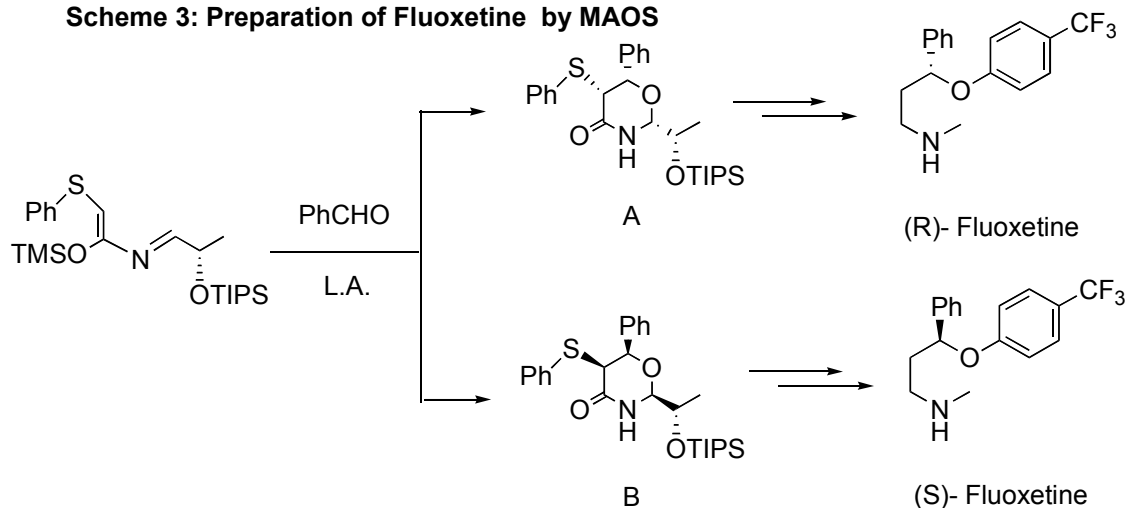
Hetero Diels-Alder reaction of this azadiene with aldehydes in the presence of lanthanides as Lewis acid and under MAOS conditions gives rise to the formation of the adducts, reported in Scheme 3, which have been elaborated to the optically active Prozac [7]. *Once again comparison of MAOS technique with classical organic chemistry has been reported* (Table 2).

The so prepared cyclic adducts have been elaborated to the desired compounds according to the reported Schemes 4 and 5.

Table 2: Conventional vs MAOS in the synthesis of Perhydroxazinone

L.A. (%)	Time	Yields	A/B
BF$_3$ (1 eq.)	-78°C 16 h	82 %	40/60
EuFOD (1%)	10 min	15 %	45/55
EuFOD (10%)	10 min	88 %	50/50
YbFOD (10%)	10 min	47 %	55/45
EuCanf. (10%)	10 min	55 %	50/50

Scheme 4: Synthesis of *(R)*-Fluoxetine

Scheme 5: Synthesis of *(S)*-Fluoxetine

a: LHMDSA, MeI, THF, 0□C, 2h; b: Ph2SiH2, RhH(CO)(PPh3)3 1%, THF, 15h, c: HCl 1N, MeOH, 90□C, 1.5h; d: p-CF3-PhCl, NaH, DMSO

5.2   Synthesis of racemic (±)-Prozac

Following the same MAOS-HDA methodology a synthesis of racemic Prozac has been achieved. Compared to the previous one this synthesis allows the preparation of the racemic drug without the needed removal of the thiophenyl group.

Scheme 6: Microwave Assisted (MAOS) HDA catalyzed by Lanthanides
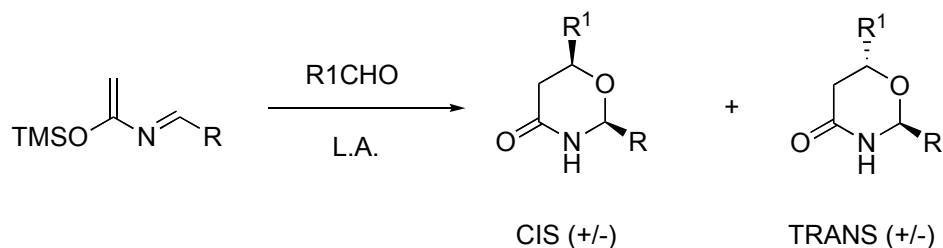
Table 3: Microwave Assisted (MAOS) HDA catalyzed by Lanthanides

R	R1	L.A. (%)	Time	Yield	Cis/Trans
Ph	Ph	BF$_3$ (1 eq.)	8 h r.t.	67 %	37/73
Ph	Ph	EuFOD (10%)	Reflux 60min	59 %	78/22
Ph	Ph	EuFOD (10%)	r.t. 7 gg.	5 %	----
Ph	Ph	EuFOD (10%)	40 min	63 %	74/26
Ph	Ph	YbFOD (10%)	40 min	47 %	86/14
Ph	Ph	EuFOD (10%)	5min	84 %	78/22
Ph	(OTIPS-phenyl)	EuFOD (10%)	30 min	38 %	75/25
Ph	(OMe-phenyl)	EuFOD (10%)	40 min	48 %	80/20
(OMe-phenyl)	(OMe-phenyl)	EuFOD (10%)	40 min	50 %	75/25
(OMe-phenyl)	(OMe-phenyl)	YbFOD (10%)	30 min	43 %	79/21

Scheme 7: Synthesis of racemic Prozac

(±)-11a-Prozac
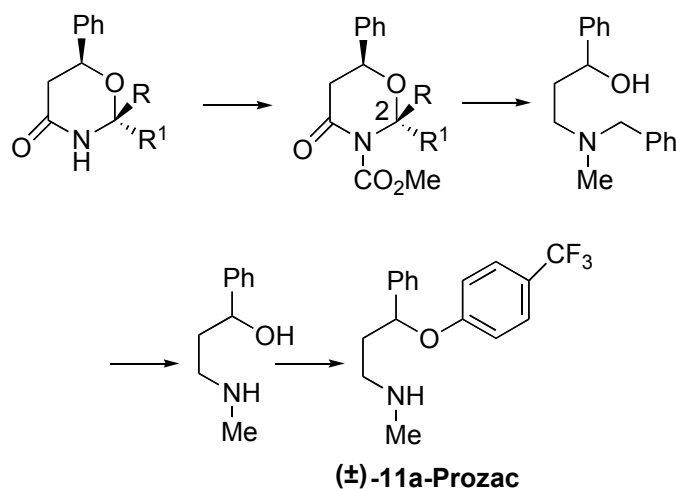
6 Microwave-assisted desulphuration by Nickel-Raney of significant biologically active compounds

Phenyl thio-substituted compounds are important intermediates in the synthesis of significant biologically active compounds. The main drawback in utilizing these intermediates lies on the relative difficulty in the reductive-elimination of the thiophenyl- or thioalkyl-group without use of toxic and/or expensive reagents. In the course of our studies on the synthesis of significant biologically active molecules we needed an efficient and safe desulphuration method. Such kind of reactions is already known and a large amount of literature is available. [8] However, there are only a few examples of desulphurization reactions of β-lactams in order to obtain 3-unsubstituted derivatives, which are known to be useful compounds with potential applications as β-lactamases or inhibitors of 3-hydroxy-3-methyl glutarate coenzyme A synthetase, human leukocyte elastase [9] poliovirus, and human rhinovirus c3-proteinase. [10] Among the different methods known in literature for this task, the cited references can be grouped in two sections: a) Ni/Raney mediated reactions [11] b) Bu$_3$SnH catalyzed reactions, [12] *e.g.* those reported by Palomo and Cossio. Both methodologies generally need long reaction times (1-2,5 hours) and high temperatures (reflux). To our knowledge there are no examples of microwave-mediated Ni/Raney catalyzed desulphuration reactions [13] of 3-phenylthio mono-substituted derivatives.

7 Desulphuration Reaction of 3-Thiophenyl-β-Lactams

Some 3-phenylthio-azetidinones, obtained according a published procedure, [3] were desulphurated by a new MW-assisted reaction using Raney/Ni as reducing agent, allowing synthesizing 3-unsubstituted-4-alkyl or 4-aryl-β-lactams in a very short time (Scheme 8 and Table 4). Comparison with an experiment performed by conventional heating showed the well-known advantages of the MAOS technique: shorter reaction times and higher yield were observed as expected. It's interesting to notice that microwave procedure used is compatible with the presence of chiral centres on the reactant species (Table 4).

Scheme 8: Desulphuration of 3-thio–β-lactams by MAOS
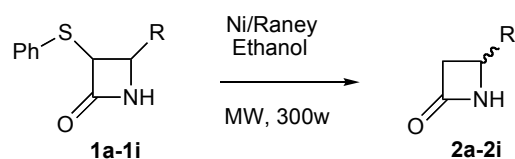
Table 4. Desulfurization of β-lactams by Ni/Ra and MAOS

Entry	R[a]	Time (min)	Yield %
1	OTIPS	240[b]	66
2	OTIPS	15[c]	76
3	OTIPS	15[c]	72
4	OTIPS	15[c]	82[d]
5	OTIPS	15[c]	85[d]
7	OTIPS	15[c]	84[d]
8	OTIPS	15[c]	85[d]
9	OTIPS, Ph	15[c]	88
10	OTIPS, Ph	15[c]	88
11		15[c]	56[d]

[a]Compounds **1a-1i** presented *trans* configuration between C_3-C_4 substituents.
[b]Conventional heating (*CH*). [c]Dielectric heating (*DH*). [d]Racemate

Indeed, the absolute configuration of the chiral centres present in the position 4 was not changed at the end of the desulphurization reaction.

8   Desulphurization reaction of 4-Thiophenyl- and 4-Thio-T -Butyl-β-Lactams

In order to extend this methodology to other β-lactam derivatives we considered to apply the MW desulphuration technology to 4-thiosubstituted β-lactam, in particular we considered the desulphurization of the 3-*tert*-butyldimethylsilyloxy-ethyl-4-thioalkyl(aryl)-azetidin-2-one (Scheme 9).

Scheme 9:Desulphuration of 4-thio–β-lactams by MAOS
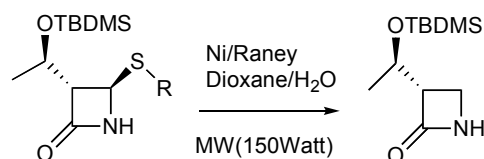
The choice of such compounds was suggested on the base of different considerations: a) a 3-*tert*-. butyldimethylsilyloxyethyl-azetidin-4-one is a compound of great interest, even from a industrial point of view, since it is an important starting material for industrial processes in the construction of antibiotics oxopenam, carbapenem and carbapenam; [14] b) the synthesis of this compound is not a simple task; [15] c) the corresponding thioderivatives, in contrast, is easily obtainable, in yield up to 70%, by literature procedures from the relatively cheap, bulky available 4-acetoxy parent [16]: last but not least application of the standard methodologies (*e.g* tributyltin hydride induced desulphuration reaction) failed in our hands.

Table 5: MW assisted desulphuration of 4-thio-lactam

Ex.	R	Method	Solvent	Temp °C	Time (min)	Y %a
1	t-But	CHb	THF/H$_2$O(2/1)	Reflux	150	45
2	t-But	DHc (300W)	EtOH	"	15	25
3	t-But	DH (150W)	THF/H$_2$O(5/1)	"	60	44
4	t-But	DH (150W)	THF/H$_2$O(2/1)	"	45	54
5	t-But	DH (150W)	Dioxane/H$_2$O (4/1)		25	60
6	t-But	DH (300W)	i-PrOH	"	60	traces
7	t-But	DH (150W)	DMF/H$_2$O (2/1)	"	60	traces
8	t-But	DH (300W)	EGMMEd	"	60	traces
9	Ph	CHb	THF/H$_2$O(4/1)	"	150	40
10	Ph	DH (150W)	Dioxane/H$_2$O (4/1)		25	27a
11	Ph	DH (150W)	THF/H$_2$O (4/1)	"	20	55
12	D	DH (150W)	DMF/H$_2$O	"	15	Traces

a:Yields are reffered on pure isolated 4 which gave spectral data superimposable with literature ones. b: CH: Convective heating; c DH: dielectric heating; d: EGMME: Ethylenglycolemonomethylether.

With the ultimate goal to find out the best experimental conditions, we performed a series of experiments changing the nature of solvents, MW power irradiations, time in order to increase the reactivity and to avoid side reactions.

Table 5 reports the most significant experiments. Moreover an experiment, using conventional heating (*CH*) (Table 5 Entry 1) was performed in order to compare its yields and time *versus* the dielectric heating (*DH*). Even in this case, comparison between the two heating procedures shows several advantages in favor of *DH*: very short reaction times, higher yields and, usually a reducing of competitive side reactions (*eg*. ring opening, displacement by an alkoxy specie, arising from the hydroalcoholic solvent, on the C4 carbon center).

9 Application of microwave assisted desulphuration to other a-thio-lactam derivatives

This last section takes into account a versatility-test of our procedure on other biologically interesting compounds containing a thiophenyl group in the position a to a lactam functionality. For this task some intermediates [17] in the synthesis of the (*R*)- and (*S*) Fluoxetines (Prozac®), were prepared by microwave assisted desulphuration reaction starting from the parent phenylthioderivatives (*see above*).

Scheme 10: Synthesis of Gabapentin intermediate
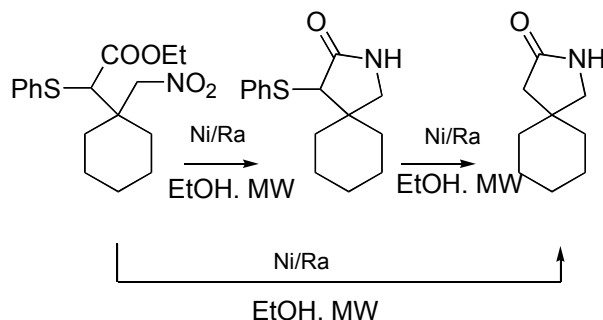
By the same procedure a new synthesis of a lactam, parent compound of Gabapentin, [18] was obtained by, eventually, simultaneous reduction of the nitro group and subsequent cyclization followed by the reductive removal of the thiophenyl group to give the desired derivative in one-pot two step reaction (Scheme 10). [21]

In conclusion, by the reported examples, we feel that a useful microwave assisted organic synthesis of different compounds has been added to the known weaponry for carry out efficient and fast libraries of biologically active derivatives.

References and Notes

1. (a) Kappe, C. O.; Dallinger, D. *Nat. Rev. Drug Discovery* 2006, AOP. published on line December *23, 2005*. (b)

Mavandadi, F.; Pilotti, A. *D. D. T.* 2006, *11*, 165. (c) de la Hoz, A.; Diaz-Ortiz, A.; Moreno, A. *Chem. Soc. Rev.* **2005**, *34*, 164-178. (d) Kappe, C. O. *Angew. Chem. Int. Ed.* **2004**, *43*, 6250-6284. (e) Lidstrom, P.; Tierney, J.; Wathey, B.; Westman, J. *Tetrahedron* **2001**, *57*, 9225-9283.

2. (a) Palomo, C.; Aizpurua, J. M.; Ganboa, I.; Oiarbide, M. *Eur.J. Org. Chem.* **1999**, 3223–3235. (b) Georg, G. I.; Ravikumar, V. T. Stereocontrolled Ketene-imine Cycloaddition Reaction. In The Organic Chemistry of

β-Lactams. Georg, G., Ed.; VCH: New York, 1993; pp 318–323. (c) Hegedus, L. S.; Montgomery, J.; Narukawa, Y.; Snustad, D. C. *J. Am. Chem. Soc.* **1991**, 113, 5784–5791. For MAOS synthesis of β-lactams see also: (a) Bandini, E.; Martelli, G.; Spunta, G.; Bongini, A.; Panunzio, M. *Tetrahedron Lett.* **1996**, *37*, 4409–4412. (b) Bandini, E.; Martelli, G.; Spunta, G.; Panunzio, M. *Synlett* **1996**, 1017–1018.

3. Panunzio, M.; Bongini, A.; Tamanini, E.; Campana, E.; Martelli, G.; Vicennati, P.; Zanardi, I. *Tetrahedron* **2003,** *59*, 9577-9582.

4. (a) Ghosez, L.; Bayard, P.; Nshimyumukiza, P.; Gouverneur, V.; Sainte, F.; Beaudegnies, R.; Rivera, M.; Frisque-Hesbain, A. M.; Wynants, C. *Tetrahedron* **1995**, *51*, 11021–11042. (b) Ghosez, L. *Pure Appl. Chem*. **1996**, *68*, 15–22. (c) Panunzio, M.; Vicennati, P. In *Recent Research Development in Organic Chemistry;* Pandalai, S. G. Ed.; Transworld Research Network: Trivandrum, India, 2002; pp. 683-707.

5. Panunzio, M.; Zarantonello, P. *Org. Process Res. Dev*. **1998**, *2*, 49–59.

6. (a) Kobayashi, S.; Jørgensen, K. A. *Cycloaddition Reactions in Organic Synthesis*; Wiley-VCH: Weinheim (Germany), 2002. (b) Boger, D. L.; Weinreb, S. M. *Hetero Diels-Alder Methodology in*

Organic Synthesis; Academic Press: New York, 1987; Vol. 47. (c) Boger, D. L. *Chemtracts-Org. Chem.* **1996**, *9*, 149-189. (d)

Jørgensen, K. A.; Johannsen, M.; Yao, S.; Audrian, H.; Thorhauge, J. *Acc. Chem. Res.* **1999**, *32*, 605-613. (e) Barluenga, J.; Suarez-Sobrino, A.; Lopez, L. A. *Aldrichim. Acta* **1999**, *32*, 4-15. (f) Palacios, F.; Alonso, C.; Amezua, P.; Rubiales, G. *J. Org. Chem.* **2002**, *67*, 1941-1946. (g) Palacios, F.; Herran, E.; Rubiales, G.; Ezpeleta, J. M. *J. Org. Chem.* **2002**, *67*, 2131-2135. (h) Jørgensen, K. A. *Angew. Chem. Int. Ed.* **2000**, *39*, 3558. (i) Buonora, P.; Olsen, J. C.; Oh, T. *Tetrahedron* **2001**, *57*, 6099-6138

7. (a) Robertson, D. W.; Jones, N. D.; Swartzendruber, J. K.; Yang, K. S.; Wong, D. T. *J. Med. Chem.* **1988**, *31*, 185. (b) Hurst, M.; Lamb, H. M. *Cns Drugs* **2000**, *14*, 51-80.

8. (a) Kang, S.-K.; Park, D.-C.; Rho, H.-S.; Yoon, S.-H.; Shin, J.-S. *J. Chem. Soc. Perkin Trans 1* **1994**, 3513-3514. (b) Bonner, W. A.; Grimm, R. A. In *The Chemistry of Organic Sulfur Compounds;* Kharasch, N.; Meyers, C. Y. Eds.; Pergamon Press: Oxford, 1966; p. 35.

9. (a) Gerard, S.; Nollet, G.; Vande Put, J.; Marchand-Brynaert, J. *Bioorganic & Medicinal Chemistry* **2002**, *10*, 3955. (b) Gerard, S.; Dive, G.; Clamot, B.; Touillaux, R.; Marchand-Brynaert, J. *Tetrahedron* **2002**, *58*, 2423.

10)(a) Firestone, R. A.; Barker, P. L.; Pisano, J. M.; Ashe, B. M.; Dahlgreen, M. E. *Tetrahedron* **1990,** *46*, 2255. (b) Skiles, J. W.; McNeil, D. *Tetrahedron Lett.* **1990,** *31*, 7277. (c) Thompson, K. L.; Chang, M. N.; Chang, Y. C. P.; Yang, S. S.; Chabala, J. C.; Ariston, B. H.; Greenspan, M. D.; Hanf, D. P.; Yudkovitz, J. *Tetrahedron* **1994,** *50*, 12049. (d) Han, W. T.; Trehan, A. K.; Wright, J. J. K.; Federici, M. E.; Seiler, S. M.; Meanwell, N. H. *Bioorg. Med. Chem.* **1995,** *3*, 1123.

10. (a) Bari, S. S.; Venugopalan, P.; Arora, R. *Tetrahedron Lett.* **2003,** *44*, 895-897. (b) Manhas, M. S.; Hedge, V. R.; Wayle, D. R.; Bose, A. K. *J. Chem. Soc. Perkin Trans. 1* **1985**, 2045-2050. (c) Ihara, M.; Fukumoto, K. *Hetyerocycles* **1982,** *19*, 1435-1438. (d) Natsugarui, H.; Matsushita, Y.; Tamura, N.; Yoshioka, K.; Ochiai, M. *J. Chem. Soc. Perkin Trans. 1* **1983**, 403-412. (e) Madan, S.; Arora, R.; Venugopalan, P.; Bari, S. S. *Tetrahedron Lett.* **2000,** *41*, 5577-5581.

12. (a) Palomo, C.; Cossío, F. P.; Odiozola, J. M.; Oiarbido, M.; Ontoria, J. M. *J. Org. Chem.* **1991,** *56*, 4418-4428. (b) Palomo, C.; Cossio, F. P.; Odriozola, J. M.; Oiarbide, M.; Ontoria, J. M. *Tetrahedron Lett.* **1989,** *30*, 4577-4580. (c) Tercio, J.; Ferreira, B.; Marques, J. A.; Marino, J. P. *Tetrahedron: Asymm.* **1994,** *5*, 641-648. (d) Bateson, J. H.; Robins, A. M.; Southgate, R. *J. Chem. Soc. Perkin Trans. 1* **1991**, 29-35. (e) Tamura, N.; Natsugari, H.; Kawano, Y.; Matsushita, Y.; Yoshioka, K.; Ochiai, M. *Chem. Pharm. Bull.* **1987,** *35*, 996-1015.

13. In the course of preparation of this manuscript a paper appeared on the Nickel/raney desulphuration assisted by Microwave: Toom, L.; Grennberg, H.; Gogoli, A. *Synthesis* **2006**, 2064-2068.

14. Martel, S. R.; Wisedale, R.; Gallagher, T.; Hall, L. D.; Mahon, M. F.; Bradbury, R. H.; Hales, N. J. *J. Am. Chem. Soc.* **1997,** *119*, 2309-2310.

15. (a) Cainelli, G.; Galletti, P.; Glacomini, D. *Tetrahedron Lett.* **1998,** *39*, 7779. (b) Ham, W.-H.; Oh, C.-Y.; Jeong, J.-H. *J. Org. Chem.* **2000,** *65*, 8372 and References therein cited.

16. Endo, M. *Can. J. Chem.* **1987,** *65*, 2140

17. Panunzio, M.; Rossi, K.; Tamanini, E.; Campana, E.; Martelli, G. *Tetrahedron: Asymm.* **2004,** *15*, 3489-3493

18. (a) Goa, L.; Sorkim, E. M. *Drugs* **1993,** *46*, 409-427. (b) Levy, H. *Antiepileptic Drugs*, 3th ed. ed.; Raven Press: New York, 1989.

19. Preparation of ethyl 2-(1-(nitromethyl)cyclohexyl)-2-(phenylthio)-acetate: Panunzio, M.; Breviglieri, G. *Manuscript in preparation*

RAPID, MICROWAVE ASSISTED SYNTHESIS OF SOLVENT FREE Mn_3O_4 NANOPARTICLES

A. Agostino, E. Bonometti, M. Castiglioni*, P. Michelin Lausarot, M.Panetta

Dipartimento di Chimica Generale ed Organica Applicata

C.so Massimo d'Azeglio, 48 – 10125 Torino, ITALY

P.Rizzi

Dipartimento di Chimica I.F.M.

Via Pietro Giuria,7 –10125 Torino, ITALY

mario.castiglioni@unito.it

Introduction

Mn_3O_4 - hausmannite synthesis has recently received some attention [1-8] in view of its use as an oxidation catalyst [9-12] and for its magnetic properties [2,5]. The main attention has been put on low temperature and/or rapid synthesis [1,2,3,4,7,8]. All the synthetic methods reported rely on solution chemistry and the time required to obtain Mn_3O_4 from the starting materials ranges from few hours to months, taking into account the preparation of the solutions, the filtration and the drying of the precipitates.

Due to their volatility and easy decomposition, transition metal carbonyls have been widely used as starting materials for the preparation of finely divided metal particles by plasma decomposition [13], by solution reaction [14,18, 20], by thermal [16] and laser decomposition [17] and by vapour-phase reactions [15,19]. Also metal oxides have been prepared by sonochemistry [20], laser pyrolysis [21,22] and solution chemistry [23,24], using metal carbonyls as starting materials. A molybdenum carbide, Mo_2C, has also been prepared from substituted metal carbonyls [25].

Microwave heating has been used in the production of small particles of different materials such as oxides [4,26-29] and sulphides [30,31].

Here we present a rapid, solid state, microwave assisted synthesis of Mn_3O_4 starting from the manganese carbonyl $Mn_2(CO)_{10}$ and oxygen gas. Though some difficulties can arise from the use of gases, dry chemistry offers, with respect to solution chemistry, the following advantages: easier handling of reactants and products, no need to remove solvents and, in some lucky cases, the purification of the products is not necessary.

Experimental

The manganese carbonyl does not absorb electromagnetic energy and cannot be directly heated by microwaves. The usual materials used as susceptors for solid state microwave assisted reactions heat too much and too rapidly to be used on heating pure metal carbonyls. To heat dimanganese(0) decacarbonyl high enough to promote the reaction, but sufficiently low to avoid extensive sublimation, a mixture of graphite and Celite™ (1:9 ratio) has been used as a susceptor. Pure $Mn_2(CO)_{10}$ (Aldrich), oxygen (SIAD) and a domestic microwave oven (SAMSUNG CE 116 KT), modified to allow inlet and outlet of gases, were used for the syntheses.

A small alumina crucible containing about 300 mg of the carbonyl and surrounded by the graphite/Celite™ (1:9 mixture) susceptor was introduced in a Pyrex vessel equipped with two connections for in and out gas. The manganese carbonyl was heated with 450 W power under slow oxygen flow for 3 minutes. The temperature of the susceptor rapidly rises up to about 100 °C, as measured with a shielded and grounded type K thermocouple. After few seconds the brown fumes evolving from the carbonyl started burning. After 1.5 minutes no further phenomena could be observed and the reaction was over. Two apparently different products were collected: a brown powder sublimed onto the walls of the Pyrex vessel (product I) and a darker powder left into the crucible (product II). Powder XRD spectra have been collected using a Siemens D5000 (Cu Kα radiation and Bragg–Brentano geometry) instrument, SEM images were obtained using a Leica Stereo Scan 420 instrument. TEM images have been obtained by using a 200 kV microscope, Jeol JEM 2010. Ft-IR spectra have been recorded using a Bruker EQUINOX 55 instrument

Results and discussion

The powder XRD spectra of both products I and II are depicted in Figures 1 and 2 respectively.

From XRD analysis, the brown product I appears to be Mn_3O_4, whereas the darker product II appears to be Mn_3O_4 contaminated by some MnO which can be formed at the high temperature reached [10] during the burning of the starting material into the crucible. The IR spectrun (KBr) of both product I and II ahows peaks at 632, 526 and 412 cm^{-1} which are in good agreement with those reported for hausmannite [32], whereas the peaks at 673, 608 and 500 cm^{-1}, which have been attributed to γ-Mn_3O_4 [7], are absent.
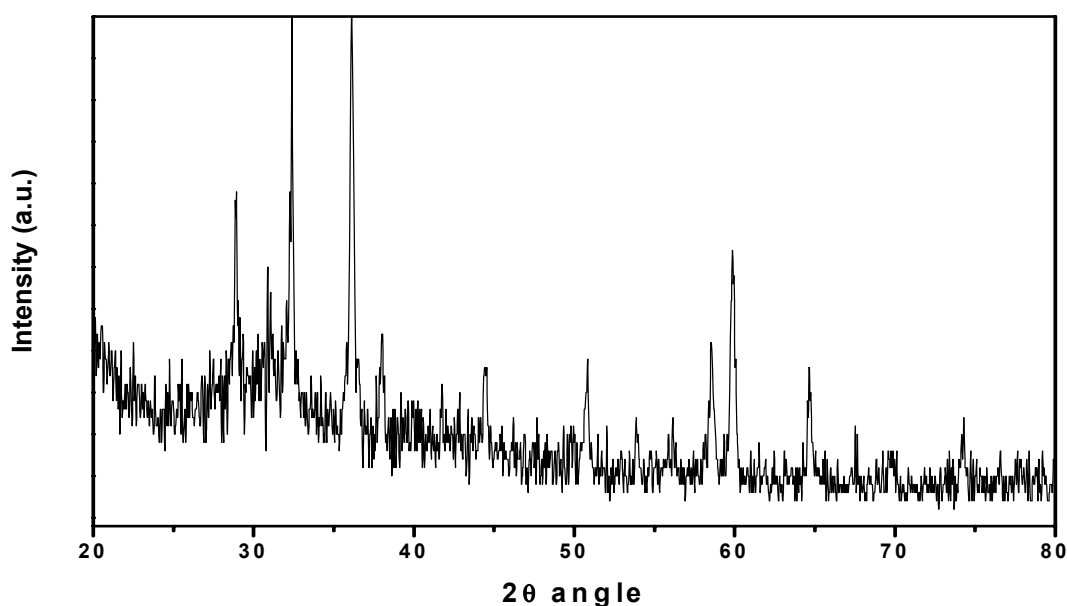
Figure 1 - Powder XRD of sublimated compound 1

66
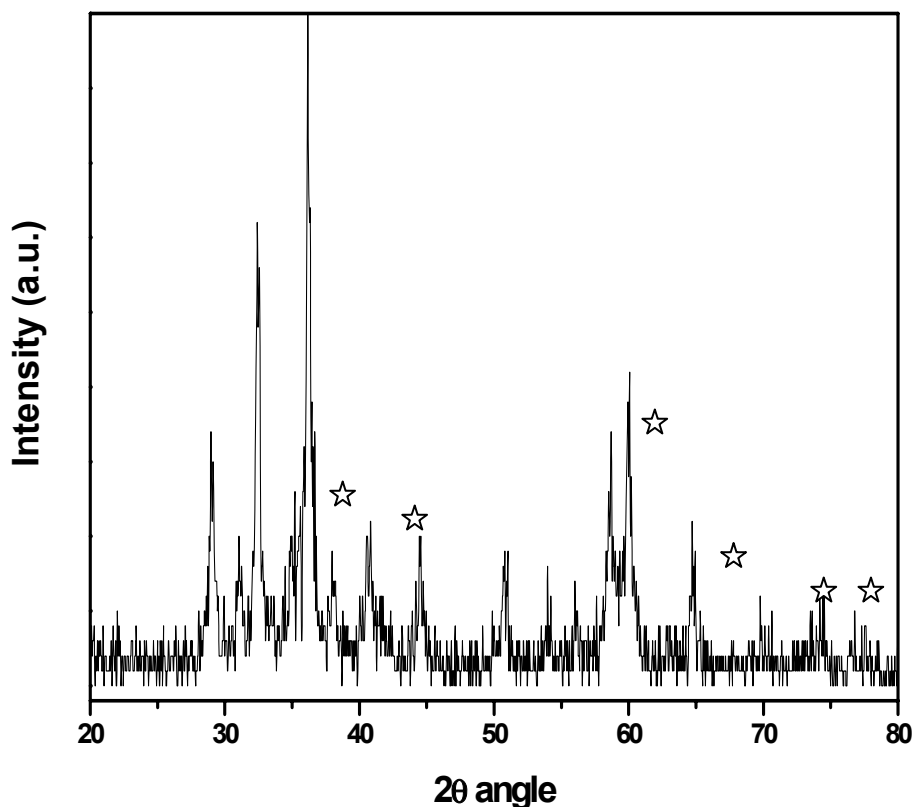
Figure 2 - Powder XRD of compound 2 left in the crucible: MnO
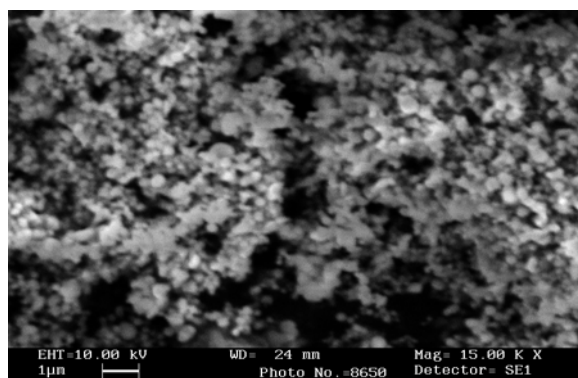
Figure 3 - SEM Image of compound I : Mn$_3$O$_4$

SEM image of compound I shows small rounded particles as depicted on Figure 3.

Product I, as observed by TEM (Figure 4), is formed by nanocrystalline rounded particles ranging from 10 nm to 30 nm that tends to aggregate by forming powders of hundreds of nm. As shown in the electron diffraction pattern (insert of Figure 4) an amorphous halo is present besides the spots typical of nanocrystals, implying that a fraction of the particles are produced in the amorphous state.

In Figure 5 TEM picture of product II is reported. Larger particles of about 50 nm are present, which appear to be completely crystalline to the electron diffraction. This finding agrees with the higher temperature experienced by compound II.
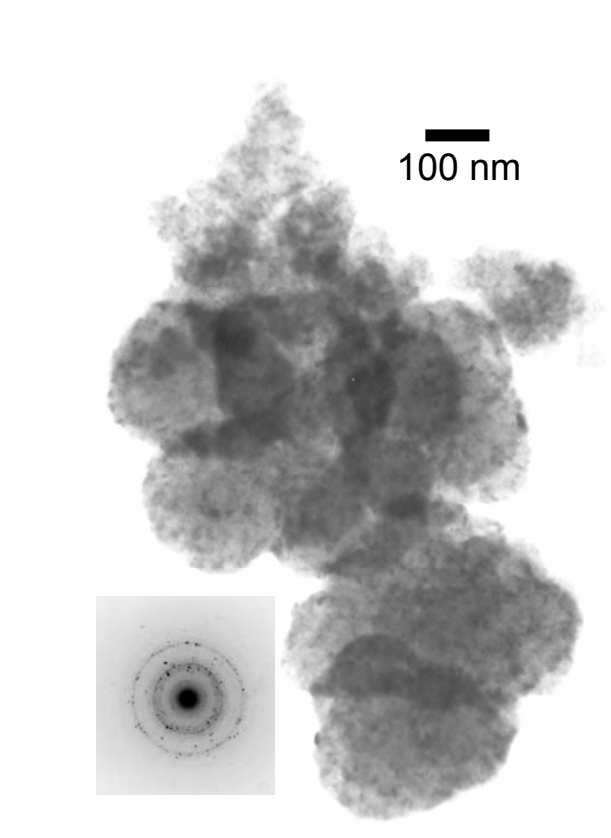
Figure 4 - TEM image of compound I
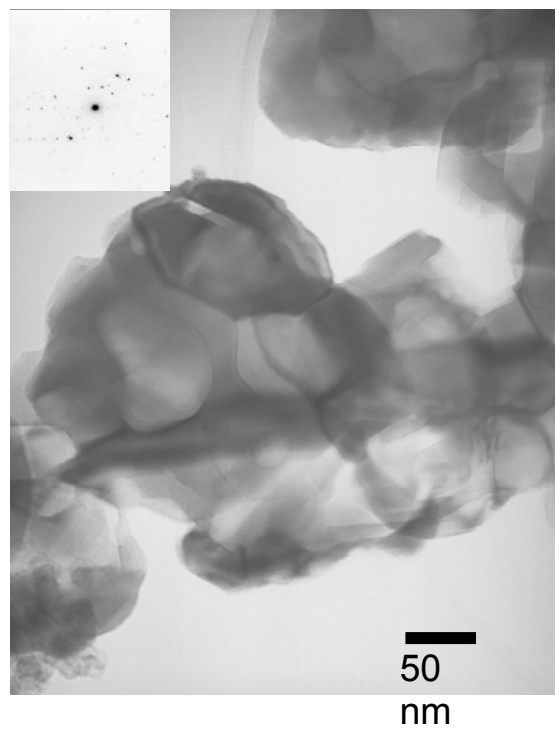
Figure 5 - TEM Image of compound II

Conclusions

Using solid state reactants, as metal carbonyls, which can be easily vaporised, together with microwave heating, it is possible to obtain highly crystalline nanometric metal oxides particles at relatively low temperature avoiding the use of solvents and tedious separation techniques.

Acknowledgements

References

[1] Y. Hu, J. Chen, X. Xue, T. Li, Mater. Lett.60 (2006) 383

[2] A. Vázques-Olmos, R.Redón, G. Rodríguez-Gattorno, M.E. Mata-Zamora, F. Morales-Leal,A.L. Fernándes-Osorio, J.M. Saniger, J. Coll.Interf.Sci. 20 (2005) 175

[3] A. Vásques-Olmos, R.Redón, A.L. Fernández-Osorio, J.M. Saniger, Appl. Phys. A 81(2005) 1131

[4] C. Bousquet-Berthelin, D. Stuerga, J. Mat. Sci. Letters 40 (2005) 253

[5] T.Ahmad, K.V.Ramanujachary, S.E. Lofland, A.k,Ganguli, J. Mater.Chem., 14 (2004) 3406

[6] Y.Liu, Z. Liu, G. Wang, Appl. Phys. A 76 (2003) 1120

[7] F.A. Al Sagheer, M.A. Hasan, L. Pasupulety, M.I. Zaki, J.Mater. Sci. Letters 18, (1999) 209

[8] Z.Weixin, W.Cheng, Z.Xiaoming, X.Yi, Q.Yitai, Sol.St.Ionics 117 (1999) 331

[9] E.J.Grootensdorst, Y.Verbeek and V.Ponec, J. Catal., 157 (1995) 706

[10] E.R.Stobbe, B.A. de Boer, J.W. Geus, Catal. Today, 47 (1999) 161

[11] L.Chen, T.Horiuchi, T. Mori, Appl.Catal. A, 209 (2001) 97

[12] G.Marbán, T. Valdés-Solís, A.B. Fuertes, Phys.Chem.Chem.Phys., 6 (2004) 453

[13] J.R.Brenner, J.B.L.Harkness, M.B.Knickelbein, G.K.Krumdick, C.L.Marshall, Nano-structured Materials 8 (1997) 1

[14] V.Le Rhun, E.Garnier, S.Promier, N.Alonso-Vante, Electrochem.Commun. 2, (2000) 475

[15] J.A.Rodriguez, J.Dvorak, T.Jirsak, J.Hrbek, Surf. Sci.490 (2001) 315

[16] M.Bron, P. Bogdanoff, S.Fiechter, M.Hilgendorff, J.Radnik, I.Dorbandt, H.Schulenburg, H.Tributsch, J.Electroanal.Chem. 517 (2001) 85

[17] S.Martelli, O.Bobatí-Miguel, L.de Dominicis, R.Giorni, F.Rinaldi, S.Veintemillas-Verdaguer, Appl.Surface Sci., 186 (2002)562

[18] L.Guczi, A.Beck, A.Horváth, D.Horváth, Topics in Catal. 19 (2002)157

[19] Z.H.Wang, C.J.Choi, B.K.Kim, J.C.Kim, Z.D.Zhang, Carbon 41 (2003) 1751

[20] A.Gedanken, Ultrason. Sonochem., 11 (2004) 47

[21] M.P.Morales, S.Veintemillas-Verdaguer, C.J.Serna, J. Mater.Res., 14 (1999) 3066

[22] S.Martelli, A.Mancini, R.Giorgi, R.Alexandrescu, S.Cojocaru, A.Crunteanu, I.Voicu, I.Morjan, Appl. Surf. Sci., 154-155 (2000) 353

[23] G.A.Rizzi, R.Zanoni, S.Di Siro, L.Piriello, G.Granozzi, Surface Sci., 462 (2000) 187

[24] R.Giordano, P.Serp, P.Kalck, Y.Kihn, J.Schreiber, C.Marhic, J.-L.Duvail, Eur. J. Inorg. Chem., (2003) 610

[25] M.K.Kolel-Veetil, S.B.Qaadri, M.Osofski, T.M.Teller, Chem. Of Mater., 17 (2005) 6101

[26] H.Wang, J-Z.Xu, J-J.Zhu, H-Y.Chen, J.Crys. Growth, 244 (2002) 88

[27] D-S.Wu, C-Y.Han, S-Y.Wang, N-L.Wu, I.A. Rusakova, Mater. Lett., 53 (2002) 155

[28] A.Agostino, A.Arrais, E.Bonometti, M.Castiglioni, C.Leonelli, MISA 2004, Ancona, Italy, October 6-8, 2004

[29] H.C.Park, S.W.Kim. S.G.Lee, J.K.Kim, S.S.Hong, D.G.Lee, S.S.Park, Mat.Sci. and Eng., A363 (2003) 330

[30] A.Agostino, E.Bonometti, M.Castiglioni, P.Michelin Lausarot, Mat.Res.Innovat., 8 (2004) 41

[31] E.Bonometti, M.Castiglioni, P.Michelin Lausarot, C.Leonelli, F.Bondioli, G.C.Pellacani, A.A.Barba, Mat.Res.Innovat., 10 (2006) 148

[32] J.B.Macstre, E.F.Lòpez, J.M.Gallardo-Amores, R.R.Casero, V.S.Escribano, E. P.Bernal, Int.J.Inorg.Materials, 3 (2001) 889

SODALITE HYDROTERMAL SYNTHESIS STARTING FROM KAOLINITE: COMPARISON BETWEEN CONVENTIONAL HEATING AND MICROWAVES HEATING

M. Savazzi, C. Mazzocchia, G. Modica, F. Martini

Dipartimento di Chimica, Materiali e Ingegneria Chimica "G.Natta"

Politecnico di Milano

Piazza Leonardo da Vinci 32, 20133 Milano - Italy

marco.savazzi@chem.polimi.it

Abstract

Sodalite was synthesized in a hydrotermal system by using conventional heating and microwaves heating, so a comparison between the two heating systems has been made. Products were characterized by means of X-ray powder diffraction (XRD) and High Resolution Scanninc Microscopy (HRSEM). Microwaves interaction with this particular reactants can increase the reaction rate and modify sodalite grain morphology. Sodalite was synthesized in 4h instead of 14h required by conventional heating and its grains were smaller than grains obtained with conventional heating. Results showed macroscopic microwaves interaction that could be related to a specific reaction step.

Introduction

Sodalite is a volcanogenic mineral belonging to the silicate class. Silicate minerals are divided into many subclasses and sodalite belongs to the feldspathoid group, same subclass of the zeolites: the tectosilicates. This subclass is often called framework silicates because their structures are tridimensional lattices made by polyhedrons $[(Si,T)O_n]$ binding connected with oxygen bridges. Usually cation T is aluminum and n = 4, so the polyhedrons are aluminosilicate tetrahedron $[SiAlO_4]$.

Sodalites have this generic formula:

$$M_m^{q+} [(Al_nSi_{12-n}O_{24})^{n-}] X_x^{r-} \cdot a Z \qquad \text{where} \qquad q\,m - r\,x = n$$

M is a divalent or monovalent cation, X is the anion, while Z can be H_2O or neutral compound. Sodalite lattice is constituted of $[AlO_4]^{5-}$ and $[SIO_4]^{4-}$ tetrahedrons which provide a total negative charge as for all silico-aluminate compounds. Some positive cations M_m^{q+} are able to coordinate themselves with active oxygen and other negative species X_x^{r-} that are in the lattice, balancing the tetrahedron negative charge. In this way the sodalite structure could contain different cations (generally alkali and alkaline-heart metals) and different anions. Furthermore it is possible to find neutral molecule (Z) like water. The ideal formula of natural sodalite is $Na_8 [(Al_6Si_6O_{24})] Cl_2$ and this kind of sodalite is the object of this work.

As described above, different sodalites can have different compositions depending on the nature of the cations, the anions and neutral molecules, but all of them have the same tridimensional lattice usually called 'sodalite-cage' or 'β-cage'. This elementary geometric structure is also the base unit of many other aluminosilicate, in particular many zeolites (Figure 1).

Sodalite can undergo a ionic exchange as many other zeolites and this capability can be exploited to prepare sodalites with different compositions, as for example reported by Taylor [1] starting from natural sodalite (Figure 2).

Sodalite is a crystalline compound which is able to include into its structure different cations and anions, in particular halides, therefore it has been studied as a possible aluminosilicate matrix that might trap the radioactive cations, in form of chloride, coming from the nuclear waste electrorefining treatment [2, 3], so it is very important to find out a simple synthesis route to produce natural sodalite with good yield.

Sodalite synthesis has already been the object of many studies, different methodologies with different starting reagents have been introduced by many authors. All these different synthesis routes can be divided into two classes: solid state reactions and hydrothermal reactions. The second ones are more interesting than the other class because they are mild reactions and simple to carry out. In general, hydrothermal synthesis is based on the preparation of a water solution with a definite pH, which is heated to low temperature and low pressure depending on the type of reaction. Friedel [4, 5], for example, was the first researcher who studied sodalite synthesis starting from mica muscovite $[KAl_2(Si_3Al)O_{10}(OH)_2]$ as silicon and aluminum source. Mica was milled finely, then it was placed in a basic water solution also containing sodium chloride and finally the solution was treated in a platinum lined autocl ave at 500 °C. Barrer et al. [6] used natural kaolinite $[Al_2Si_2O_9H_4]$ as Si and Al source and used milder reaction conditions with respect to Friedel.

In this work is presented a detailed study of the methodology proposed by Barrer et al. [6] to optimize the natural sodalite synthesis and, in particular, it has been taken into account two different heating system: conventional heating and microwaves heating. It has been done a comparison between the two reaction system underlining differences and specific advantages of the new microwave technology.
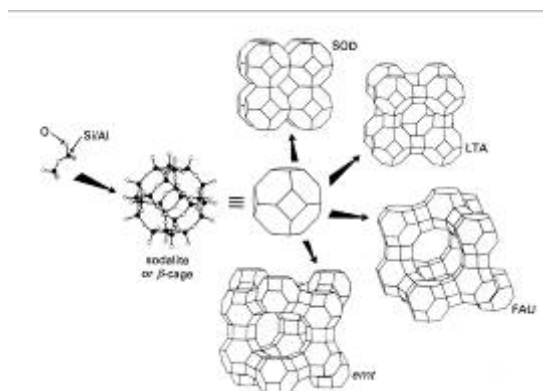
Figure 1 - Zeolite structures made by sodalite cages

Experimental section

The synthesis method proposed by Barrer et al. [6] has been used to produce sodalite starting from a natural reagent without heavy reaction conditions: 90 °C and ambient pressure. It has been decided to use the same reaction conditions of the original method but using only a tenth of the original reagents weights. In this way it has been possible to use only a little volume of reaction.

All the synthesis have been made adding 0.2 g of kaolinite and 1 g of NaCl into a 20 ml of a basic water solution (NaOH 4 M). Afterwards the solutions have been put into closed cylindrical reactor vessels made by Teflon (100 ml volume) which seal was guaranteed by a polypropylene external structure. The synthesis temperature has been fixed at 90 °C so the reactions have been made at nearly ambient pressure. The reactor vessels and the reactancts concentrations have been the same for all the synthesis, instead the reaction times have been changed to study the rate of the reaction.

Since the main aim of this work has been to investigate the synthesis of sodalite with particular attention for the heating method, many reactions have been carried out with two different heating methods identical conditions except for duration. Some synthesis have been made inserting the reactor vessels in a conventional heater (Mazzali Vuototest) which had been preheated at 90 °C, on the contrary other syntheses have been irradiated with microwaves. In this case the vessels have been put on a rotary plate into a microwave heater and the temperature has been measured with a thermocouple into one of the vessels. The microwave oven used for this study was a Milestone, mod. Ethos 1600, operating at a frequency of 2.45 GHz with a maximum power of 1 kW. All the syntheses have been made without magnetic stirring.

After the heating treatment the reactor vessels have been cooled down to room temperature, the content have been filtered and washed with plentiful water. The powder produced was separated from solution on filtering membrane (Pall HT-450 100/Pk with 47 mm diameter and 0.45 μm pore diameter) using a vacuum separation induced by a water pump. In the same separation system the powders have been washed with plentiful water and then have been dried at 110 °C overnight. Finally the products have been milled and analyzed.

$$Na_8 [(Al_6Si_6O_{24})]Cl_2$$

$$Li_{4.4}Na_{3.6} [(Al_6Si_6O_{24})]Cl_2$$

$$Li_8 [(Al_6Si_6O_{24})]Br_2$$

$$Li_8 [(Al_6Si_6O_{24})]Cl_2$$

$$Na_{5.5}K_{2.5} [(Al_6Si_6O_{24})]Cl_2$$

$$Na_8 [(Al_6Si_6O_{24})]I_2$$

$$Na_{0.3}K_2Rb_{6.3} [(Al_6Si_6O_{24})]Cl_2$$
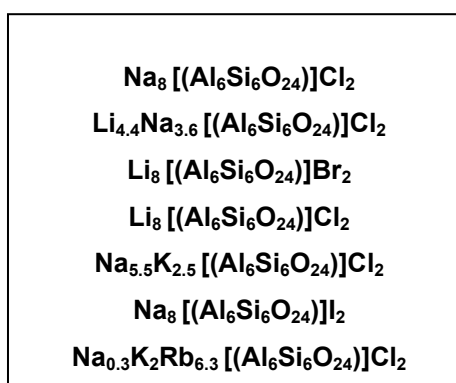
Figure 2 - Sodalite compositions produced by Taylor [1]

Characterization

The powders have been analyzed by X-ray powder diffraction (XRD). The XRD patterns have been recorded with a diffractometer Philips, PW 1710 ($\lambda = 1.542$) working at 40 kV and 30 mA with a scansion speed of 1° 2θ/min. Furthermore powder morphology was examined with high resolution scanning electron microscopy (HRSEM), using a FEG-SEM LEO, Mod. 1530, equipped with a secondary high resolution electron detector over the objective lens, a conventional secondary electron detector positioned into the chamber and a retro diffused sparking electron detector Centaurus, RBSD Rutherford Back Scattering Detector.

Natural kaolinite

Firstly natural kaolinite, which is the precursor of Al and Si and which come from a quarry of Sardinia, has been characterized to understand its degree of purity and its main properties. Kaolinite is a natural clay so it might not be pure as the commercial reagents but it is cheaper than the latter. Different techniques have been used to analyze kaolinite: XRD, SEM, TG and chemical analysis.

First an X-ray diffraction of the natural kaolinite has been done and in Figure 3 the XRD pattern has been compared with the kaolinite peaks coming from a XRD database. It has been observed that the powder was not composed only by kaolinite but there was also an allotropic form of silica: cristobalite. Cristobalite main peaks, which are the highest of the whole spectrum, cover four secondary kaolinite peaks (20÷23° in 2 θ). To confirm this result a chemical analysis of the powder has been made and the result has shown the Si/Al weight ratio of 6.18 which is about six times bigger than the stoichiometric Si/Al kaolinite ratio ($Al_2Si_2O_5(OH)_4$). Therefore kaolinite purification method has been developed.
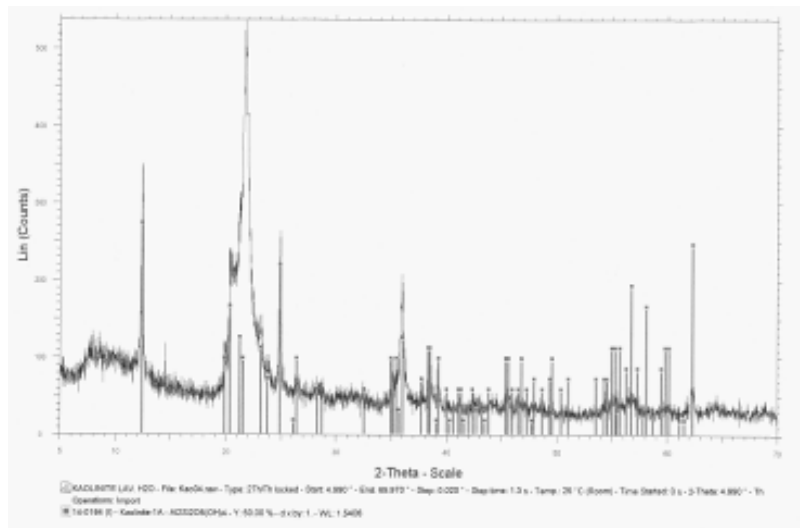
Figure 3 - X-ray spectrum of natural kaolinite compared with standard kaolinite peaks (vertical lines)

Since kaolinite does not dissolve in sodium hydroxide concentration less than 2M, whilst cristobalite easily does also in solutions with lower molar concentration, the purification of kaolinite has been obtained using 0.5 M NaOH solution at 60 °C for 7h under magnetic stirring. After purification a total weight loss which has never exceed 62% was recorded as well as XRD analysis (Figure 4) which demonstrated a decrease in cristobalite peaks.

Scanning electron microscopy observations to evidence difference in the morphology of the natural and purified kaolinite are reported (Figure 5a and 5b). In the purified kaolinite it has been observed the typical lamellar hexagonal structure while, on the contrary, natural kaolinite shows unstructured, fine and inhomogeneous crystals.

Finally thermogravimetric analysis of natural kaolinite and purified kaolinite have been collected to detect the cristobalite amount into the starting kaolinite. The kaolinitic crystal can be decomposed into an amorphous material, called metakaolinite, with the structural water release caused by thermal treatment at 500-700 °C. On the contrary cristobalite withstand this thermal treatment without any weight change.
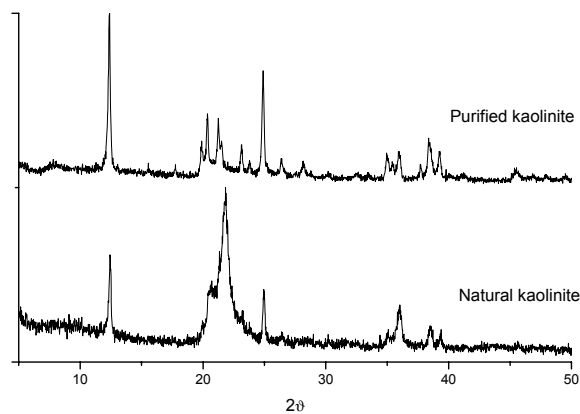
Figure 4 - Natural and purified kaolinite XRD spectrum
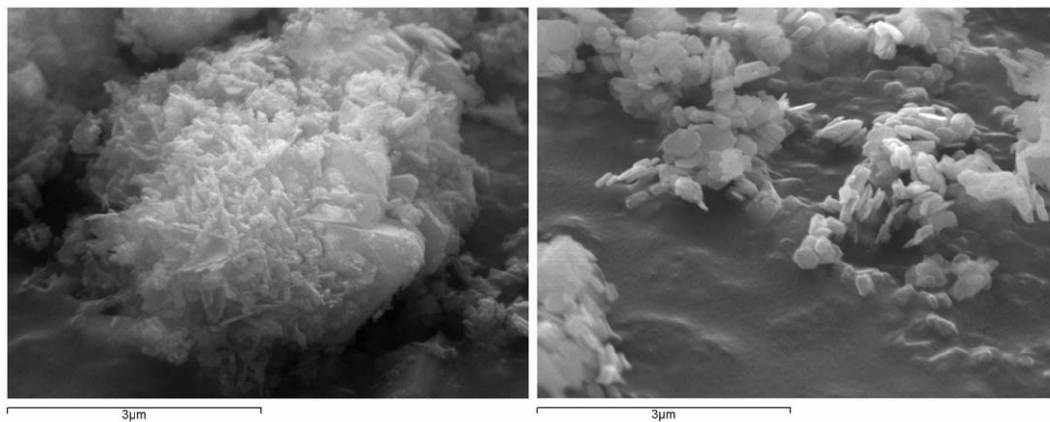
Figure 5 - a) Natural kaolinite; b) Purified kaolinite

The decomposition reaction can be represented with this stoichiometry [7]:

$$Al_2Si_2O_5(OH)_4 \xrightarrow{500°C-700°C} Al_2Si_2O_7 + 2H_2O$$
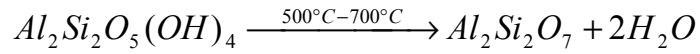
The purified kaolinite TG analysis showed that the weight loss between 500 °C and 700 °C was 12.3% witch represent only the structural water loss, instead the natural kaolinite TG analysis showed a weight loss of 4.7% witch represent the kaolinite, mixed with cristobalite structural water loss, so it has been possible to calculate the kaolinite quantity into the starting powder since the weight loss could be related only to the kaolinite decomposition: *4.7/12.3*100=38.21%*. This result has confirmed the weight loss measured during the purification process.

Results and discussion

Sodalite synthesis has been made starting with purified kaolinite. The hydrothermal reaction can be easily represented with this ideal stoichiometry equation:

$$3Al_2Si_2O_9H_4 + 2NaCl + 6NaOH \xrightarrow{water} Na_8Al_6Si_6O_{24}Cl_2 + 9H_2O$$
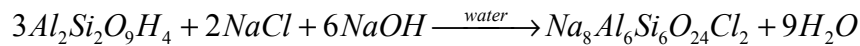
A lot of tests have been made at different reaction times using the two heating systems whose comparison represents the main objective of the work.

Conventional heating results

The reactor vessels were inserted into the heater preheated at 90 °C so that to reduce the transition time necessary to raise the water solution temperature till 90 °C. However the transition time has been overlooked compared with the long reaction times. Powders obtained from each synthesis have been analyzed with XRD analysis and the yield has been calculated taking into account the theoretical reaction stoichiometry only for every reaction that produced pure sodalite.

The experimental results have shown that the synthesis path starting from kaolinite till the pure sodalite in less than 15 hours (Figure 6) showed a slow disappearance of kaolinite peaks and a fast increase of sodalite peaks. After 15 hours, kaolinite peaks have completely disappeared. In Figure 6, 14 hours test XRD analysis exhibits all the peaks from sodalite crystals together with the kaolinite main peak at 12.39 of 2θ°. During the transformation from kaolinite to sodalite no other crystalline phases have ever been formed. A lot of tests have been also done with reaction times longer than 15 hours and the sodalite yields have been calculated, but the yield growth has never been so high as during the first 15 hours. The plot reported in Figure 7 shows the reactions' yields evolution with treatment time: between 15h and 24h the yield increases by only 6.63 percentage points in 9 hours, on the contrary in the first 15 hours the yield grows up to 66.2%.
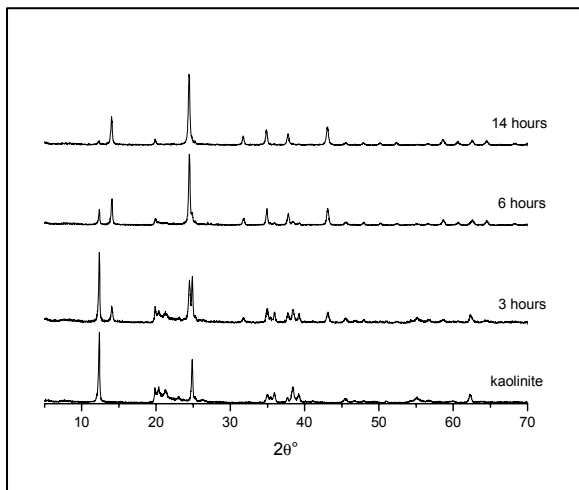
Figure 6 - XRD analysis (conventional heating)   **Figure 7 - Reactions yield**
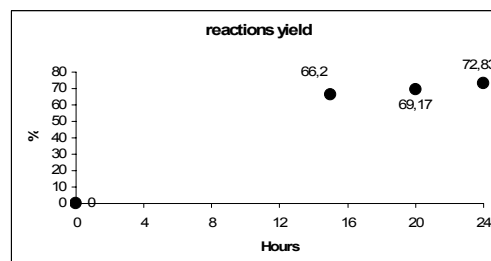
Accordingly to these results and in order to compare the two different synthesis methods, it has been decided to consider the total kaolinite disappearance and the achievement of pure sodalite as the end of the reaction since from this point on the yields have not grown so much.

Pure sodalite obtained in conventional heating reaction has been analyzed with high resolution scanning electron microscopy. Figures 8a, 8b and 8c show three images of the same product at increasing magnification. They have shown the grain dimension being approximately 200 nm. Figure 8d (enlargement of Figure 8c) shows a sodalite grain with the proper unit cell shape: truncated octahedron made up of six square faces and eight hexagonal faces (to be compared with Figure 1).

Microwaves heating results

The same reactor used for conventional heating tests have been used in the microwave oven. The vessel was put into a rotary carousel so that microwaves could interact with the water solutions in a more homogeneous way and the reaction temperature was controlled with a thermocouple inserted into one vessel. The microwave oven is equipped with an automatic power control to keep the heating rate following the programmed rate: in 10 minutes from room temperature to 90 °C followed by soaking with a fluctuating power emission always less than 150 W. The achievement of 90 °C has been considered as the starting point of reactions.

Tests have been made starting with treatment of 30 minutes to longer than 4 hours; at the end the products have been analyzed with XRD (Figure 9). The analysis have shown the same results of conventional heating reactions, sodalite has been quickly produced and, on the contrary, kaolinite has been slowly dissolved, but the synthesis time has been different from conventional heating reaction time: pure sodalite has been obtained only after 4 hours. Afterwards tests have been made with reaction time longer than 4 hours to measure the yield but it has been observed a low yield increase even after very long synthesis. After 4 hours of reaction the yield of sodalite was 80.23%.
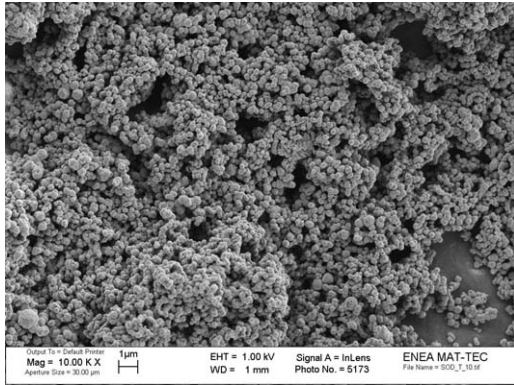
Figure 8a
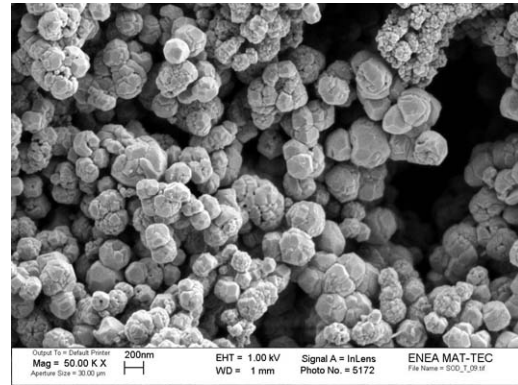
Figure 8b
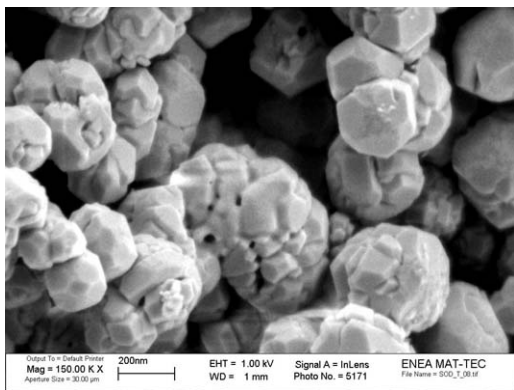
Figure 8c
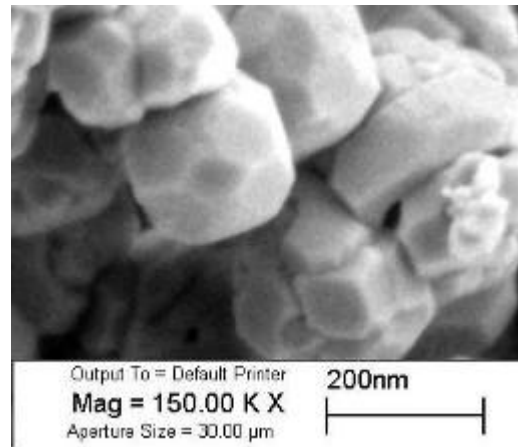
Figure 8d

Figure 8 - Sodalite obtained in conventional heating reaction analyzed with HRSEM
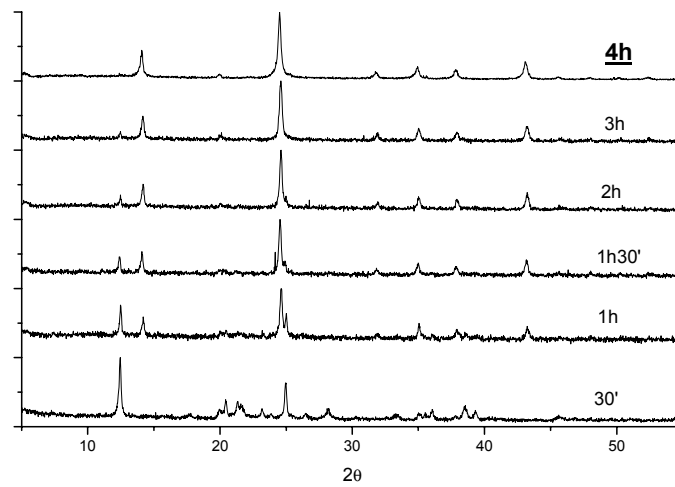
Figure 9 - XRD analysis (microwaves heating)
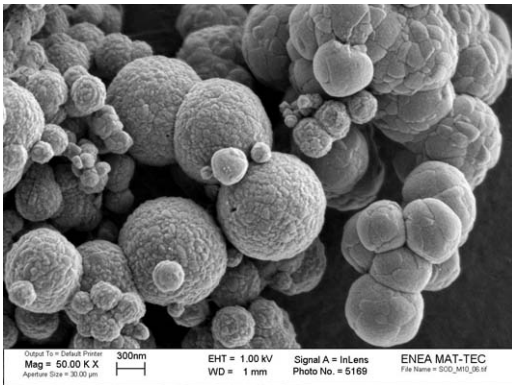
Figure 10a
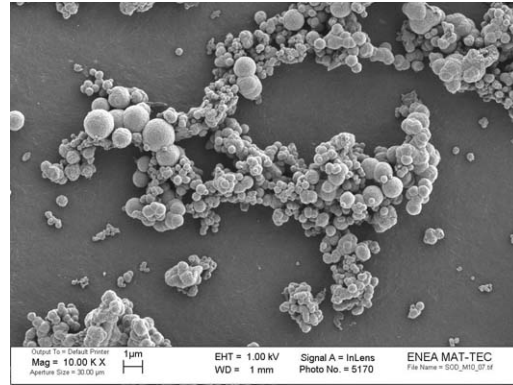
Figure 10b
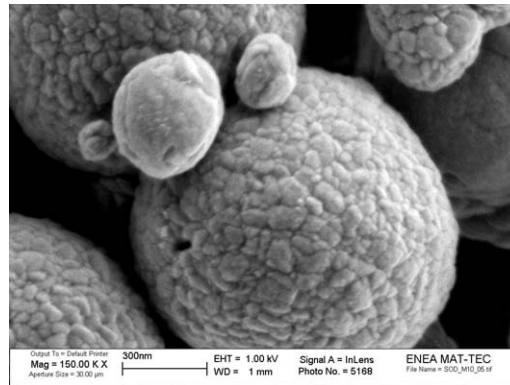
Figure 10c

Figure 10 - Sodalite obtained in microwaves heating reaction analyzed with HRSEM

Pure sodalite obtained in microwaves heating reaction has been analyzed with high resolution scanning electron microscopy to compare the morphology with sodalite grains obtained in conventional heating reaction. Figure 10 shows three images where a great difference from the images of sodalite obtained by conventional heating can be observed. Spherical agglomerates made up of sodalite crystals 40-70 nm in diameter without a well-defined geometric shape are visible.

Cristobalite effect

All the results reported above have been obtained starting with purified kaolinite. In this section we describe the cristobalite effect on the sodalite reaction to verify the importance of the purification process of kaolinite before reaction. A lot of syntheses have been made with the same methodology described above but using natural kaolinite as received, so the reactions have been made also in presence of cristobalite.
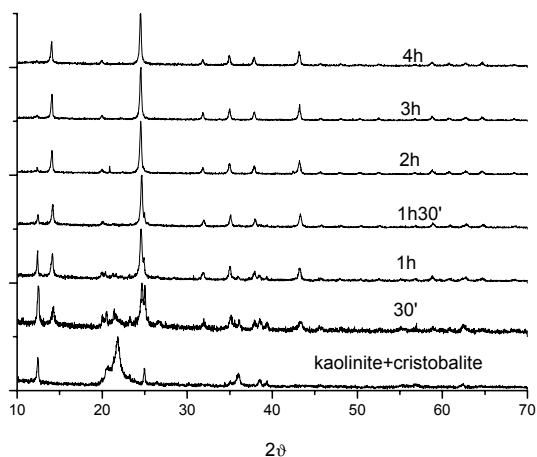
Figure 11a - Microwaves heating
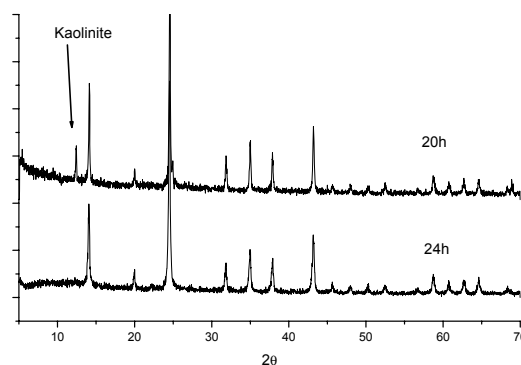
Figure 11b - Conventional heating

Products have been analyzed with XRD diffraction and some results are shown in Figure 11a (microwave heating) and 11b (conventional heating). Pure sodalite has been obtained in both heating methods and, also in this case, it is possible to see the reaction rate increase as a consequence of microwaves irradiation. Cristobalite has not affected the sodalite synthesis, since it dissolves at the beginning of reaction and probably it has not participate to the formation of sodalite since the reaction yields, taking into account only the real quantity of kaolinite, are similar to the yields obtained from purified kaolinite: *76.08%* microwave heating after 4h; *72.66%* conventional heating after 24h. These results have shown that cristobalite does not affect the reaction yield so the purification process is not absolutely necessary.

Discussion

Sodalite synthesis comparing conventional heating and microwaves heating has provided a lot of experimental data. They have shown two important macroscopic results about microwaves effect on hydrothermal synthesis:

- *Reaction rate*: Pure sodalite has been produced faster than conventional heating with a remarkable reduction in the reaction time;

- *Morphology*: Sodalite crystals have smaller dimensions than crystals obtained in conventional heating but they do not have a specific geometric shape and they agglomerated in spherical systems.

Besides macroscopic results, analysis of the microwaves effects at microscopic point of view could be greater attractive to understand the interactions between microwaves and chemical reactions, so it has made an attempt to explain the results of this work. The exact microwave effect on chemical reaction is difficult to understand deeply but with experimental results and other literature works it has been possible to suppose some interaction mechanisms that should be verified with specific experimental tests.

Microwaves could interact with chemical substance and materials in different ways depending on substances physical and chemical proprieties [8]. In this work microwaves interact with water quickly increasing the system temperature, but this effect could not explain the lower reaction time obtained in microwave heating.

80
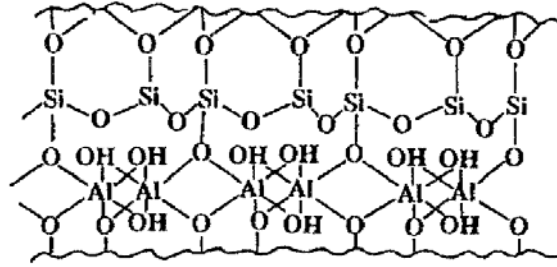
Figure 12 - Kaolinite layer

To better understand the positive microwave effect a deep insight of the sodalite synthesis mechanism should be considered. Bauer et al. [9, 10] had studied the kaolinite dissolution kinetics and mechanism in basic solution with KOH concentration between 0.1 M and 4 M, with temperatures between 35 °C and 80 °C. Their work is based on the determination of silicon and aluminum concentration after different treatment time, and on products XRD analysis. Bauer showed that kaolinite, in basic solutions, dissolves with rate depending on KOH concentration, temperature and solid/solution ratio. Furthermore he studied the chemical mechanism of kaolinite dissolution.

Moreover it should be considered that kaolinite is a clay layered mineral in which each layer is made up of one silicon tetrahedral sublayer bonded with one aluminum octahedral sublayer, and layers are bonded to each other with hydrogen bonds (Figure 12). Dissolution rate of kaolinite depends on aluminum or silicon surface sublayers detachment which is related to the superficial charge taken by the two different superficial sublayers, this phenomenon strictly depends on solution pH: if pH is less than 11, charges are mainly concentrated on silicon tetrahedral sublayers, on the contrary charges are mainly located on aluminum octahedral sublayers [9].

In this work sodalite synthesis have been made into high pH solution so kaolinite dissolution is related with the detachment of octahedral aluminum sublayers due to the higher concetration of negative charges on those structures. Bauer et al. [10] workfinally showed that kaolinite dissolution rate is related with the Al-O-Si hydrolysis, which is the cause of the detachment of aluminium sublayers, and hence to the total dissolution rate of kaolinite. The surface charges on aluminium sublayer (OH-) promotes the hydrolysis reaction represented in this stoichiometric equation [9, 10]:

$$O_{3/2} \equiv Si - O_{2/2} - Al = (OH)_{4/2S} + H_2O_L + OH^- \longrightarrow O_{3/2} \equiv Si - OH + Al(OH)_4^-$$
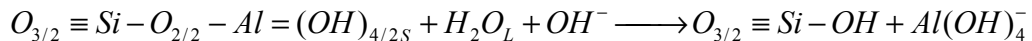
The experimental results presented in this work indicate that the rate determining step of sodalite synthesis is kaolinite dissolution because sodalite crystallization is faster than it, as a matter of fact, XRD analysis showed slow disappearance of kaolinite and a fast crystallization of sodalite. If this result is interpreted with Bauer's theory the microscopic microwaves effect should be evidenced in the kaolinite dissolution reaction and in particular in the Al-O-Si bonds hydrolysis. Due to the presence of hydroxyl groups (bonded with Al) kaolinite is certainly susceptible to microwaves [11] and it is possible to suppose that this interaction could promote exactly the hydrolysis of aluminum sublayers increasing the kaolinite dissolution and then enhancing the sodalite formation rate. Besides the effect on reaction rate, microwaves interact also with the crystallization step giving different sodalite crystals morphology, mainly smaller in size,

when compared to conventional heating. Solid crystallization in hydrothermal system occurs following the Ostwald rule [9], furthermore two steps characterize it: nucleation and crystal growth.

SEM analysis have shown conventional heating reactions produced regular grains near 200nm, on the contrary microwaves reaction produced irregular grains smaller than grains obtained with conventional heating. This result implies a microwave interaction with nucleation and crystal growth: microwaves could increase nucleation rate bringing about the slowing down of crystals growth.

Conclusion

The comparison between conventional heating and microwave heating on the hydrothermal sodalite synthesis showed that microwaves interaction with this particular reactants can increase the reaction rate and modify sodalite grain morphology.

It has been made an attempt to identify the real microscopic interaction between microwaves and sodalite synthesis. This interaction is great difficult to identify exactly but it has been possible to determine the reaction steps in which microwaves could cause macroscopic effect obtained with experimental results.

Acknowledgment

References

[1] Taylor D. – "Cell parameter correlations in the aluminosilicate sodalites" – Contrib. Minerl. Petrol, 51 (1975) 39-47

[2] J.J. Laidler, J.E. Battles, W.E. Miller, J.P. Ackerman, E.L. Carls – "Development of Pyroprocessing Technology" – Progress in Nuclear Energy 31 (1997) 131-140

[3] J.P. Ackerman, T.R. Johnson, L.S.H. Chow, E.L. Carls, W.H. Hannum, J.J Laidler – "Treatment of wastes in the IFR fuel cycle" – Progress in Nuclear Energy 31 (1997) 141-154

[4] Ch. G. Friedel - Bull.soc.fr.Min. 13 (1890) 129

[5] Ch. G. Friedel - Bull.soc.fr.Min. 13 (1890) 182

[6] R.M. Barrer, J.F. Cole, H. Sticher – "Chemistry of soil minerals – part V: Low Temperature Hydrotermal Transformations of Kaolinite" – Chem. Soc. (A) (1968) 2475

[7] "Ullmann encyclopedia of industrial chemistry – Wiley-VCH, 6th ed" Weinheim 2003, p.635

[8] K.J. Rao, B. Vaidhyanathan, M. Ganguli, P.A. Ramakrishan – "Synthesis of inorganic solid using microwaves" – Chem. Mater. 11 (1999) 882

[9] A. Bauer, B.Velde, G. Berger – "Kaolinite transformation in high molar KOH solutions" – Applied Geochemistry 13 (1998) 619-629

[10] A. Bauer, G. Berger – "Kaolinite and smectite dissolution rate in high molar KOH solutions at 35 °C and 80 °C" – Applied Geochemistry 13 (1998) 905-916

[11] M. Panneerselvam, K. J. Rao – "Novel microwave method for the synthesis and sintering of mullite from kaolinite" – Chem. Matter. 15 (2003) 2247-2252

SYNTHESIS OF FUNZIONALIZED MESOPOROUS SILICA ASSISTED BY MICROWAVE IRRADIATION

M. L. Saladino, A. Spinella, E. Caponetti, D. Chillura Martino

Dipartimento di Chimica Fisica, Università degli Studi di Palermo

Parco d'Orleans II, Viale delle Scienze pad. 17 – 90128 Palermo - Italy

Abstract

The microwave assisted synthesis of neat mesoporous silica, functionalized with neodymium oxide is presented and compared with that performed by conventional methods. The mesoporous silica, whose properties such as a high specific surface area, tuneable pore size and a narrow pore size distribution are well known, was prepared at 30 °C by using cetyltrimethylammonium bromide micelles as template and then calcinated in the presence of air at 550 °C for 4 hours. Once synthesized, mesoporous silica was impregnated with neodymium oxide by using the incipient wetness method. Microwave irradiation was undertaken in both steps, synthesis of mesoporous silica and its impregnation, by using an apparatus operating at 2.45 GHz frequency and tuneable power. Samples were characterized by X-Ray Diffraction, Scanning Electron Microscopy and Energy Dispersive X-ray technique.

1. Introduction

Mesoporous materials known as MCM (Mobil Composition of Matter) represent one of the most interesting discoveries in the field of material chemistry. These materials can be depicted as arrays of pores having size in the range between 2 and 50 nm, organised in hexagonal (HMS and MCM-41), cubic (MCM-48) or lamellar (MCM-50) structures. Such materials are characterised by long-range order, surface area higher than 700 m^2g^{-1} and easy pores accessibility. These features have allowed the use of MCM materials in the catalysis for many petrol-chemical processing [1-4], for redox process in liquid phase [6,7], as heteropolyacid supports [5], and as highly efficient adsorbents [8,9].

Among the various classes of structures, MCM-41 can be considered the most important mesoporous material. Cylindrical pores, whose length results in the range of microns, separated by amorphous silica walls and organised in a hexagonal long-range structure, constitute it. The HMS material assumes a similar structure even if the pores order extends to lower distances [10].

Functionalised mesoporous materials display interesting properties. Materials obtained by using mixtures of silicates and aluminates as precursors, exploiting the acid properties of aluminium, have been successfully used in the catalitic cracking [11,12], those containing alkaline-earth and transition metals display basic and redox properties, respectively, and have been used as catalysts [13,14]; materials containing lanthanide ions assume acid properties [15,16]. Particular attention has been devoted to rare earth oxides supported on solid surfaces since their photophysical properties may be modified by interaction with the host structures [17-19]. These properties are interesting for the development of new materials in optoelectronic technology applications such as optical memory devices, lasers and fluorescence matrices [20].

MCM-41 synthesis procedure, proposed firstly by Kresge et al. in 1992 [21], is based on the acid (or basic) hydrolysis of silicate precursors by using ionic surfactant liquid crystals as templates. Several reaction mechanisms have been proposed [22, 23]. Beck and coworkers [22] have asserted that the material structure is determined by the self-organisation of surfactant in the liquid crystals. In the first step of the synthesis, the surfactant molecules self-assemble forming cylindrical micelles that organise themselves in a hexagonal structure. This step is followed by the inorganic skeleton (silica or silica-alumina) formation around the cylindrical liquid crystal structure. Other authors [23] have demonstrated that both surfactant and silicate anion contribute to the formation of a supramolecular structure. Changing opportunely the chemical nature of surfactant and of silicate precursors, their concentration, the synthesis temperature and the reaction time, it is possible to control the pores diameter and the walls thickness. A final calcination process allows destroying the surfactant aggregates from inside the pores and to obtain the mesoporous material. The hexagonal structure of the liquid crystals is maintained after calcination [22, 23].

The hexagonal mesoporous silica (HMS) is obtained, by applying the same method, from a solution of a non-ionic surfactant. The material forms because the neutral inorganic precursor interacts with the non-ionic surfactant via hydrogen bonds [24].

Recently, the microwave-assisted synthesis of molecular sieves is considered to be a promising field of research due to several fascinating advantages including the homogeneous heating throughout the reaction vessel that results in a more homogeneous nucleation and shorter crystallization time [25-29] compared to the conventional hydrothermal method. Most of microwave preparations reported in literature involve the use of microwave ovens in which the temperature achieved is up to 100-150 °C.

This work focuses on the microwave-assisted synthesis of mesoporous silica at room temperature. In addition, MCM-41 was functionalized with neodymium oxide by following the incipient wetness method under microwave radiation. Both materials have been structurally and morphologically characterised; results have been compared with those obtained from the same material produced by means of conventional methods.

2. Experimental

2.1 Materials

Cetyltrimetylammonium bromide (CTAB, Aldrich), hydrochloric acid (Aldrich, 37%), tetraethoxysilane (TEOS, Fluka) and neodymium nitrate hexahydrate (Aldrich) were used as received. Solutions were prepared by weight adding conductivity grade water.

2.2 MCM-41 synthesis

MCM-41 was prepared by adding the silica precursor tetraethoxysilane to an aqueous solution containing cetyltrimethylammonium bromide (CTAB) and hydrochloric acid [22]. The reactants molar ratios were: $CTAB/SiO_2=0.21$, $HCl/SiO_2=2.1$ and $H_2O/SiO_2=146$.

The mesoporous synthesis under microwave irradiation was carried out in a radiation exposure apparatus (SAIREM) operating at 2.45 GHz frequency and a tuneable power up to 300 W.

This apparatus was designed in order to attain a homogeneous field distribution inside the sample holder. It allows measuring the microwave power absorbed by the sample and results easy in use; more details on this apparatus and its field dosimetry are reported elsewhere [30, 31]. The main remarkable feature is the possibility to irradiate samples keeping constant their temperature that is continuously measured by a non-perturbative optical fibre thermometer (Nortech Reflex-TP21M02).

In order to keep the sample temperature at 30 ± 1 °C, the incident microwave power was varied from 12 to 15 W and the sample holder was cooled by a thermostated (20 ± 0.1 °C) water jacket externally surrounding the waveguide.

A white precipitate appeared after 20 minutes. As soon as the precipitation was considered complete (2 irradiation hours), the resulting powder was filtered, washed and dried at room temperature. To remove CTAB molecules from the hexagonal mesoporous material, the sample was calcined in air at 550 °C for 4 hours.

The reference material was synthesised at the same conditions of concentrations and temperature, but in absence of microwave irradiation. The precipitate appeared after 45 minutes and, even in this case, it was filtered after two hours and then calcined in air at 550 °C for 4 hours.

2.3 MCM-41 impregnation

Nd-MCM-41 sample, with Nd/Si atom ratio equal to 0.05, was prepared, following the incipient wetness method [32]. The calcined MCM-41 mesoporous silica (reference material) was progressively wetted by adding drop wise an ethanolic solution of $Nd(NO_3)_3 \cdot 6H_2O$ at the appropriate concentration.

The sample was divided in two aliquots, both were maintained at 60 °C: one was treated with microwave, to evaporate the ethanol, by tuning the incident power from 40 to 50 W and setting the water temperature, circulating in the jacket externally surrounding the waveguide, at 20 ± 0.1 °C.

For comparison the remaining aliquot was located in an oven. The dry materials were thermally treated at 550 °C for 5h in order to transform the neodymium nitrate in neodymium oxide. The white MCM-41 powder turns out violet after impregnation.

2.4 Characterization techniques

X-Ray Diffraction spectra have been collected by means of a Philips PW 1050/39 diffractometer in the Bragg-Brentano geometry using Ni filtered Cu Kα radiation (λ = 1.54178 Å). The X-ray generator worked at a power of 40 kV and 30 mA and the resolution of the instrument (divergent and antiscatter slits of 0.5°) was determined using α-SiO_2 and α-Al_2O_3 standards free from the effect of reduced crystallite size and lattice defects.

Scanning Electron Microscopy investigation has been performed by using a Philips XL30 equipped with an Energy Dispersive X-ray device. Samples were supported on the stubs by carbon paint and coated with gold in order to make the sample a good conductor. The accelerating voltage ranged between 18 and 25 kV during SEM investigation, while it was set at 25 kV for EDX analysis.

3. Results and discussion

3.1 MCM-41 powder

XRD patterns of the two, microwave irradiated and reference material, uncalcined mesoporous samples are reported in Figure 1. The XRD patterns do not show significant differences. Beside the three (100), (110), (200) reflections characteristic of the MCM-41 hexagonal lattice symmetry [33] (showed in the inset), both samples show some peaks that could be ascribed to the CTAB, whose XRD pattern is also reported. In the same Figure, the diffraction pattern of crystalline silica (tridymite) [34] is also reported. It clearly emerges that the formation of crystalline silica can be excluded.

The unit cell parameter (a_0) that in the hexagonal structure indicates the pores centre-centre distance, is correlated with (100) distance (d_{100}) by means of the equation $a_0 = 2d_{100}/\sqrt{3}$ [35]. For this sample, being d_{100}, computed by means of the Bragg law, 39.40 Å the a_0 value results 45.50 Å.
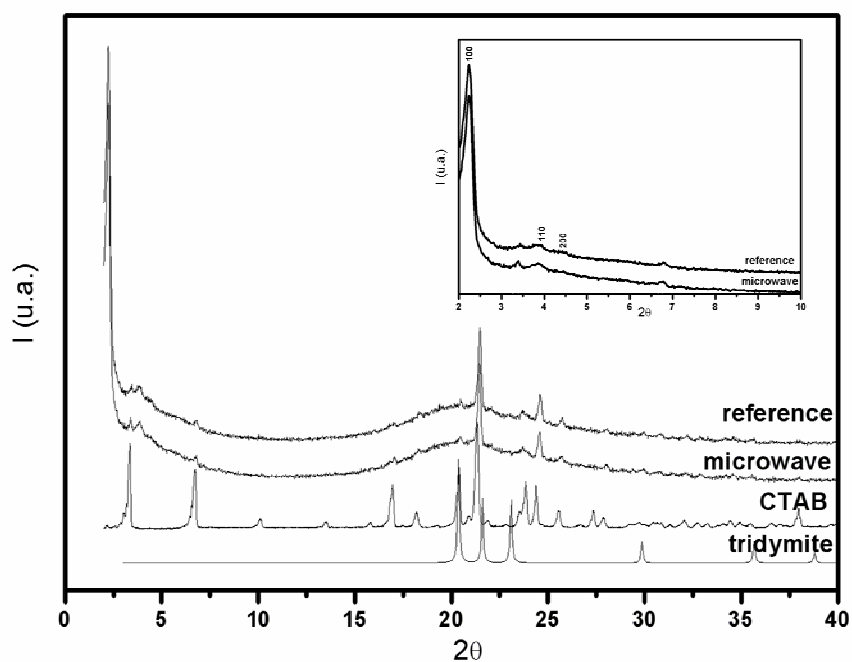
Figure 1 - XRD patterns of MCM-41 reference material and prepared by using microwave irradiation together with the ones of CTAB and tridymite

Some differences are indeed observable in the XRD patterns of the two above samples after calcination (see Figure 2).
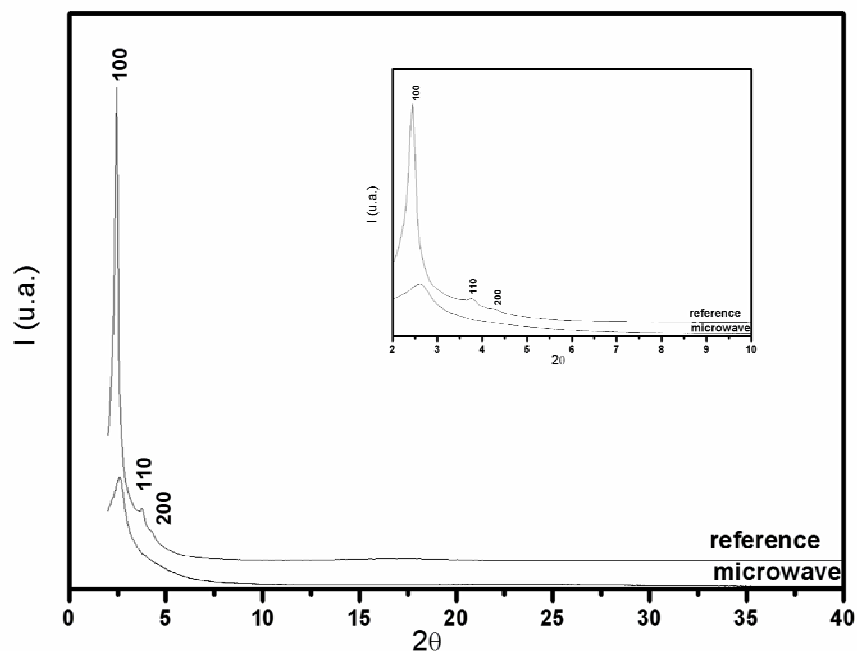
Figure 2 - XRD patterns of calcined MCM-41 samples prepared by using microwave irradiation and of the reference

The XRD pattern of the reference mesoporous calcined sample shows the three (100), (110) and (200) peaks, indicating that the MCM-41 hexagonal structure is maintained. The disappearance of all other peaks confirms the correctness of attribution to the CTAB crystalline structure. For this sample, the d_{100} and the a_0 values, were 36.03 Å and 41.60 Å, respectively.

In the XRD pattern of the calcined microwave irradiated sample, it is possible to observe the disappearing of (110) and (200) secondary peaks which indicates that the long range order of the hexagonal MCM-41 structure is lost; the XRD pattern looks similar to that of HMS type material having a wormhole-like pore structure [24,36]. Compared with the previous pattern, the lower intensity of the (100) diffraction peak is probably ascribable to an increased number of defect sites and bond strain. In addition, a little shift of the (100) peak toward higher θ values can be noticed: the d_{100} and a_0 values were 33.69 and 38.90 Å, respectively. This shift indicates that the mesoporous silica prepared by using microwave irradiation has pores narrower than the ones prepared with traditional method, even if the structure, in particular the a_0 value, of the un-calcined material was identical.

SEM micrographs of the two mesoporous calcined samples, microwave irradiated and reference material, are shown in Figure 3.
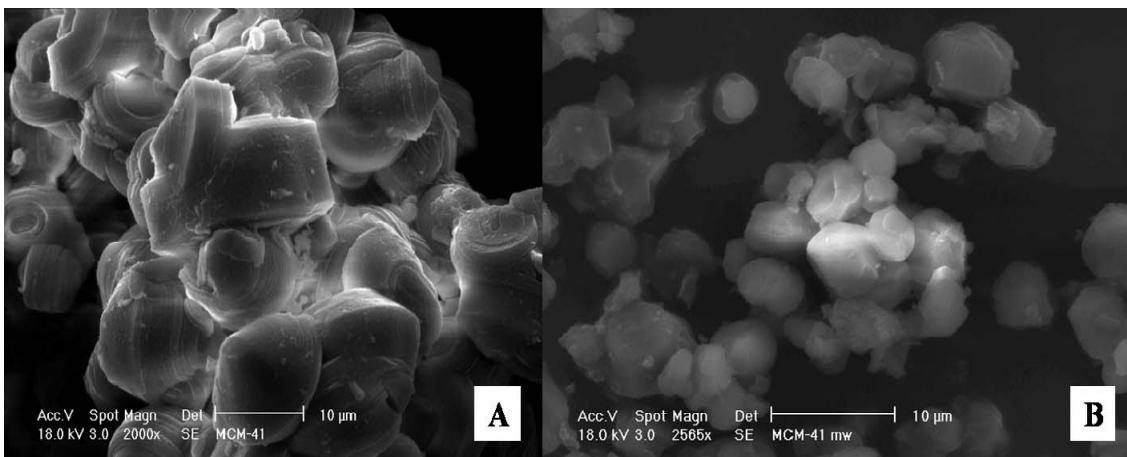
Figure 3 - SEM micrographs of the two calcined mesoporous samples: (A) reference sample and (B) sample prepared under microwave irradiation

The mesoporous morphology is that of the typical ordered hexagonal structures for both samples [27]. Microwave irradiation causes the formation of smaller particles. This finding could be explained by considering the shorter crystallization time upon microwave irradiation in comparison with conventional method. Usually, the preparation needs at least 45 min. to allow crystalline MCM-41 to form, whereas the microwave preparation takes only 20 min at 30 °C. It is worth noticing that during the treatment, temperature was kept constant to make the method really comparable with the traditional one. However, the shorter synthesis time freezes the structures without having reached the equilibrium, thus causing the formation of smaller particles having a weaker hexagonal structure that can evolve during the thermal treatment, becoming more similar to the HMS than to MCM-41 mesoporous material.

3.2 Nd_2O_3-MCM-41 impregnated

Even if the colour of the impregnated Nd_2O_3-MCM-41 sample is indicative of neodymium presence in the sample, micro EDX spectra were collected for the samples obtained by using traditional incipient method and by using microwave irradiation. Spectra are reported in Figure 4.
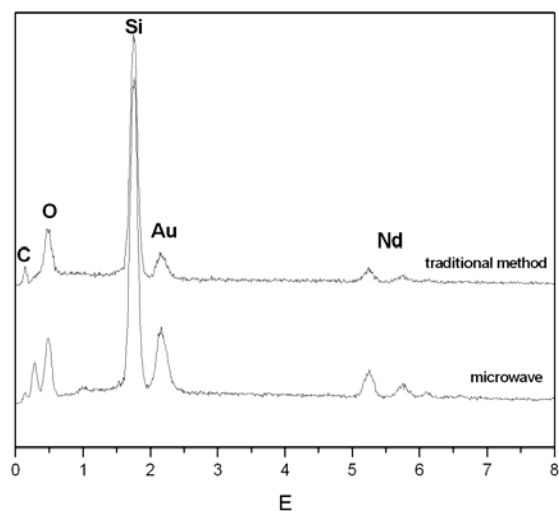
**Figure 4 - EDX spectra of Nd2O$_3$ impregnated MCM-41 samples prepared by the
traditional and the microwave assisted incipient wetness method**

Beside the fluorescence K lines of silicon and oxygen, components of MCM-41, the K lines for carbon from the stub and the L lines of gold coating, the presence of neodymium was recognized by the presence of Lα and Lβ1 at 5.23 and 5.72 keV, respectively.

The diffraction patterns of the Nd$_2$O$_3$ impregnated MCM-41 prepared by using traditional and microwave assisted incipient wetness method are compared with the XRD pattern of the MCM-41 reference material in Figure 5.
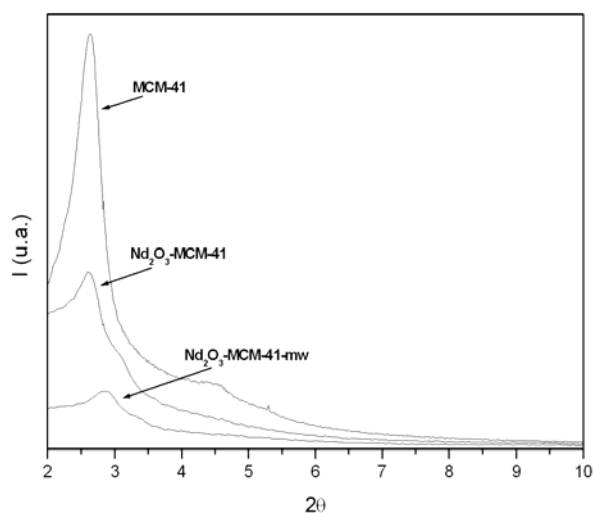
**Figure 5 - XRD patterns of MCM-41 reference sample and of the two Nd2O$_3$ impregnated
MCM-41 samples prepared by the traditional and the microwave assisted (mw)
incipient wetness method**

For both impregnated samples, the MCM-41 structure is preserved even after the additional five hours treatment at 550 °C. However, the intensity reduction of the principal diffraction peak (100) indicates that the number of defect sites and bond strain increase upon neodymium oxide addition. As discussed in the previous section, the intensity decrease of the secondary peaks (110) and (200) suggests the loss of long-range order, that can be consequence of the incorporation of Nd_2O_3 in the MCM-41 pores, in agreement with the literature [37-39].

The (100) peak position for the Nd_2O_3 impregnated MCM-41 prepared by using traditional incipient wetness method results unvaried with respect to the reference material. On the contrary, Nd_2O_3-MCM-41 prepared by microwave assisted (mw) incipient wetness method shows a shift of the principal peak (100) to higher angles. The a_0 values were 39.20 and 35.76 Å, respectively. These results indicate that the impregnation performed by using microwave irradiation, even if it does not change significantly the original MCM-41 structure, reduces the centre-centre distance of the pores

SEM micrographs of the impregnated samples prepared by conventional methods (A) and by using microwaves (B) are shown in Figure 6.
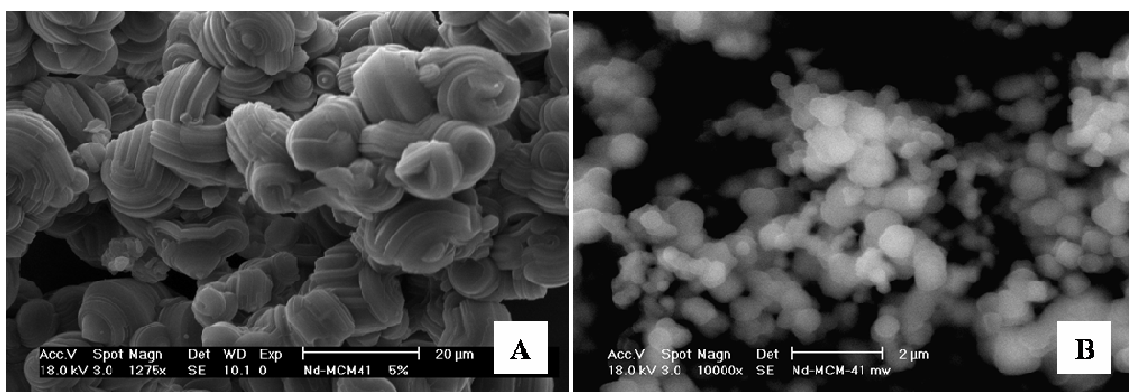
Figure 6 - SEM micrographs of Nd2O3-MCM-41 samples prepared by the traditional (A) and the microwave assisted (B) incipient wetness method

The morphology of Nd_2O_3-MCM-41 sample obtained by traditional method is the same of that of MCM-41 support (shown in Figure 3) confirming the XRD data analysis. The particles shape of Nd_2O_3-MCM-41 sample obtained by microwave assisted incipient wetness method is spherical and they are smaller in size with respect to the MCM-41 reference sample suggesting that microwaves cause a fragmentation of the former structure.

4. Conclusion

Mesoporous silica was prepared by using the conventional method and the microwave assisted one. The synthesis assisted by microwave irradiation causes the formation of a material with a weaker structure that changes after the calcination. The obtained material has a structure similar to HMS mesoporous with a more narrow pores size that the one prepared with traditional method.

A composite material, constituted by MCM-41 and neodymium oxide, was prepared by impregnation following the incipient wetness method assisted by microwave. For comparison the same material was prepared by using the same method without microwave assistance.

Evidence of the presence of neodymium in the silica matrix was obtained from EDX. XRD patterns showed that the impregnation does not change significantly the structure and morphology of the MCM-41, even if the Nd_2O_3-MCM-41 samples prepared by using microwave irradiation shows a smaller centre-centre distance of the pores.

Acknowledgment

References

[1] K. Moller, T. Bein, *Chem. Mater.*, **10** (1998) 2950.

[2] M.J. Girgis, Y. P. Tsao, *Ind. Eng. Chem. Res.*, **35** (1996) 386.

[3] C.Y. Chen, H. X. Li, M.E. Davis, *Microporous Mater.,* **2** (1993),17.

[4] K. R. Kloestra, H.J. Van Bekkum, *J. Chem. Res. S.,* (1995) 26.

[5] C.T. Kresge, D.O. Marler, J.S. Rav, B.H. Rose, U.S. Patent, **366** (1994) 945.

[6] S. Gontier, A. Tuel, *Zeolites*, **15** (1995) 601.

[7] A. Sayari, *Chem. Mater.*, **8** (1996) 1840.

[8] X. Feng, et al., *Science*, **276** (1997) 923.

[9] L. Mercier, T. Pinnavaia, *J. Adv. Mater.* **9** (1997) 500.

[10] H. Lin, Y. Chen, *J. Porous Mater.*, **12** (2005) 95.

[11] M. Busio, J. Janchen, J.H.C. Van Hooff, *Microporous Mater.,* **5** (1995) 211.

[12] Z. Luan, Ch.F. Chen, H. He, J. Klinowski, *J.Phys.Chem.* **99** (1995) 10590.

[13] T. Blasco, A. Corma, M.T. Navarro, J. Perez-Pariente, *J. Catal.* **156** (1995) 65.

[14] W. Zhang, T.J. Pinnavaia, *Catal. Lett.* **118** (1996) 9164.

[15] M.F.B. Joana et al., *Journal of Alloys and Compounds* **374** (2004) 101.

[16] S. C. Laha, P. Mukherjee, S. R. Sainkar and R. Kumar, *J. Catal.* **207,** (2002) 213.

[17] H. Yokoyama, *Science* **256** (1992) 66.

[18] F.S. Richardson, *Chem. Rev.* **82** (1982) 541.

[19] G.E. Buonocore, H. Li, B. Marciniaak, *Coord. Chem. Rev.***99** (1990) 55.

[20] O.A. Serra, I.L.V. Rosa, C.L. Medeiros, M.E.D. Zaniquell, *J. Lumin.* **60&61** (1994) 112.

[21] C.T. Kresge, M.E. Leonowicz, W.J. Roth, J. Vartuli, *Nature* (London), **359** (1992) 710.

[22] Beck et al. *J. Am. Chem. Soc.* **114** (1992) 10834.

[23] M.E. Davis, et al. *Microp. Mater.* **2** (1993) 17.

[24] P.T. Tanev, T.J. Pinnavaia, *Chem. Mater.* **8** (1996) 2068.

[25] J.C. Jansen, A. Arafat, A.K. Barakat, H. van Bekkum, in: M.L. Occelli, H.E. Robson (Eds.), Synthesis of Microporous Materials, vol. 2, Van Nostrand Reinhold, New York, 1992, p. 507.

[26] H.M. Sung-Suh et al. *Res. Chem. Intermed.*, **26** (2000) 283.

[27] S.G. Deng, Y.S. Lin *J. Mater. Sci. Lett.,* **16** (1997) 1291.

[28] U. Oberhagemann et al. *Microporous and Mesoporous Materials* **33** (1999) 165.

[29] S.E.Park et al. *Res. Chem. Intermed*. **26 (3)** (2000) 283.

[30] R. Massa, G. Petraglia, E. Caponetti, L. Pedone, *Materials Research Innovations* **8** (2004) 48.

[31] Caponetti et al., pag. 135-145 in questo volume.

[32] J. Santamaria-Gonzales et al., *Catalysis Letters* **64** (2000) 209.

[33] G. Behrens, G.D. Stucky, *Angew. Chem., Int. Ed. Engl.* **32** (1993) 696 and references therein.

[34] Inorganic Crystal Structure Database *http://icsdweb.FIZ-Karlsruhe.de.*

[35] J. Aguado, D.P. Serrano, J.M. Escola, *Microp. Mesop. Mater.* **34** (2000) 43.

[36] W. Zhang, T.R.Pauly and T.J.Pinnavaia, *Chem. Mater.* **9** (1997) 2491.

[37] M. Froba, R. Kohn, G. Bouffaud, O. Richard, G. van Tendeloo, *Chem. Mater*. **11** (1999) 2858.

[38] R. Kohn, M. Froba , *Catal. Today* **68** (2001) 227.

[39] J.M.F.B. Aquino et al. , *Journal of Alloys and Compounds* **374** (2004) 101.

Section 3. Materials and processes

LIQUID PHASE MICROWAVE SINTERING OF ALUMINA

B. Cioni, E. Origgi, A. Lazzeri

Department of Chemical Engineering, University of Pisa,

Via Diotisalvi 2, 56126 Pisa, Italy

beatrice.cioni@ing.unipi.it

Abstract

Microwave sintering of liquid-phase-sintered (LPS) alumina was carried out for the first time in this work, to the authors' knowledge. The purposes of this investigation were to verify the feasibility of microwave processing on spherical mill grinding media, with dimensions used in industrial milling applications, and to compare the resulting properties with those of conventionally produced samples. The obtained ceramic mill grinding media were characterized by density measurements, microstructure analysis, mechanical properties determination and standard wear tests commonly used in industrial grinding. Preliminary results on pilot scale microwave apparatus showed the possibility of microwave sinter a significant number of alumina mill grinding media in a competitive industrial process.

Keywords

Microwave processing; Milling; Hardness; Al_2O_3; Liquid Phase Sintering (LPS)

Introduction

Microwave technology is a perspective alternative respect to conventional heating methods because of its potential energy and cost savings properties [1-3]. The process can be carried out for drying, curing, concentrating, rapid heating and waste remediation. Specific advantages of this technology for industrial and environmental applications include: selective heating capabilities, more energy efficient during heating and drying with significant time savings, low waste, improved product quality, greater control and reduced equipment size [4]. The cost of microwave power systems is generally considerably greater than that of conventional heating systems. Moreover, the cost of installation, operating power, maintenance and financing must be weighed against potential savings in labor, space, yield, productivity and energy [5-6]. Despite these extra costs and limitations, microwave heating has become a well-known efficient process for several industrial applications: ceramics manufacturing, reactivation of carbon and catalytic powders, sludge dewatering, incineration of biomedical waste.

In particular microwave processing of ceramics has recently received a growing interest, because of rapid volumetric heating, high densification rate, decreased sintering activation energy, improved microstructure and low energy consumption [7-8].

During microwave sintering the green material has to couple with microwaves, then it volumetrically absorbs the electromagnetic energy and transforms it into heat inside the material body. This eliminates the need for spending energy on heating the walls of the furnace or reactor, its massive components and heat carriers.

The volumetric nature of energy deposition accelerates heating, with significant energy saving and reduction in process time.

According to a study carried out by Patterson et al. [9], the specific energy consumption in the sintering of silicon nitride-based ceramics at 1600 °C is about 3.1 kWh/kg for microwave heating versus 19.7 kWh/kg for fast conventional heating in a resistive oven with an energy saving of about 78%. However, it should be noted that the energy saving is not the only benefit of using microwave energy in high-temperature processes. In many cases microwave processing is capable of improving the product quality or leads to results that cannot be achieved by conventional heating. Enhanced densification behaviors were also observed in microwave processing due to a reduction in the apparent activation energy following in an acceleration of the sintering by microwave heating [8]. Another characteristic of microwave heating is that the densification of some ceramic materials can be achieved at lower temperatures and in shorter times than those required in conventional processing [10].

Recently various structural ceramics and composites have been successfully sintered by microwave heating: Al_2O_3 [11-12], yttria (Y-TZP) [12-16], ceria-stabilized-tetragonal zirconia polycrystals (Ce-TZP) [17] are only a few of the materials that are more actively investigated. In the literature there are examples of pure alumina (99.99%) powder sintered by 2.45 GHz microwave heating up to 91.7% of its theoretical density. Furthermore Janney and Kimrey [18] noticed that alumina was sintered more rapidly by microwave sintering than by conventional heating, obtaining densification of submicronic alumina powder up to the 97.76% of the theoretical density with more homogenous microstructure.

Notwithstanding the promising results that have been obtained [19], a few problems are still unresolved: in particular the difficulty of coupling between some ceramic materials and microwave energy at low temperature, during microwave heating [20-21]. This is due to the different crystal structure and loss mechanism in various ceramics that causes some differences in their microwave absorption levels [7], therefore the degree of interaction between microwave and ceramic changes with temperature [20]. Al_2O_3, ZrO_2 and Si_3N_4 have low absorption ability at lower temperature, until some critical value (T_{cr}) is obtained after which the coefficient of dielectric loss grows exponentially causing thermal instability and sometimes avalanche temperature increase (thermal runway). This rapid increase in temperature, in radio-transparent ceramics, could be associated with the softening of the amorphous phase, which increases the surface conductivity [22], and then overheating of separate regions can be reached.

Meek et al. reported [11] 93.3% and 91.7% of the theoretical density respectively for ZrO_2-Y_2O_3 and Al_2O_3 by microwave sintering. The difficult coupling at low temperature and the problem of the localized overheating can be improved with the help of hybrid heating scheme that combines microwave and convective heating by the use of susceptors to bring the temperature of the material to its critical MW coupling temperature. Materials with high loss factor (susceptors) are installed together with the green ceramic bodies in the microwave cavity in between the heat insulation and the samples. By hybrid heating it is possible to reduce thermal stresses, decreasing the temperature gradients in the body and increasing considerably the rate of the process [23].

Another method of hybrid heating is the addition of susceptors in the form of SiC powder or whiskers around or on top of the material to be treated [1; 6], but this is a method restricted only to those cases in which the additives will not affect the performances of the products.

The aim of this research is to verify the feasibility of microwave processing of alumina-based samples with industrial milling applications. One of the most industrially significant powder densification processes is the liquid phase sintering (LPS). This process consists of heating a mixed powder compact until a small amount of chemically stable liquid phase forms and greatly accelerates the sintering of powders [24-26]. Mortensen [27] subdivided the densification proceeding into three stages: the first consists in a relatively rapid rearrangement of solid particles beginning immediately upon the liquid formation, then the second stage is a solution-reprecipitation phenomenon observed only in systems where the remaining solid phase features some solubility in the liquid phase. Finally in the third stage there is the formation of solid bridges between touching solid particles. Our purpose is to combine the advantages offered by liquid phase sintering (increased sintered rate, the possibility of obtaining particular properties, by varying the type of additives) with the peculiarities of the microwave heating. Moreover the liquid phase during sintering could aid coupling between the alumina-based material and microwave energy at low temperature, because of the higher loss factors of the additives. This paper will focus on microwave sintering of alumina–based powder containing 10% of additives in order to evaluate the possibility of an efficacious alternative process respect to the traditional heating.

Experimental section

A commercial alumina (Alubit[®] from Industrie Bitossi, Sovigliana - Italy) containing Al_2O_3 (90%), SiO_2, $CaCO_3$, $MgCO_3$ and other components, was used for the experimental trials. All samples had a green density of about 58% of theoretical density (3,64 g/cm^3) and a weight of about 100 g.

Sample processing

Tests of simultaneous microwave sintering of 5 spherical samples of diameter 1½ in. were performed on pilot scale microwave oven, equipped with a 6 kW 2.45 GHz magnetron, in order to evaluate the possibility of industrial application of the process. Due to the complexity of the apparatus it was possible to monitor the temperature of only one sample, i.e. the sphere placed in the center of the chamber. The sample temperature in the pilot scale microwave apparatus was measured by a EUROTRON IRtec 60 series optical pyrometer in the range of 300-1300 °C. The pyrometer was connected to a computer that recorded one measurement every 10 seconds. The measuring spot had a diameter of 1 cm at a distance of approximately 5 cm.

A scheme of the microwave apparatus is shown in Figure 1: a variable power 6 kW water-cooled microwave generator (Muegge Gmbh equipped with a TOSHIBA E3327 magnetron) supplies the energy needed for the sample heating. The microwave generator is coupled to the applicator by means of a three-stub auto tuner used for impedance matching, i.e. to minimize reflections back toward the source.
Between the generator and the auto tuner a three-port circulator directs the reflected power from the applicator into a water-cooled dummy load to protect the magnetron from possible damage.
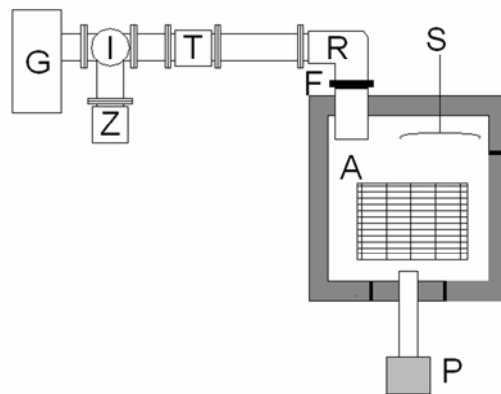
Figure 1 - Scheme of the microwave apparatus used for the pilot scale microwave sintering (G: generator 2.45 GHz, 6 kW; I: three port circulator; Z: water cooled dummy load; T: auto tuner; R: connected transition; F: quartz window; A: applicator; S: mode stirrer; P: pyrometer)

A directional coupler equipped with a sensor was also used to monitor both forward and reflected power. Microwaves are directed from the generator to the applicator by means of a rectangular wave-guide equipped with a connected transition. A steel/aluminum multi-blade mode stirrer is used to continuously perturb the field distribution in the oven.

In Figure 2 a schematic sketch of the set-up for pilot scale microwave sintering is reported: a few samples are placed inside of the chamber made of an insulating material (Al_2O_3 fiberboard), which has a low density and has not significant dielectric losses at the operating frequency. Samples were placed within a fiberboard box, in which SiC rods were used as susceptors in a picket fence assembly, for hybrid heating the low-loss alumina samples in the initial low temperature regime [1].
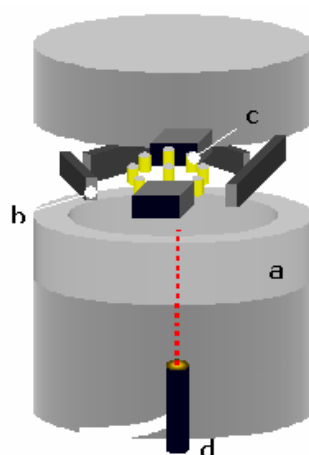
Figure 2 - Schematic sketch of the set-up for pilot scale microwave sintering; (a) alumina fiber (insulation), (b) SiC road, (c) sample, (d) pyrometer

Characterization of the sintered samples

Density was measured on the green pellets–by geometrical evaluation and on the sintered samples-by the Archimedes method using deionized water as medium.

Alubit® Powder and Alubit® pellets after exposure to microwaves were examined by X-ray diffraction (XRD) using a Siemens Kristalloflex 810 diffractometer.

The microstructure of the samples was observed by means of a Philips SEM 515 scanning electron microscope (SEM) on polished and etched sections.

Hardness and fracture toughness measurements

Vickers hardness (HV) and fracture toughness (K_{IC}) were determined by indentation tests at different loads, using an automatic durometer according to UNI-ENV 834-4. At least three measurements at each indentation load were performed. Both Vickers microhardness and Vickers macrohardness were performed on a plane surface of a half part of the double-step heated samples, previously cut by a diamond blade. The following formula is applied to determine the Vickers hardness (1):

$$HV = 1.854 \cdot \frac{F}{d^2} \qquad (1)$$

where F is the applied load (N) and d is the mean of diagonals (mm).

Indentation fracture toughness, K_{IC} was obtained from the Anstis Equation (2):

$$K_{IC} = 0.016 \cdot \left(\frac{E}{H} \right)^{1/2} \cdot P \cdot c^{-3/2} \qquad (2)$$

where, E is the elastic modulus (GPa), H the Vickers Hardness (GPa), P the indentation load (N) and c is the crack length (m) measured by SEM micrographs.

Wear test

Wet-milling tests were performed in a ball mill at room temperature, according to the typical industrial procedure (Figure 3). About 3 kg of commercial alumina grinding spheres, Alubit®, used as a reference and filled with cobalt oxide in such a way to assume a blue color, and the same amount of microwave sintered alumina grinding media, were loaded together into the ball mill with the aqueous medium (de-ionized water) and were run for a period of 10 hours as initial conditioning, then for 6 cycles of 23 hours. After each ball-milling run, the test specimens were cleaned in a bath with water jet, dried and thereafter accurately weighed (to give wear as difference in weight) The wear surfaces were examined by scanning electron microscopy (SEM).
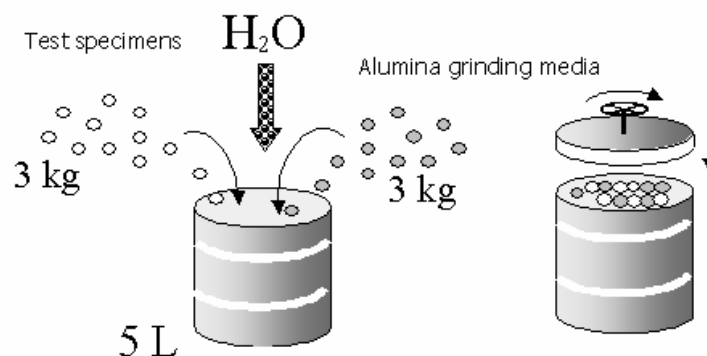
Figure 3 - Schematic sketch of the set-up for the wear test

Results and discussion

After the preliminary wear test [28] carried on the sintered alumina spheres in a single cycle (1 hr at 1100 °C), it was noted that more than 80% of the samples were undamaged, but a few samples showed the well-known core-shell morphology with hard shell and black core (Figure 4a).

It is well known the "black coring" that usually occurs during the firing process when carbon inside the clay body has not been sufficiently eliminated [29-30]. The green spheres contain some carbonaceous matter, which oxidizes during firing between approximately 500 °C and 700 °C, producing carbon dioxide that escapes from the sample. If the presence of oxygen in the kiln atmosphere is insufficient, the carbon cannot be eliminated from the clay and it is left in a weaker state. This tends to occur more during a "reduction" firing where oxygen in the kiln atmosphere is reduced.

If the heating process (conventional or with microwaves) is too quick, the porosity in the more external area begins to close before that in the inner. Then a layer where sintering is almost completed grows from the inside to the outer surface until to a depth that starts to prevent the outlet of the inner gases. As a consequence, the combustion gases accumulate within the sample causing a pressure build-up, which can only be compensated by the formation of a spherical crack between the external shell and the core. Moreover the hard shell of the already sintered material not only obstructs the regular expulsion of the ligand but also hinder the flux of oxygen necessary to its oxidation. Therefore a certain amount of ligand remains trapped in the inner part of the sample and pyrolize giving the inner core its dark colour due to the formation of carbonaceous material.
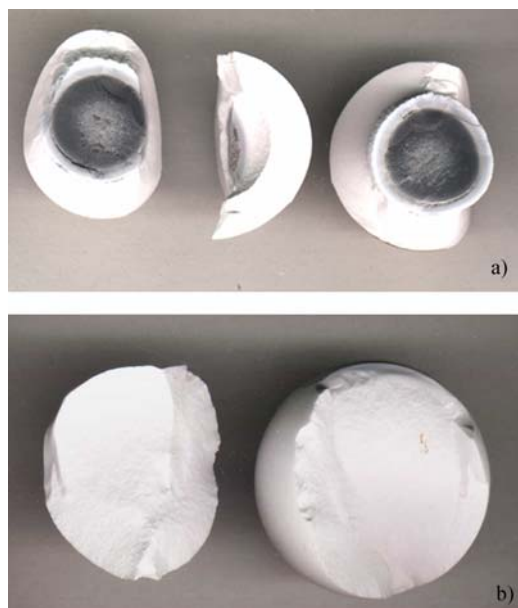
Figure 4 - Image of the internal part of samples after single-step thermal cycle (a) and after a double-step thermal cycle (b)

In order to avoid the formation of the black core the thermal cycle was modified by subdivision of the process in two different phases: the first with the aim of completely eliminate the ligands and the second to carry out the sintering (Figure 5). The double cycle gave satisfactory results with a medium volumetric shrinkage of 41.7% and density of 3.5 g/cm^3, equal to the 96.1% of the theoretical density. The elimination of the black core defect, confirmed by an image of the section of one sample reported in Figure 4b), allowed wear results for the MW sintered samples similar to those showed by conventionally sintered ones.
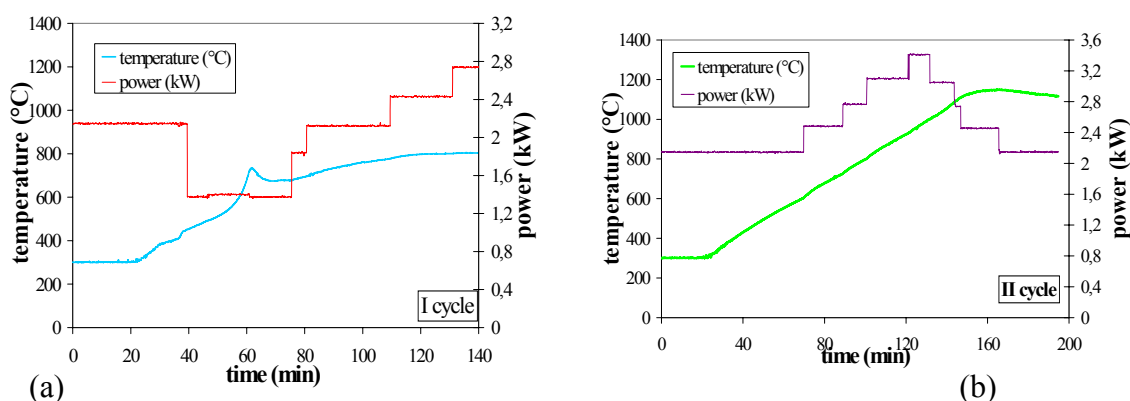
Figure 5 - Double-step cycle of microwave sintering: the first cycle (a) and the second cycle (b)
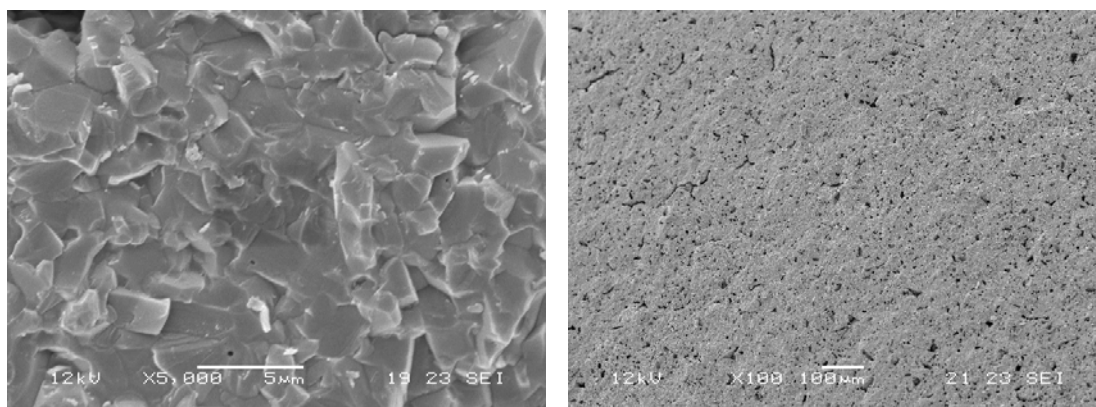
(a)   (b)

Figure 6 - SEM image of surface of the double-step heated samples after wear test, under 5000 x magnification (a) and 100 x magnification (b)

SEM images in two different magnifications (Figure 6a) and Figure 6b) of surface after wear test showed that the surface of the sample after the wear test were not particularly damaged. The double-step heated samples manifested approximately a similar rate of consumption respect to the conventionally sintered mill grinding mediaThere is an evident difference between values of temperature observed in conventional industrial sintering of this type of alumina (1550 °C) and values of temperature observed in spherical specimens during a treatment on pilot scale apparatus.

A possible explanation of this evidence is that the spherical specimens have large dimensions, and then there are probably gaps between the surface temperature (lower) and the temperature in the core (higher) of spheres caused by the greater tendency of the surface to disperse the heat.

Furthermore it must be underlined that the pyrometer measures the temperature of the sample placed in the center of the chamber, position where the sphere is more distant from susceptors than the other four samples. It is presumable that the temperature of the other four spheres was higher than the detected one as confirmed by their mean volumetric shrinkage, which is about 4% higher than that of central sample.

The percent volumetric shrinkage of the four samples placed around the central specimen results sufficiently homogeneous, being around 41.7, leading to approximately 96.1% of theoretical density. The conventionally processed samples achieved almost the same density (95.5%) at higher temperature, 1550 °C.

The causes of these significant differences in densification degree for microwave versus conventionally treated samples are identified in the internal heating phenomenon associated with microwave processing [10].

When the inside of the sample achieved high density before complete densification of the surface layers, fewer pores are 'trapped' inside the sample minimizing the internal porosity.

This phenomenon is particularly evident in alumina, mainly as the sample size is quite large as in this case. In a previous study Clark and co-workers [31] reported that the sample density enhanced when the sample size was increased from 6 to 20 g.

Figure 7 compares a typical X-ray diffraction (XRD) pattern of a sample of microwave sintered alumina (a) with that of the corresponding green sample (b).

The XRD peaks of the green samples are sharper and clearly defined with respect to those of the sintered sample where the peaks are generally wider (this could be attributable to the fact that all grains were not subject to the same stress). In the MW sintered alumina there are some peaks on the background with different intensity respect to the powder. Also the background due to the amorphous phase appears much more intense after sintering, then it is possible to conclude that the amorphous constituents were probably absent in the powder before the sintering process. Except for the amorphous phase, these XRD patterns exactly tallied with the standard Al_2O_3 (corundum) powder XRD pattern. The labelling and the identification of the diffraction peaks, reported in Figure 7, has been carried out following the National Institute of Standards & Technology Certificate of Analysis for Standard Reference Material® 676 accessed through the NIST Standard Reference Materials website[*], reported in Table 1.
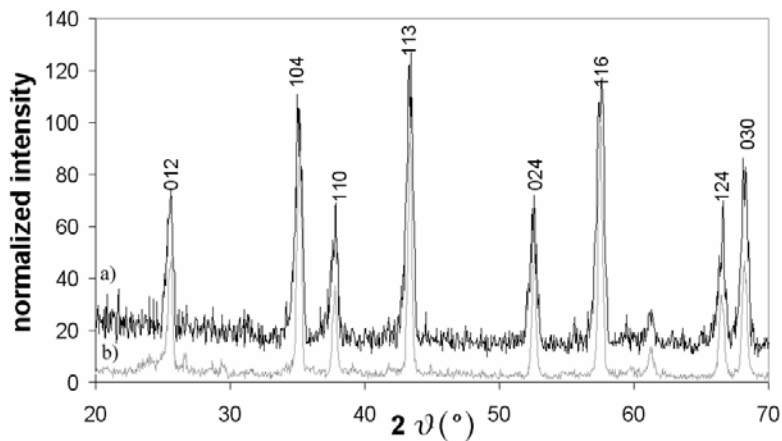
Figure 7 - X-ray diffraction pattern of a microwave sintered alumina sample (a) and a green sample (b)

Table 1 - Certified Relative Intensity Data

Reflection (hkl)	Scan Angles		Relative Intensity	
	Low	High	Value	Uncertainty
012	23.9°	27.1°	57.96	1.80
104	33.8°	36.5°	87.40	0.65
110	36.5°	38.8°	36.32	0.19
113	42.0°	45.0°	100.0	---
024	50.7°	54.0°	47.18	0.41
116	55.7°	58.9°	95.59	1.21
124	65.1°	67.2°	36.02	0.78
030	67.2°	69.6°	55.75	1.26

---

[*]http://ts.nist.gov/ts/htdocs/230/232/232.htm
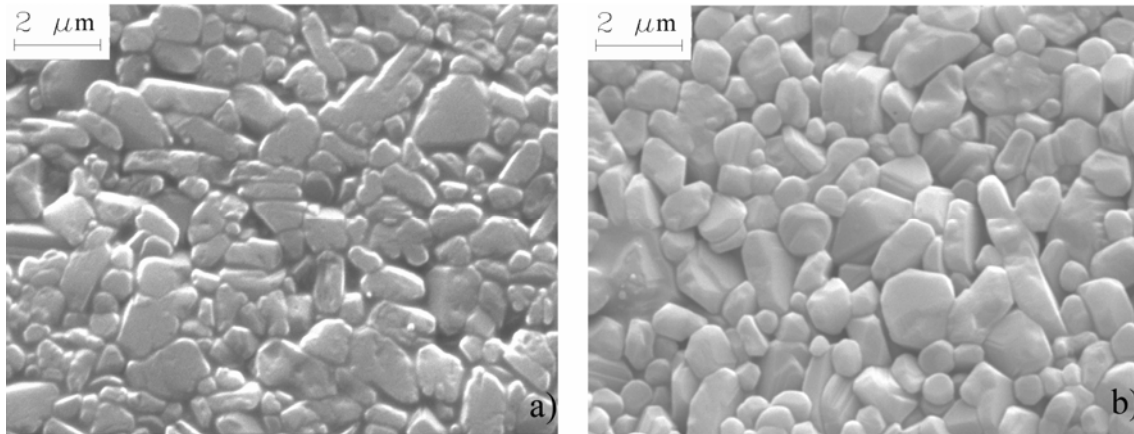
Figure 8 - Scanning electron micrograph of (a) microwave sintered alumina and (b) conventionally sintered after thermal etching

A comparison between the microstructure of a microwave (a) and a conventionally (b) sintered sample is shown by two representative micrographs in Figure 8. The two micrographs were obtained after thermal etching the samples at 1400 °C for 30 min.

The type and the dimension of the grains were almost the same: they presented irregular structure of discs as well some polyhedral shapes. In addition in the case of microwave sintering all grains appeared more compact as if a higher densification degree were reached. In literature there were observed some substantial differences concerning grain growth during the microwave treatment.

Some researchers [31] hypothesised that by microwave energy, thanks to the higher heating rate and shorter sintering cycles, it was possible reduce grain sizes. Patterson and co-workers [32] compared alumina sintering by conventional heating and microwave, obtaining average grain sizes of 4.38 mm and 3.19 mm respectively for the samples with 99.6% of the theoretical density (conventional) and for those with 99.3% (microwave).

The results achieved by Samuels and Brandon [33] showed that the microwave-sintered specimens presented slightly larger grain sizes, as would be expected from their higher densities. Therefore it is evident that the grain size mainly depends on the densification degree of the alumina compact, the higher the density the larger the grains.

In this work, the difference in the obtained density, for the conventionally (95.5%) and for the microwave (96.1%) sintered samples, is so slight that only a little difference in grain size could be noticed between the two materials.

Actually the microwave sintered sample presented greater intragranular porosities (Figure 8a) with respect to the conventionally sintered sample (Figure 8b), although there were no significant differences in density values.

No visible cracks were observed in the microwave sintered samplesVickers microhardness tests were carried out with load of 0.5 kg applied for 15 s, their results are shown in Table 2. The mean value of the microhardness resulted 7.3 GPa.

Table 2 - Vickers microhardness of microwave-sintered samples

d_1 (μm)	d_2 (μm)	F (kg)	HV (GPa)	HV_{mean} (GPa)
34	36	0.5	7.4	
38	40	0.5	6.0	
41	37	0.5	6.0	
33	34	0.5	8.1	
32	34	0.5	8.3	7.3
37	37	0.5	6.6	
32	40	0.5	7.0	
34	35	0.5	7.6	
31	34	0.5	8.6	

Table 3 - Vickers macrohardness of microwave sintered samples

d_1 (μm)	d_2 (μm)	F (kgf)	HV(GPa)	HV_{mean} (GPa)
201	196		4.6	
196	185	10	5.0	4.5
		(98N)		
206	224		3.9	
285	291		6.6	
291	315	30	5.9	6.3
		(294N)		
290	288		6.5	

Vickers macrohardness results are reported in Table 3 with indentation load of 10 kgf and 30 kgf applied on the specimen during 15 s.

Figure 9 shows the SEM image of Vickers macrohardness indentation at 30 kg load carried out on a microwave sintered sample. The mean value for Vickers macro-hardness tests with an indentation load of 98 N on MW sintered samples was 4.5 GPa was obtained, while with an indentation load of 294 N, an average value 6.3 was found. Sglavo et al. reported that the Vickers hardness measured at indentation load of 294 N (30 kg) on a conventionally sintered commercial Alubit® was 10.4±0.6 GPa [34].

The discrepancy between our data and those published by Sglavo et al. might be originated by a difference in raw material quality or in the reliability of the instruments used for measuring hardness. Nevertheless the values of hardness measured for MW sintered LPS alumina are similar to those found for conventionally sintered samples of the same material. The measured K_{IC} was 2.9 MPa·m$^{1/2}$ in the case of the microwave sintered samples while values in the range 2.5-3.5 MPa m$^{1/2}$ for the conventionally sintered samples of similar composition have been reported [34-35]. This leads to the conclusion that the fracture properties of the sintered samples by microwave and conventional methods are comparable.
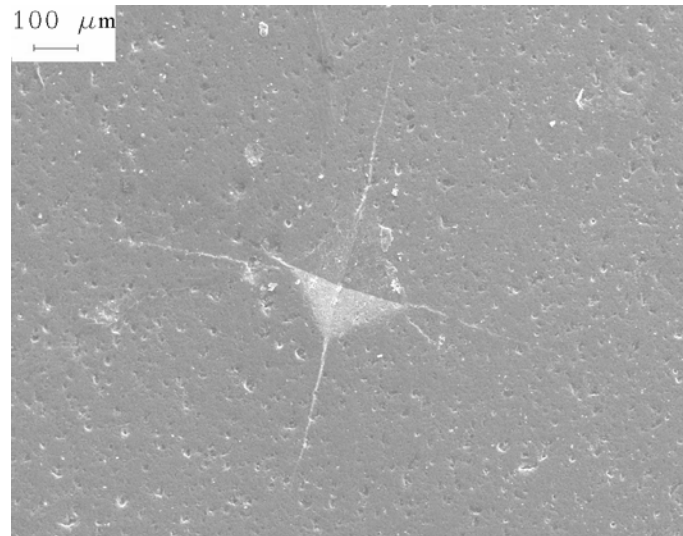
Figure 9 - SEM image of Vickers macrohardness at indentation load of 30 kgf

Conclusions

A series of hybrid sintering experiments on LPS alumina samples by 2.45 GHz was performed. The experimental tests were carried out on a pilot scale 6 kW microwave oven in order to sinter several samples simultaneously. Sintering with susceptors avoided the problems of direct microwave sintering of a low-loss ceramic as alumina is. Alumina samples were sintered to more than 96% of the theoretical density by rapid heating during about 6 hr in case of double-step cycle of microwave sintering, with considerable timesavings compared to the conventional process, 72 hrs. Higher heating rates, although easily achievable by using microwaves, are not desirable because of the presence of ligands and carbonates that form gases during the combustion. Too fast heating rates can give rise to black core defects and the formation of subsurface spherical cracks that separate the samples into a fully sintered outer shell and a more porous black core. The microstructure observed for MW sintered samples displayed an irregular structure and shape with long and narrow grains, but there are no substantial differences between the morphology obtained by the microwave and the conventional sintering process. The mechanical properties (Vickers hardness and fracture toughness) of the sintered samples by microwave and conventional methods are comparable.

In order to investigate the performance of the obtained ceramic samples in the sector of mill grinding media they were subjected to standard wear tests. The preliminary results were quite satisfactory regard to the wear properties once choosing the proper heating rate prevented the formation of black core defects. There are nevertheless many interesting results about mechanical properties (hardness and indentation fracture toughness) that reveal attractive perspective of microwave applications in the ceramic field. Moreover the preliminary experiments on the pilot oven showed the possibility of microwave sintering of a significant number of spherical alumina samples in a competitive industrial process.

Acknowledgements

References

[1] Tinga, W. R., Fundamentals of microwave-material interactions and sintering. In Microwave Processing of Materials, ed. W. H. Sutton, M. H. Brooks and I. J. Chabinsky. Materials Research Society, Pittsburgh, PA, 1988, vol. 124, pp. 33-43.

[2] Metaxas, A.C. & Binner, J. G. P., Microwave processing of ceramics. In Advanced Ceramic Processing Technology, ed. J.G.P. Binner. Noyes Publications, New Jersey, USA, 1990, 285-367.

[3] Janney, M.A. & Kimrey, H.D., Diffusion-controlled processes in microwave fired oxide ceramics. In Materials Research Society Symposium Proceedings, Microwave Processing of Materials II, ed. W. B. Snyder, Jr, W. H. Sutton, M. F. Iskander and D. L. Johnson. Materials Research Society, Pittsburgh, PA, 1991, vol. 189, pp. 215-227.

[4] Jones, D.A., Lelyveld, T.P., Mavrofidis, S.D., Kingman, S.W. & Miles, N.J., Microwave heating applications in environmental engineering-a review, Resour. Conserv. Recy., 2002, 34, 75-90.

[5] Sheppard, L.M., Manufacturing ceramics with microwaves? The potential for economical production, Am. Ceram. Soc. Bull., 1988, 67[10], 1656-1661.

[6] Katz, J.D. & Blake, R.D., Microwave sintering of multiple alumina and composite components, Am. Ceram. Soc. Bull., 1991, 70[81], 1304-1307.

[7] Xie, Z., Yang, J., Huang, X. & Huang, Y., Microwave processing and properties of ceramics with different dielectric loss, J. Eur. Ceram. Soc., 1990, 19 [3], 381-387.

[8] Zhao, C., Vleugels, J., Groffils, C., Luypaert, P.J. & Van Der Biest, O., Hybrid sintering with a tubular susceptor in a cylindrical single-mode microwave furnace, Acta mater., 2000, 48 [14], 3795-3801.

[9] Patterson, M.C.L., Apte, P.S., Kimber, R.M. & Roy, R., Batch processes for microwave sintering of silicon nitride (Si3N4). In Materials Research Society Symposium Proceedings, Microwave Processing of Materials III, ed. R. L. Beatty, W. H. Sutton, and M. F. Iskander. Materials Research Society, Pittsburgh, PA, 1992, Vol. 269, pp. 291-300.

[10] Clark, D.E., Folz, D.C. & West, J.K., Processing materials with microwave energy, Mat. Sci. Eng. A-Struct., 2000, 287 [2], 153-158.

[11] Meek, T. T., Holcomb, C. E. & Dykes, N., Microwave Sintering of Some Oxide Materials Using Sintering Aids, J. Mater. Sci. Lett., 1987, 6 [9], 1060-1062.

[12] Blake, R. D. & Meek, T. T., Microwave processed composite materials, J. Mater. Sci. Lett., 1986, 5 [1], 1097-1098.

[13] Nightingale, S. A., Worner, H. K. & Dunne, D. P., Microstructural Development during the Microwave Sintering of Yttria-Zirconia Ceramics, J. Am. Ceram. Soc., 1997, 80 [2], 394.

[14] Janney, M. A., Calhoun, C. L. & Kimrey, H. D., Microwave Sintering of Solid Oxide Fuel-Cell Materials .1. Zirconia-8 Mol-Percent Yttria, J. Am. Ceram. Soc., 1992, 75 [2], 341-346.

[15] Nightingale, S. A., Dunne, D. P. & Worner, H.K., Sintering and grain growth of 3 mol% yttria zirconia in a microwave field, J. Mater. Sci., 1996, 31 [19], 5039-5043.

[16] Wilson, J. & Kunz, S. M., Microwave Sintering of Partially Stabilized Zirconia, J. Am. Ceram. Soc., 1988, 71 [1], C40-C41.

[17]   Xie, Z., Huang, Y., Zhang, R., Yang, J. & Wang, S., Microwave sintering of Ce-Y-ZTA composites, Am. Ceram. Soc. Bull., 1997, 76 [11], 46-50.

[18]   Janney, M.A., Calhoun, C.L. & Kimrey, H.D., Microwave sintering of zirconia-8 mol% yttria. In Ceramic Transactions, Microwaves: Theory and application in Materials Processing, ed. D.E. Clack, F.D. Gac and W.H. Sutton. American Ceramic Society, Westerville, OH, 1991, Vol. 21, pp. 311-317.

[19]   Cheng, J., Agrawal, D., Zhang, Y. & Roy, R., Microwave sintering of transparent alumina, Mater. Lett., 2002, 56 587-592.

[20]   Sutton, W.H., Microwave Processing of Ceramic Materials, Am. Ceram. Soc. Bull., 1989, 68 [2], 376-386.

[21]   Holcombe, C. E. & Dykes, N. L. Microwave sintering of titanium diboride, J. Mater. Sci., 1991, 26[14], 3730-3738.

[22]   Suvorov, S. A., Turkin, I. A., Printsev, L. N. & Smirnov, A. V., Microwave Synthesis of Materials from Aluminum Oxide Powders, Refractories and Industrial Ceramics, 2000, 41[9], 295-299.

[23]   Spotz, M. S., Skamser, D. J. & Johnson, D. J., Thermal stability of ceramic materials in microwave heating, J. Am. Ceram. Soc., 1995, 78[4], 1041-1048.

[24]   Eremenko, V. N., Naidich, Y. V. & Lavrinenko, I. A., Liquid Phase Sintering, Consultants Bureau, New York, 1970.

[25]   German, R. M., Liquid Phase Sintering, Plenum Press, New York, 1985.

[26]   Goswami, A. P. & Das, G. C., Role of fabrication route and sintering on wear and mechanical properties of liquid-phase-sintered alumina, Ceramics International, 2000, 26, 807-819.

[27]   Mortensen, A., Kinetics of Densification by Solution-Reprecipitation, Acta mater., 1997, 45[2], 749-758.

[28]   A. Lazzeri, B. Cioni, G. Baldi, Atti 2° Convegno Nazionale Microonde nell'Ingegneria e nelle Scienze Applicate MISA 2004, p. 17, (2004)

[29]   Negre, F., Barba, A., Amoros, J.L. & Escardino, A, Oxidation of black core during the firing of ceramic ware. 2. Process kinetics, Br. Ceram. Trans J, 1992, 90, 5-11.

[30]   Negre, F., Barba, A., Orts, M.J. & Escardino, A, Oxidation of black core during the firing of ceramic ware .3. Influence of the thickness of the piece and the composition of the black core, Br. Ceram. Trans J, 1992, 91, 36-40.

[31]   De', A.S., Ahmad, I., Whitney, E.D. & Clark, D.E., Microwave (hybrid) heating of alumina at 2.45 GHz: I. Microstructural uniformity and homogeneity. Ceram. Trans., 1991, 21, 319–339.

[32]   Patterson, M.C.L., Kimber, R.M. & Apté, P.S., The Properties of Alumina Sintered in a 2.45 GHz Microwave Field. In Mater. Res. Soc. Symp. Proc.: Microwaves Processing of Materials II, ed. W. B. Snyder, W. H. Sutton, D. L. Johnson and M. F. Iskander, Materials Research Society Pittsburgh, Pennsylvania: 1990, Vol. 189, pp. 257-266.

[33]   Samuels, J. & Brandon, J.R., Effect of composition on the enhanced microwave sintering of alumina-based ceramic composites, J. Mater. Sci., 1992, 27[12], 3259-3265.

[34]   Sglavo, V.M. & Pancheri, P., Crack Decorating Technique for Fracture-Toughness Measurement in Alumina, J. Eur. Ceram. Soc., 1997, 17, 1697-1706.

[35]   O'Donnel, H.L., Readey M.J. & Kovar, D. Effect of glass additions on the indentation-strength behaviour of alumina. J. Am. Ceram. Soc. 1995, 78, 849–856.

STRUCTURAL EVOLUTION DURING THE DIELECTRIC HEATING OF STARCH MATRIXES

[1]Domenico Acierno, [2]Anna Angela Barba, [2]Matteo D'Amore

[1]Dipartimento di Ingegneria dei Materiali e della Produzione, Università degli Studi di Napoli "Federico II", Piazzale V. Tecchio – 80125 Napoli – Italy

[2]Dipartimento di Scienze Farmaceutiche, Università degli Studi di Salerno
Via Ponte Don Melillo – 84084 Fisciano (SA) – Italy – *aabarba@unisa.it*

Abstract

Microwaves have been used to the drying of starch products (*Solanum tuberosum* cv *Monalisa*) as a fast heating process for dissipative media.

Effects of simultaneous heat and mass transfer phenomena on the sample structures have been analysed and compared with results obtained in conventional processes.

Introduction

Drying is an unit operation devoted to transfer a liquid (or vapour) phase from a solid (or vapour) phase. It is largely used in different industrial applications, such as treatment of foods, production of cosmetics and pharmaceuticals, manufacturing of paper, wood and building materials, polymers and so on.

The drying involves the simultaneous transfer of heat and matter, i.e. heat and mass exchanges between the product under processing and the surrounding bulk. In food treatments water is the liquid phase, contained in solid or semi-solid matrixes, to be transferred in a fluid drier, typically dry, warm air if convective methods are used.

Aim of the drying operation in foods treatments is to enhance their shelf life by reducing the water activity and consequently the microbiologic degradation [1].

The drying operation, that involves heat transfer, can damage the food constituents. The damage is related to the methods that are used to warm up the foods (temperature and time of exposure to hot conditions) and can imply physical (structural and morphologic modification such us shrinkage) or chemical (degradation of sensitive nutrients such us protein, vitamin, aroma etc.) alterations [2].

Dielectric heating

The development of dehydration technology is divided in four groups or generations. Drying technology that used microwaves and RF is proposed as an innovative process of the fourth generation, after convective methodologies (cabinet, kiln, bed, conveyor, and spray drier and drum drier in the first and the second process generations, respectively) and freeze dehydration and osmotic methods (third generation) [3].

The chemical and physical implications above outlined are the real limits to the production of high-quality food and beverages, where nutritional characteristics must be preserved during the treatments. Mild technologies currently adopted are the present stage of the evolution in food technology.

Dielectric heating can be used as a technique capable to realize HTST (high temperature short time) conditions. Exposures to high temperatures when performed in reduced times minimize both loss of nutrients and structural damages in foods.

Starch matrixes

Drying of fruit, vegetables and pasta is one of the most important industrial applications of the microwaves technology. Actually, packaged pre-cooked, cooked, dried and crisped foods have an enormous market success, basically since social factors and availability of innovative materials for packaging have promoted a new style of eating. Vegetables, in particular potatoes, are largely used in the production of soups, salads, gnocchi, accompaniment dishes etc. [4, 5].

Potato matrixes have homogenous, hygroscopic non-porous structures, with a parenchyma characterized by small cells, which are structurally less complex than for other starch vegetables. Thus, they are suitable to drying study purposes [6].

Aim of this work is to analyze the different structural properties of starch products dried either by convective and dielectric methods. Attention will be focused on kinetic studies, shrinkage of samples and rehydratation.

Experimental

Materials, apparatuses and methods

Potatoes (*Solanum tuberosum*), *Monalisa* cultivar, are used in experimental runs. In order to ensure highly reproducibility of results, all the samples are achieved from a single grower, are stored in darkened conditions at 6 °C and selected for homogenous shape and size. Prior to experimental investigations (measures and treatments), the samples are taken out of the refrigerator and left to stabilize at room temperature.

Convective drying treatments are performed using a ventilate thermostatic oven (*ISCO serie 9000*).
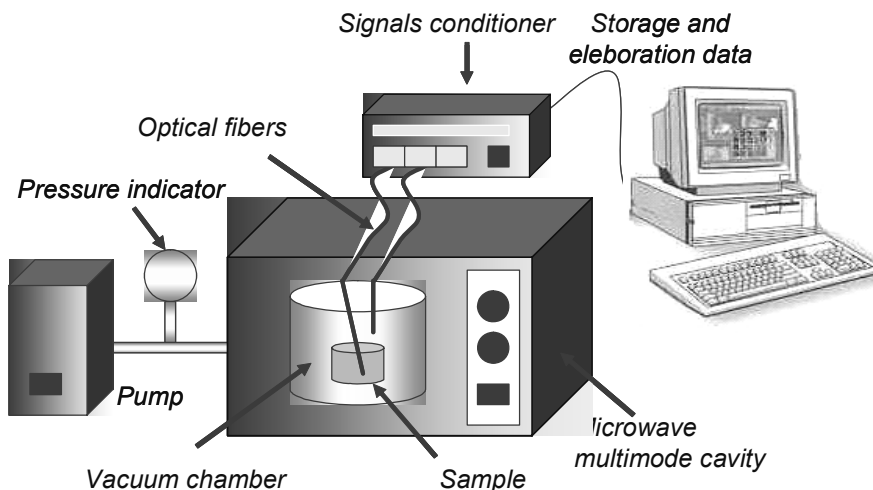
Figure 1 - Schematic representation of the sep-up apparatus for dielectric drying experiments

Dielectric drying runs are carried out in a closed multimode applicator (*De Longhi mod. 314 MW Easy*) operating at 2.45 GHz and at different power levels. The multimode applicator is equipped with an optical thermometer (*FISO, mod. UMI 8*) with teflon probes (*Fort Fibre Ottiche FOT L*) to measure and to record the temperature profiles in the potato tubers during microwave processing. The vacuum treatments are performed using a pyrex chamber placed in the cavity and connected to a membrane pump (*KNF LABOPORT N.842.3 FT40.18*). In Figure 1 the experimental set-up is sketched.

A network analyser instrument (8753ES Agilent Technologies) with a dielectric probe meter (85070D Agilent Technologies), in the frequency range from 1 to 6 GHz, is used to perform the dielectric characterizations of the potato samples.

Samples are cut in cylindrical shape, 31 mm in diameter and 20 mm in thickness (Figure 2). Sample dimensions have been determined on the basis of potato size and dielectric properties to obtain a representative model-matrix and a volumetric heating (penetration depth bigger than diameter/thickness values). Before microwave drying, each sample is pre-treated by blanching (in hot water for two minutes and then in cool water).
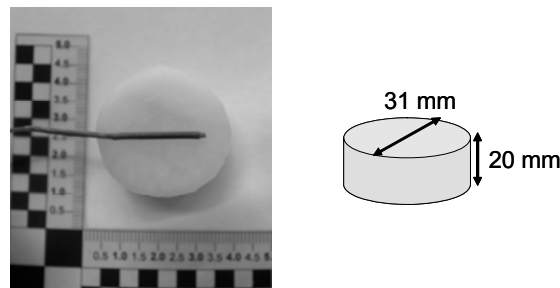
Figure 2 - Sample preparation

The temperature profiles of samples and bulk have been monitored by optical fibers. Data acquisition procedure has been performed by a PC with a dedicated software.

The potato samples drying and rehydratation tests have been carried out via gravimetric methods.

Results and discussion

Figure 3 shows a typical dielectric spectrum of the raw potatoes used in this work, in the range 1 to 6 GHz. The values obtained outline the highly dissipative behaviour of the starch matrixes, due to the strong interaction between electromagnetic field and the matrixes themselves. This is related to their large water content and to the synergic interaction water-starch chains (interacting mixtures) [7] [8].

Viceversa, the thermal diffusivity (i.e. the ratio thermal conductivity to capacity) of potatoes is very low, such as for vegetables and fruits (see Figure 4) [9] [10]. As a consequence, traditional drying methods, which are based on heat convection and conduction phenomena, require extremely long treatment times.
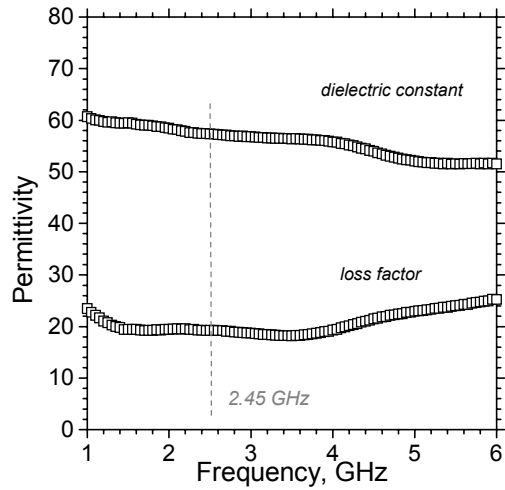
Figure 3 - Dielectric constant and loss factor of raw potato samples
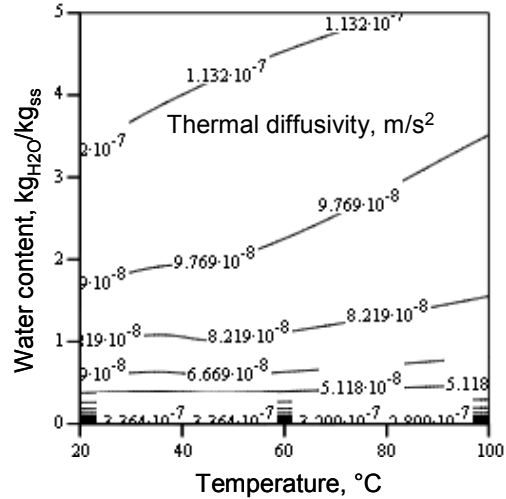
Figure 4 - Contour plot of thermal diffusivity of potato
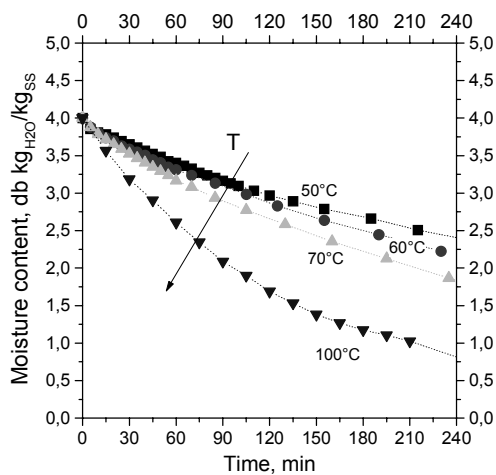
Figure 5 - Drying curves of potato samples. Convective method at different bulk temperatures (50 °C, 60 °C, 70 °C and 100 °C)
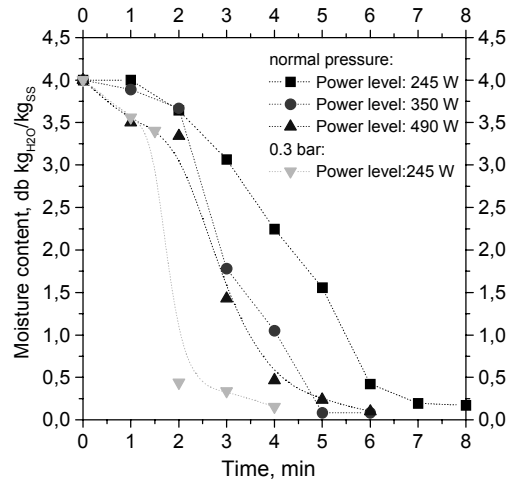
Figure 6 - Drying curves of potato samples. Microwave heating at different conditions (245 W, 350 W and 490 W)

It has to be noted that both rates and temperatures of the drying processes strongly affect morphological and structural properties of the final products. In particular, the rate of mass transfer inside the matrixes determines the parenchyma cell modifications and the related starch matrix shrinkage. As a matter of fact, slow drying rates lead to highly shrunken, very dense materials. The potatoes dried in the convective oven with the long processing times required (see Figure 5) show a progressive elongation of parenchyma cells with time and consequently a progressive starch structure densifications [11]. Moreover, slow mass and heat transfer rates allow the solutes migration from the core to the surface matrixes. This phenomenon generates a crust that could hinder both further mass losses and the eventual rehydratation processes.

Note that the crust could even cause internal fractures and breakages due to water vapour overpressures.

In dielectric drying, high heating rates have as a consequence high rates of mass transfers and, in turn short treatment times. In Figure 6 are reported the drying curves of potato samples obtained at different power levels. As can be see, the treatment times are in the order of minutes.

During microwave heating the water can leave the liquid phase and diffuse as vapour flux even inside the matrix core. Water diffusion as a vapour phase avoids the solutes migration and, thus, the crust formation. Furthermore, the generation of a puffed structure in the material under drying reduces the shrinkage phenomena (see Figure 7).

The same physical features are observed in the drying processes under vacuum conditions, even if reduced external pressures could implicate an enhancement of the puffing structures.

Thus, microwave treatments avoid solutes migration and crust generation, but can produce puffed structures. This latter characteristic has a crucial role on rehydratability processes and represents a desired feature for crunchy snacks. However, a strong puffing can seriously damage the dried products.

In Figure 8 the results of rehydratation tests of potato samples dried via convective methodology and by microwave treatments are reported. As it is shown, the better restore of the potatoes initial moisture content is obtained for both (atmospheric and 0.3 bar in pressure) the experimental conditions used in microwave techniques.
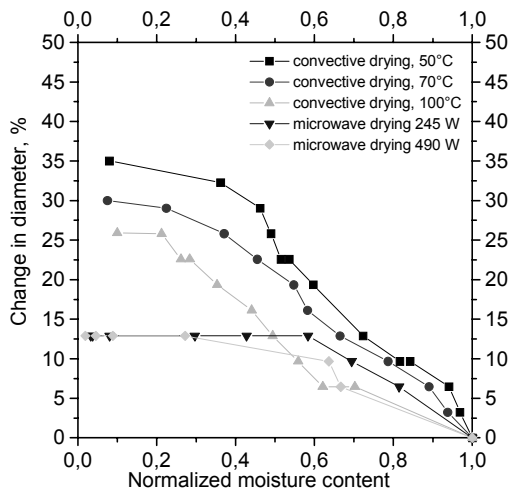
Figure 7 - Percentage change in diameter with moisture content during convective (50 °C, 70 °C, 100 °C) and microwave (245 W and 450 W) drying tests
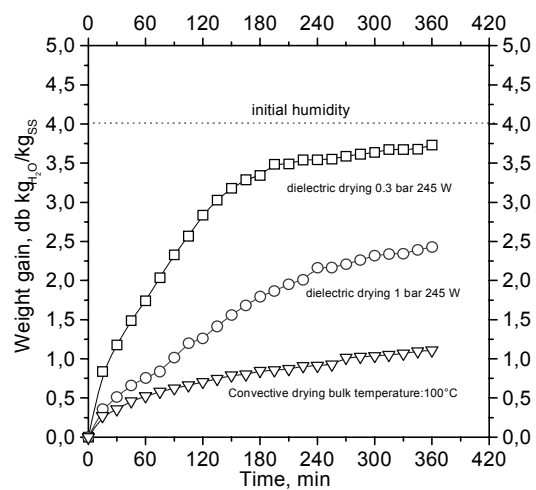
Figure 8 - Weight gain of potato samples dried by different techniques (rehydratation at 20 °C)

Conclusions

Dielectric drying of starch matrixes of *Solanum tuberosum* is characterized by short treatment times if compared to convective methods.

The rate of the simultaneous heat and mass transfer phenomena has a crucial role on the structural properties of the dried products obtained. Samples dried via microwaves show a porous structure (puffed aspect) and a reduced shrinkage.

The absence of a superficial crust allows a good performance in the rehydratation tests.

References

[1] Cappelli P., Vannucchi V., Chimica degli Alimenti, Zanichelli Ed., Bologna, 2000

[2] Nijhuis H. H., Klock W., Leguijt C., Muresan S., Torringa H.M., Yuksel D., "Approaches to improving the quality of dried fruit and vegetables," Food Sci. & Tech., 9 13-20 (1998)

[3] Vega-Mercado H., Gòngora-Nieto M., Barbosa-Cànovas V.G., "Advances in dehydration of foods," J. of Food Eng., 49 271-289 (2001)

[4] Torringa

[5] Tang J., Hao F., Lau M., "Microwave Heating in Food Processing"; pp. 1-44 in Advanced in: Bio-processing Engineering, X.H. Yang and J. Tang Eds., Word Scientific Ltd., New Jersey, 2002

[6] Khraisheh M.A.M., McMinn W.A.M, Magee T.R.A., "A multiple regression approach to the combined microwave and air drying process," J. Food Eng., 43 243-250 (2000)

[7] Mudgett R.E., "Electrical properties of foods"; pp. 49-87 in Engineering properties of foods, Rao M.A. and Rizvi S.S.H., Eds., Marcell Dekker Inc., New York, 1986

[8] Pace W.E., Goldblith A., Van Dyke D., Westphal B., "Dielectric properties of potatoes and potato chips," J. of Food Sci., 33 37-42 (1997)

[9] Liang X.G, Zhang Y., Ge X., "The measurement of thermal conductivities of solid fruits and vegetables," Meas. Sci. Technol., 10 N83-N86 (1999)

[10] Sweat V.E., "Thermal properties of foods"; pp. 329-390 in Engineering properties of foods, Rao M.A. and Rizvi S.S.H., Eds., Marcell Dekker Inc., New York, 1986

[11] Wang N., J.G. Brennan, Change in structure, density e porosity of potato during dehydration, J. of Food Eng., 24 61-76 (1995)

MICROWAVE PROCESSING OF SiC - MATRIX COMPOSITES BY CHEMICAL VAPOUR INFILTRATION (CVI)

B. Cioni, E. Origgi, A. Lazzeri

Department of Chemical Engineering, University of Pisa,

Via Diotisalvi 2, 56126 Pisa, Italy

beatrice.cioni@ing.unipi.it

Abstract

Processing by means of MicroWave assisted Chemical Vapour Infiltration (MWCVI) of silicon carbides, SiC matrix composites based and their physical-chemical characterization has been carried out in this work. A new pilot scale microwave assisted CVI reactor was designed and built. In order to easily carry out a scale up of this process, typical lab-scale technical solutions have been carefully avoided. Silicon carbide was infiltrated inside of pores that exist between the fibres tows by the decomposition at 1000 °C of methyltrichlorosilane according to the following reaction:

$$CH_3SiCl_3(g) + H_2(g) \rightarrow SiC(s) + 3HCl(g) + H_2(g)$$
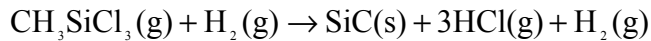
The microstructure of the samples obtained from the preliminary infiltration trials was observed by scanning electron microscopy in order to evaluate the quality and the degree of densification that has been achieved within the fibre tows. Preliminary results suggest that MWCVI is a perspective method to produce SiC-matrix composites with high densification degree and purity on large scale.

Keywords

Microwave, silicon carbide, composites, chemical vapour infiltration.

Introduction

Ceramic matrix composites (CMCs) represent the latest entry in the field of composites for applications involving high temperature and harsh operating conditions, since a major shortfall of conventional ceramics is that they possess low fracture toughness, which can results in brittle failure [1]. They combine the thermal and chemical resistance of monolithic ceramics with the mechanical strength of ceramic reinforcements with improved fracture toughness when compared with ordinary ceramics.

For the past 15 years, research and development of CMCs has been sustained because of their potential for military and commercial applications, including (a) aircraft engine components, such as combustors, turbines, compressors and exhaust nozzles; (b) ground-based and automotive gas turbine components, such as combustors, first and second stage turbine vanes and blades, and shrouds; (c) aerospace engines for missiles and reusable space vehicles; and (d) industrial applications, such as heat exchangers, hot gas filters, and radiant burners [2,3].

There are several ways of producing ceramic matrix composites [1], some of these techniques are no more than variants on the processing of monolithic ceramics. The processing of CMCs should be considered an integral part of the whole process of designing a CMC component: in fact any damage to the reinforcement because of processing will result in a decrease of final performances or the reinforcement orientation resulting from the processing could influence the mechanical response of a CMC to an applied load.

Among industrially available matrix densification techniques, chemical vapour infiltration (CVI) best meets the quality requirements for CMCs [4], particularly for the production of SiC ceramic reinforced with SiC fibres (SiC$_f$-SiC composites) that present excellent high temperature properties including: high strength, high modulus of elasticity, low coefficient of thermal expansion and hence good wear and thermal shock resistance, chemical stability and a greater fracture toughness than for unreinforced SiC.

This technique is based on the common principle of filling the porosity inside the fibre preforms with a SiC matrix resulting from decomposition of gaseous precursors (CVI). The CVI process involves fabricating ceramic fibres preforms in the shape of final parts. Fibres such as silicon carbide are woven, braided, and wound to produce the desired shape. The preforms are infiltrated with chemical vapours that react at elevated temperatures to form a silicon carbide matrix onto and in between the fibres.

The maintaining of the preform porosity open until the end of the densification process is the key point of the CVI process [5]. If the outside temperature of the preforms is higher than the interior one, than the deposition is preferential at the exterior of the preform and does not advance in the interior of the sample. CVI is a relative slow technique since it has to be performed at low deposition rates in order to maintain interconnected open porosity. This implies long process times and high costs. In order to reduce the CVI process time, to lower the cost of this typically expensive technology and to improve the material quality, avoiding fibre degradation, an innovative Microwave Assisted Chemical Vapour Infiltration (MWCVI) pilot plant [6] was recently developed by our research group.

Microwave radiation has been used as an alternative route to conventional radiant heating techniques in the chemical vapour infiltration (CVI) process to produce fibre reinforced ceramic composites. The degree at which a ceramic material adsorbs MW radiation is dependent on its dielectric properties: silicon carbide, alumina, zirconia for example are all susceptible materials and can be heated by microwaves [7-10]. Microwave heating is different from conventional heating in that the energy is deposited uniformly through the component being heated. The atmosphere surrounding the component will not be directly affected by the MW energy and will hence be at lower temperature than the surface of the component. Radioactive loss from the surface may results in an inverse temperature profile: this basically means that the surface of the component will be at a lower temperature than the centre. Then the deposition of the ceramic matrix proceeds from the inside to the outside, avoiding the problems connected with the sealing of the external pores of the preform [11].

Rapid heating is also possible due to the uniform heating of the component, which reduces the thermal stresses generated by temperature gradients. These gradients in case of MW heating are generally much lower if compared to conventional heating methods.

By means of the MWCVI process high purity and high density SiC matrices can be obtained and preforms of very complex geometry can be successfully infiltrated, at operating temperatures between 900 and 1200 °C. Since the pressure required by the process is low (1-100 kPa), the damaging of fibres and their reactions with the matrix are limited. Previous works carried out by Binner et al. [12,13], based on SiC$_f$/SiC components (50 mm diameter, 10 mm thick), has shown that by using microwaves to enhance the CVI process, fabrication times can be reduced from hundreds of hours to around 30 hrs.

Respect to the work of Binner et al. [12,13] the MWCVI pilot plant developed in this work presents the important characteristic of carefully avoiding typical lab-scale technical solutions, like the use of large components in quartz or other materials that are not suitable for industrial production plants, in order to easily carry out a scale up of this process. This approach has leaded us in coping with many new problems that required innovative solutions.

Experimental section

In order to design and build the new MWCVI system (Figure 1) it has been necessary to prepare: a system for generation and transfer of microwave energy to the preform to be heated (a Muegge Gmbh variable power, water cooled, 6 kW 2.45 GHz microwave generator, equipped with a Toshiba E3327 magnetron), a flow system for the reagent and carrier gases in order to bring them in contact with the preform without contamination and in safety conditions, a system for the treatment of exhaust gases, and an advanced electronic apparatus of process control and management.

(a)　　　　　　　　　　　　　　　(b)

Figure 1 - An image of the MWCVI pilot plant (a) and the control station (b)

The Pilot Plant was designed after modelling thermal and electromagnetic fields distribution [14]. Abaqus 6.1.1 F.E.M. package [15] was used to perform the thermal modelling, while Ansoft HFSS [16] enabled the electromagnetic modelling. Simulation results showed that the electric field inside of the chosen insulator produced a negligible heating. The electric field was reasonably constant within the sample, allowing foreseeing uniform heating. This could produce an uniform deposition of the SiC precursor compound on silicon carbide fibres. Moreover the analysis revealed the need of a mode stirrer to achieve a better distribution of microwave power improving the process efficiency. Specific software, developed with the Intelluxion FIX 7.0 [17] programming suite, controls the microwave power directed to the MWCVI reactor in order to obtain the desired temperature profile during the deposition.

Methyltrichlorosilane (MTS, Sigma-Aldrich, 99% of purity)) was used as the precursor material for SiC deposition. MTS is generally preferred over other reactants because it has a one to one ratio of carbon to silicon that yields stoichiometric SiC over a wide range of operating conditions [18]. The MTS gas (boiling point: 66 °C) was produced by the vaporization of liquid MTS in a suitable temperature controlled vessel. When heated to around 1000 °C it decomposes into SiC and HCl according to the following reaction:

$$CH_3SiCl_3(g) + H_2(g) \rightarrow SiC(s) + 3HCl(g) + H_2(g)$$
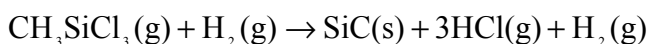
MTS was carried to the reaction chamber using a mixture composed of 97.2% Ar and 2.8% H_2 as gas carrier, with the gas flow passing through the sample thickness, as indicated by the arrow in Figure 2. The first layer (layer 1) is the nearest sample surface with respect to the reagent gas flux, the 7th layer (layer 7) is in the centre of the composite and the 15th layer (layer 15) is on the upper surface.

The MTS concentration could be controlled by the gas flow rate within the range 10-20 mol/hr, maintaining the MTS liquid at constant temperature of 40 °C. The molar H_2/MTS ratio was chosen between 500-1000. The total pressure of the reaction chamber was adjusted to 1.01 bar and the products of the reaction were removed with a scrubber system consisting of an aqueous solution of sodium hydroxide (Carlo Erba reagents, 97% of purity) with a concentration of 15 g/l.
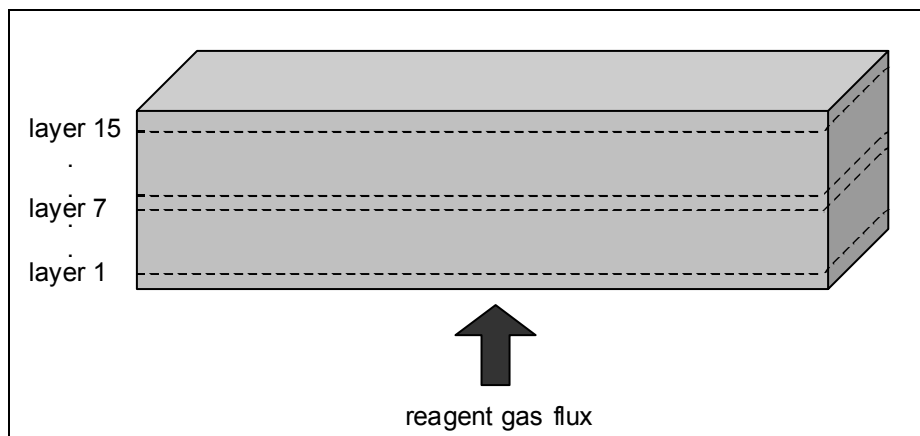
Figure 2 - Scheme of the SiC$_f$/SiC sample
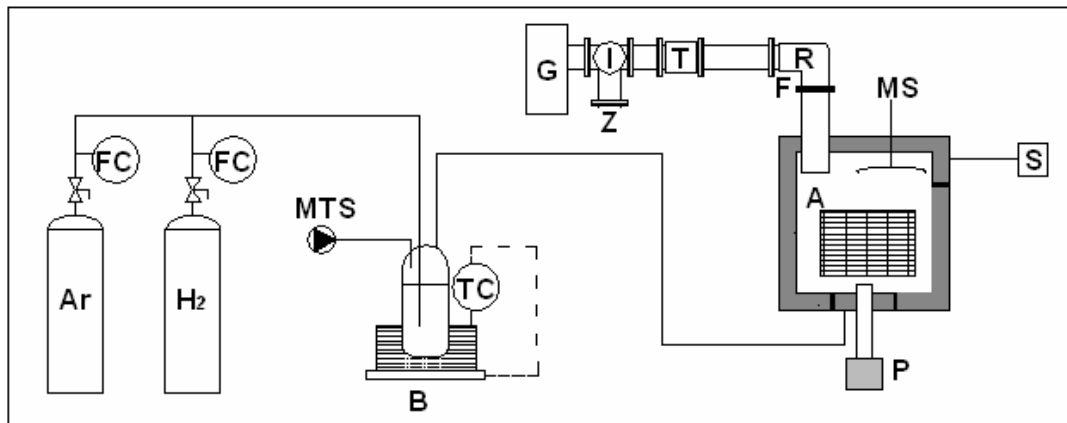
Figure 3 – Scheme of the MWCVI reactor (G: generator 2.45 GHz, 6 kW; I: three port circulator; Z: water cooled dummy load; T: auto tuner; R: connected transition; F: quartz window; A: applicator; MS: mode stirrer; P: pyrometer; S: scrubber system; B: bubbler; FC: feed controller; TC: temperature controller)

The residual gas (including H_2 and Ar and MTS unreacted decomposition products) are vented into a fume head. At the end of infiltration, the MTS-H_2 stream and microwave power were shut off and argon was allowed flowing through the reaction vessel for a minimum of 2 hr until the sample had cooled down to room temperature and the toxic by-products were completely removed and neutralized.

A schematic diagram of the MWCVI system used to infiltrate the silicon carbide fibre preforms is reported in Figure 3. SiC preforms were obtained using 15-layer Ceramic Grade Nicalon NL 202 woven fabric in the form of bricks of 20x40x80 mm in size. The percentage weight composition, density and other characteristics of the Nicalon Fibres used in this work are reported in Table 1.

Morphology of the composites was examined using a JEOL JSM 5600 Scanning electron microscopy (SEM) and electron probe microanalysis based on energy dispersive X-ray spectroscopy (EDS) was used in order to obtain a semi-quantitative composition of samples before and after the MWCVI process, determination of oxygen by LECO TC400 Series, by employing the inert gas fusion principle, was carried out in order to confirm data about the oxygen content in the samples.

Table 1 - Chemical-physical and mechanical properties of Ceramic Grade Nicalon NL 202 fibres [19]

	Si	C	O
Composition (wt%)	56.6 %	31.7%	11.7%
Density (g/cm^3)	2.55		
Young's Modulus (GPa)	199		
Strenght (GPa)	3		

Results and discussion

In Figure 4 is reported a typical temperature profile recorded during an experimental infiltration trial. Temperature is measured by an optical pyrometer placed under the Nicalon preform (see Figure 3).
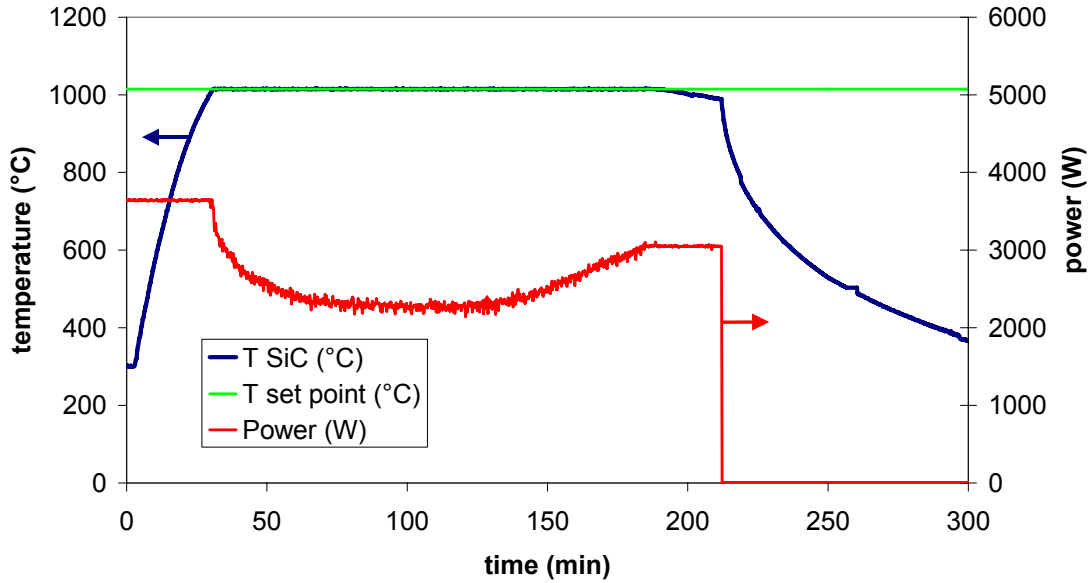
Figure 4 - Temperature profile for microwave chemical vapour infiltration for SiC/SiC sample

The sample was initially heated by microwave irradiation at constant power and with a flux of the Ar/H_2 mixture up to 1000 °C was reached. About 3.5 kW of microwave power was required to heat the sample until the temperature of 1000 °C in only 30 minutes, because of the high dielectric constant of silicon carbide. At this point MTS was allowed into the chamber to start the infiltration. The sample temperature was maintained constant by the action of a PID controller that adjusted the power in order to keep the temperature constant.

a)   b)
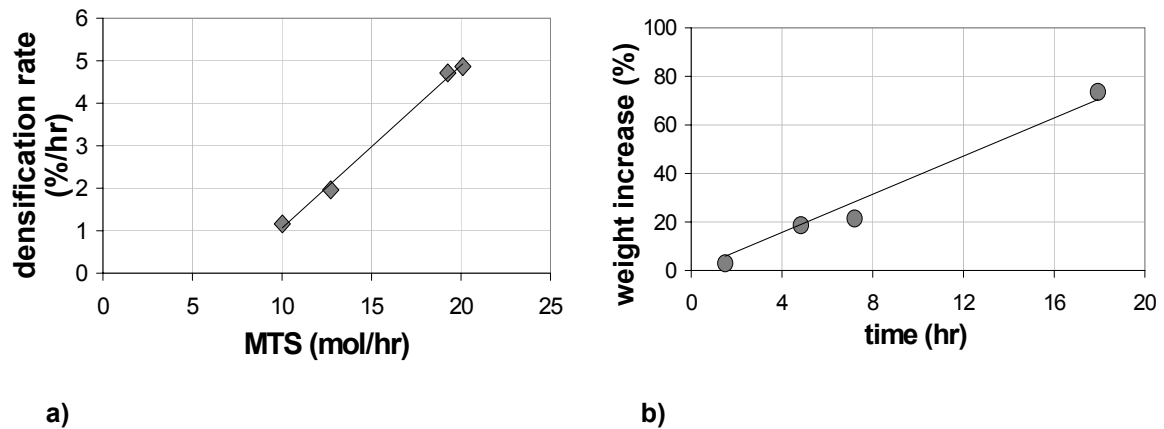
Figure 5 - a) Densification rate of 15-layer fibre preforms as a function of the MTS molar flux, during a multi-cycles process of 18 hr; b) Weight increase (%) vs. time during a multi-cycles process of MWCVI, with an average MTS molar flux of 15 mol/hr

The densification rate of 15-layer fibre preform is shown in Figure 5a) as a function of the MTS molar flow rate. It is clear that the densification rate enhanced with the increase of the reagent molar flux. In Figure 5b) the weight increase vs. time is reported, showing that about 18 hr are needed to reach the 70% of weight increase, with an average MTS molar flux of 15 mol/hr. The overall deposition of silicon carbide from the MWCVI process was a linear function of the time.

The layer 1 (Figure 6a) and Figure 6b)), directly in contact with the reagent gas flux, resulted completely infiltrated with lack of porosity. This lower surface appeared very dense and compact. This type of deposition is not desirable since it can make the proceeding of the infiltration difficult if not impossible, due to the sealing of the outer pores of the perform. Figure 6c) presents a SEM micrograph at 35 x magnification and Figure 6d) at 1000 x magnification of the layer 7 of the SiC_f/SiC composite surface after the microwave assisted infiltration.
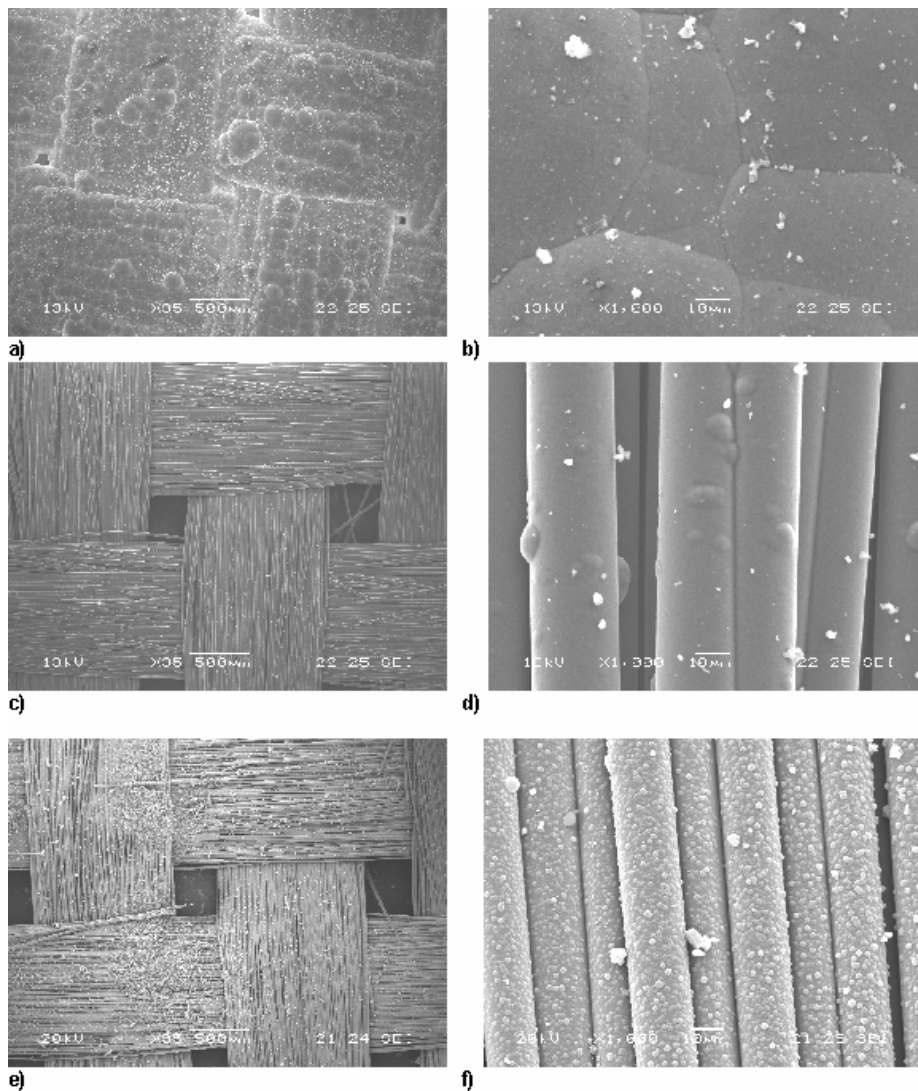
Figure 6 - SEM image showing the silicon carbide deposit produced via MWCVI at 35 x magnification (a, c, e) and SEM image of single fibres with SiC deposition layer at 1000-x magnification (b, d, f)

Although a certain number of micro crystals of silicon carbide were visible on the fibre surface in that zone, the composite contained an evident inter-tow porosity. The upper surface (layer 15), as shown in Figure 6e) and Figure 6f) resulted more infiltrated than the inner layers. This effect is probably due to the fact that a portion of the gaseous reactive mixture bypassed the sample, flowing around it, filling up the chamber and infiltrating the sample from the opposite side respect to the inlet flux. In other terms, the mechanism of deposition in the outer layers was mostly due to convective mass transfer while in the inner layers only diffusion can take place during the infiltration. Comparing the layer 1 with the layer 15 it is evident that, for the upper surface, the process was comparatively slower, resulting in a higher degree of porosity. Nevertheless the deposition resulted quite uniform with a large number of spherical micro crystals.

The fibre diameters were found to be in range of 9-10 microns in samples before the treatment, with a percentage increase of the coating thickness on the fibres of 63%, 12% and 6% respectively for the layer 1 (Figure 7a), the layer 2 (Figure 7b) and the layer 4 (Figure 7c), after the MWCVI trials.

a)   b)   c)
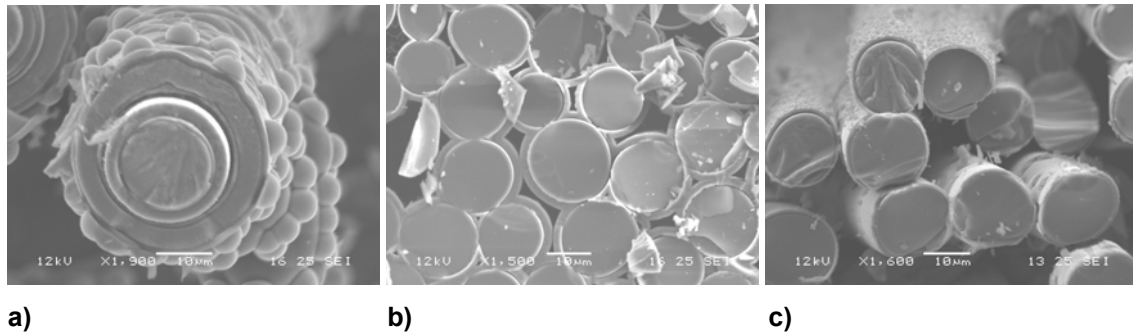
Figure 7 - SEM image showing sections of the SiC$_f$/SiC sample under 1500-x magnification in the layer 1 (a), layer 2 (b) and layer 3 (c)

These results were apparently in disagreement with the inverse temperature profiles that could be produced via microwave heating, with the associated preferential densification of the SiC$_f$/SiC composites from the inside out [11]. The gas reagent flux, in this case, was probably not well optimised, in fact MTS went straight against the lower surface of the composite and there it decomposed mainly by filling the more external pores present on the first layers. The gas mixture progressively decreases its content in reactive component (MTS) and also reaches the upper surface with a reduced mass flow rate. This can explain the reduced deposition observed for the outer layer. In general it is evident that, for the outer and the inner layers, the most of the inter- and intra-tow porosities were not fully infiltrated and sealed. However this fact is known also for composites produced with standard CVI, which generally contain macroscopic inter-fibre bundle pores which hamper several important properties related with composite rigidity and transport properties.

Further MWCVI cycles will be needed in order to completely densify the perform, but in order to reduce the processing time a future development of this research will be the combination of MWCVI with polymer impregnation and pyrolysis (PIP) [20] process for the preparation of SiC$_f$/SiC composites.
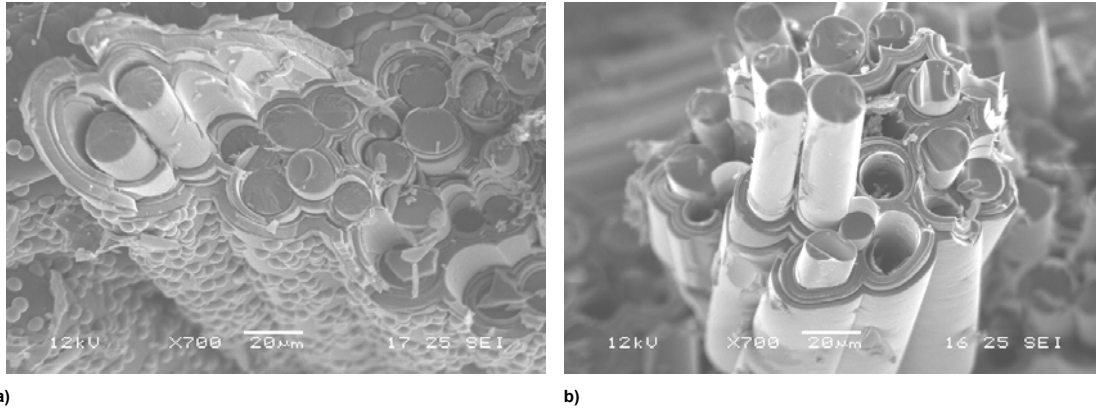
Figure 8 - SEM micrograph of a composite fracture surface, showing debonding within the matrix around the interface and consequently some fibre pull-out in the first layers a) and in the inner layers b)

In this way it will be possible to considerably reduce the time to infiltrate the macro-pores that exist between the fibre tows. These can be hundreds of micrometres wide and consequently infiltrate much more slowly than the micropores that exist between the fibres within the tows.

By a rough preliminary analysis, the composite failure behaviour seemed to be related with a certain degree of fibre pull-out (Figure 8). That result is normally associated with a weak interface between fibres and matrix, although no attempt has been made in this work to optimise the interphase adhesion. In fact, it is well known that in SiC_f/SiC composites, the interphase between SiC fibres and SiC matrix is very important in order to obtain excellent mechanical properties since it allows the deflection of cracks at the interphase. The fibre pullout during fracture leads to excellent interfacial shear strength and the ductile-like failure modes to produce good mechanical properties [21].

The EDS analysis showed a noticeable difference between the samples before and after the MWCVI process (Table 2). The oxygen content values, declared from the manufacturer [19], were confirmed by a LECO analysis. The discrepancy with the EDS results can be expected since this type of analysis provides only semi-quantitative results, with the determination of the oxygen content by the gas fusion methods allows precision of the order of a few ppm. Three major peaks were observed in the EDS spectra from the untreated samples, which include silicon (Si), carbon (C) and oxygen (O). The former two elements originate from the main constituents of the SiC fibres and the last element (O) probably pertains to the O-rich amorphous phase in which SiO_xC_y has been identified [22]. When the MWCVI treated samples were detected a much greater C-peak and a reduced Si and O-peak were found. This suggests that some oxygen atoms and silicon were replaced by carbon atoms forming an increased level of C-rich phase.

Table 2 - Composition (wt%) obtained by EDS micro-analysis of SiC_f (before MWCVI) and SiC_f/SiC (after MWCVI)

	Composition (wt%)		
	Si	C	O
SiC_f	60	21	19
SiC_f/SiC	33	61	6

The sensible decrease of oxygen content in the obtained composite is an important result because the high temperature mechanical properties of SiC_f/SiC composites get considerably worse when oxygen is present in the material. Nevertheless the Nicalon NL202 SiC-based fibres used in this work, are not pure SiC, but Si–C–O fibres, referred to as SiC-based fibres of first generation, consisting of SiC-nanocrystals (1–2nm in size) and free carbon embedded in an amorphous SiCxOy matrix [22]. Recently, SiC-based fibres of second generation (such as Hi- Nicalon) have been developed: they are oxygen-free fibres consisting of a mixture of SiC-nanocrystals (5 nm in mean size) and free carbon [C/Si (at) ratio=1.39]. Moreover the SiC fibres of third generation (such as Hi-Nicalon S, Tyranno SA or Sylramic) are oxygen-free and quasi-stoichiometric [with C/Si (at)=1.00–1.08], with an excellent thermal stability. These advanced SiC fibres are currently extremely expensive due to the small size of their market [23] and have not been taken into consideration in this study, which is mainly focused at optimising the operating conditions of the MWCVI Pilot Plant.

Conclusions

Results obtained up to now from the preliminary infiltrations carried out on preforms, not previously pre-treated; show the feasibility of the industrial scale-up of MWCVI process. An average weight increase of about 70% respect to the initial sample was achieved in 18 hr of microwave treatment. The silicon carbide deposition inside the sample was sufficiently homogeneous and compact, with an evident inter-tow porosity was still present. The densification of the SiC_f/SiC composites results deeper from the lower to the upper surface, because the gas reagent flux was not yet well optimised. The oxygen content in the MWCVI treated sample was considerably decreased respect the untreated fibres, therefore the plant was well-sealed and suitable in order to carried out operations in absence of moisture and air, which maybe responsible of silica and SiC_xO_y formation. Silica can cause deposition inside the piping system and possible blockage of the gas flow, while the presence of SiC_xO_y would hamper the mechanical properties of the SiC_f/SiC composites.

Acknowledgements

References

[1] Chawla, K.K., Ceramic matrix Composites, Chapman & Hall, 1993.

[2] Naslain, R., Design, Preparation and Properties of non-Oxide CMCs for Application in Engines and Nuclear Reactors: an Overview, Compos. Sci. Technol., 2004, 64, 155-170.

[3] Lamouroux, F., Bertrand, S., Pailler, R., Naslain R., Cataldi, M., Oxidation-Resistant Carbon-Fibre-Reinforced Ceramic-Matrix Composites, Compos. Sci. Technol., 1999, 59,1073–1085.

[4] Besmann, T.M., McLaughlin, J.C., Lin, H.T., Fabrication of Ceramic Composites: Forced CVI, J. Nucl. Mater., 1995, 219, 31-35.

[5] Bertrand, S., Lavaud, J.F., El Hadi, R., Vignoles, G., Pailler, R., The Thermal Gradient-Pulse Flow CVI Process: a New Chemical Vapor Infiltration Technique for the Densification of Fibre Preforms, J. Eur. Ceram. Soc., 1998,18, 857-887.

[6] Lazzeri, A., Cioni, B., Origgi, E., Cercignani, G., Nardini, G., Production of Ceramic Matrix Composites by Means of an Innovative Pilot-Plant for Microwave Assisted Chemical Vapour Infiltration (MWCVI), 10th International Conference on Microwave and High Frequency Heating, pp. 322-325, Modena 2005.

[7] Tinga, W. R., Fundamentals of microwave-material interactions and sintering. In Microwave Processing of Materials, ed. W. H. Sutton, M. H. Brooks and I. J. Chabinsky. Materials Research Society, Pittsburgh, PA, 1988, vol. 124, pp. 33-43.

[8] Metaxas, A.C. & Binner, J. G. P., Microwave processing of ceramics. In Advanced Ceramic Processing Technology, ed. J.G.P. Binner. Noyes Publications, New Jersey, USA, 1990, 285-367.

[9] Clark, D.E., Folz, D.C. & West, J.K., Processing materials with microwave energy, Mat. Sci. Eng. A-Struct., 2000, 287 [2], 153-158.

[10]   Xie, Z., Yang, J., Huang, X., Huang, Y., Microwave Processing and Properties of Ceramics with Different Dielectric Loss, J. Eur. Ceram. Soc., 1999, 19, 381-387.

[11]   Jaglin, D., Binner, J., Vaidhyanathan, B., Calvin, P., Prentice, Shatwell, B., Grant, D., Prentice, C., Shatwell, B., Grant, D., Microwave Heated Chemical Vapor Infiltration: Densification Mechanism of SiCf/SiC Composites, J. Am. Ceram. Soc., 2006, 89 [9], 2710–2717.

[12]   Yin, Y., Binner, J.G.P., Cross, T.E., Microwave Assisted Chemical Vapour Infiltration for Ceramic Matrix Composites, Ceram. Trans., 1997, 80, 349-356.

[13]   Timms, L.A., Westby, W., Prentice, C., Jaglin, D., Shatwell, R.A., Binner, J.G.P., Reducing Chemical Vapour Infiltration Time for Ceramic Matrix Composites, J. Microsc., 2001, 201(2), 316-323.

[14]   Nenciati, F., Origgi, E., Lazzeri, A., Thermal and Electromagnetic Characterization of a new Pilot-Plant for the Production of Ceramic Matrix Composites by Microwave Chemical Vapour Infiltration, 9th International Conference on Microwave and High Frequency Heating, pp. 1-5, Loughborough University, UK. 2003.

[15]   Abaqus is a product of ABAQUS, Inc., Rising Sun Mills, 166 Valley Street, Providence, RI 02909-2499 USA *http://www.abaqus.com/*.

[16]   Ansoft HFSS is a product of Ansoft Corporation, 225 West Station Square Drive, Suite 200, Pittsburgh, PA 15219 USA *http://www.ansoft.com/*.

[17]   Intellution Fix 7.0 Industrial Automation Software.

[18] Stinton, D.P., Hembree, D.M., More, K.L., Sheldon, B.W., Besmann, T.M., Headinger, M.H., Davis, R. F., Matrix Characterization of Fibre-Reinforced SiC Matrix Composites Fabricated by Chemical Vapour Infiltration, J. Mater. Sci., 1995, 30, 4279-4285.

[19] Nippon Carbon Co., LTD. Technical datasheet.

[20] Nannetti, C.A., Riccardi, B., Ortona, A., La Barbera, A., Scafe, E., Vekinis, G., Development of 2D and 3D Hi-Nicalon Fibres/SiC Matrix Composites Manufactured by a Combined CVI–PIP Route, J. Nucl. Mater., 2002, 307–311, 1196–1199.

[21] Jacques, S., Guette, A., Langlais, F., Naslain, R., C(B) Materials as Interphases in SiC/SiC Model Microcomposites, J. Mater. Sci., 1997, 32, 983-988.

[22] Chollon G., Pailler R., Naslain R., Laanani F., Monthioux M., Olry P., Thermal stability of a PCS-derived SiC fibre with a low oxygen content (Hi-Nicalon), J. Mater. Sci., 1997, 32, 327-347.

[23]   International Town Meeting on SiC/SiC Design and Material Issues for Fusion Systems, Oak Ridge National Laboratory, January 18-19, 2000, *http://aries.ucsd.edu/PUBLIC/SiCSiC*.

MICROWAVE ENHANCEMENT OF THE EARLY STAGES OF SINTERING OF METALLIC POWDER COMPACTS AND METAL-CONTAINING COMPOSITES

P. Veronesi, C. Leonelli, G. Poli

Dipartimento di Ingegneria dei Materiali e dell'Ambiente

Università degli Studi di Modena e Reggio Emilia

Via Vignolese 905, 4110 Modena - Italy

paolov@unimore.it

Abstract

Coupling numerical simulation of the electromagnetic field during sintering of metallic powder compacts and metal-containing composites with the experimental results, it has been possible to demonstrate the existence of a microwave enhancement of the early stages of sintering. The main phenomena involved resulted to be the electromagnetic field concentration in the regions among the conductive particles, as well as direct microwave absorption within the skin depth of the metal particles. This local concentration of the electric field, occurring exactly in the regions of necks formation, can have intensity higher than the dielectric strength of the medium, thus favouring breakdown phenomena, leading to arcing and local plasma formation, which trigger more efficient mass transport mechanisms during sintering.

Three different cases has been numerically simulated and experimentally tested: sintering of micrometric steel and brass spheres, sintering of millimetric pure metals and brass spheres, sintering of glass matrix composites reinforced with metal fibres.

I.   Introduction

Microwave sintering of metals is a relatively new technology, whose main reported benefits regard higher densification, rounder pores shape, lower temperature and shorter processing time with respect to conventional heating treatments [1-6]. However, a complete understanding of the mechanisms responsible of the enhanced microwave sintering is still missing. The microwave absorption within the skin depth of the metal powders cannot completely explain the microwave-matter interaction and the experimentally measured rapid heating of metallic powder compacts. As a matter of fact, conductive particles aggregates, immersed in relatively high intensity electromagnetic fields, can be subjected to other phenomena.

Different explanations have been proposed in the past years, and the most promising ones regard the role of the magnetic field [7-9] or the presence of an insulating oxide layer, which usually covers metallic powders. The presence of such layer not only leads to an increase in the microwave power absorbed by the metallic compacts, but it also changes how heat is generated in the sample volume [10]. Some of the authors recently proposed a further mechanism involved in the microwave heating of metal compacts demonstrating that for small spherical particles the local electromagnetic field distribution can be seriously affected by the spatial arrangement of the conductive particles [4]. This phenomenon can lead to dielectric breakdown conditions, involving arcing and plasma formation near the necking regions.

The aim of this work is to present detailed experimental evidences and numerical simulation results demonstrating the importance of the electromagnetic field concentration in determining the sintering behaviour and the resulting microstructure of metallic compacts and metal-containing composite materials, in particular during the early stages of sintering. Comparative tests were also performed in conventionally heated furnace, in similar geometrical and thermal conditions, to highlight differences with the microwave processing route.

II. Sintering of conductive spherical powders

Spherical particles are often used to produce metal compacts by powder metallurgy routes. The conventional sintering of such compacts is well known and it involves different mechanisms, ranging from solid state diffusion to more efficient mass transport phenomena in presence of liquid or gaseous phase [11]. In case of multi-component systems, microwave selective heating can lead to peculiar results, like different microstructure and densification levels compared to conventional (resistance) heating.

II.I Experimental

Microwave sintering in air of spherical powders generated during EDWC (Electrical Discharge Wire Cutting) has been studied. The starting powders were made mainly by Cu/Zn and Fe/Cr/Ni micro spheres, deriving respectively from the cutting wire and the cut steels. Particle size smaller than 75 µm was selected by sieving the powders after drying in air. Figure 1 shows the X-ray diffraction pattern of the dried powders.
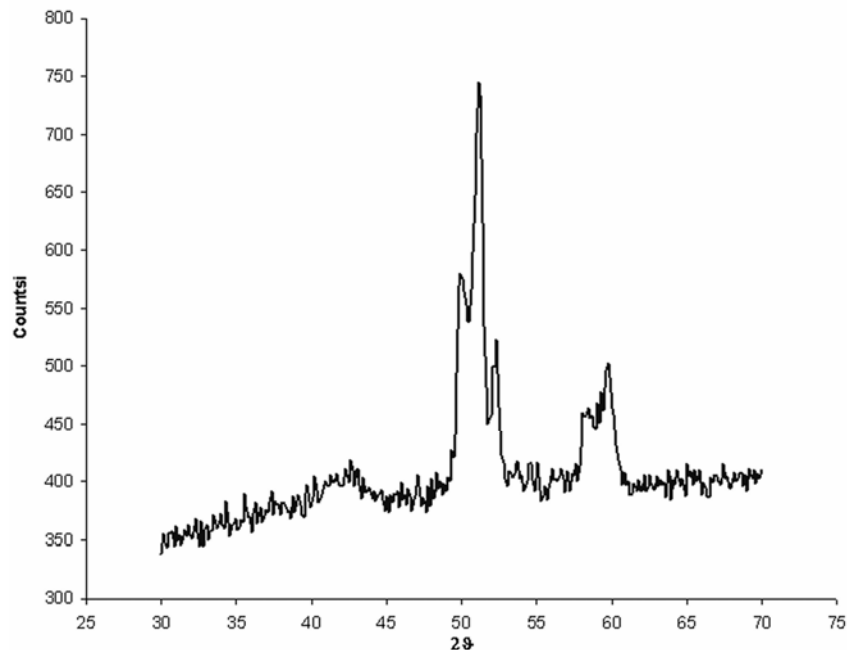
Figure 1 - X-ray diffraction pattern of the dried powders, showing their composition is mainly Cu/Zn and Fe/Cr/Ni

126

The peaks corresponding to d = 2.12, 2.06, 1.83 Å can be ascribed to brass presenting the rombohedric cell of Zn (JCPDS 25-322). The peaks at d = 2.06, 1.79 Å correspond to the CFC structure of austenite (JCPDS 31-619), but the higher planar distances indicate the presence of a solid solution, containing Ni and Cr (JCPDS 33-397), as detected by SEM/EDS analysis. The d = 2.02 Å peak can be ascribed to the CCC structure of Fe α (JCPDS 6-696).

The dried powders have been used after a pre-treatment at 200 °C for 2 hours, which proved not to alter the X-ray diffraction pattern, to prepare 1g compacts having 12 mm diameter, obtained by uniaxial pressing at 34.6 MPa. Average green density of the compacts was 2.52 ± 0.02 kg/dm^3.

Sintering tests have been performed by conventional heating in an Opto.Lab electric furnace, used for Mac Quaid tests, and by microwave heating at 400W forward power, using a single mode TE$_{10n}$ (n= 3 or 4), fed by a magnetron operating at 2.45 GHz, depicted in Figure 2 and described in details elsewhere [4].
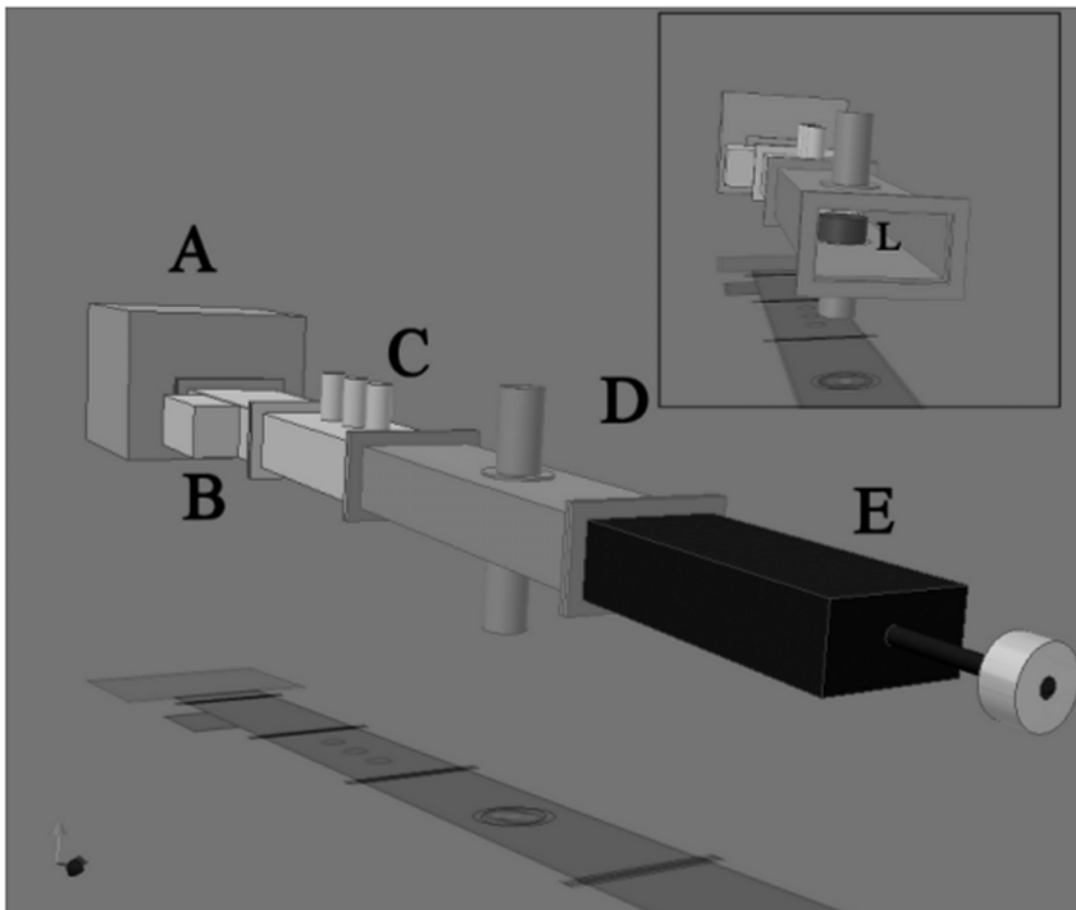
Figure 2 - A) microwave generator @ 2.45 GHz; B) 3-port circulator + dummy load; C) three-stub tuner; D) applicator with measuring ports/gas flux inlets; E) shorting plunger; L) typical load position in the applicator (maximum of electric field)

Thermal insulation of the samples was achieved using coarse alumina powder. An auxiliary absorber (SiC disc) has been introduced in some tests to vary the temperature and electromagnetic field distribution.

Maximum sintering temperature for conventional sintering has been set to 700, 800, 900 and 1000 °C, while microwave heating sintering was performed only at 600, 650, 700 and 800 °C, maintaining in both cases a 4 °C/s heating rate.

Temperature has been measured during microwave sintering by means of optical pyrometers, namely a non-contact Sitel IKS-T14-09 (surface temperature) and a Mikron M680 (inner core temperature), the latter measuring the temperature (above 600 °C) contacting the sample by means of a sapphire fibre.

II.II   Modeling

The software Concerto 4.0 (Vector fields, U.K.) was used to model in 3D a portion of the system, simulating a 400 W microwave generator operating at 2.45 GHz feeding a TE_{103} applicator loaded with a single disc-shaped compact (12 mm diameter, 6 mm height), immersed in alumina powders and contained in a cordierite crucible. A further optional SiC disc (30 mm diameter, 4 mm thickness) placed under the sample was modeled. Two different scales (macro- and micro-) have been used to simulate the microwave heating behaviour of the whole system. The macro-scale allowed the calculation of the SAR (specific absorption rate, in W/kg) of the sample, represented by an equivalent load, as a function of the experimental setup configuration (with or without SiC auxiliary absorber), while the micro-scale was used to evidence local variations of the electromagnetic field distribution near the metallic particles.

The SAR distribution showed that, as expected, under 400 W microwave irradiation the SiC element lowers the maximum electric field near the load surfaces facing the SiC element itself, and it absorbs part of the available microwave power. A detailed analysis of a similar case can be found in [12].

The distribution of the electromagnetic field around the metal particles composing the compact has been obtained considering a 3D model of a small aggregate of 4 spherical particles (diameter 20,15,15 and 6 μm), whose electric and magnetic properties are representative of brass (20 μm sphere, P-CuZn20) or stainless steel (15,15 and 6 μm spheres, AISI 304). Two different conditions have been simulated, the first one considering the very initial stages of sintering, using the electric properties of the metals at room temperature, with particles only contacting, and the second one after a significant necking occurred (neck area of the larger particles equal to 15% of the largest particle cross section), using the materials' electric properties at 600 °C. In both cases, the particles are considered to belong to the surface of the sample (disc-shaped compact), and they are exposed to a microwave forward power of 400 W, at 2.45 GHz. Figure 3 summarises the modeling results, referred to a section of the 3D model.

It is evident (Figure 3a) that in the early stages of sintering, before necking occurs, a pronounced electromagnetic field concentration rises in the space among the particles, and its intensity can reach the air dielectric strength ($3 \cdot 10^6$ V/m), thus favouring arcing or ionisation of the air surrounding the necking region. Both mechanisms can lead to a localised overheating, forming a liquid phase among the particles (molten metal) or providing a further mass transport contribution due to evaporation-condensation.
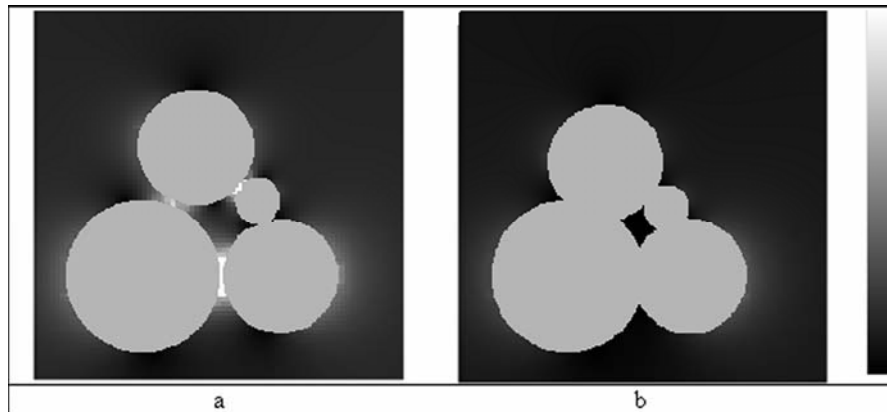
Figure 3 - Electric field envelope in the mid-section of the 4-spheres aggregate: a) before particles necking; b) after particles necking; c) scale maximum= $3 \cdot 10^6$ V/m

After necking occurred (Figure 3b), the modeling results show that the maxima of the electric field are no longer in the space among the particles, nor they reach the same intensity as before. In this condition, arcing is less likely to occur and the sample is most probably heated by direct microwave absorption and by heat transfer from other nearby regions, not necked yet, and thus prone to arcing.

II.III   Results and discussion

Microwave sintered samples without the use of the auxiliary absorber presented some difficulties in maintaining the desired heating rate, and were visibly subjected to arcing. The high electric field intensity among the particles, as expected from the modeling results, probably surpassed the dielectric strength of the air surrounding the particles, creating a conductive path and a localised overheating. Samples subjected to pronounced arcing were severely cracked and distorted, and presented white residua whose composition, determined by X-ray diffraction, proved to be mainly ZnO, coming from the oxidation of the brass particles.

The use of the auxiliary absorber (SiC disc) helped reducing the electric field intensity among the particles, and provided a more controllable heating, as well as a heat source external to the samples. Conventional and microwave sintering results using the SiC disc, expressed in terms of samples' dimensional variation of diameter (D) and height (H) are depicted in Figure 4.
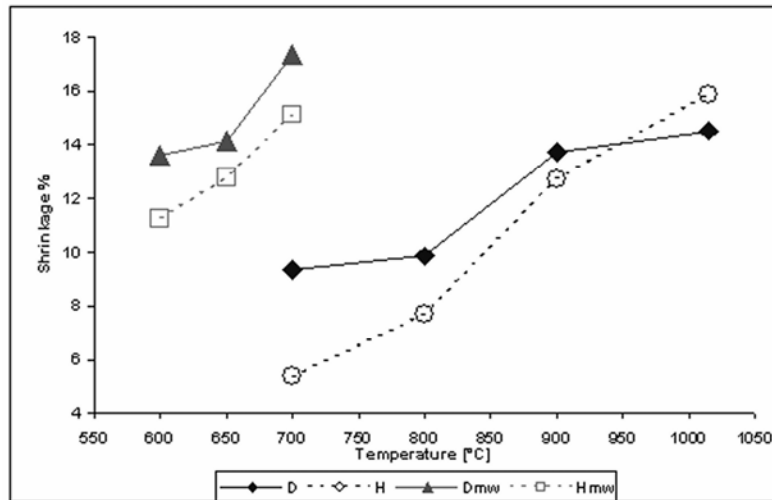
Figure 4 - Samples average diameter and height variation as a function of temperature after sintering using conventional heating (D, H) and microwave heating (Dmw, Hmw)

The maximum densification occurred in case on microwave heating, at temperature significantly lower than conventional heating. No sample heated conventionally was able to reach the shrinkage levels of microwave sintered samples, despite the higher temperatures. The microstructure of sintered samples presented pronounced variations, depending on the experimental conditions, as shown in Figure 5.

Microwave sintered samples (Figure 5a) presented a higher percentage of non-oxidised metallic spherical inclusions, immersed in a partially oxidised matrix, whose composition was determined by X-ray diffraction to be mainly magnetite (Fe_3O_4) and ZnO. The spherical inclusions composition corresponds to secondary copper and Fe/Cr/Ni alloy. Conventionally sintered samples presented the formation of CuO starting from 700 °C, and at 900 °C the resulting microstructure is a more oxidised matrix of iron and copper oxides, embedding a dispersion of Fe/Cr/Ni alloy microspheres. ZnO is detected on the surface of the conventionally heated samples only at temperatures above 900 °C.
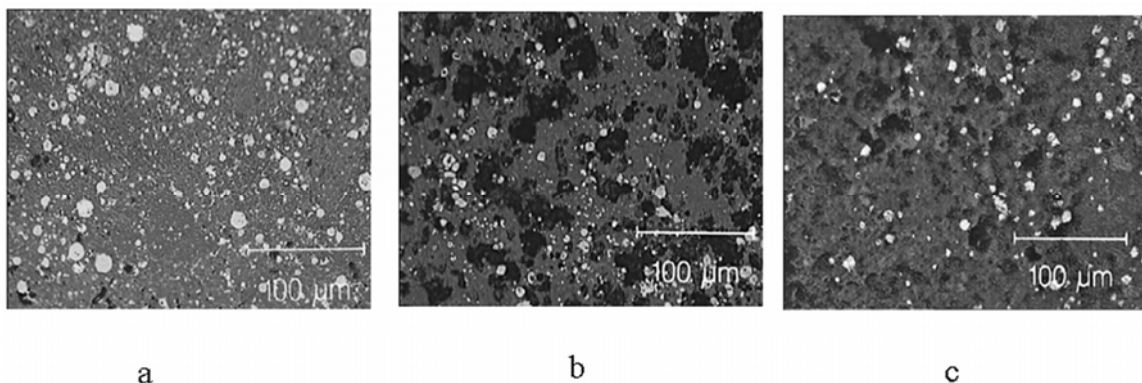
Figure 5 - Optical microscope micrographs of samples: a) microwave sintered at 700 °C; b) conventionally sintered at 700 °C; c) conventionally sintered at 900 °C

130

This phenomenon seems to confirm the local overheating of the metallic particles, since the oxidation of Zn occurred during microwave heating starting from a measured surface temperature of 650 °C. This result is in agreement with the electromagnetic field concentration emerged from the numerical simulations.

III. Sintering of millimetric metallic powders

Compared to the previous case, larger, but still spherical, metallic powders should reduce the ratio between the volume of the material directly heated by microwaves (corresponding to a shell having the thickness equal to the skin depth at the operating frequency) and the overall volume.

III.I   Experimental

Metallic millimetric spheres made of pure (99.9%) Cu, Ag, Au and brass (P-CuZn20), having an average diameter of 2mm have been used for the sintering tests. Controlled quantities of spheres have been placed in mullite and SiC crucibles (Figure 6a). The first crucible is representative of an almost microwave-transparent material, while the second crucible is used to provide a pronounced attenuation of the electromagnetic field impinging on the metal particles. The same single mode applicator of the previous tests was used, sintering the samples in air and in Ar flux (20 Nml/min), with microwave forward power ranging from 300 to 1000 W.

III.II   Modeling

The system composed of crucible and metallic spheres, subjected to microwave heating at 2.45 GHz in the single mode applicator of Figure 2, has been numerically simulated using the software Concerto 4.0. Figure 6 represents a typical configuration of copper spheres, in a SiC crucible (a), and the corresponding 3D model (b).
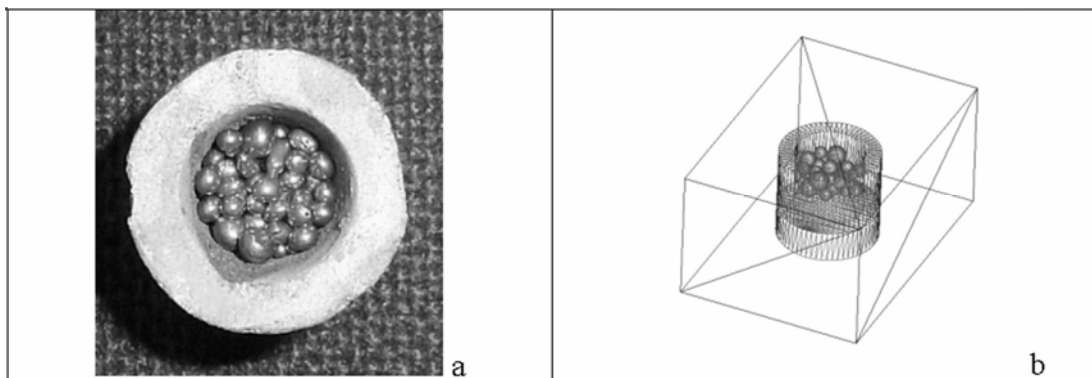
Figure 6 - Copper spheres in a SC crucible and correspondent model of the loaded applicator

131
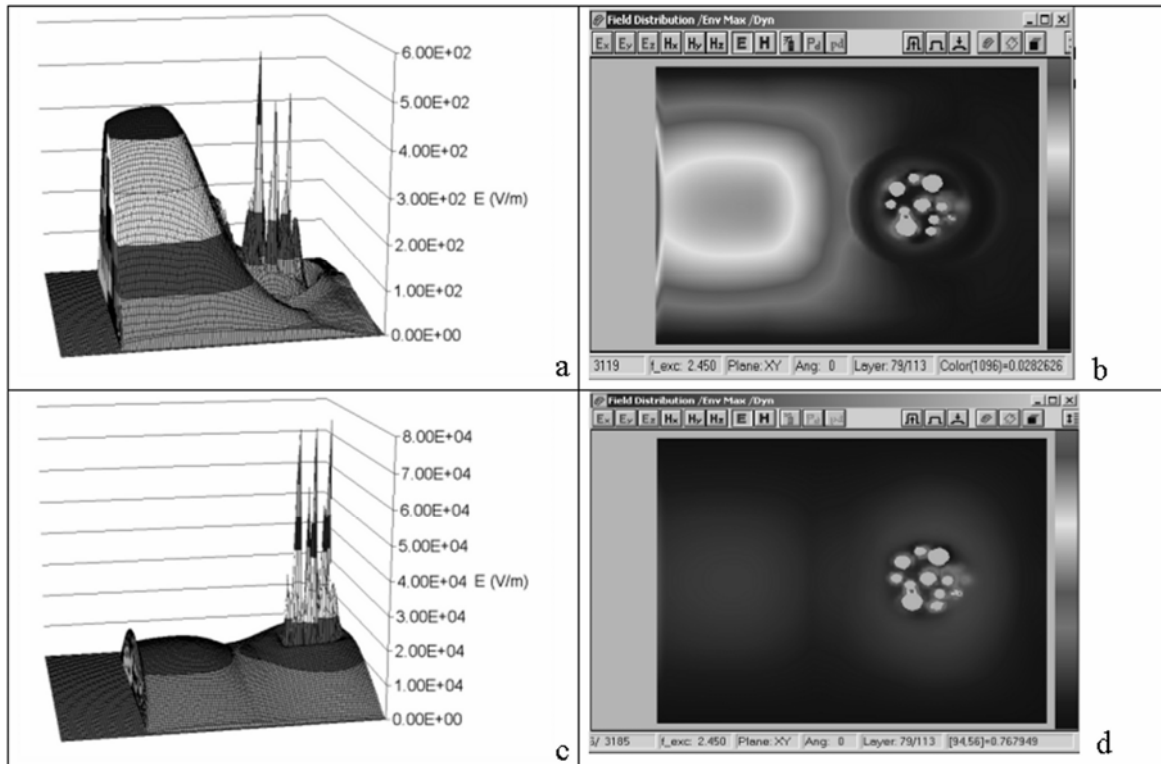
Figure 7 - Envelope (3D graph and thermal plot) of the electric field (V/m) in the mid horizontal section of the applicator loaded with metallic spheres, placed in: a,b) SiC crucible; c,d) mullite crucible

Varying the crucible material (mullite or SiC) and maintaining unaltered the microwave forward power, the envelope of the calculated electric field is deeply affected by the different conditions, as shown in Figure 7. In Figures 7 a) and b), referred to microwave sintering in a SiC crucible, the calculated electric field envelope in the mid horizontal section of the system is represented. The maximum field intensity occurs among the particles (round shapes in the right of Figure 7a), but its value is similar to the one existing on the outside of the crucible, i.e. almost 500 V/m. In Figures 7 c) and d), referred to microwave sintering in a mullite crucible, the calculated electric field envelope in the mid horizontal section of the system is maximum among the particles (round shapes in the right of Figure 7d), and its value is in excess of 7000 V/m, more than 2 orders of magnitude higher than the field intensity outside the crucible.

Comparing the two cases (Figure 7a and 7c), it is evident a variation of more than 2 order of magnitude of the electric field envelope in the region near the metallic spheres, confirming the expected attenuation in presence of SiC crucible. In both cases, pronounced E-field intensity maxima are present in the space among the particles, as evident in the thermal plots of Figure 7. The different order of magnitude makes the system with the mullite crucible much more prone to arcing among the particles with respect to the SiC crucible one. In the first case, it is very likely to have a direct microwave absorption by the metal spheres, and the formation of necks due to the electromagnetic field concentration in the space near the spheres, while in the second case an indirect microwave absorption (heat generated preferentially in the crucible and transmitted to the spheres) is expected.

III.III Results and discussion

Representative sintering results, regarding a brass and a copper sample, sintered in air in a mullite and a SiC crucible, are reported respectively in Figure 8a and 8b.
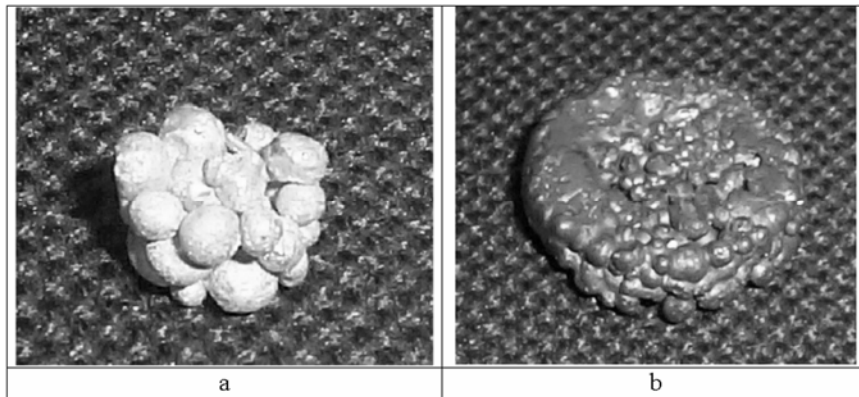
Figure 8 - Microwave sintered samples of: a) brass spheres in mullite crucible, b) copper spheres in SiC crucible

It is evident that the sample sintered in the mullite crucible (8a) underwent direct microwave absorption, since all necks are in the inner part of the sample and there is no evidence of melting of the outer particles.

On the contrary, the sample sintered in the SiC crucibles (8b) presented melted regions on the outer surface while the inner regions were only starting to form necks, indicating that a higher temperature (melting point) was reached in the parts of the sample in direct contact with the microwave absorbing crucible.

In this case, the indirect microwave absorption can be considered equivalent to conventional heating. SEM observation of the necking regions in samples subjected to direct microwave absorption evidenced a kind of etching of the surfaces near to the necking regions, as reported in Figure 9, referred to a silver sintered sample.

This phenomenon could be ascribed to the electric discharge and plasma formation occurring in that region, locally removing matter from the sphere, and adding it to the necking region.

133
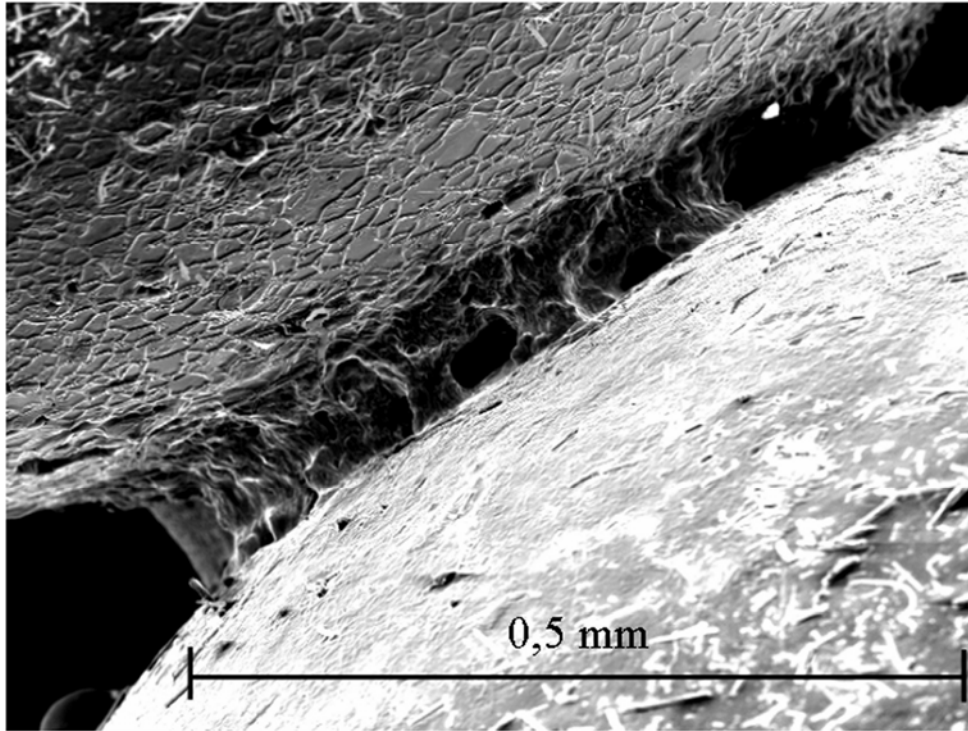
Figure 9 - SEM micrograph of a neck between two silver spheres, obtained by microwave sintering. An apparently etched microstructure is evident in the upper sphere

IV. Sintering of metal-fibre reinforced composites

The electromagnetic field concentration occurring near metal particles can be successfully employed to over-heat a dielectric material in which the conductive particles are dispersed. It is a well-known phenomenon that the addition of conductive particles to a low-loss dielectric matrix improves its microwave coupling [13-16] and this has also been used in the past to produce functionally graded materials [17-18].

The controlled introduction of metal particles, having a certain shape and aspect ratio, can lead to a very localised heating of a dielectric matrix, improving its adhesion to the reinforcement

IV.I Experimental

Duran® borosilicate glass powder was used as a matrix and was mixed to up to 10% volume of Hastelloy X fibres, as reported in a previous work [19]. The fibres had an average length of 100 μm. Cylindrical samples (diameter: 10 mm, height: 4 mm) were obtained by uniaxial pressing the mixed composite powders at room temperature. Green densities of ~ 60% of the theoretical density were achieved. The calculated skin depth of this kind of fibres, at room temperature and at 2.45 GHz, is 11 μm.

Microwave sintering of the glass matrix composite was performed in the single mode applicator described Figure 2, but placing the samples in the maximum of the electric (central part of the applicator) or magnetic (side of the applicator) field.

IV.II   Modeling

A portion of the unsintered (green) compact was chosen for micro-scale modeling of its interaction with the electromagnetic field generated by a microwave source operating at 2.45 GHz. Three Hastelloy X fibres where considered parallel, while a fourth fibre was set perpendicularly to the previous ones. The glass matrix, homogenous, was supposed to embed the fibres with complete contact and no pores. Results are referred only to the case of samples placed in the maximum electric field position of the applicator.

The modeling results are shown in Figure 10, where the electric field envelope in the glass matrix surrounding the fibres and in close proximity of the fibres' surface is qualitatively depicted.
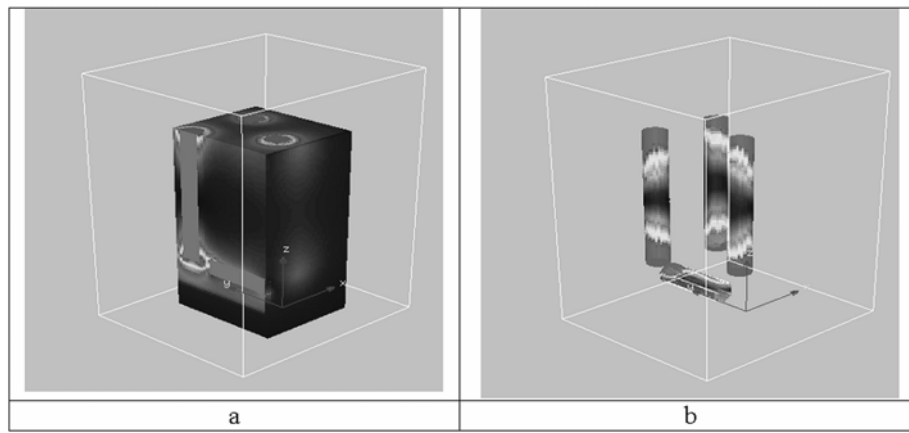
Figure 10 - Modeling results of the electric field envelope: a) in the glass matrix; b) in the glass matrix surrounding the Hastelloy X fibres. Arbitrary scale

It is evident, once again, the electric field concentration near the fibres' tip, and the electric field is maximum in the space among two nearest fibres' tip. Since the microwave power density in a dielectric material is proportional to the square of the local value of the electric field [20], during sintering of the composite it is expected a pronounced overheating of the glass matrix near the end sides of each fibre.

Moreover, if the electric field concentration reaches high value, breakdown phenomena could occur, involving temperatures higher than the melting point of the Hastelloy X fibres (1355 °C).

IV.III   Results and discussion

Sintering of the composite, depending on the sintering conditions and fibres content, provided different results (porous and foamed materials, partially dense materials, toughened glass matrix composites) [21-23]. Microwave sintering in the maximum of the magnetic field provided higher heating rates, but less controllable processes [22].

A more homogenous microstructure, with spherical pores, could be obtained positioning the samples in the maximum of the electric field. However, for high microwave forward power, the high electric field intensity leads to local and uncontrolled overheating of portions of the samples, which presented severely distorted regions.

135

A SEM investigation of the regions affected by overheating confirmed the presence of molten metal fibres, as shown in Figure 11.
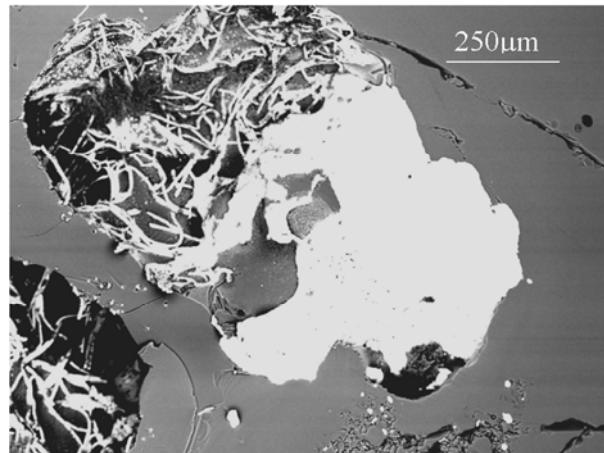
Figure 11 - BSD SEM micrograph of an overheated region of a 10% fibre sample processed in the maximum of the electric field. EDS analysis of the white region corresponded to average Hastelloy X composition

V.   Conclusions

Coupling the electromagnetic field simulation on a macro- and micro-scale with the experimental results, it has been possible to demonstrate the microwave enhancement of the early stages of sintering of conductive compacts. In particular, it has been shown that:

- microwave sintering is strongly affected by phenomena of local concentration of the electric field;

- there are concurrent phenomena of direct microwave heating, within the skin depth of the metals, mainly due to the magnetic field, and phenomena of breakdown and plasma formation, mainly due to the high electric field intensity, which give a further, and often determinant, contribution to heating;

- necking is favoured in case of microwave heating of spherical powders, since the electric field concentration is maximum in the zone among the particles, which corresponds to the zone of formation of necks during sintering;

- breakdown phenomena causes other more efficient mass transport mechanisms (liquid phase, evaporation-condensation) to occur during sintering of metal powders. This can partially explain the faster and more pronounced densification observed in many microwave sintered parts;

- it is possible to use advantageously the electromagnetic field concentration to obtain peculiar microstructures, for instance using metallic fibres, or to properly choose the refractory/insulating supports to prevent or to promote breakdown phenomena, at the same overall microwave power output from the generator.

Acknowledgements

References

[1] Rödiger K, Dreyer K, Gerdes T, Willert-Porada M, *Int J. Refract Metals H* 5 (6), (1998) p. 409.

[2] Leparoux S, Vaucher S, Beffort O, *Adv Eng Mater* 5 (2003) p. 449–453.

[3] Cheng JP, Agrawal DK, Komaneni S, Mattis M, Roy R, *Mat Res Innovt* 1 (1997), p. 44–52.

[4] Veronesi P, Leonelli C, Bassoli E, Gatto A, Iuliano L., *Proceedings of the Sintering 2003 Conference*, 15-17 September 2003, Penn State University, Pennsylvania, USA, CD-ROM.

[5] Fang Y, Agrawal DK, Roy R, Angerer P, Skandan G., *Proceedings of the Sintering 2003 Conference*, 15-17 September 2003, Penn State University, Pennsylvania, USA, CD-ROM..

[6] Upadhyaya A, Sethi G, Agrawal D., *Proceedings of the Sintering 2003 Conference*, 15–17 September 2003, Penn State University, Pennsylvania, USA , CD-ROM.

[7] Cheng J, Roy R, Agrawal D, *J. Mats. Sci. Lett.* 20 (2001) p.1561-l563.

[8] Cheng J, Roy R, Agrawal D, *Mat. Res. Innovat.*, 5 (2002) p.170-177.

[9] Agrawal D, Cheng J, Peelamadu RD, Roy R., *Proc. of Intl. Symp. on Microwave Science and its Application to Related Fields,* Nara (Japan), (2002) p. 8-9.

[10] Rybakov KI, Semenov VE, Bykov YV, Egorov SV, Eremeev AG, Plotnikov IV, *Proc. of the Fourth World Congress on Microwave and Radio Frequency Applications*, Edited by R.L. Schulz, D.C. Folz , Austin, Texas, (2004) p. 459-468

[11] German R.M. *Powder metallurgy science*, 2nd ed. Princeton (NJ): MPIF 1994

[12] R. Sola, "Use of microwaves in the SHS of Ni,Al–based intermetallic compounds" – in Italian, Bachelor thesis in Materials Engineering, University of Modena and Reggio Emilia, 2005

[13] Carr G L, Perkowitz S, Tanner GL, *Infrared and Millimeter Waves* 13 (1985), p. 171–263

[14] Bykov YV, Rybakov KI, Semenov VE, *J. Phys. D: Appl. Phys.* 34 (2001), p. R55–R75

[15] Boccaccini AR, Veronesi P, Leonelli C, *J. Europ. Ceram. Soc.* 21 (8) (2001) p.1073-1080

[16] Veronesi P, Leonelli C, Pellacani GC, Fiumara V, Barba AA, D'Amore M, *Materials Engineering* 13 (4) (2002) p. 65-72

[17] Bykov YV, Egorov SV, Eremeev AG, Rybakov KI, Semenov VE, Sorokin AA, *Mater*. 8 (2001) p. 71–76

[18] Gerdes T, Willert-Porada M, *Microwave Processing of Materials V (Materials Research Society Symp. Proc. vol 430)*, ed M F Iskander et al (Pittsburgh, PA: Materials Research Society), (1995) p. 175–180.

[19] Minay EJ, Boccaccini AR, Veronesi P, Cannillo V, Leonelli C, *Advances in Applied Ceramics* 104 (2) (2005) p. 49-54

[20] Metaxas AC, Meredith RJ, I*ndustrial microwave heating*, Peter Peregrinus, London (1993), p. 97-102

[21] Veronesi P, Leonelli C, Pellacani GC, Boccaccini AR, *Journal of Thermal Analysis and Calorimetry* 72 (2003) p. 1141-1149

[22] Minay EJ, Boccaccini AR, Veronesi P, Cannillo V, Leonelli C, *Journal of Materials Processing Technology* 155-156 (2004) p. 1749-1755

[23] Minay EJ, Veronesi P, Leonelli C, Boccaccini AR, *Journal of the European Ceramic Society* 24 (2004) p. 3203-3208

MICROWAVE DEHYDRATION OF WATER IN OIL MICROEMULSION CONTAINING NANOPARTICLES SYNTHESIZED IN SITU

M. L. Saladino, E. Caponetti, D. Chillura Martino, A. Spinella

Dipartimento di Chimica Fisica, Università degli Studi di Palermo

Parco d'Orleans II, Viale delle Scienze pad.17– 90128 Palermo - Italy

Abstract

In this work the dehydration process of a nanoparticles-microemulsion system, promoted by microwave, will be discussed. Samples have been irradiated by using a microwave apparatus, operating at 2.45 GHz and tunable power up to 800 W, by setting the operative power in order to achieve a constant temperature (35 °C) during the experiment. The nanoparticles size and the water amount in the irradiated system were monitored by using Uv-vis and FT-IR spectroscopy, respectively. Data analysis showed that irradiation causes the water evaporation from the micellar core without affecting the nanoparticles size significantly. Microwave irradiation, since it does not use any chemical, turned out to be a technique swift, clean and with a low ambient impact, useful for the dehydration of a complex system such as nanoparticles-microemulsion.

1.   Presentation

It is well known that the high surface energy of nanoparticles is responsible of their tendency to grow in size and/or, for very tiny particles, to coalesce. In order to reduce this tendency, the effort of researchers is focused to carry out new synthesis protocol able to produce stable nanoparticles having a desired structure, composition and morphology.

Many investigations have exploited the applicability of water in oil (W/O) micro-emulsion to the synthesis of nanoparticles. This route revealed to be a very powerful technique [1-3]. A W/O microemulsion is a thermodynamically stable system where water droplets and the continuum oil region are spatially separated by amphiphilic (surfactant) molecules. The generated micro- or nanoheterogeneities are dynamical entities, known as inverse micelles [1-3], which can be used as nanoreactors to perform several kinds of reactions.

This is a consequence of the inverse micelles ability to exchange their content, so enabling the synthesis of materials "in situ" *in order to* obtain nanoparticles. Therefore, when two W/O microemulsions containing reactants are mixed, the reaction takes place. If at least one of the products is insoluble, the exchange of material among micelles promotes the formation of clusters followed by a growth process. The confined micelles structure prevents the indefinite clusters growth, allowing a control of their size. Besides, surfactant molecules stabilize the nanoparticles. Several kinds of nanoparticles, such as sulphides, selenides, oxides, metals, polymers, alloys and others have been produced by means of this synthesis procedure [4-6].

Recently, it has been shown that the dimension of nanoparticles is regulated by the reactants concentration, the water to surfactant molar ratio, inverse micelles size and the temperature [7-10]. Due to the dynamics of the system, this synthetic approach introduces some drawbacks; in fact, the ripening phenomenon (growth of the biggest particles to the expenses of the smaller ones) takes place.

This phenomenon reveals to be hardly controllable since the role of the parameters and of the growth mechanisms are not still fully understood.

Due to their tendency to coalesce, bare nanoparticles, thermodynamically unstable, tend to loose their peculiar properties. In order to circumvent this drawback, several researchers have attempted to passivate the nanoparticle surface by using suitable capping agent as thiol, ammines, pyridines, i.e. electron donors or acceptors species that bond to the nanoparticles surface thus avoiding coalescence [11-16].

A disadvantage of this procedure comes out when bare nanoparticles are required. After the synthesis, the clusters must be separated by the solvent (water and oil) and re-dispersed in apolar solvent in order to inhibit the ripening process. Alternative, the full microemulsion dehydration can be obtained by using a dehydration agent as phosphorus pentoxide [17]. In both cases, the process involves a samples manipulation.

Recently, we have undertaken a detailed investigation on CdS nanoparticles synthesis in microemulsion assisted by microwave. The electromagnetic irradiation causes some significant effects on mechanism and reaction's kinetics [18-20]. Microwave irradiation causes a local heat of water nanodrops with the formation of strong thermal gradient, leading to an increase of nucleation rate and a stabilization of nanoparticles.

In the present work, the microwave irradiation is discussed as an alternative method with respect to the traditional methods for the dehydration of microemulsion systems and, consequently, for the stabilization of nanoparticles in microemulsion. The irradiation was performed at 2.45 GHz by setting the external cooling system at 20 ± 1 °C and by opportunely varying the power in order to keep the sample temperature constant at 35 ±1 °C. Results are compared with those obtained by using conventional dehydration method.

2. Experimental

2.1 Materials

Sodium bis(2-ethylhexyl) sulphosuccinate (AOT, Aldrich 98%) was dried under vacuum for two days. Cadmium sulphate (Aldrich, 99%), sodium sulphide nonahydrate (Fluka, 99%), n-heptane (Aldrich, 99%) and phosphorus pentoxide (Sigma, 99%) were used as received. Conductivity grade water was used to prepare aqueous solutions.

2.2 Instrumentations

The scheme and a photograph of microwave apparatus are reported in Figure 1. The instrumentation was a SAIREM downstream microwave source working at 2.45 GHz [21]. The main characteristics of this exposure set up are: the homogeneous fields distribution inside the sample holder, the ability to measure the microwave power absorbed by the sample, the simplicity in use.

The microwave apparatus has been connected with an UV-Vis spectrophotometer by a peristaltic pump that carries the irradiated microemulsion inside the spectrophotometer cell; after the measurement, the microemulsion is brought back in the sample holder. By using this apparatus, it is possible to irradiate liquid samples and at the same time, to obtain information about the kinetics of reactants or products that present optical activity in the UV-Vis range.
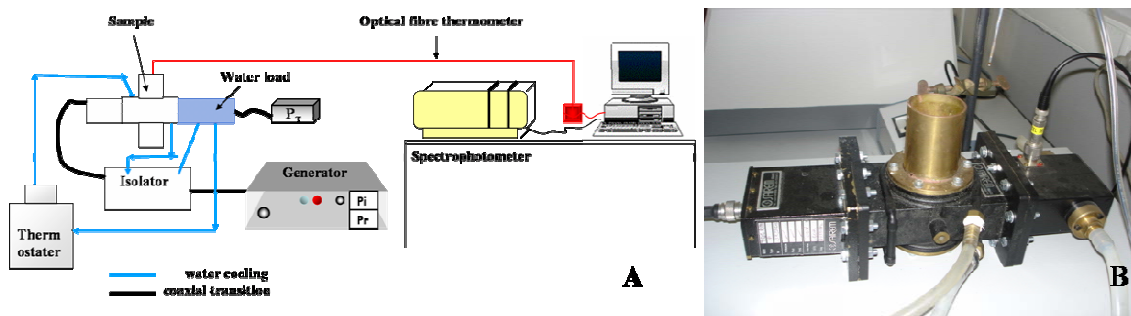
Figure 1 - Microwave apparatus: A) scheme;
B) photograph of the wave guide and sample holder

The incident (Pi), reflected (Pr) and transmitted (Pt) powers were continuously measured by means of power sensors and power meters connected before (by means of a reflectometer bridge) and after the sample holder, respectively. In this way, it was possible to control accurately the power absorbed by sample (Pa= Pi - Pr - Pt). More details on this apparatus and its field dosimetry are reported elsewhere [22].

UV-Vis spectra were recorded in the 200÷600 nm range by means of a double beam Beckman DU-640 spectrophotometer with a resolution of 1.0 nm.

FT-IR spectra were measured in the range 4000-500 cm^{-1} using a Perkin Elmer BXI FT-IR spectrometer with a spectral resolution of 1 cm^{-1} and 100 scans.

3. Nanoparticles synthesis

CdS nanoparticles were synthesised by mixing two water/AOT/n-heptane microemulsions, A and B, differing only in the type of aqueous phase. The aqueous phase of microemulsion A was a 0.2 mol kg^{-1} $CdSO_4$ solution, whereas the aqueous phase of microemulsion B was a 0.2 mol kg^{-1} Na_2S solution. The AOT concentration in n-heptane was 0.15 mol kg^{-1} and the water/surfactant molar ratio was 5 [7]. Microemulsions A and B were mixed at 25 °C, and the mixture was placed in an open glass cylinder positioned inside a water bath maintained at 35.0 ± 0.1 °C.

Nanoparticles growth was followed for two hours by monitoring the CdS UV-Vis absorption spectra. Some of the spectra are reported in Figure 2.
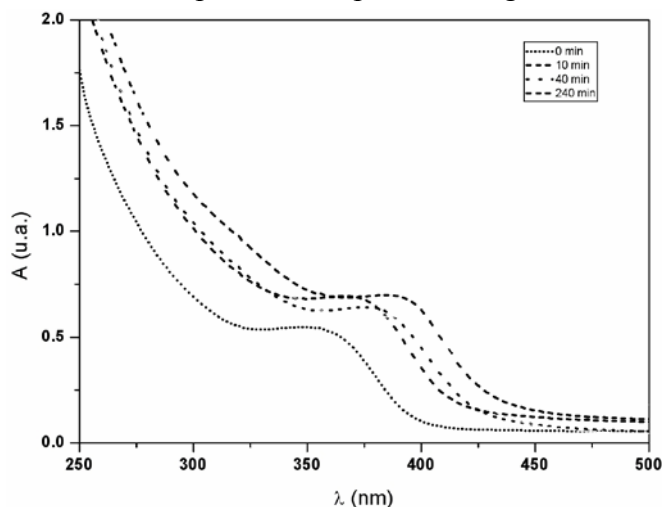
Figure 2 - UV-Vis adsorption spectra of CdS nanoparticles during synthesis
at different times

A well-defined absorption band at about 375 nm, ascribed to the first exciton (1s-1s) transition of the CdS nanoparticles [7,24], is present. The position of the band maximum moves towards higher wavelengths without appreciable changes in the curve shape. Both theoretical studies [25] and experimental results [26] have shown the existence of a correlation between the onset of the absorption band and the size of CdS particles. According to this, the clear peak shift and the absorption onset shift towards higher wavelengths as a function of time indicate that nanoparticles grow with time. Moreover, the width of this absorption band can be related to the distribution of nanoparticles sizes or to the presence of indirect transitions, whereas the molar extinction coefficient at the band maximum is related to the morphology of the surface [27].

By using a suitable UV-Vis spectral analysis [23], nanoparticles sizes were estimated. Results are reported as a function of time in Figure 3.

The fast growth process observed in the first stage of the synthesis is followed by a slower process which tends to level off at long times.
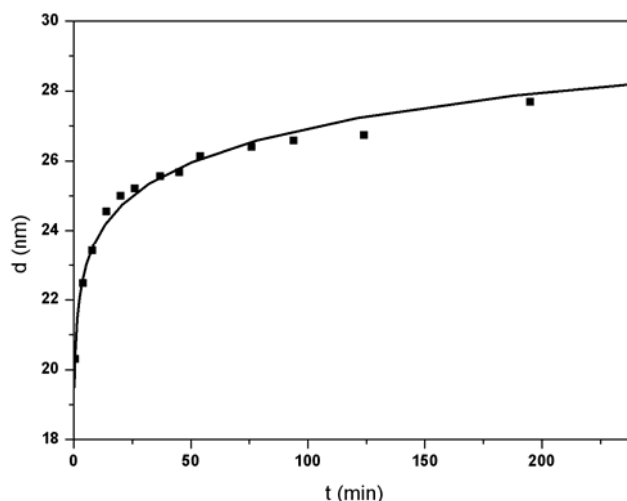
Figure 3 - CdS nanoparticles diameter (d) as a function of time (t) for water/AOT/n-heptane microemulsion (R = 5)

4.   Microwave assisted dehydration

The CdS in microemulsion sample, as above prepared, was placed in a glass cylinder, inserted in the waveguide and irradiated. Due to dielectric properties of microemulsion components, the energy is absorbed almost completely by the water droplets causing a local temperature increase, but it suddenly distributes to all the system thus reducing the strong local thermal gradients.

For this reason, in order to maintain the sample temperature at 35 ± 2 °C, the sample holder was cooled by a thermostated (25 ± 0.1 °C) water jacket externally surrounding the waveguide. By means of this setup, cooling water does not interact with the microwave field. Moreover, as it will be clear later, the decrease of water content in the system reduces its ability to absorb the microwave radiation.
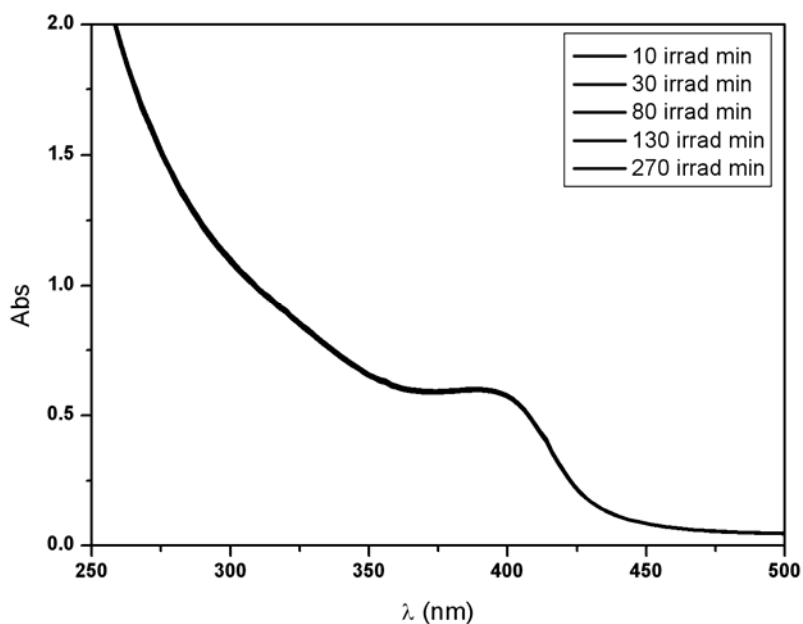
Figure 4 - UV-Vis adsorption spectra of CdS nanoparticles system irradiated for different times

This implies that, in order to maintain the sample temperature at 35 ± 2 °C the incident microwave power was increased from 22 up to 30 W. Sample temperature was continuously monitored during the treatment by using a non-perturbative optical fibre thermometer (Nortech Reflex-TP21M02).

The nanoparticles size was checked by recording the UV-vis spectra [23] for about eleven hours. The coincidence of the CdS absorption bands, a continuous line in Figure 4, during microwave irradiation indicates that no variation of nanoparticles size occurs.

Several aliquots at various irradiation times were withdrawn from the sample in order to investigate, by FTIR technique, the structural changes that the microemulsion and nanoparticles underwent at different microwave irradiation doses.

In order to compare the microwave effect with that of dehydration traditional method, the non-irradiated aliquot was shaken with phosphorus pentoxide powder for 60 minutes. The resulting suspension was filtered and analyzed by means of FT-IR technique.

Spectra, registered for the system before irradiation and after eleven hours of irradiation, are reported in Figure 5.

The significant features of the spectra concern the water OH stretching (≈ 3480 cm^{-1}), CO stretching (≈ 1730 cm^{-1}), H_2O bending (≈ 1642 cm^{-1}), and SO_3 stretching (≈ 1045 cm^{-1}).

The absorbance in the frequency range where the OH stretching falls is reported in Figure 6 (dotted lines), at various irradiation times.

143
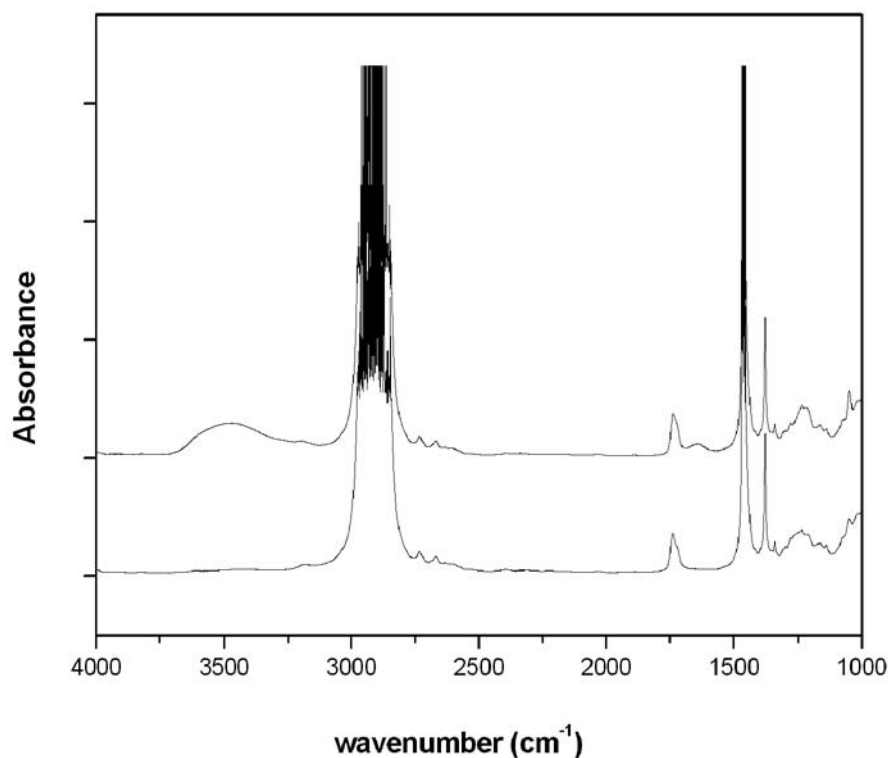
Figure 5 - FT-IR spectra of CdS nanoparticles/water/AOT/n-heptane system before irradiation (lower spectrum) and after irradiation for eleven hours (upper spectrum)
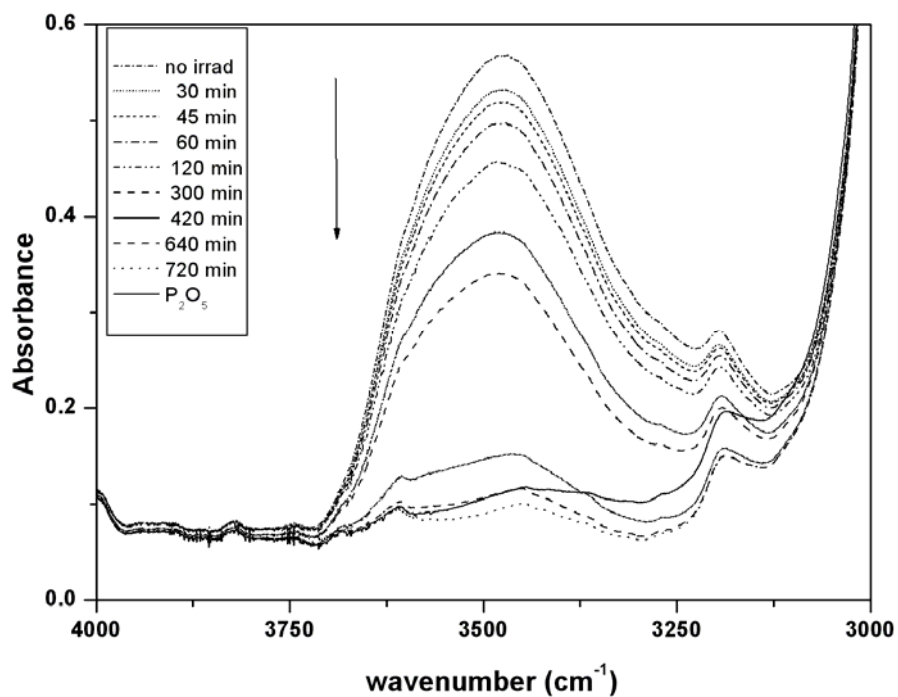
Figure 6 - OH stretching band of nanoparticles/water/AOT/n-heptane system for different irradiation times (min). For comparison, the spectrum of the same system dehydrated with phosphorus pentoxide is reported as continuous line

The OH stretching (3480 cm^{-1}) signal decreases as a function of irradiation dose. This indicates a progressive decrease of the water amount. The evident changes in the line profile of the band indicate the presence of different spectral contributions ascribable to the water molecules feeling the effects of various environments and of selective microwave irradiation effects; work is in progress to analyze in detail the different components of this band and their assignment to water molecules in interactions with different environments.

After eleven hours, the disappearance of OH band indicates that the system can be considered anhydrous. The coincidence, to some extent, of the above spectrum with that collected for the sample treated with phosphorus pentoxide indicates that both methods are effective to dehydrate the system.

However, by a close inspection of the bands of the system dehydrated with phosphorus pentoxide, it is possible to evidence some variations in the two SO$_3$ stretching bands suggesting that phosphorus pentoxide causes some modification of the ester groups of the surfactant molecule.

This effect is evidenced in Figure 7. On the contrary, spectra of the microwave dehydrated system indicate that irradiation, even for prolonged times (up to eleven hours) does not alter the surfactant structure.
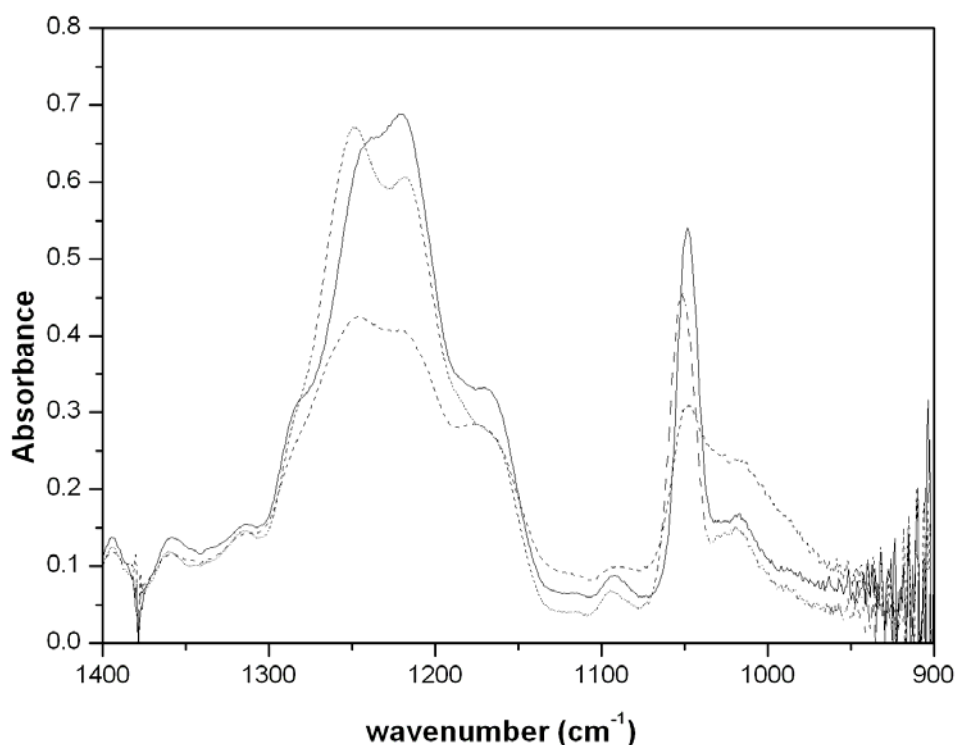
Figure 7 - Stretching vibration bands of SO$_3$ of AOT surfactant before (continuous line), after (dashed line) microwave treatment and after (dotted line) treatment with phosphorus pentoxide

4.   Conclusion

It has been proved that microwave irradiation of water/AOT/n-heptane microemulsion containing CdS nanoparticles, at constant temperature, causes a progressive dehydration of the system. The method presents some advantages with respect to the treatment with phosphorous pentoxide.

Microwave irradiation stabilizes the nanoparticles against indefinite growth, leaving the other component unchanged. The constancy of nanoparticles size can be attributed to the significant decrease of water content in the inverse micelles that inhibits the material exchange among micelles and, consequently, the nanoparticles growth.

The dehydration effect of microwave irradiation has been proved by FT-IR spectra investigation. By comparing the spectra of the irradiated system and that of the sample dehydrated with phosphorus pentoxide, it clearly emerges that, notwithstanding the latter process is the most rapid one; it causes variations in the SO_3 stretching bands of the surfactant molecules.

The microwave irradiation method can be considered safe for the ambient because it avoids the use of substances extraneous to the system and circumvents treatments that can damage the system itself and/or increase the pollution.

Acknowledgment

References

[1] M.P. Pileni, T. Zemb, C. Petit, *Chemical Physics Letters* **118(4)** (1985) 414.

[2] A.L. Compere et. al., *J. Phys. Chem. B,* **101** (1997) 7139.

[3] E. Caponetti, A. Lizzio, R. Triolo, W.L. Griffith, J.S. Johnson *Langmuir* **8** (1992) 1554.

[4] H.P. Li et al. *Optical Materials* **14** (2000) 321.

[5] E.J. Kim, S. Kim, S.H. Hahn *J. Mat. Sci.* **37** (2000) 1455.

[6] M. Rong, M. Zhang, H. Liu, H. Zeng *Polymer* **40** (1999) 6169.

[7] E. Caponetti et al. *Mat. Sci. Eng. C* **23** (2003) 531.

[8] C. Petit, P. Lixon, M.P. Pileni, *J.Phys.Chem.* **94** (1990) 1598.

[9] A. D'Aprano, F. Pinio, V. Turco Liveri, *J. Solution Chemistry* **20** (1991) 301.

[10] J.P. Wilcoxon, R. Williamson, R. Baughman, *J.Chem.Phys.* **98** (1993) 9933.

[11] R.R. Chandler, *J. Phys. Chem.* **97** (1993) 9767.

[12] G.C. Lisensky, R.L. Penn, C.J. Murphy, A.B. Ellis, *Science* **248** (1990) 840.

[13] C.R. Cowdery, D.G. Whitten, G.L. McLendon, *J. Chem. Phys.* **176** (1993) 377.

[14] T. Dannhauser et al. *J. Phys. Chem.* **90** (1986) 6074.

[15] P.V. Kamat, N.M. Dimitrijevic, *J. Phys. Chem.* **93** (1989) 4259.

[16] P.V. Kamat, Isr. *J. Chem.* **33** (1993) 47.

[17] P. D. I. Fletcher, D. D. Grice and S. J. Haswell, *Phys. Chem. Chem. Phys.*, **3** (2001) 1067.

[18] M. Shen, Y. Du, P. Yang, L. Jiang, *J. Phys. and Chem. Sol.* **66** (2005) 1628.

[19] E. Caponetti, D. Chillura Martino, M. Leone, L. Pedone, M. L. Saladino, V. Vetri, *submitted*

[20] G. Calvaruso, A. Ruggirello, V. Turco Liveri, *J. Nanop. Res.*, **4** (2002) 239.

[21] E. Caponetti, L. Pedone, R. Massa, *Materials Research Innovations*, **8** (2004) 44.

[22] R. Massa, G. Petraglia, E. Caponetti, L. Pedone, *Materials Research Innovations* **8** (2004) 48.

[23] S. Komarneni, D. Li, B. Newalkar, H. Katsuki, A.S. Bhalla *Langmuir* **18** (2002) 5959.

[24] L. E. Brus, *J. Chem. Phys.* **80** (1984) 4403.

[25] T.F. Towey, A. Khan-Lodhi, B.H. Robinson, *J. Chem. Soc. Faraday Trans.* **86(22)** (1990) 3757.

[26] A. Henglein, *Chem. Rev.,* **89** (1980) 1861.

[27] H. Weller et al. *Chem. Phys. Lett.* 124 (1986) 557.

SCREENING OF CATALYSTS FOR SOOT OXIDATION BY MICROWAVES

Vincenzo Palma, Paola Russo, Giuseppa Matarazzo, Paolo Ciambelli

Department of Chemical and Food Engineering, University of Salerno

via Ponte Don Melillo, 84084 Fisciano (SA), Italy

vpalma@unisa.it

Abstract

Recently microwaves (MW) heating has been proposed as effective technique to shorten the time of oxidation of soot collected on diesel particulate filter (DPF). In this work a screening of catalysts for soot oxidation in a specifically designed MW apparatus has been performed. In particular, the effect of the catalyst support on the activity of Cu/V/K catalyst towards the oxidation of soot in the presence of microwaves was investigated.

1.   Introduction

The most appealing device to control particulate at the exhaust of diesel engine is based on an efficient diesel particulate filter (DPF). Once particulate is collected on the filter, it has to be continuously or periodically removed by thermal regeneration [1]. The regeneration system should have the capability to achieve high efficiencies by burning all the soot collected on it without any structural filter damage. The various regeneration techniques differ mainly by the way wherein particulate is heated until a hot reaction zone.

Among the various techniques investigated that using microwaves (MW) as energy source has proven to be promising, since MW heating is more efficient and faster than conventional heating. However, a specific regeneration system must be designed in order to achieve a satisfactory performance. In particular, it must be taken into account that the different dielectric properties of materials involve a selective mechanism of heating, i.e. carbon particulate has a very high dielectric loss factor, ceramic materials as Al_2O_3 are microwaves transparent, while SiC exhibits a very strong ability of absorbing microwaves [2]. Although an increase in the microwave power supplied could increase the regeneration efficiency, with a decrease in the total regeneration time, it is limited by the occurrence of high thermal stresses inside the filter [3]. Therefore, temperature controlled regeneration obtained by continuously varying the power supplied during regeneration as function of the measured filter temperature can lead to particulate oxidation minimizing the thermal stresses of the filter [4].

The regeneration of diesel soot filters by microwave was investigated in the past and this technique was proven to be simple, effective and reliable [3]. Although several diesel particulate trap systems using MW energy as heating source have been investigated, only few attempts combine this heating technique with catalysis [5-11]. The possibility of combining catalytic and permittivity properties of the filter components (catalyst and support material) with the microwave absorbing properties of soot results in enhanced performance of soot loaded filter regeneration.

Recently, we reported [10-12] that combining catalytic (Cu/V/K) filter and microwave heating allowed performing filter regeneration at temperature typical of diesel exhaust. In particular, the presence of catalyst assures lower soot ignition temperature, higher selectivity to CO_2, higher soot combustion rate and higher microwave energy saving.

In this work, the effect of the catalyst support on the activity of Cu/V/K catalyst towards the oxidation of soot in the presence of microwaves was investigated.

2. Experimental

2.1 Materials

Catalysts samples were prepared by supporting the active species of Cu/V/K catalyst on different ceramic materials: Al_2O_3: high purity alumina; Al_2O_3 (92%): 92% Al_2O_3 + SiO_2; SiC: high purity silicon carbide; SiC (50%): 50% SiC + 40.5% Al_2O_3 + 9.5% SiO_2; TiO_2: 98% TiO_2 + 2% SO_2; Cordierite; PSZ(Mg): 97% ZrO_2 + 3% MgO. All catalysts were prepared by wet impregnation with aqueous solution of inorganic salts: NH_4VO_3, KCl and $CuCl_2 \cdot 2H_2O$ in the molar ratio Cu:K:V= 2:2:1. The suspension was stirred and heated at 573 K for 2 h and then dried at 393K for 2 h. The powder catalyst obtained was calcined in static air at 973 K overnight.

Soot was collected directly at the exhaust of a gas-oil burner equipped with a nozzle giving a gas-oil mass flow rate of 1.9 kg/h (commercial gas-oil with H/C molar ratio of 1.75 and S content of 0.05 wt%).

2.2 Apparatuses and procedures

The activity of catalysts during electrical heating was investigated by air flow temperature-programmed oxidation of soot-catalyst mixtures with a TA Instruments Q600 thermobalance (TGA). The initial catalyst-soot mass ratio was 10, the air flow rate was 100 (STP)cm^3/min; the temperature was increased from 290 K to 970 K at 10 K/min heating rate.

In order to perform the catalyst screening in the presence of microwaves, a MW apparatus, reported in Figure 1, was specifically designed. The core of the apparatus is a MW system (Fricke und Mallah) including: i) a power supply that allows smoothly and stepless adjusting the magnetron output power up to 2000 W, driven by an external analog signal; ii) a 2.45 GHz water cooled 2 kW Magnetron head, fitted on a suitable launcher.

The latter is connected to a circulator with a water dummy load in order to protect the MW generator from the reflected power. The forward and the reflected power are measured by a dual bidirectional coupler. It is fitted on a waveguide at the circulator output. The coupler output is connected to an electronic card that linearizes and amplifies the output signal. Moreover, a motorized three stub tuner is fitted on the waveguide at the coupler output in order to match the load impedance and minimize the amount of reflected power. A quartz annular reactor (De=18 mm, Di=15 mm) is located in the centre of the waveguide, perpendicular to the direction of MW propagation, in the region of the maximum field. This particular geometry for the MW reactor was chosen in order to minimize the temperature radial gradient inside the catalytic bed. The sample temperature is measured by an optical pyrometer (Raytek), with a spot of about 40 mm, on the external reactor surface.

	(1) power supply
	(2) magnetron head
	(3) magnetron launcher
	(4) circulator
	(5) dual bidirectional coupler
	(6) motorized three stub tuners
	(7) annular quartz reactor
	(8) gas mass flow controllers
	(9) spot measurement pyrometer
	(10) gas analyzers
	(11) vent
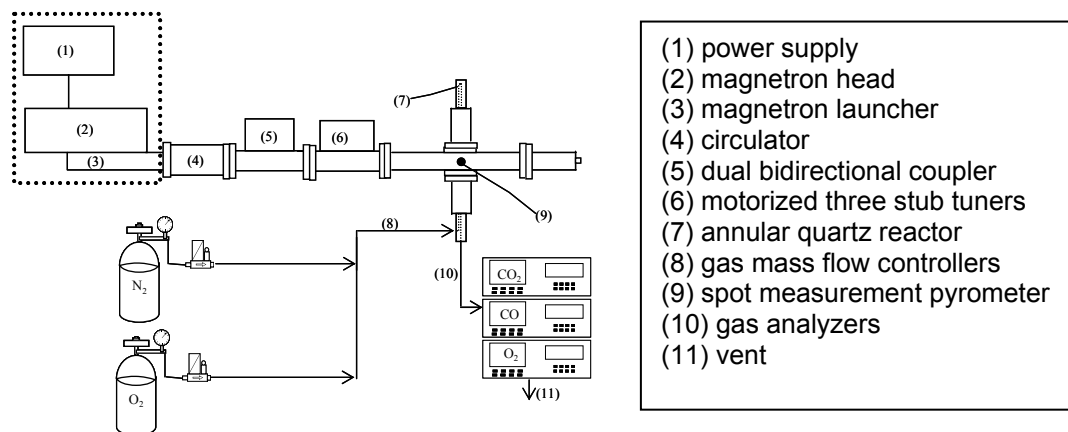
Figure 1 - Scheme of the apparatus for catalyst screening in the presence of microwaves

The pyrometer is connected to a PID controller for the incident power. The inlet gas mixture was fed to the reactor by mass flow controllers (Brooks) and the rector outlet was sent to specific analysers (ABB, Uras 14 and Magnos 106) to continuously detect CO, CO_2 and O_2 concentrations.

The activity tests in the presence of microwaves were carried out on mixtures of soot and catalyst obtained by carefully grinding the two components in an agate mortar (tight contact). The initial amount of soot loaded was about 25 mg. The catalyst-soot mixture, with an initial mass ratio of 10, was diluted with quartz powder (180-355 µm) in a mass ratio of about 10. Typical condition test are the following: controlled heating rate (20 °C/min up to 920 K) with a continuously variable power supplied; inlet gas flow rate (10.5 % vol O_2 in N_2) of 1000 (STP)cm^3/min.

3.   Results and discussion

From tests carried out in thermobalance the PSZ (Mg) supported Cu/V/K catalyst results the most active assuring a soot ignition temperature of about 540 K and a maximum oxidation rate at about 610 K. Soot oxidation profiles for the TiO_2, Al_2O_3 and cordierite supported catalysts are similar with a maximum oxidation rate occurring at 640-650 K. Both Cu/V/K-SiC supported catalysts are the least active towards soot oxidation, showing ignition and maximum oxidation rate at respectively 605 and 685 K for SiC and 660 and 750 K for SiC (50%).

In Figure 2a results of uncatalytic soot oxidation by microwaves are reported. From CO and CO_2 concentrations it appears that the soot ignition temperature is about 750 K and that during the reaction the CO_2/CO ratio remains unchanged at a value of about 1.8. In terms of required power, the incident power decreases from about 450 W at room temperature to about 150 W when the sample temperature reaches 420 K.

Behind this temperature the incident power is minimised as long as the soot is not yet enough oxidized. Indeed, once reached high soot conversion (90%) at a temperature of about 870 K the incident power quickly increases from 150 W to 1000 W, with a corresponding decrease of the absorbed with respect to the reflected power, while a sample temperature decrease is observed. Indeed, the incident power is the sum of the absorbed and reflected power.
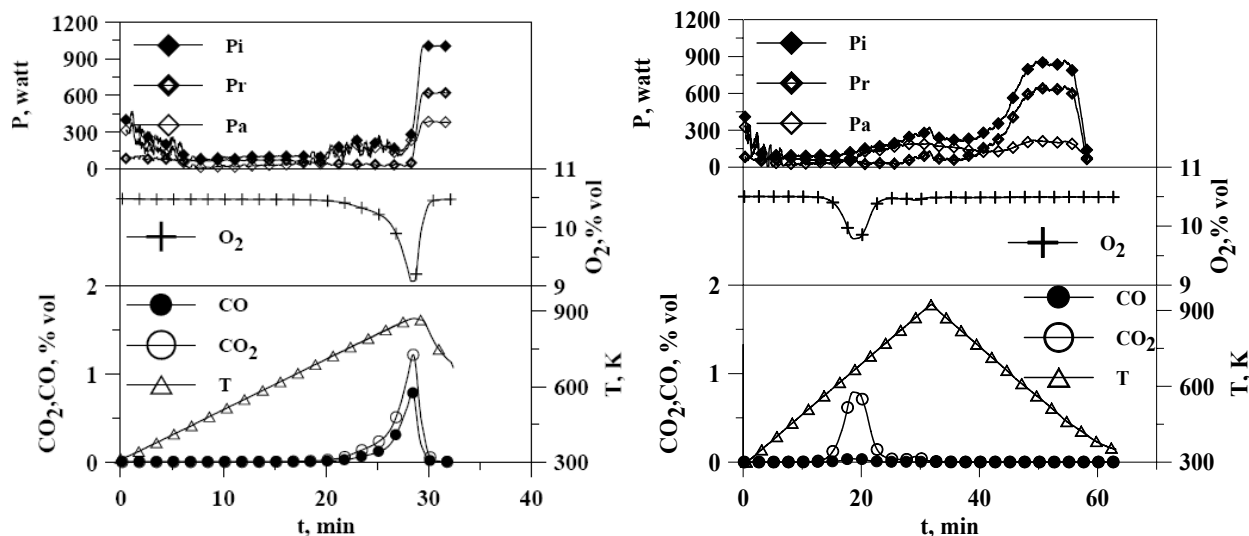
**Figure 2 - a) Uncatalysed and b) Cu/V/K catalysed soot oxidation test
in the presence of microwaves**

Typical results of catalytic soot oxidation performed by temperature programmed test are shown in Figure 2b for Cu/V/K-TiO$_2$ catalyst. Similarly to the uncatalytic case the required incident power decreases from about 450W at room temperature to about 150 W when the sample temperature reaches 420 K.

The CO$_2$ profile indicates that the catalytic oxidation begins at about 550 K and reaches a maximum at about 650 K (CO$_2$/CO=20). In this range of temperatures both incident and absorbed power slightly increase. Similar behaviour is observed even after total soot conversion and up to 920 K.

To evaluate the power required for catalyst heating in the absence of soot as function of temperature, a controlled cooling from 920 K to about 370 K was performed after catalytic soot oxidation (Figure 2b).

It clearly appears that at high temperatures (770-920 K) the required power is about 250 W and it is almost absorbed by the catalyst, while it increases at lower temperature (450-770 K), reaching a maximum (about 850 W) in the temperature range 450-550 K.

Results of microwave soot oxidation on Cu/V/K catalysts supported on the other ceramic materials give a soot ignition temperature for all the catalysts in the range 540-580 K and a maximum oxidation rate in the range 655-705 K. Except for Cu/V/K-SiC which is less active with a maximum oxidation rate occurring at about 780 K, all the catalysts give total soot oxidation and CO$_2$/CO ratio in the range 15-20.
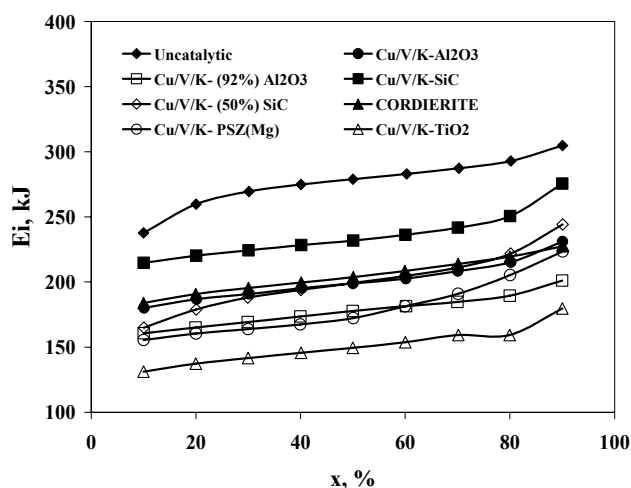
Figure 3 - Microwave energy required to reach different soot conversions
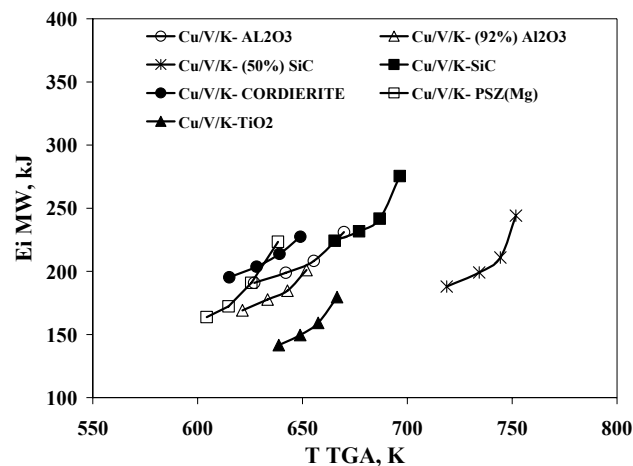
Figure 4 - MW energy required to reach different soot conversions against temperature as evaluated by TGA test

In terms of incident power, the energy required reaching a fixed conversion for the uncatalytic and catalytic soot oxidation was evaluated and reported in Figure 3. It appears that the energy required performing soot oxidation increases with soot conversion, being the soot the main microwave absorber. However, the presence of the catalyst assures a lower energy requirement with respect to the uncatalytic oxidation. In particular, the $Cu/V/K-TiO_2$ catalyst is the most efficient requiring the lowest energy to perform soot oxidation: at 50% soot conversion the energy saving with respect to the uncatalytic case is about 46%, while it is about 28% for $Cu/V/K-SiC$, the lowest efficient catalyst. In general, the energy saving obtained in the presence of the catalyst is due to the specific activity towards soot oxidation which allows reaching the same conversion at lower temperatures and hence in a shorter time with respect to the uncatalytic oxidation. In order to evaluate the contribute in terms of specific microwave absorbing properties of each catalyst, the energy required to reach 30, 50, 70 and 90% carbon conversion was related to the temperature at which this conversion is reached during electrical heating in TGA tests (Figure 4).

In particular, experimental results do not correlate with the specific catalytic activity obtained by TGA tests, but a different scale of energy requirement for a given soot conversion is obtained. Indeed results show that catalysts supported on PSZ(Mg), Al_2O_3, and cordierite allow reaching 30% carbon conversion at temperatures lower than $CuVK-TiO_2$ and $Cu/V/K-SiC$, while in terms of energy required to reach this conversion the $CuVK-TiO_2$ catalyst results the most efficient. This result suggests that the microwave absorbing properties of ceramic support in the oxidation of soot in the presence of MW have a primary role like the specific catalyst activity.

To this aim the energy required for reaching 10% soot conversion was related to the dielectric properties of the ceramic powder support in terms of loss factor [6]. Results reported in Figure 5 confirm that TiO_2 powder requires lower energy showing the highest value of the loss factor.

153
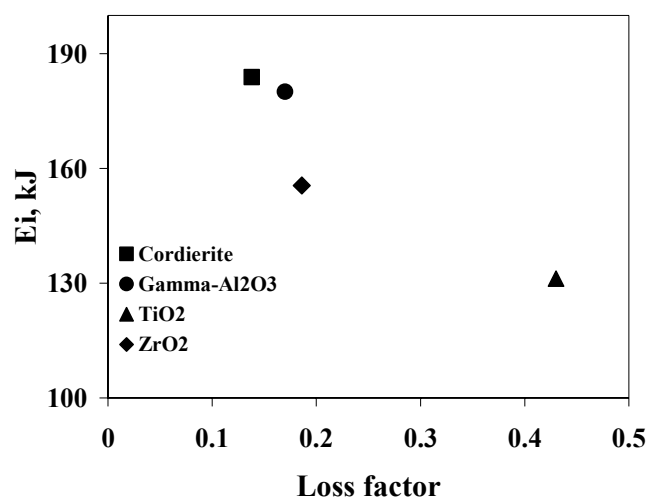
Figure 5 - Energy required reaching 10% soot conversion as function of loss factor of the some ceramic powder support

4. Conclusions

In the microwave assisted catalytic oxidation of soot improved regeneration efficiency and energy saving can be achieved in the presence of a catalyst having either specific activity for soot oxidation and good MW absorption properties. Experimental results indicate that microwave absorbing properties of ceramic support have a primary role like the specific catalyst activity.

In particular, with respect to the uncatalytic case the energy saving obtained in the presence of the catalyst is due to the specific activity towards soot oxidation which allows reaching the same conversion at lower temperatures and hence in a shorter time. In addition tests performed with different ceramic powder supports confirm that the material with the highest value of the loss factor (TiO_2 powder) requires the lowest energy to reach a given soot conversion.

References

1. A. Mayer, encyclopaedic article on "Particulate-Filter-Systems, Particle-Traps" (2003).
2. Z. Ning, Z. Guanglong, L. Yong, L. Junmin, G. Xiyan, L. Lunhui, C. Jiahua, *SAE Paper* 952058 (1995).
3. Z. Ning, Y. Yongsheng *SAE Paper* 991470 (1999).
4. V. Palma, M. D'Amore, P. Russo, A. D'Arco, P. Ciambelli, *Comb. Sci. Technol.* 174 (2002) 11.
5. F. B. Walton, P. J. Hayward, D. J. Wren, *SAE Paper* 900327 (1990).
6. J. Ma, M. Fang, P. Li, B. Zhu, X. Lu and N.T. Lau, *Appl. Catal.A-Gen.* 159 (1997) 211.
7. A. Bliek, Y. Zhang-Steenwinkel, Patent: EP1304456 (2001).
8. Y. Zhang-Steenwinkel, L.M. van der Zande, H.L. Castricum A. Bliek,. R.W. van den Brink, G.D. Elzinga, Top. Catal. 30/31 (2004) 257.
9. Y. Zhang-Steenwinkel, L.M. van der Zande, H.L. Castricum A. Bliek,. R.W. van den Brink, G.D. Elzinga, *Chem. Eng. Sci.* 60 (2005) 797.
10. V. Palma, P. Russo, M. D'Amore, P. Ciambelli, *Top. Catal.* 30/31 (2004) 261.
11. P. Ciambelli, V. Palma, P. Russo, M. D'Amore, *Stud. Surf. Sci. Catal.* 145 (2003) 367.
12. V. Palma, P. Russo, G. Matarazzo, P. Ciambelli, *Proceedings of the 7th World Congress of Chemical Engineering*, Glasgow, United Kingdom, July 10-14, 2005

MICROWAVE PROCESSING OF CHLORIDE WASTE TO FORM A GLASS-CERAMIC USING A SYNROC STRATEGIC APPROACH.
MISA 2006

M. La Robina[1], P. Veronesi [2], M. Poli [3], C. Leonelli [2]

1. Institute of Materials and Engineering Science, Australian Nuclear Science and Technology Organisation. (ANSTO) New Illawarra Road – Lucas Heights, NSW 2234 – Australia

michael.larobina@bologna.enea.it, michael.larobina@ansto.gov.au

Currently visiting scientist at ENEA, Centro di Recerca Bologna.

2. Dipartimento di Ingegneria dei Materiali e dell'Ambiente, Facolta' di Ingegneria, Universita' degli Studi di Modena e Reggio Emilia. Via Vignolese 905/A 41100 Modena

3. ENEA, Ente per le Nuove Tecnologie, l'Energia e l'Ambiente, Centro di Ricerche, Via Martire di Monte Sole, 4, 40129 Bologna

Abstract

With ANSTO's entry into EUROPART, a project that is co-funded by the European Commission, a new class of waste forms is being investigated. The waste is a result of reprocessing spent nuclear fuel using pyrometallurgical techniques to electrolyse the spent fuel elements and to recover the unused plutonium and uranium for recycling in other forms of fuel elements. The waste resulting from this work is a mixture of various chlorides that contain radiotoxic isotopes like Cs^{137} and Sr^{90} as well as minor actinides like Am, Cm and Np which can also be recovered and either disposed of as a waste, or redirected for transmutation and subsequently disposed of. The waste is a highly conductive material, so it lends itself very well for processing with such technologies as microwaves and radio-frequencies. We propose to develop a waste form based on the SYNROC (SYNthetic ROCk) technology by designing a ceramic or a glass -ceramic that is capable of hosting these alkali and alkaline earth chlorides and immobilising them. The glass ceramic composition devised using this strategy is being tested for suitability. Here we report the preliminary experiments and the results obtained, highlighting the problems and how we might deal with them.

Introduction

<u>Background:</u>

A brief summary of where the waste comes from and what is the wastes that are we interested in will be given. Nuclear waste has many wide and varied sources:

1.   Nuclear fuel production.

   a.   <u>Uranium mining</u> produces vast amounts of waste during the processing of the ore to produce the uranium oxide yellow cake.

   b.   <u>Uranium enrichment</u> the second stage of nuclear fuel production also produces new waste.

   c.   And clearly the actual <u>fabrication of fuel rods</u> will produce more waste in the form of waste material and contamination of the production plant.

2.   Fuel burn up in a reactor:

a.   Once the fuel rod are burned, the spent rods contain highly radioactive fission fragments such as ^{137}Cs and ^{90}Sr and unburnt nuclear fuel such as plutonium (^{239}Pu) and uranium (^{235}U) together with minor actinides that form by transmutation of ^{238}U, i.e., americium, neptunium and curium.

3.   Production of weapons such as low yield tactical fission bombs and extremely high yield fusion weapons that are triggered by a fission device.

4.   Production of isotopes for use in nuclear medicine which are produced in reactors and cyclotrons to make radiopharmaceuticals.

5.   Fuel reprocessing:

a.   Spent fuel rods have significant quantities of unburnt fuel as well as minor actinides. These are clearly valuable and need to be recovered by reprocessing the spent fuel rods. As a result, the chemistry undertaken to do this reprocessing will inevitably increase the inventory of waste.

b.   One of the processes that produce such waste is the pyrometalurgical electro-refining method used to electrolytically separate the uranium and plutonium from the spent fuel rods. This is one of two methods used in the European project EUROPART.

With ANSTO's entry into EUROPART, we are now looking at ways of treating this new class of waste form and various techniques are being investigated. This paper is concerned with designing a ceramic or a glass-ceramic that is capable of hosting these alkali and alkaline earth chlorides and immobilising them.

The EUROPART waste consists of the following: 63% Li-KCl eutectic, 12% NaCl, 10% CsCl, 7% $BaCl_2$ and 8% $SrCl_2$. Radio Frequencies (RF) and microwaves are extremely efficient and rapid ways of heating materials that couple and absorb this kind of energy. As seen from the literature, the chlorides are excellent absorbers of microwaves so this frequency was chosen as a starting point in the processing.

What is SYNROC

SYNROC was invented some 25 years ago in Australia at the Australian National University. Its inventor Prof. Ringwood argued that the best way to immobilise radioactive isotopes was to mimic nature. He had found that there were a large number of naturally occurring minerals that contained radio active elements in the crystal lattice and also were part of the mineral ensemble that formed extremely ancient and durable rocks. He therefore set out to recreate these minerals in the laboratory and try to form an ensemble of minerals that would result in a synthetic rock.

Hence the word SYNROC from *syn*thetic *roc*k was coined. With this in mind a search was made for some naturally occurring mineral that could take up the chloride, the alkali metals and the alkaline earth metals as well as the caesium and strontium. Some of the mineral building blocks being considered are shown in Table 1.

Table 1 - Mineral phases in the chloride waste

Mineral Phase	Composition
Pollucite	$(Cs,Na)_2Al_2Si_4O_{12} \cdot (H_2O)$
Chlorartinite	$Mg_2(CO_3)Cl(OH) \cdot 3(H_2O)$
Hollandite	$Ba(Al,Ti)_2Ti_6O_{16}$
Natural Hollandite	$(Ba,Sr)(Mn^{+4},Mn^{+2})_8O_{16}$
Chlorothionite	$K2Cu(SO_4)Cl_2$
Chlormanganokalite	K_4MnCl_6

The initial choice was to deal with the chloride waste having all the isotopes present, i.e. ^{137}Cs, ^{90}Sr and americium, neptunium and curium[§]. Clearly, being able to minimise the process steps would present an enormous cost advantage. Against this has to be weighed the formation of durable mineral phases. To form an ensemble of durable mineral phases, the composition may need to be adjusted in order to ensure that durable mineral phases form. To achieve this, may require the removal of some of the isotopes from the waste and dealing with them separately. Koyama *et al* [1] have proposed the use of sodalite as the most favourable mineral phase in order to immobilise chlorides while Leturcq *et al* [2] has also suggested the use of silver to remove the chloride and then dealing with the remaining radiotoxic isotopes using well proven ceramic compositions such as those of synroc or various compositions of borosilicate glass, which can not hold the chloride ions. This work aims to find an assemblage of mineral phases that behave similarly to the synroc mineral assemblage, which ranges from ceramics to glass-ceramics. Although the work has the aim as stated, we focus this report on the actual process and the use of microwaves.

Experimental

The composition selected was designed to give the various mineral phases shown in Table 1. Two compositions were prepared, 281105 and 291105. Both were essentially the same and the composition shown in Table 2 can be taken as representative of both. The variation was only slight and well within the experimental error of the weighing process.

[§] Americium, curium and neptunium are minor actinides which would require the addition of mineral phases such as Pyrochlore $[(Ca,ACT,REE)_2(Ti,Fe,Nb)O_7]$, Zirconolite, $[(Ca,ACT,REE)Zr(Ti,Al)_2O_7]$, and Brannerite, $[(ACT,Ca,REE)(Ti,Fe)_2O_6]$, which can take up the actinides (ACT) as well as rare earth elements (REE) into their crystal lattice. For the sake of simplicity we only deal with the caesium and strontium which can be taken up by Perovskite, $[ABO_3, (Ca,REE,Sr)TiO_3]$, Hollandite, $[Ba_xCs_yTi_{8-2x-y}M^{3+}_{2x+y}O_{16}]$.

Table 2 - The column labelled "Required" are the weights calculated based on the composition given above. The compounds shown are the compounds actually used simply because they were what were available

Compound		Required	Actual	Compound	Required	1/10	Actual
			Added				Added
KCl		**110.21**	11.032	SiO_2	44.27	4.4	4.407
LiCl		**62.67**	6.274	$Al2O_3$	18.4	1.8	1.804
NaCl		**32.93**	3.295	$MgCO_3$	143.62	14.4	14.404
CsCl		**27.44**	2.71	$CaCO_3$	20.30	2.0	2.03
$SrCl_2$	Hydrated 176.54	**24.45**	2.459	$CuSO_4.5H_2O$	179.22	17.9	17.922
$BaCl_2$	Hydrated 244.28	**33.33**	3.33	MnO_2	86.00	8.6	8.604
				$Fe2O_3$	11.00	1.1	1.104
				$Pb(CH_3CO_3).Pb(OH)_2$	41.6	0.41	0.416
				TiO_2	72.7	7.3	7.309
				$BaCO_3$	13.00	1.3	1.304

The composition design shown in Table 2, is aimed at maximising the waste loading in the resulting waste form. To do this the synroc approach or strategy is used. The synroc strategy involves using the waste and adding a precursor which consists of a mixture of oxides (or other compounds as in our case) to give the targeted mineral phases when the waste and the precursor have been treated. In addition, the waste components were considered to be part of the mineral phase being designed so that the precursor alone would not be sufficient to make the required phases. This approach ensures a higher waste loading than otherwise could be obtained. The waste and the precursor were prepared separately and subsequently mixed to form the mixture for processing.

Once the waste and precursor mixture was thoroughly mixed, some borosilicate glass frits were added. Two lots were prepared for processing; the first lot was a 1:1 mixture and the second lot of a 2:1 mixture of waste form to borosilicate glass frits. The 1:1 ratio was selected because the behaviour of these materials was unknown and the aim was to produce a glass ceramic which consists of a glass matrix with the selected mineral phases throughout. The mixtures were placed in a cordierite/mullite crucible and heated in a microwave oven at the University of Modena and Reggio Emilia in the MAG - Microwave Application Group Laboratory for various time intervals measuring the temperature as heating progressed. The experiments with the same compositions were repeated in the microwave laboratory at ENEA, Bologna. Once the samples were prepared, they were sent to ENEA in Brasimone to have the microstructure examined by the SEM lab there.

Results

The two lots of samples prepared produced a green glass as shown in Figure 1. The rapid heat treatment that is a major advantage with MW can be seen in Figure 2. Here the temperature readings measured as the mixture was processed are plotted against time. Melting occurred at low temperatures as was evident from the presence of liquid glass ceramic in the crucible once removed from the microwave oven.
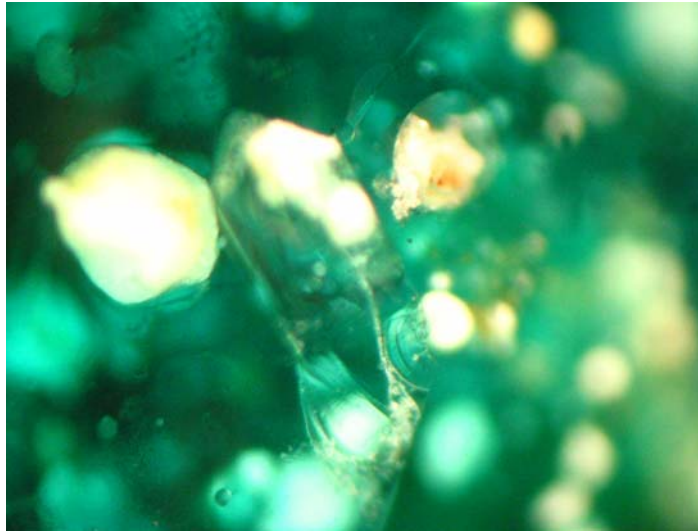
Figure 1 - Optical microscope image of the green glass formed
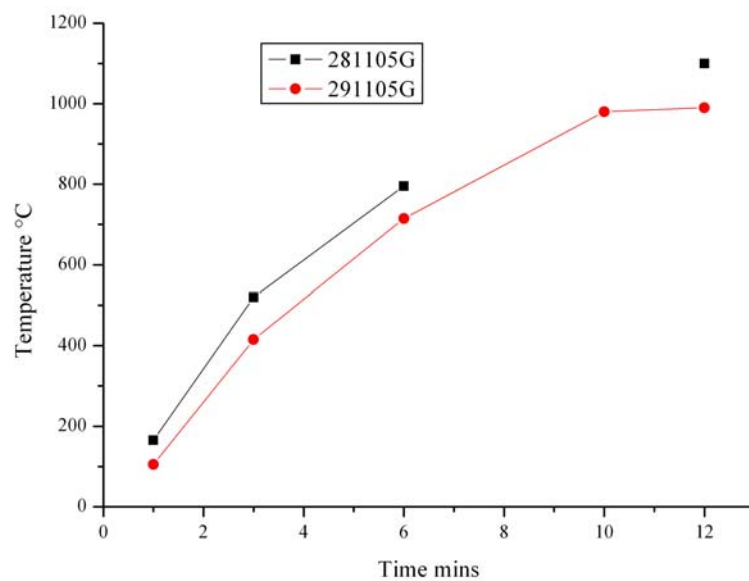
Figure 2 - The two temperature graphs vary slightly, because of a slight difference in composition but the trends are the same

SEM

The SEM showed a wide variety of phases and a good glass matrix.
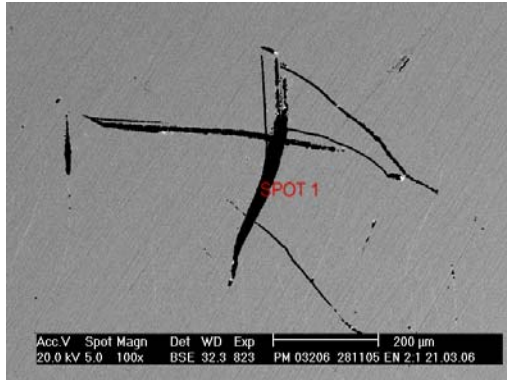
Figure 3 - Matrix
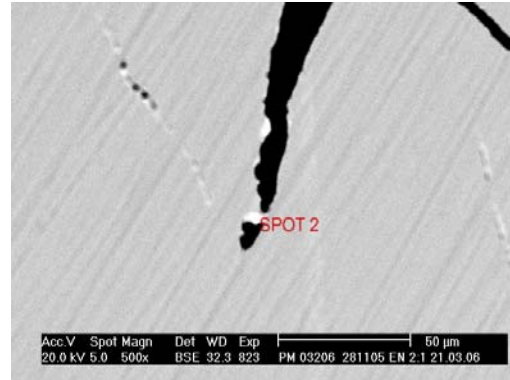
Figure 4 - Black long phase
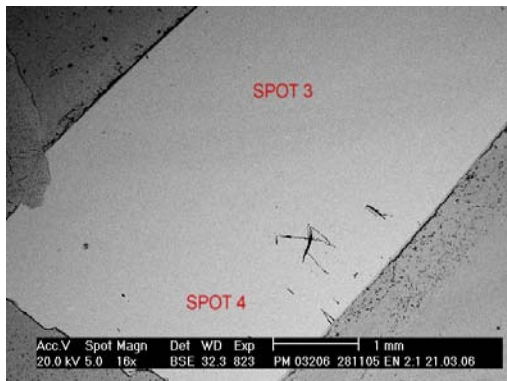
**Figure 5 - Spot 3 Grey polygonal phase
and spot 4 White spot in grey phase**

Figure 6 - Spot 5 White round phase

Table 3 - EDS analysis of the various spots shown in Figures 3 to 6

SPOT	O	Na	Mg	Al	Si	S	Cl	K	Ca	Ti	Fe	Cu
1	75.46	3.59	4.58	1.16	10.97	0.15	0.38	0.48	0.37	1.66	0.23	0.97
2	64.04		5.42		19.74			0.39	0.28	2.84	1.38	2.11
3	21.26	3.73	9.28	3.13	42.08		0.87	1.74	1.57	6.35	1.87	5.91
4	20.62	2.70	9.52	3.38	44.03		0.92	1.60	1.15	6.53	1.86	7.70
5	34.75		36.48	5.09	6.18		0.47			0.78	0.95	8.11
6	69.88	1.46	4.14	2.02	15.29		0.32	0.72	0.50	3.09	0.48	15.29

PM 03206 281105 EN 2:1 6-April-2006
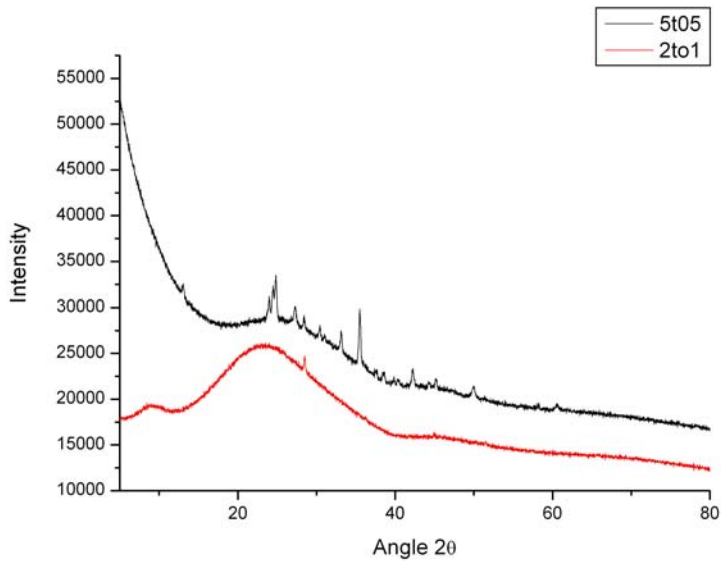
Figure 7 XRD of two samples One was of the 1:1 ration waste to glass (5to5) while the other is the 2:1 ratio of waste to glass. As can be seen a better glass was formed with 2:1 (smooth amorphous curve with no peaks) than with the 1:1

Conclusions

Clearly a glass matrix did form although the mineral phases targeted were not evident, the matrix does have a complex composition which could be interpreted as a mixture of various phases, for example as determined from EDS:

$Na_{4.97}K_{1.03}Ca_{0.51}Mg_{5.99}Cu_{3.95}Fe_{0.72}Al_{1.54}Ti_{3.03}Si_{30.69}Cl_{0.49}O_{47.09}$

(PM 03006 281105 GMO 5:5) and

$Na_{3.9}K_{2.33}Ca_{1.09}Mg_{6.19}Cu_{3.58}Fe_{1.29}Al_{2.13}Ti_{4.53}Si_{33.58}Cl_{0.67}O_{40.71}$

(PM 03506 291105 EN 2:1)

The matrix composition from sample to sample was consistent even if some variation of element content was shown – it was clear that a glass was formed. A variety of other phases were observed with there compositions as determined by EDS summarised below

$Na_{1.42}Mg_{1.54}Ca_{0.12}Cu_{1.32}Ti_{33.83}Si_{7.34}Cl_{0.29}O_{54.17}$ (PM 03006 281105 GMO 5:5) and

$Na_{2.84}K_{1.34}Ca_{1.34}Mg_{14.61}Cu_{4.14}Fe_{1.66}Al_{2.02}Ti_{5.06}Si_{26.66}Cl_{0.54}O_{39.80}$ (PM 03506 291105 EN 2:1)

From sample: PM 03306 291105 EN 5:5 we get the following phases.

1. $Na_{4.27}Mg_{6.52}Al_{2.41}K_{1.67}Ca_{0.68}Fe_{1.81}Cu_{4.76}Ti_{3.68}Si_{50.03}Cl_{0.91}O_{23.26}$

2. $Na_{4.93}Mg_{3.08}Al_{0.96}K_{0.39}Ca_{0.24}Fe_{0.13}Cu_{0.46}Ti_{0.91}Si_{12.69}Cl_{0.21}O_{76.01}$

3. $Mg_{31.12}K_{1.04}Ca_{0.87}Fe_{1.56}Cu_{7.27}Ti_{3.24}Si_{39.61}Cl_{0.68}O_{14.6}$

4. $Mg_{7.70}Al_{1.31}K_{0.51}Ca_{0.32}Fe_{3.14}Cu_{4.99}Ti_{65.47}Si_{8.01}Cl_{0.29}O_{8.25}$

5. $Na_{15.14}K_{22.23}Cs_{1.66}Fe_{0.75}Cu_{18.96}Si_{2.32}Cl_{9.60}O_{29.34}$

6. $Sr_{13.63}K_{6.35}Ca_{4.55}Ba_{45.06}Cu_{16.07}Cl_{14.33}$

Clearly there needs to be some additional work done in interpreting what these phases are and how they all fit together in the matrix. Due to shortness of time, leach tests were not conducted and are planned for a future run of experiments. Some problems with volatilisations was observed, so that future experiments are planned to be conducted in a controlled atmosphere chamber operating at above one atmosphere to suppress the volatile fumes from forming. From point of view of the process, that is the application of the microwaves to melt the mixture and form a glass, the experiments can be described as successful. It was found however that the particular waste form, i.e. the chlorides mix alone would not form a low viscosity melt, instead it formed a very viscous mass which did not appear react very well with several of the component chemicals still present in their original form. It was also found that the minimum amount of borosilicate glass that could be used was 30% of the mixture mass. It appears that with less glass frits added, there is not enough thermal mass to absorb the microwave energy to sufficiently raise the temperature of the mixture to make it become liquid. All in all the results are promising and worthy of further investigation to optimise the process so that it can be applied to the problem at hand.

Acknowledgements

References

1) Tadafumi Koyama, Chiaki Matsubara, Toshio Sawa and Hioshi Tanaka, "Waste form development for immobilization of radioactive halide salt generated from pyrometalurgical reprocessing." Proceedings from GLOBAL 1997, Vol. 1, pp. 610-615.

2) G. Leturcq, A. Grandjean, D. Rigaud, P. Perouty, M. Charlot "immobilization of fission products arising from pyrometallurgical reprocessing in chloride media", Journal of Nuclear Materials 347 (2005) 1–11.

Section 4. Modelling and applicator design

NUMERICAL SIMULATION OF A CONTINUOUS MICROWAVE DRIER FOR EXTRUDED TILES

D. Boccaccini, C. Leonelli, G.C. Pellacani, M. Romagnoli, P. Veronesi

Dipartimento di Ingegneria dei Materiali e dell'Ambiente

Università degli Studi di Modena e Reggio Emilia

Via Vignolese 905, 4110 Modena - Italy

paolov@unimore.it

Abstract

Drying of extruded ceramic tiles is a time-consuming process, because thermal gradients or not homogenous shrinkage must be avoided in order to ensure tiles' integrity. Preliminary experimental microwave drying tests have been performed on the extruded tiles, with 18% moisture level, in order to assess the maximum power density bearable by the material. Dielectric properties measurement provided the input data for the numerical simulation of the microwave drying of the extruded tiles, in a multi-feed (2 ports module) multimode applicator. Simulated microwave feeds position and orientation lead to different results in terms of energy efficiency, evaluated in terms of the scattering matrix coefficients.

I.   Introduction

Ceramics materials, including glasses, can benefit from the use of microwaves, due to their usually low thermal conductivity. Moreover, in drying or de-binding applications, the selective heating can be successfully exploited, and, depending on the power penetration depth, shorter processing times can be achieved [1].

Using accurate process controls, if necessary employing hybrid (i.e. hot air, ohmic, etc...) heating systems, it is possible to regulate the flux of water leaving the body, avoiding the creation, during drying, of a completely dried surface layer which impedes the remaining water molecules diffusion towards the ambient.

This problem is instead frequently encountered using conventional drying methods. Even if microwave assisted drying can be carried out up to ten times faster than the rate obtainable by means of hot air or IR lamps, the process has an intrinsic limit due to mechanical resistance of the green (unfired) body. A too rapid power transfer would cause the water to instantaneously vaporise, deforming, cracking or even breaking the ceramic body [2].

On the other side, the combined use of different heating techniques can help reducing the thermal gradient between the outer and the inner parts of the ceramic bodies, allowing for faster processing [3].

II.   Experimental

Preliminary microwave drying tests have been conducted in a modified multi-mode applicator, equipped with mode stirrer and hot air generator (from 75 to 200 °C, 650 W resistance power). Microwave power could be varied from 150 to 950 W, stepwise, and the power controller was of the simple on/off type. It has been chosen the power level of 650W, to compare with the hot air heating treatment. A series of rectangular shaped samples (160x120x20 mm) was cut starting from the extruded green plates (18% moisture) provided by Olivastri Forni Srl. Samples weight was 750±100 g; each sample, one per run, was placed on two alumina supports (1x10 cm, thickness 0.8 cm) to allow air circulation.

The software Design Expert 6.1 (Stat-Ease, USA) was used to setup the most appropriate Design of Experiment, able to minimise the number of tests needed to quantify indeterminate measurements of factors and interactions between them, statistically, through observance of forced changes made methodically and experiments run in a random order to avoid introducing bias into the results. As a result, mathematical models describing the factors (variables) interactions can be obtained, and local maxima or minima can be calculated (optimisation) and experimentally tested for validation. A Response Surface Method (RSM) with Central Composite Design (CCD) was chosen for its ability to suit process optimisation. Independent variables were: overall treatment time (1-12 minutes), microwave treatment time (0-100%) and sample movement in the applicator (On/Off). Dependent variables were water removed (g), maximum temperature difference at the end of the treatment (°C) and measured MOR after 2 days (N/mm^2). The CCD lead to 28 experimental conditions (microwave power = 650W, hot air temperature=75 °C), some of which repeated, as shown in table I.

Further tests have been conducted in a prototype multimode applicator presenting a single horn feed in the upper part, connected to a 3 kW microwave generator (SM1150 power supply + TM030 head, Alter, Reggio Emilia). Square samples having the dimensions of 200x200x20 mm were placed, one per run, in the plane perpendicular to the microwave propagation direction in the feeding waveguide, ad different height from the applicator bottom. A 4-channel fibre optic temperature measurement system (Neoptix, Canada) was used to measure the temperature raise of the samples during microwave exposure, in order to evaluate the heating homogeneity in case of stationary load and no hot air flux (critical condition).

Each sample, immediately after the complete treatment, was weighed, and placed vertically to eventually finish its drying at ambient conditions. Visual assessment of the damage (cracks, distortion, swelling) was also performed. Modulus of Rupture (flexural strength in a three-point bending test) was measured 2 days after the treatment, when most of the samples looked satisfactory dried. Modulus of Rupture measurements, conducted using a 3-point bending apparatus (CCR-Faenza) were used to estimate the sample damage induced by microwave exposure.

Permittivity of the samples at different moisture levels were measured by an Agilent 85070E Dielectric probe kit connected to an HP 851907B vector network analyser. The measurement technique consists in converting complex reflection coefficient into complex permittivity. Calibration is achieved using distilled water, open and short circuit loads.

164

Table I - Experimental conditions (microwave power = 650W; Hot Air temperature= 75 °C)

Sample	time tot	t MW	t Hot Air	Movement
n°	min	min	min	(ON/OFF)
1	3	0	3	ON
2	10	10	0	ON
3	3	3	0	OFF
4	3	3	0	ON
5	6.5	3.25	3.25	ON
6	3	0	3	OFF
7	6.5	3.25	3.25	OFF
8	10	0	10	OFF
9	10	0	10	ON
10	6.5	3.25	3.25	OFF
11	6.5	3.25	3.25	OFF
12	6.5	3.25	3.25	ON
13	6.5	3.25	3.25	ON
14	10	10	0	OFF
15	6.5	6.5	0	OFF
16	6.5	0	6.5	ON
17	6.5	6.5	0	ON
18	6.5	3.25	3.25	OFF
19	6.5	3.25	3.25	ON
20	11.45	5.725	5.725	OFF
21	6.5	3.25	3.25	OFF
22	6.5	0	6.5	OFF
23	1.55	0.775	0.775	OFF
24	6.5	3.25	3.25	ON
25	6.5	3.25	3.25	ON
26	1.55	0.775	0.775	ON
27	11.45	5.725	5.725	ON
28	6.5	3.25	3.25	OFF

Three series of samples, one as received (moist), one after 1-day exposure to ambient conditions (partially moist) and one completely dried (dry) were subjected to dielectric properties measurement in the 1-3 GHz frequency range.

Numerical simulation of a new multi mode applicator, based on the horn-feed applicator tests, was performed using the commercial software Concerto 4.0 (Vector Fields, U.K.).

The software, given a parameterised model geometry, the dielectric and electric properties of the materials, and the characteristics of the input/output ports, is able to calculate the system scattering matrix as well as to visualise the electromagnetic field distribution in the applicator and in the load. This can result particularly useful to calculate the Specific Absorption Rate (SAR, in W/kg), corresponding to the amount of power dissipated (or heat generated) into the unit mass of the load. The built-in optimisation procedure of the software allows changing the model geometry, varying one or more parameters, in order to minimise an objective function, such as the reflected power or the crosscoupling between different microwave generators.

III.   Results and discussion

Preliminary tests in the modified hot air/microwave multimode applicator showed a good reproducibility of the results in terms of water loss, a shown in Table II. However, the same can not be said concerning MoR, and this is mainly due to the random occurrence of the damage in the sample, but also to the measurement uncertainties typical of the 3-point bending test. Not in all cases it was possible to obtain a fracture along the centre line of the sample (which corresponds to the maximum flexural moment), and this could be considered an evidence of an existing damage able to weaken the resistance in sections different from the most loaded one. The treatment consisting of 3.25 minutes of microwaves followed by 3.25 minutes of hot air while moving the sample – samples 5, 12, 13, 19, 24, 25 – did not damage the material (MoR is in the average value), while it removed 7 times more water than a conventional (hot air) drying lasting the same amount of time – samples 16, 22. As a matter of fact, on the average, the combined treatment removed 27.6 g of water, while the conventional hot air treatment was able to remove only 3.8 g. A prolonged exposure to microwaves, however, despite allowing more water to be removed, lead to severe sample cracking, as confirmed by the low MOR values of samples 2 and 14.

Statistical analysis of the results is represented in Figure 1. The analysis confirms some expected results, i.e. the sample movement does not affect the amount of water removed (Figure 1 a and b), but surprisingly it does not seem to affect the MoR values (Figure 1 c and d), despite its strong influence on sample homogenous heating (Figure 1 e and f). Increasing microwave exposure time allows more water to be removed (Figure 1 a and b), while it has some detrimental effects on MoR and sample homogenous heating, especially in case of stationary sample. This suggest the existence of an upper limit to the maximum microwave continuous exposure time bearable by the material, which roughly corresponds to the removal of more than 35 g of water from the sample: in that case, MoR values fall dramatically.

Heating tests in the horn-feed applicator showed that in case of stationary samples, heating homogeneity is difficult to achieve, as shown in Figure 2b, but it is not impossible to dry the sample by pure microwave heating, provided the forward power is carefully controlled. In the experimental conditions used, 650 W of continuous microwave irradiation on 0.8 kg samples caused the appearance of small surface cracks.

Table II - Preliminary tests results (microwave power = 650W; Hot Air temperature= 75 °C)

sample	time tot	t MW	t Hot Air	Movement	H2O removed	MoR	ΔT
n°	min	min	min	(ON/OFF)	g	N/mm2	°C
1	3	0	3	ON	1.2	0.78	0.5
2	10	10	0	ON	88.7	0.20	22.5
3	3	3	0	OFF	19.6	1.01	16.5
4	3	3	0	ON	17.8	0.74	13
5	6.5	3.25	3.25	ON	25.5	0.77	4.5
6	3	0	3	OFF	1.9	0.88	0.5
7	6.5	3.25	3.25	OFF	30.2	0.66	16
8	10	0	10	OFF	6.1	0.88	1.5
9	10	0	10	ON	5.6	0.98	0.5
10	6.5	3.25	3.25	OFF	28.8	0.83	21
11	6.5	3.25	3.25	OFF	34.3	0.94	17
12	6.5	3.25	3.25	ON	26.4	0.65	6.5
13	6.5	3.25	3.25	ON	26.2	0.77	6
14	10	10	0	OFF	89.8	0.23	45
15	6.5	6.5	0	OFF	53.1	0.10	34.5
16	6.5	0	6.5	ON	3.9	0.73	0.5
17	6.5	6.5	0	ON	57.5	0.03	3
18	6.5	3.25	3.25	OFF	27.1	0.95	12.5
19	6.5	3.25	3.25	ON	33.4	0.66	7
20	11.45	5.725	5.725	OFF	54.6	0.16	19.5
21	6.5	3.25	3.25	OFF	27.4	1.18	12.5
22	6.5	0	6.5	OFF	3.7	0.54	0.5
23	1.55	0.775	0.775	OFF	3.2	0.74	8
24	6.5	3.25	3.25	ON	28.2	0.69	3.5
25	6.5	3.25	3.25	ON	26.0	0.85	4
26	1.55	0.775	0.775	ON	2.8	0.74	3
27	11.45	5.725	5.725	ON	53.8	0.17	1
28	6.5	3.25	3.25	OFF	26.9	0.76	8

.
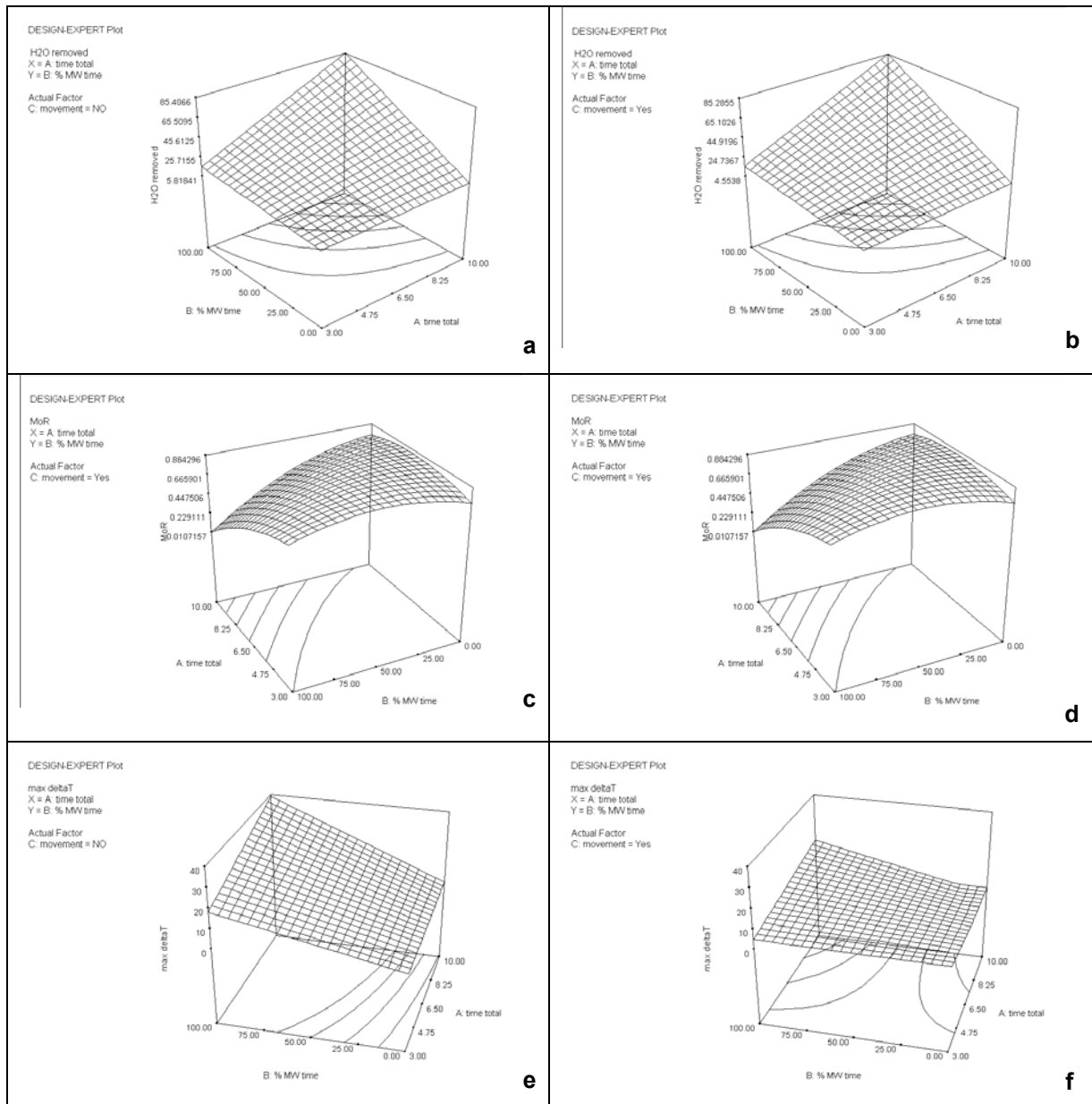
Figure 1 - Statistical analysis of preliminary tests results: dependence on treatment time and microwave exposure time of: a) water removed in case of stationary sample; b) water removed in case of sample movement; c) MoR in case of stationary sample; d) MoR in case of sample movement; e) temperature difference in case of stationary sample; f) temperature difference in case of sample movement

The preliminary results, obtained in existing applicators, evidenced the need for a new applicator, able to increase more homogenously the sample temperature, without damage, but with high efficiency. For this reason, based on the obtained results, a new tunnel applicator was designed, presenting horn-like feeds, and the possibility of moving (translation) the load while exposing it to hot air. Moreover, the obtained results, suggested not using microwaves to remove significant percentages of water, since this could lead to cracking and swelling of the sample.
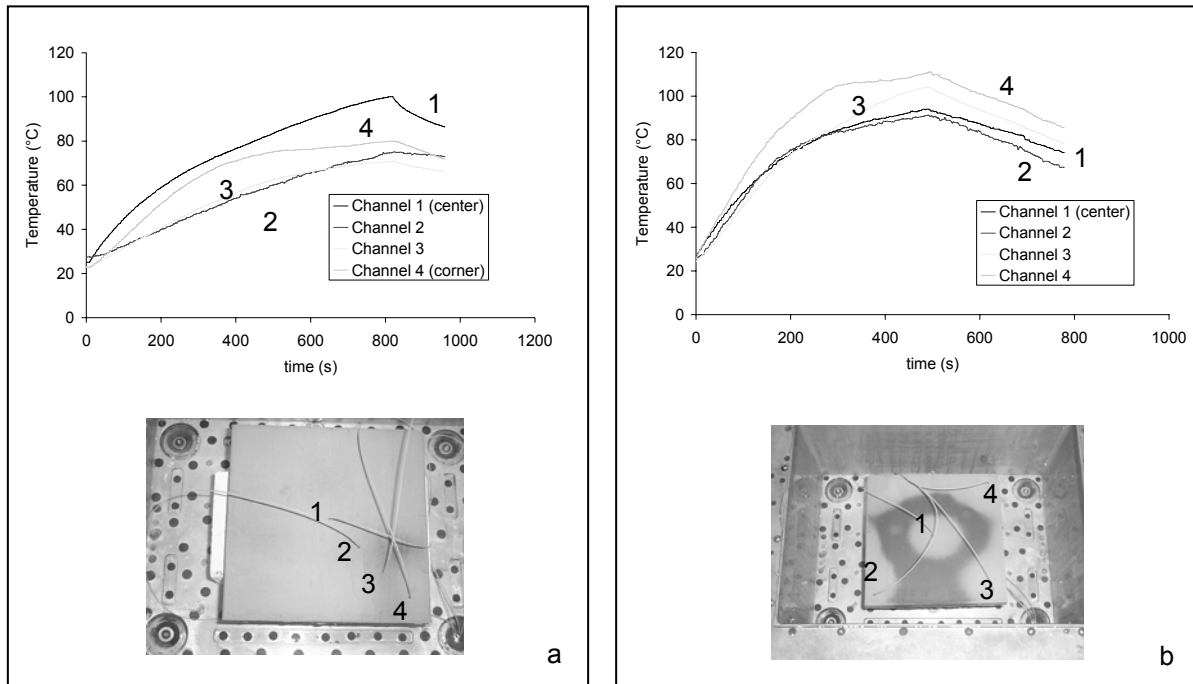
Figure 2 - Differential heating of the samples placed in the horn-feed applicator in 2 different positions: a) centre overheating but fairly homogenous drying; b) heating unhomogeneity and incomplete drying

Table III - permittivity measurements

Moisture	ε'	ε''	$tan\ \delta$	Dp (mm)
18%	27.7	8.1	0.29	13.1
9%	19.4	4	0.21	22.1
3%	6.2	0.9	0.15	54.7

The design procedure required the dielectric properties of the material to be known, at least in some of its status (moist, partially dried and almost dry). Dielectric properties measurement, reported in Table III, showed a progressively increasing power penetration depth at 2.45 GHz, as expected. However, the moist samples present a small penetration depth, which can be a limiting factor for the overall thickness of the tiles to be dried

Based on the permittivity measurement results, a modular applicator has been designed, containing two feeds (microwave sources) per module. Each feed, of the horn type, was parameterised and optimised in terms of minimum reflected power, under different loading conditions. A drawing of the module, in one of the possible waveguide configurations, is shown in Figure 3a. A load composed of 16 square tiles, four of which not equally spaced from the others (Figure 3b), in order to take into account possible deviation from the ideal conditions, was set at a fixed distance from the bottom of the applicator.

169
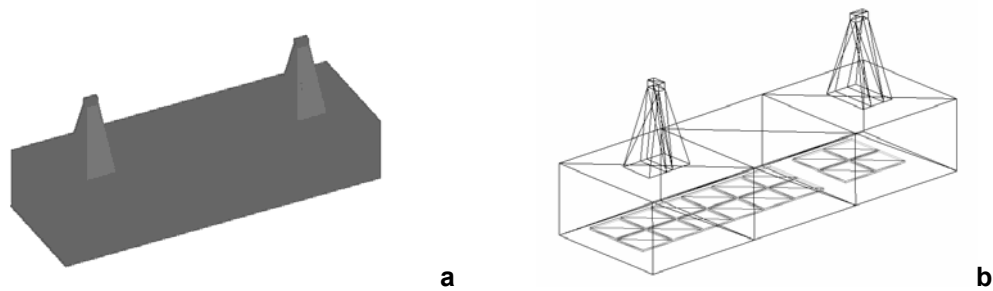
**Figure 3 - Module of the microwave drier a) in the V-V configuration
b) in the O-V configuration, showing the load position**

A first series of simulations was performed considering the case of moist tiles, with the aim of using microwaves only to increase samples' temperature, and not removing water. A second series regarded the case of partially moist samples, in the hypothesis that 9% moisture corresponds to the starting of well know phenomenon of the decrease in the drying rate by pure hot air [4], and that the water temperature raise due to microwaves could be used to increase water diffusion from the inner parts towards the sample surface. In both cases, the load position was varied in the applicator, simulating the presence of a conveyor belt moving the samples. The average of the absolute values of the scattering matrix coefficient calculated for different load positions was used to compare energy efficiency of competing solutions. The optimisation (applicator height and width, constrained by the maximum layout occupation allowed) was conducted minimizing an objective function obtained summing these values, squared.

Depending on the waveguide configuration, different scattering matrices could be obtained for the same set of optimised applicator height and width. In particular, in case of moist material, at 2.45 GHz, in the configuration shown in Figure 3a (V-V, i.e. the exciting field in the waveguide is oriented parallel and transversally to the direction of sample movement), the calculated $|S11|$ is 0.45, while $|S12|$ is 0.22, indicating a pronounced mismatch and crosscoupling. Instead, in case one feed is rotated by 90°, as depicted in Figure 3b (configuration O-V), the calculated $|S11|$ is 0.23 and $|S12|$ is 0.0007. A similar behaviour was obtained in case of homogenous partially dried load. These results indicate that the O-V configuration (exciting fields in the waveguides perpendicular to each other) results much more favourable, as expected, as far as crosscoupling is concerned.

The optimised applicator ports were excited sinusoidally in order to calculate the SAR in the load. Its distribution on the first layer of the tiles, for one possible sample position, is represented qualitatively in Figure 4. The calculation results show that the O-V configuration provides a more homogenous heat generation in the load, which will benefit also from the movement along the tunnel length. As expected, the lack of material passing under the microwave feeds (for instance, due to a non ideal loading condition) causes more power to be locally generated in the load: the four top tiles of Figure 4 present a higher SAR with respect to the remaining twelve. This phenomenon will have to be taken into account when realizing the control system of the applicator, which should be able to vary the microwave forward power depending on the loading conditions (presence of input material, amount of input material and its spatial distribution).

V-V configuration	O-V configuration
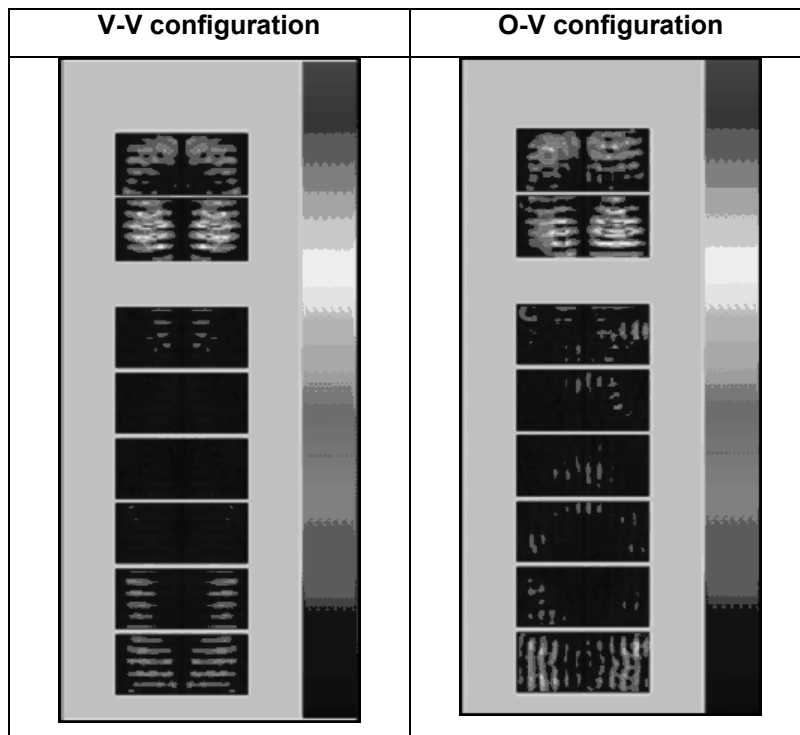
Figure 4 - Qualitative SAR distribution in the tiles surface layer

IV.   Conclusions

Numerical simulation of a new microwave drier for extruded tiles proved to be a useful tool to optimise the design of the applicator, helping to improve its efficiency and the proper heating homogeneity. The use of the MoR measurements helped assessing the tiles damage due to the microwave exposure, thus determining the maximum power density which the material can stand without being negatively affected in its mechanical strength.The experiments evidenced some benefits deriving from the use of microwaves to reduce the drying time of extruded ceramic tiles. In particular, it can be concluded that:

• there is a ratio greater than 1:15 in the drying rate, in the considered experimental conditions, between pure microwave and pure hot air drying. This does not implies that sample integrity is retained;

• as long as microwaves do not remove significantly water from the product, mechanical properties of the green bodies are retained; hybrid systems should be used for complete drying;

• in a more homogenous microwave applicator, like the horn-feed one, pure microwave drying is feasible, but a SAR lower than 800W/kg should be preferred;

• homogeneity of heat generation in the sample is mandatory, and the use of mode stirrers, combined with the movement of the load, could help reducing temperature gradients in the sample. Numerical simulation helped optimizing, in terms of energy efficiency and heating homogeneity, the modules of the continuous drier.

References

[1] Veronesi P., Siligardi C., Franchini M., Leonelli C., *Intl. Cer. Journal* (feb 2001), 57-62.

[2] Jansen W., Visscher K., Beuse R., Weber J., *Proc. of the 7th Intl. conf. of microwave and high frequency heating* (1999), 481-484.

[3] Mizuno M., Obata S., Takayama S., Ito S., Kato N., Hirai T., Sato M., *J. Europ. Cer. Soc.*, 24[2], 8th International Conference on Ceramic Processing (2004), 387-391.

[4] Metaxas A.C., Meredith R.J., "Industrial microwave heating", Peter Peregrinus, London (1993), 43-96.

INNOVATIVE THECNOLOGY FOR THE ARTISTIC AND CULTURAL HERITAGE

A. Diaferia, N. Diaferia, F. D'Imperio, V. Rosito

Emitech s.r.l.

Via Olivetti – Zona ASI 70056 Molfetta (BA) - Italy
Phone: 080.99.00.295   Fax: 080.99.00.297
www.emitech.it   emitech@emitech.it

Abstract

Works of art and antiques undergo ageing processes and can be also damaged by external factors of biologic, chemical and physical origin. Pests and micro-organisms are the main agents of bio-deteriorations of documentary and archival assets and of works of art. A wide range of methods is available for eliminating pests such as fumigation, hot water, hot air, heat and cold treatments, but all these disinfesting processes present the disadvantage of toxicity and/or long duration of the cycle. In the last years microwave processing of materials, for industrial and civil scopes, has been of considerable interest for applied electromagnetism since microwave heating has a large number of applications. These are advantageous in terms of time saving and quality of the final product unlike the conventional heating method.

This work presents how electromagnetic energy at microwave frequencies can be employed for the disinfesting treatments of the artistic heritage and for the disinfection of documentary and archival assets. The tests on insects mortality and on microwaves effects on paper were performed with the collaboration of "Centro di Fotoriproduzione Legatoria e Restauro degli Archivi di Stato" (CFLR - Ministero per i Beni e le Attività Culturali, Rome) using a reverberating chamber realized by Emitech s.r.l..

Microwave systems

The disinfesting system is composed of a metallic shielded chamber reverberating at the microwave frequencies.

The device can be provided with one or more multimodal agitators (stirrers) whose function allows obtaining a statistically uniform and homogenous electromagnetic field in the volume in which the treatment takes place.

The system has also a fiber optic thermometer which allows measuring temperatures during the irradiation notwithstanding the electromagnetic interferences. Moreover, by means of an electronic precision balance, it is possible to remark changes of weight in the treated object.

The operating system is completely automated by means of a PLC (Programmable Logic Controller) interfaced with a touch-screen. Thanks to this configuration, there is a better and easier control of the variables during the disinfesting process.

The microwaves emission is stopped automatically by the PLC when the temperature and the weight reach the pre-established values.

Figure 1 shows one of the devices used for the experimentation characterized by the following features:

Dimensions   L = 1200 mm W = 800 mm H = 1110 mm;

Maximum power emitted by the magnetron 2 or 6 kW at a frequency of 2,45 GHz.

The measurements of the field uniformity were taken using a signal generator (19 dBm at 2.45 GHz) HP 83731 B, an isotropic sensor or Wandel & Goltermann TYPE 18, an EM Radiator Meter EMR 300 situated into the chamber at 20 cm (level A), 40 cm (level B) and 60 cm (level C) from the bottom of the treatment chamber.

The measurements of the electromagnetic field were taken with a sample time of 2 s and in an interval of 360 s. The average value of the field was measured for every point in both conditions: with the stirrer set in motion or off in order to remark the differences of field uniformity.

Figure 1 - Microwave device realized by Emitech

.

Table 1 - Measures of field uniformity with a still stirrer and with a moving stirrer

stirrer off

LEVEL A

	1	2	3
a	25,98	25,38	18,15
b	25,19	13,68	21,07
c	13,19	14,79	21,62

LEVEL B

	1	2	3
a	22,20	16,33	15,85
b	30,09	21,88	12,29
c	15,79	23,06	15,92

LEVEL C

	1	2	3
a	17,18	22,29	14,01
b	21,59	18,22	12,74
c	22,43	15,09	17,69

stirrer on

LEVEL A

	1	2	3
a	18,77	18,12	18,34
b	20,57	17,69	16,60
c	17,71	18,16	19,77

LEVEL B

	1	2	3
a	18,18	17,36	19,52
b	17,23	17,53	16,88
c	18,05	18,41	17,67

LEVEL C

	1	2	3
a	17,54	17,54	17,48
b	18,48	18,05	18,07
c	19,25	17,53	18,31

Another disinfestation system is the Mi.Sy.A container (Figure 2). The device consists in a metallic shielding chamber characterized by the following dimensions: L = 6040 mm; W = 2430 mm; H = 2590 mm.

It is composed of a treatment chamber and a technical area. The former is isolated from the latter where electronic and electromechanical devices are situated (microwaves generator, switchboard, PLC, cooling systems, airing system).

The treatment chamber is shielded and reverberating: it is provided with a stirrer and a shielded and automated door with pneumatic pistons.

Figure 2 - Mi.Sy.A. container realized by Emitech
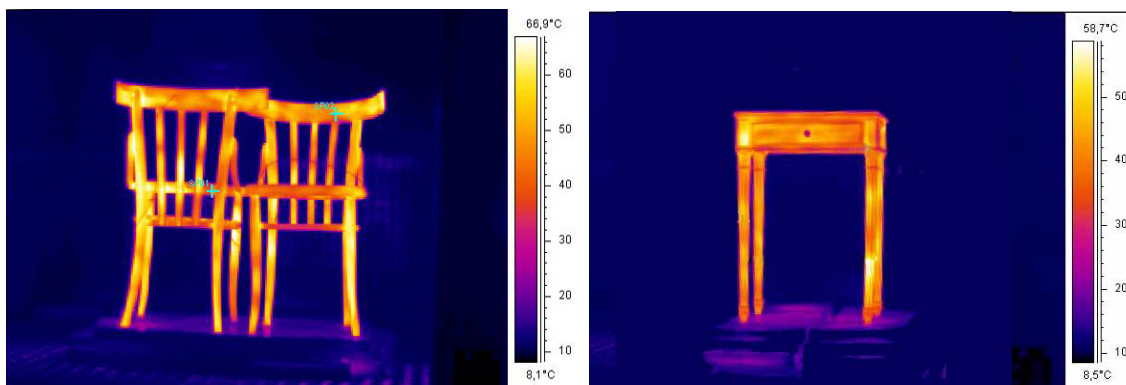
Figure 3 - Thermographic images of a beechwood bedside table and chairs

The electromagnetic energy at the frequency of microwaves is produced outside the chamber by one or more generators and is introduced through appropriate openings in the walls. Its power can be varied in order to reach the lethal temperature of pests.

A PLC and a dedicated software allow the management of the process parameters (power, time, temperature of the treated object) and the control of safety devices, alarms, opening and closing of the door.

The temperature of the treated object can be measured in real-time using the fiber optic sensors which are included in the system.

Figure 3 shows a beechwood bedside table and two chairs after an irradiation at 6 KW of power for 100 s in a reverberating chamber; thanks to an infrared thermo-camera (FLIR system) it is possible to remark the uniformity of the surface temperature.

Tests on insects mortality and effects on wood and paper objects

The results of the experimental work about the insects resistance against microwaves are illustrated here. The entomological samples employed in the tests on paper belong to the Stegobium paniceum L. species, a Coleoptera Anobiidae widespread in archives (Figure 4 A). It produces irreversible damages like holes and tunnels in the infested material (Figure 4 B).

Figure 4 A and B - Insects Stegobium Paniceum (larva and adult) on the left; damaged manuscript, on the right

*Table 2 - Tests on insects mortality

Test N°	Volume Thickness (cm)	Volume Wt (g)	Paper Humid. (%)[1]	Irrad. Time (s)	Pow. (kW)	Sample position	Final temp. (°C)	Sample Average wt (mg)[2]	Results[2]	Mortality
1	1.5	374.45	9.5	60	1	Middle	55.14	L:1.6 A:0.9	L:3 d A:3 d	100%
						Superficial	47.26	A:0.9 A:1.0	L:2 d;1 a[3] A:3 d	83%
2	4	948.60	7.8	120	1	Middle	51.57	L:0.9 A:1.0	L:3 d A:3 d	100%
						Superficial	58.56	L:1.0 A:1.1	L:3 d A:3 d	100%
3	8	1866.43	7.8	180	1	Middle	58.03	L:1.2 A:1.3	L:3 d A:2 d; 1l	83-100%
						Superficial	46.12	L:1.0 A:1.2	L: 2d ; 1 a[3] A: 2d; 1l	67-83%
4	8	1870.62	8.5	240	1	Middle	69.62	L:0.4 A:0.8	L: 3 d A: 3 d	100%
						Superficial	55.70	L:0.9 A:0.9	L: 3 d A: 3 d	100%
5[4]	8	1872.54	7.6	0	0	Middle	19.44	L:2.0 A:0.8	L: 3 a A: 3 a	0%
						Superficial	-	L:1.6 A:0.9	L: 3 a A: 3 a	0%

1) Measured by Aqua-Boy
2) L= larva of Stegobium paniceum L.; A = adult of Stegobium paniceum L: d = dead ; a = alive; l = lost.
3) This larva was apparently dead soon after the treatment, but it has recovered 24 hours afterward.
4) "White" test; the book with the entomological specimens is set inside the Mi.Sy.A. system the door closed, stirrer and pump in service over 180 s time, without going through microwaves irradiation.

The experimentation has been carried out applying a maximum power of 1 kW at variable times: table 2 shows the operating conditions which are necessary to obtain the mortality of samples (larvae and adults).

Tests were carried out in order to value the microwaves irradiation effects on paper. We irradiated two piles of paper sheets (23 x 14 cm, height 8 cm) Whatman n. 1 chromatographic paper, for 164 s and Fabria 100 paper by Cartiere Miliani Fabriano, at a power of 1 kW, for 220 s till to reach 55 °C in the coldest area. Some treated sheets were artificially aged in a climatic chamber at 80 °C, 65% R.H. (ISO 5630/3) for 24 days in order to study the long-term effects on irradiated paper.

*Table 3 - Physical and chemical tests on paper

	WHATMAN[1]			
	Untreated	Aged	Irradiated	Irradiated and aged
Brightness (%)[3]	92.9	89.9	94.2	90.5
Double Folds MD (n°)[4]	12	11	12	11
pH[5]	6.50	6.67	6.45	6.30
DPv[6]	1400	1184	1379	1287
A.R.[7]	-	-	-	-
	FABRIA[2]			
Brightness (%)[3]	92.0	80.1	91.8	80.5
Double Folds MD (n°)[4]	455±161	231±74	433±142	288±62
pH[5]	9.33	9.33	9.39	9.33
DPv[6]	852	711	841	724
A.R.[7]	1.61	1.55	1.73	1.54

1)87 g/m^2, pure cotton cellulose with no fillers, sizings and other additions. Final temperature T_f = 74.88 °C

2)100 g/m^2, chemical paste from conifer and broadleaf tree, paste sizing with dimerous alkyl ketene (Aquapel), surface sizing with potatoes starch.

3) UNI 7623.

4) TAPPI T 423 om – 89.

5 UNI 10177.

6) Degree of polymerization UNI 8282.

7) Alkaline Reserve(%CaCO$_3$) UNI 10183.

*G. Arruzzolo and other authors, "Action of Microwaves on noxious insects to paper supports", Modena, 12-15 September 2005.

Table 3 shows the results of chemical, physical and mechanical methods used to analyze any damage incurred, weakening or properties changes.

The heating effects on three slabs of poplar, prepared and depicted with several techniques that were used in the past, were studied.

The effects of heating were evaluated in terms of warpings of the wood and possible chinks: these changes can damage a pictorial layer that could be present.

Temperatures were constantly measured using a fiber optic thermometer whose extremity was inserted in the sample through a hole (Ø 1 mm); the sample was treated for 5 minutes at 55 °C.

Before the treatment, there were no chinks and detachments of the pictorial layer. Samples were photographed through the microscope before and after the microwaves treatment; photograms were compared to remark chinks or detachments of the pictorial layer. Chinks, detachments and deterioration of the pictorial layer were not found in any case (Figure 5).
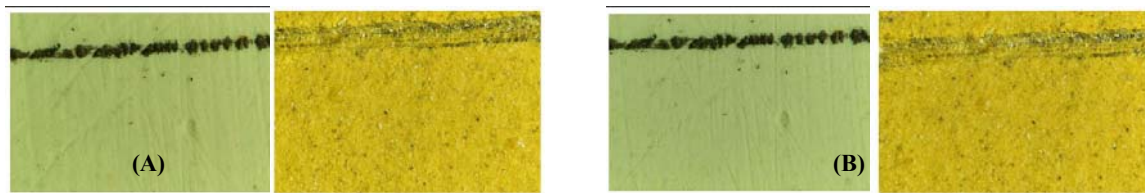
Figure 5 - Particulars of depicted slabs photographed through the microscope; the frame is 1 mm wide; the pictures on the left were taken before the treatment (A), the pictures on the right after it (B)

Conclusions

The presence of modal agitators (stirrers) in the presented microwaves devices allows identifying an area, in the inner volume of the reverberating chamber, where the uniformity of the electromagnetic field there is assured.

In the experimental tests, realized using Emitech's microwave devices, the experimental conditions proved to be effective against noxious insects and completely harmless for both operators and treated objects.

References

[1]   G. Arruzzolo, G. Marinucci, E. Ruschioni, E. Veca, U. Cesareo, L. Botti, G. Impagliazzo, O. Mantovani, L. Residori, D. Ruggiero, B. Orioni, "Progetto MI. SY. A.(parte I): azione delle microonde su insetti dannosi per i supporti di carta", IX Salone dei Beni e delle Attività Culturali, Restaura - Venezia, 2-4 dicembre 2005.

[2]   G. Arruzzolo, G. Marinucci, E. Ruschioni, E. Veca, U. Cesareo, L. Botti, G. Impagliazzo, O. Mantovani, L. Residori, D. Ruggiero, B. Orioni: "Action of Microwaves on noxious insects to paper supports" - *10th International Conference on Microwave and High Frequency Heating Modena*, 12-15 September 2005.

[3]   N. Diaferia, F. D'Imperio, *Electromagnetic characterization of an asymmetrical reverberating chamber*, 2° Convegno Nazionale MISA 2004 Ancona, 6-8 ottobre 2004.

[4]   D. Andreuccetti, M. Bini, A. Ignesti, A. Gambetta, R. Olmi, Microwave Destruction of Woodworms, *Journal of Microwave Power and Electromagnetic Energy,* vol. 29, n. 3, 1994.

SAR EVALUATION IN GTEM CELL FOR IN VITRO DOSIMETRY

M. Bozzetti, G. Calò, A. D'Orazio, M. De Sario, L. Mescia,
V. Petruzzelli, F. Prudenzano*

Dipartimento di Elettrotecnica ed Elettronica, Politecnico di Bari
Via Re David, 200 – 70125 – Bari

* Dipartimento di Ingegneria dell'Ambiente e per lo Sviluppo Sostenibile, Politecnico di Bari
Viale del Turismo, 8 - 74100 – Taranto

petruzzelli@poliba.it

Abstract

In this paper we deal with the design of a novel GTEM cell suitable for in vitro dosimetry. The first prototype of the GTEM cell and the measurement setup useful to perform the dosimetric experiments are proposed too. Finally, the Specific Absorption Rate (SAR) of in vitro biological samples exposed in the GTEM cell is evaluated by means of numerical and experimental techniques based on electric field and temperature measurements.

1. Introduction

Although well investigated all over the world, in vitro dosimetry is still of great interest for international organizations and research laboratories actively involved in preventing human health hazards. In fact, possible biological effects due to mobile-phone usage have been often contradictorily assessed owing to inconsistencies of the results obtained by different laboratories due to the impossibility of a rigorous replica of the experimental conditions.

The need of properly designing an exposure system for dosimetric experiments is obviously of primary importance. Accordingly, the accurate definition of the exposure conditions (i.e. electromagnetic (e.m.) source frequency, e.m. field strength, exposure time and amount of e.m. power absorbed by the exposed sample) is crucial for the interpretation of the observed biological effect and for the correlation with the inducing e.m. field.

The exposure system we chose in order to meet the in vitro dosimetry requirements is a GTEM cell suitably designed to be included in a conventional incubator (of size 0.60 m x 0.50 m x 0.50 m), necessary for the survival of the biological sample during the dosimetric experiments. The first GTEM cell prototype, inserted in the incubator is shown in Figure 1. The proposed GTEM cell, designed for in vitro dosimetry, differs from the conventional one for the noticeably reduced sizes (maximum size L=0.45 m) if compared with the several-meter-long GTEM cells for Electromagnetic Compatibility (EMC) tests. Moreover, accurate and repeatable measures can be performed in this GTEM cell for frequencies up to a few GHz being the propagating TEM wave characterized by uniformity and controllable intensity [1-4].

Figure 1 - GTEM cell prototype in the incubator

2. GTEM cell simulations

To design the GTEM cell for in vitro dosimetric experiments, the electromagnetic propagation has been simulated by a homemade computer code based on the Transverse Resonance Diffraction (TRD) method [5]. By applying the TRD technique, the GTEM cell has been simulated at the two typical operating frequencies of the dual band GSM mobile phone system, f=900 MHz and f=1800 MHz. The TE, TM and TEM propagating modes can be separately identified with acceptable CPU computer time.

Figure 2 outlines the relevant geometrical parameters of the GTEM cell. In order to allow a good 50-Ω impedance matching with the external instrumentation and to achieve the maximum power transfer to the exposure system, the transversal sizes of the GTEM cell must be chosen according to the following equations:

$$\begin{cases} a(z) = 2\ z\ \tan(\alpha) \\ b(z) = z\left[\tan(\gamma) - \tan(\theta)\right] \\ d(z) = z\left[\tan(\gamma) + \tan(\theta)\right] \\ c(z) = \xi\ a(z) \end{cases} \tag{1}$$

The suitable values assuring the characteristic impedance Z_0=50 Ω are: ξ=0.29, α=π/12, γ=π/18, θ=π/36. According to eq.1, the characteristic impedance along the propagation direction remains constant since the tapered shape of the GTEM cell slowly changes along the longitudinal z direction.
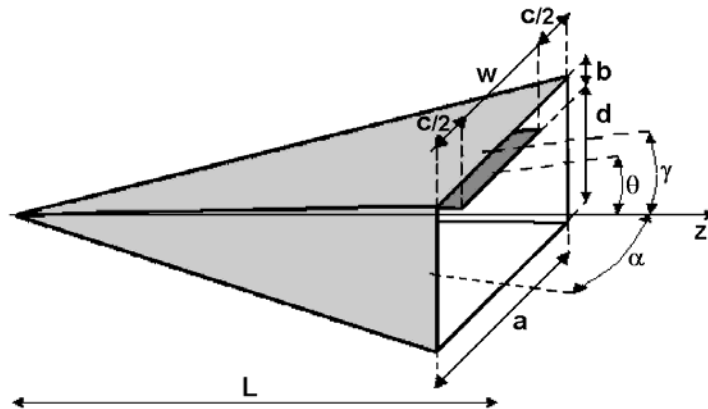
Figure 2 - Sketch of the GTEM cell

Furthermore, the TRD simulation, stated that the optimal length L=0.45 m, chosen to allow the insertion of the GTEM cell in the incubator, assures the propagation of the only TEM mode along almost all the GTEM cell for the two aforesaid typical operating frequencies of the dual band GSM. Thanks to the negligibility of the higher order modes, a uniform e.m. field distribution is assured in the inner region, located between z=0.23 m and z=0.30 m, where the biological sample under test must be placed.

As an example, Figure 3 illustrates the contour lines of the E_x (a) and the E_y (b) electric field components together with the |E| electric field modulus of the TEM mode (c) at frequency f=1.8 GHz in the z=0.230 m section, corresponding to an input power P_{in}=1 W. The dashed and solid lines refer to negative and positive electric field values (expressed in V/m), respectively. As Figure 3 shows, the TEM mode assumes an almost uniform pattern in the region under the inner conductor, thus allowing exploiting a large region (y<-0.040 m and -0.080 m<x<-0.040 m) for the Specific Absorption Rate (SAR) measurement.
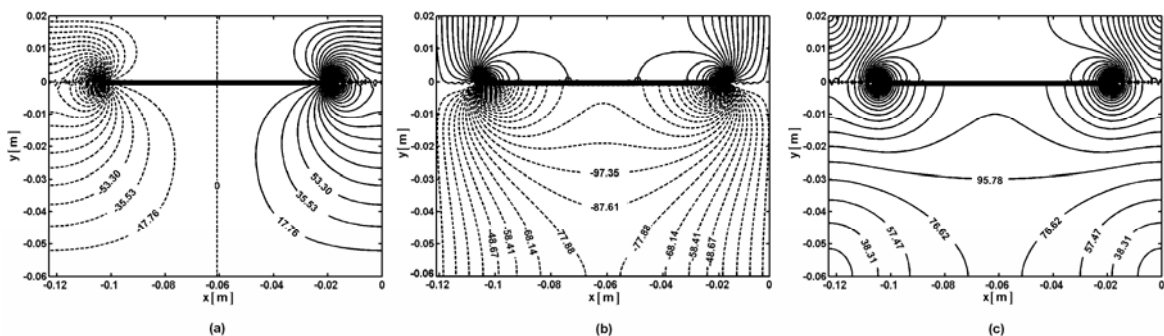
Figure 3 - Electric field contour lines of the TEM mode: positive (solid lines) and negative (dashed lines) values of: a) E_x component [V/m], b) E_y component [V/m] and c) electric field modulus |E| [V/m] at z=0.230 m and f=1.8 GHz

183

3. GTEM cell prototype

The photo of the GTEM cell prototype, enclosed in the incubator, is shown in Figure 1. In particular, the GTEM cell walls are made of aluminum, whereas the internal septum is made on a copper printed circuit board (PCB) shaped to maintain the optimal aspect ratio to assure the 50-Ω characteristic impedance. Moreover, a 50-Ω resistive network load is inserted in the PCB to connect the septum to the GTEM cell terminal wall thus allowing the low-frequency impedance matching.

According to the biological experiment constraints, suitable apertures were made on the GTEM cell walls for the air flux and the thermodynamic conditioning of the inner test volume. These small apertures, having 5-mm diameter, fulfill the cut-off condition at the dual-band GSM operating frequencies without affecting the electromagnetic shielding. In addition, as Figure 1 shows, a cut-off waveguide aperture on the GTEM cell side door was made for the insertion of control probes during the exposure.

The experimental characterization of the GTEM cell was carried out performing the Standing Wave Ratio (SWR) and the Time Domain Reflectometry (TDR) measurements.

The TDR measurement has shown an almost constant (Z_0=50±2 Ω) characteristic impedance along the propagation direction in good agreement with the design values. Nevertheless, a maximum impedance mismatch (50±10 Ω) was measured in correspondence of the input section, where the transition from SMA connector to septum occurs. Accordingly, a reduction of the power transfer to the GTEM cell is expected.

Major efforts have been devoted to the terminal load optimization in order to prevent standing waves from perturbing the e.m. field uniformity. The measured SWR is lower than 1.5 at both the dual band GSM frequencies.

According to the aforesaid measurement results, the e.m. field irradiating the biological sample within the GTEM cell is expected to be uniform.

4. GTEM cell dosimetry

4.1 SAR evaluation

Aiming at the evaluation of the exposure conditions during the dosimetric experiments, a combined technique involving experimental and numerical electric field data has been used for indirectly assessing the SAR of the sample under test. Specifically, the electric field modulus has been measured by means of an innovative optical probe [6] in nine points located in the test region.

The numerical evaluation of the SAR has been carried out by a full-scale numerical model of the realized GTEM cell developed by CST MW Studio [7]. A value of SAR_m=1 W/kg, averaged over the sample volume has been achieved for input power P_{in}=0.78 W, at f=1.8 GHz. Moreover, the electric field has been evaluated in nine points around the sample position both numerically (by CST) and experimentally. By comparing the corresponding simulated and measured E-field values, the SAR of the biological sample can be evaluated.

The same exposure condition during the experiment (i.e. unchanged values of the incident E-field strength and mean SAR) has been obtained for an input power slightly higher than that used for the CST simulation. Under the above circumstances, a $SAR_m=1$ W/kg is achieved at 1.8 GHz for $P_{in}= 1.5$ W.

4.2 SAR validation

SAR of the exposed biological sample can be indirectly estimated by measuring the induced temperature variation. In particular, the actual overall temperature variation, as a function of time t, results from a balance between heat gain and loss in the biological sample.

A valuable method for the SAR assessment is based on the analysis of the temperature values measured in consecutive heating and cooling time intervals [8]. On this purpose, the temperature T is expressed as a function of time t as follows:

$$T(t) = \begin{cases} T_0 & 0 \leq t \leq t_0 \\ T_0 + \dfrac{A}{k}\left(1 - e^{-k(t-t_0)}\right) & t_0 \leq t \leq t_0 + \tau \\ T_0 + \Delta T_{on} e^{-k(t-t_0-\tau)} & t \geq t_0 + \tau \end{cases} \tag{2}$$

where T_0 is the initial temperature corresponding to the thermodynamic equilibrium reached before the e.m. irradiation for $0 \leq t \leq t_0$, whereas $\Delta T_{on} = T(t_0 + \tau) - T(t_0)$ is the temperature increase due to the electromagnetic irradiation during the power-on interval, $t_0 \leq t \leq t_0 + \tau$. The unknown parameters k, A, and ΔT_{on} of eq.2 are evaluated in dependence on the measured temperature data by a linear regression analysis. The average SAR is calculated as follows:

$$SAR = c\,A = c\,\frac{k\,\Delta T_{on}}{1 - e^{-k\tau}} \tag{3}$$

where c is the sample specific heat capacity.

For the SAR evaluation and for the validation of the simulation results, the aforesaid heating-cooling curve analysis (eqs.2-3) has been applied.

Figure 4 shows the temperature measurement setup scheme of GTEM cell. The signal generator and the amplifier are linked to the GTEM cell and a personal computer performs, via GPIB interface, different electromagnetic exposure conditions. An optical temperature control probe is inserted in the biological sample during the exposure and is connected, through the GTEM cell side door aperture, to its remote unit by an optical fiber. The temperature is recorded during the experiment by the computer connected to the remote unit via RS232.

Figure 5 reports the temperature values during a consecutive power-on and off interval. By analyzing the measured data (dots), the fitting curve (solid curve) is calculated by eq. 2. Therefore, by eq. 3, a SAR=1.1 W/kg is obtained for $P_{in}=1.5$ W.
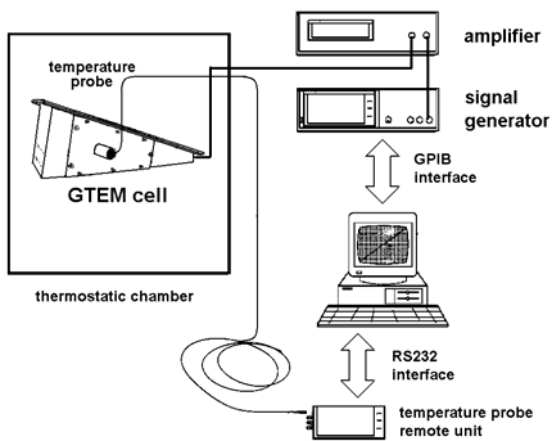
Figure 4 - Temperature measurement setup
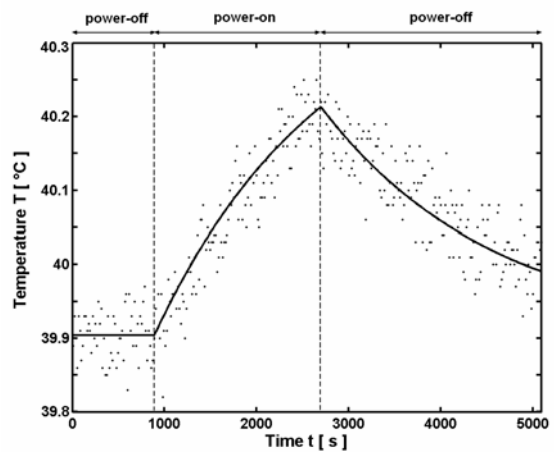
Figure 5 - Biological sample temperature vs time: measured values (dots) and fitting curve (solid curve)

5. Conclusion

A GTEM cell, designed to be included in a conventional incubator (of size 0.60 m x 0.50 m x 0.50 m), has been proposed for dosimetric experiments. The first prototype of the GTEM cell has been characterized by means of SWR and TDR measurements. Furthermore, a numerical and experimental procedure for the evaluation of the SAR of an exposed biological sample has been performed. A good agreement between numerical (SAR=1 W/kg) and experimental (SAR=1.1 W/kg) results has been achieved for an input power P_{in}=1.5 W.

References

[1] G. Calò, F. Lattarulo, V. Petruzzelli: GTEM Cell Experimental Setup for In Vitro Dosimetry, 13th International Conference on Software, Telecommunications and Computer Networks, SoftCOM 2005, Split, Marina Frapa (Croatia), September 15-17, 2005.

[2] G. Calò, A. D'Orazio, M. De Sario, L. Mescia, V. Petruzzelli, F. Pudenzano: GTEM Cell Exposure Device for GSM Mobile Frequency in vitro Experiments, EMC Europe Workshop 2005, Rome, Italy, 19-21 September 2005.

[3] Bozzetti M., G. Calò, A. D'Orazio, M. De Sario, L. Mescia, V. Petruzzelli, F. Prudenzano, G. Cibelli, and R. Zefferino: A novel GTEM cell for in vitro dosimetric experiments, Proc. 3rd Int. Workshop Biological Effects of Electromagnetic Fields, Kos, Greece, I, 11-17, 2004.

[4] IEC 61000-4-3, (2003), Electromagnetic compatibility (EMC) testing and measurement techniques – radiated, radio frequency, electromagnetic field immunity test.

[5] De Leo R., T. Rozzi, C. Svara, and L. Zappelli: Rigorous analysis of the GTEM cell, IEEE Trans. Microwave Theory Tech., MTT-39(3), 488-499, 1991.

[6] W. Mann, K. Petermann: VCSEL-based miniaturised E-field probe with high sensitivity and optical power supply, Electronics Letters, vol. 38, pp. 455-456, May 2002.

[7] CST GmbH, Bad Nauheimer 19, D-64289, Darmstadt, Germany.

[8] Handbook of Biological effects of Electromagnetic fields, CRC Press, 2nd edition, 1996, Florida USA.